FIRST EXPERIMENTS

Spallation Neutron Source
Second Target Station

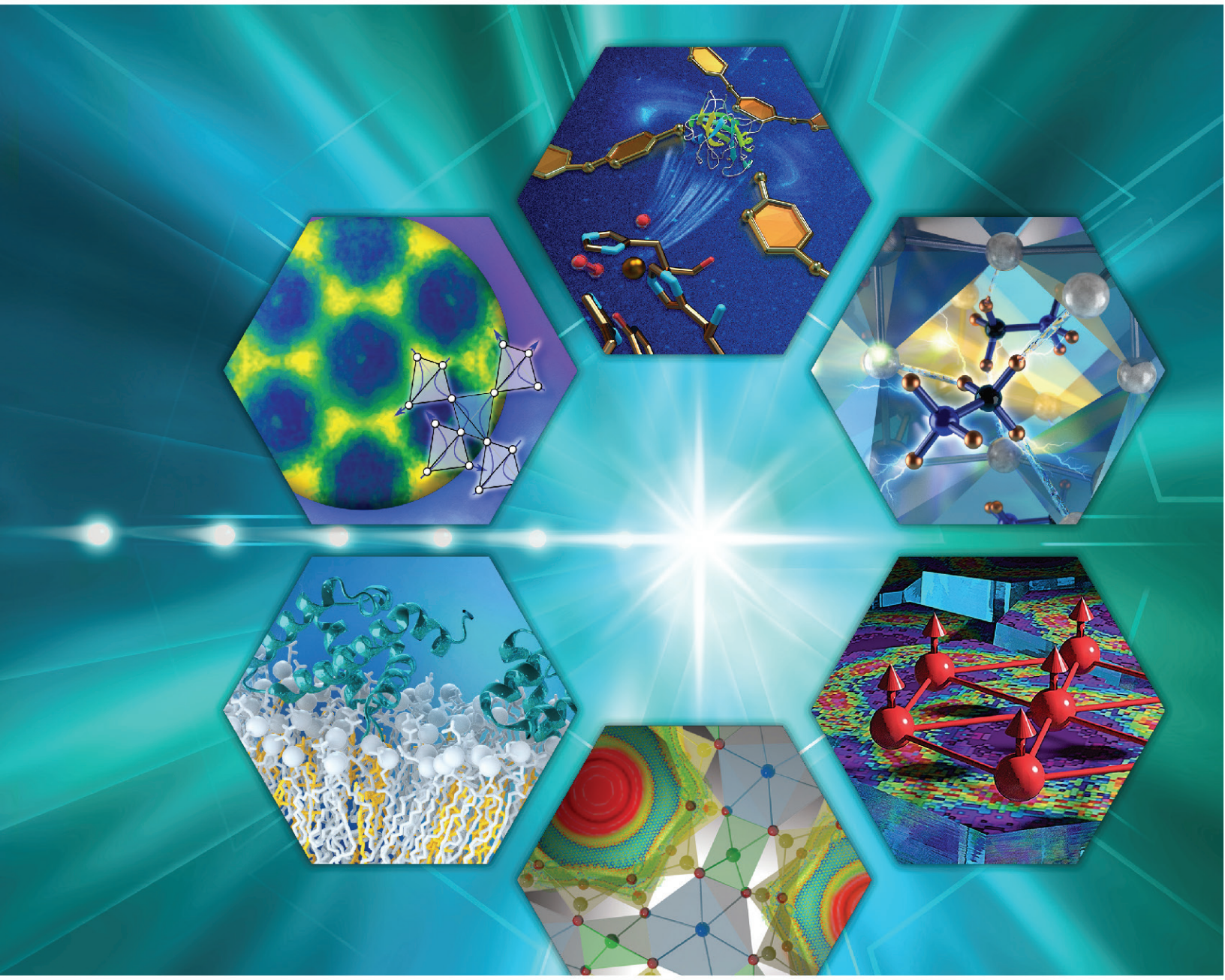

Managed by UT-Battelle LLC for the US Department of Energy

OAK RIDGE National Laboratory

DOCUMENT AVAILABILITY

Reports produced after January 1, 1996, are generally available free via US Department of Energy (DOE) SciTech Connect.

Website www.osti.gov

Reports produced before January 1, 1996, may be purchased by members of the public from the following source:

National Technical Information Service
5285 Port Royal Road
Springfield, VA 22161
Telephone 703-605-6000 (1-800-553-6847)
TDD 703-487-4639
Fax 703-605-6900
E-mail info@ntis.gov
Website http://classic.ntis.gov/

Reports are available to DOE employees, DOE contractors, Energy Technology Data Exchange representatives, and International Nuclear Information System representatives from the following source:

Office of Scientific and Technical Information
PO Box 62
Oak Ridge, TN 37831
Telephone 865-576-8401
Fax 865-576-5728
E-mail reports@osti.gov
Website http://www.osti.gov/contact.html

ORNL/SPR-2019/1407

First Experiments: New Science Opportunities at the Spallation Neutron Source Second Target Station

Date Published:
December 2019

Prepared by
OAK RIDGE NATIONAL LABORATORY
Oak Ridge, Tennessee 37831-6283
managed by
UT-BATTELLE, LLC
for the
US DEPARTMENT OF ENERGY
under contract DE-AC05-00OR22725

On the Cover

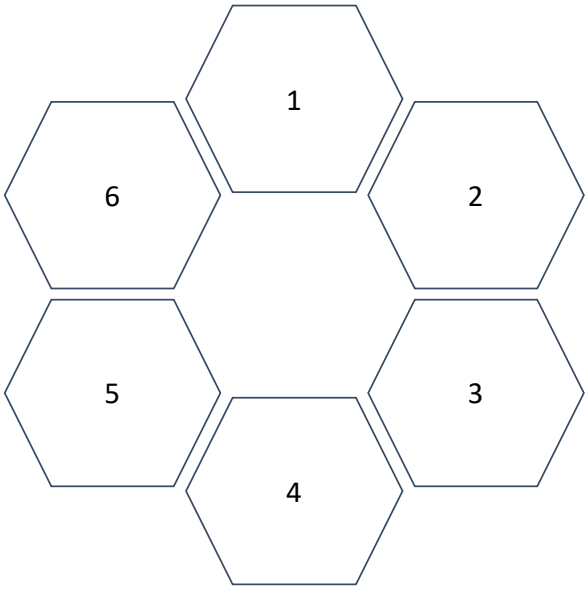

1. Neutron scattering (in combination with X-ray scattering) provided new insights into how a fungal lytic polysaccharide monooxygenase breaks down cellulose. Knowing how oxygen molecules (red) bind to catalytic elements (illustrated by a single copper ion) will guide researchers in developing more efficient, cost-effective biofuel production methods [O'Dell, W. B.; Agarwal, P. K.; Meilleur, F. *Angew. Chem. Int. Ed.* **2017,** *56,* 767–770]. Neutron instrument used: IMAGINE at HFIR. Image source: ORNL/Jill Hemman.
2. Neutron interactions revealed the orthorhombic structure of the hybrid perovskite stabilized by the strong hydrogen bonds between the nitrogen substituent of the methylammonium cations and the bromides on the corner-linked $PbBr_6$ octahedra [Yang, B.; Ming, W.; Du, M-H.; Keum, J. K.; Puretzky, A. A.; Rouleau, C. M.; Huang, J.; Geohegan, D. B.; Wang, X.; Xiao, K. *Adv. Mater.* **2018,** *30,* 1705801]. Neutron instrument used: TOPAZ at SNS. Image source: ORNL/Jill Hemman.
3. Neutrons were used to examine the origins of unusual magnetic behavior in ytterbium-magnesium-gallium-tetraoxide ($YbMgGaO_4$), a rare earth–based metal oxide that is a quantum spin liquid candidate [Paddison, J. A. M.; Daum, M.; Dun, Z.; Ehlers, G.; Liu, Y.; Stone, M. B.; Zhou, H.; Mourigal, M. *Nature Phys.* **2017,** *13,* 117–122]. Neutron instruments used: CNCS and SEQUOIA at SNS. Image source: ORNL/Jill Hemman.
4. Neutron scattering and ab initio simulations were used to document the discovery of a new "quantum tunneling state" of the water molecule confined in 5 Å channels in the mineral beryl [Kolesnikov, A. I.; Reiter, G. F.; Choudhury, N.; Prisk, T. R.; Mamontov, E.; Podlesnyak, A.; Ehlers, G.; Seel, A. G.; Wesolowski, D. J.; Anovitz, L. M. *Phys. Rev. Lett.* **2016,** *116,* 167802]. Neutron instruments used: SEQUOIA and CNCS at SNS; VESUVIO at ISIS Neutron and Muon Source, Rutherford Appleton Laboratory. Image source: ORNL.
5. Neutrons were used to determine how cholesterol enhances the binding of proteins to cell membranes [Doktorova, M.; Heberle, F. A.; Kingston, R. L.; Khelashvili, G.; Cuendet, M. A.; Wen, Y.; Katsaras, J.; Feigenson, G. W.; Vogt, V. M.; Dick, R. A. *Biophys. J.* **2017,** *113,* 2004–2015]. Neutron instrument used: EQ-SANS at SNS. Image source: ORNL/Jill Hemman.
6. Neutron scattering revealed a pattern characteristic of the emergent electron motion in the quantum spin liquid state in the three-dimensional antiferromagnet $NaCaNi_2F_7$ [Plumb, K. W.; Changlani, H. J.; Scheie, A.; Zhang, S.; Krizan, J. W.; Rodriguez-Rivera, J. A.; Qiu, Y.; Winn, B.; Cava, R. J.; Broholm, C. L. *Nature Phys.* **2019,** *15,* 54–59]. Neutron instruments used: HYSPEC at SNS and MACS spectrometer at the NIST Center for Neutron Research. Image source: Brown University/Kemp Plumb and ORNL/Genevieve Martin.

Contents

On the Cover ..... **ii**
List of Figures ..... **vii**
List of Tables ..... **viii**
Executive Summary **1**
1. Introduction **5**
2. Overview of STS Neutron Beam Production **9**
2.1 Production of Proton Pulses **9**
2.2 Compact Source Design **10**
3. Polymers and Soft Materials **13**
3.1 Introduction **13**
3.2 New STS Experimental Capabilities for Soft Materials Research **15**
3.3 First STS Experiments **17**
3.3.1 Macromolecular Assembly in External Fields 17
3.3.2 Making Hierarchical Structures Using Charged Polymers 19
3.3.3 Watching Polyelectrolytes at Work 21
3.3.4 Discovering Advanced Soft Matter Composites In Situ 22
3.3.5 Controlling Structure and Flow in Complex Fluids 24
3.4 Conclusion **25**
4. Quantum Matter **28**
4.1 Introduction **28**
4.2 New STS Experimental Capabilities for Quantum Materials **29**
4.3 First STS Experiments **30**
4.3.1 Revealing the Fundamental Interactions in Quantum Disordered Materials 30
4.3.2 Exploring Magnetism Beyond Thermal Equilibrium 33
4.3.3 Understanding Structure and Dynamics of Topological Quantum Matter 35
4.3.4 Tuning Emergent Quantum States of Matter 36
4.3.5 Exploiting Advances in Heterostructure Fabrication for Applications of Quantum Matter 38
4.4 Conclusion **41**
5. Materials Synthesis snd Energy Materials **46**
5.1 Introduction **46**
5.2 New STS Experimental Capabilities for Materials Synthesis and Energy Materials **47**
5.3 First STS Experiments **48**
5.3.1 Mastering Hierarchical Assembly and Crystallization from Complex Solutions 48

5.3.2 Discovery and Synthesis of Functional Materials via High Pressure 51
5.3.3 In Situ Examination of Dynamic Interfaces in Batteries and Supercapacitors 53
5.4 Conclusion 56
6. Structural Materials 59
6.1 Introduction 59
6.2 New STS Experimental Capabilities for Structural Materials 60
6.3 First STS Experiments 62
6.3.1 Understanding How to Overcome the Strength-Ductility Trade-off 62
6.3.2 Exploring the Fundamentals of Additive and Metamorphic Manufacturing 64
6.3.3 Understanding Fundamental Corrosion Mechanisms 66
6.4 Conclusion 67
7. Biology and Life Sciences 69
7.1 Introduction 69
7.2 New STS Experimental Capabilities for Biological Function 71
7.3 First STS Experiments 73
7.3.1 Time-Resolved Disorder in Amyotrophic Lateral Sclerosis 73
7.3.2 Understanding the Structure, Dynamics, and Function of the Microbial Cell Envelope 75
7.3.3 Photosystem II: The Light-Activated Water-Splitting Enzyme 77
7.3.4 Harnessing the Catalytic Power of a Versatile Family of Enzymes 78
7.4 Conclusion 80
8. Applying Advances in Neutron Instrumentation and Technologies to the STS 83
8.1 Introduction 83
8.2 Neutron Optics 84
8.2.1 Neutron Beam Transport 84
8.2.2 Neutron Focusing/Imaging Optics 85
8.2.3 Polarizing Supermirrors 85
8.3 Polarized Neutrons and Larmor Methods 85
8.4 Neutron Detectors 87
8.5 Data and Computing 89
8.5.1 Comprehensive Data Architecture 90
8.5.2 Smart Neutron Scattering Instruments in a Converged Data and Computing Ecosystem 90
8.5.3 Advanced Data Reduction and Analysis 91
8.6 STS Experimental Approaches 93
8.6.1 Time-of-Flight Experimental Approaches 93

8.6.2 Time-Resolved and Cinematic Measurements of Kinetic Processes and Beyond-Equilibrium Matter 93
8.6.3 Smaller Sample and Beam Sizes 95
8.6.4 Simultaneous Measurements Across Unprecedented Length Scales 95
8.7 STS Instrument Concepts 96
8.7.1 SANS Instrument 97
8.7.2 Simultaneous SANS/WANS Instrument 98
8.7.3 Neutron Reflectometer with Horizontal Sample Surface 99
8.7.4 Cold Neutron Chopper Spectrometer 101
8.7.5 Multimodal Instrument for Studies at High Magnetic Field 102
8.7.6 Single-Crystal Diffractometer for Small Samples 104
8.7.7 Versatile Diffractometer for Magnetic Structure Studies 105
8.7.8 Versatile Multiscale Materials Engineering Beamline 106
9. Contributors 111
Appendix A. Community Workshops and Activities in Support of STS, 2013–2018 117
Appendix B. Acronyms, Abbreviations, and Initialisms 119

(Intentionally left blank)

List of Figures

Fig. 2.1. Schematic layout of the SNS complex, including the proposed STS (at right). viii
Fig. 2.2. Rotating tungsten target and moderator configuration. 11
Fig. 2.3. Pulse shapes emitted from FTS and STS cold, coupled moderators at a wavelength of 5 Å (a typical benchmark for cold neutrons). 11
Fig. 2.4. Peak and time-averaged brightness of current (closed circles) and planned (open circles) neutron sources, illustrated at 5 Å. 12
Fig. 3.1. Dynamic exchange reaction of vitrimers. 18
Fig. 3.2. Schematic of an ABA block copolymer complex coacervate. 20
Fig. 3.3. Crystalline domains of ODPA-P3 matrix containing 2.4 vol% SWCNTs. 23
Fig. 3.4. Hierarchical structures in the complex fluid used in the PUREX process. 25
Fig. 4.1. Fractionalized excitations in candidate QSL materials result in a diffuse response in INS experiments. 31
Fig. 4.2. Single crystals of the organic superconductor κ−$(BEDT\text{-}TTF)_2Cu[N(CN)_2]Br$. 31
Fig. 4.3. Machine learning using neural networks leading to visualization of glass formation in a cooled spin liquid. 33
Fig. 4.4. Schematic of a pyrochlore Ising ferromagnet. 34
Fig. 4.5. Energy level scheme for the chromium-8 molecule. 34
Fig. 4.6. Emergent electrodynamics of topological spin structures: deflection of an electron when passing through a skyrmion. 35
Fig. 4.7. Exploring the properties of SmB_6. 36
Fig. 4.8. Representative phase diagram of a cuprate superconductor as a function of temperature and hole doping. 37
Fig. 4.9. Pressure as a parameter for tuning superconductivity. 38
Fig. 4.10. An organic superlattice consisting of 1D pthalocyanine chains can be used to generate custom, variable spin, 1D chains. 40
Fig. 4.11. CeO_2 nanotrees. 40
Fig. 5.1. Mechanisms of crystallization from aqueous solutions. 49
Fig. 5.2. Simulated neutron scattering data. 50
Fig. 5.3. Details of the new phase of silicon. 52
Fig. 5.4. Simulated performance of a reflectometer designed for the STS, derived from fitted reflectivity data obtained on the FTS Liquids Reflectometer. 55
Fig. 6.1. Schematic of real-time in situ multimodal experiments at the STS. 63
Fig. 6.2. Schematic of powder-fed additive manufacturing setup with a scanning focused laser beam for heating. 64
Fig. 6.3. Schematic of an electrochemical split cell for in situ neutron reflectometry measurements. 67
Fig. 7.1. Application of deuterium labeling and contrast matching. 70
Fig. 7.2. Isotopic contrast variation. 73
Fig. 7.3. Hijacking membrane-less organelles in ALS. 74
Fig. 7.4. Computer model of the cell envelope of a Gram-negative bacterium. 76
Fig. 7.5. Photosystem II and the Kok cycle. 77
Fig. 7.6. The dimeric aspartate aminotransferase (AAT) enzyme and two active sites. 79
Fig. 8.1. Illustration of the range of Fourier time and momentum transfer measured by a wide-angle NSE at the STS. 87
Fig. 8.2. Scintillator Anger camera detector technology. 88
Fig. 8.3. Advancing detector technology. 89

Fig. 8.4. Illustration of the power of cinematic data collection. 94
Fig. 8.5. Cartoon of extreme high field magnet, illustrating limited access to the sample location. 95
Fig. 8.6. Schematic view of the STS target building and experiment halls, showing 16 of the 22 instruments that will be part of the STS when it is fully outfitted. 96
Fig. 8.8. Simulated scattering patterns for the STS SANS instrument. 97
Fig. 8.7. Arrangement of stepped arrays of Anger camera detector modules for the STS SANS instrument. 97
Fig. 8.9. Detector configuration for STS SANS/WANS instrument concept. 98
Fig. 8.10. Kinetics of the crosslinking reaction of a polyelectrolyte hydrogel. 100
Fig. 8.11. Schematic view of the STS horizontal surface reflectometer concept. 100
Fig. 8.12. Functional layout of the STS cold neutron chopper spectrometer concept. 102
Fig. 8.13. Performance of the FTS and STS cold neutron chopper spectrometers. 102
Fig. 8.14. Spectrometer and diffraction arms surrounding the magnet of the multimodal instrument concept. 103
Fig. 8.15. Range of energy and momentum transfer simultaneously accessed by the analyzer arms of the multimodal instrument concept for a single instrument configuration. 104
Fig. 8.16. Schematic of the optics design for STS single-crystal diffractometer for small samples 105
Fig. 8.17. Detector layout for STS diffractometer optimized for magnetic structure studies. 106
Fig. 8.18. Detector layout for the STS engineering materials instrument. 107
Fig. 8.19. Simulated diffraction data from VULCAN at the FTS (left) and the engineering diffractometer at the STS. 107

List of Tables

Table 8.1. STS SANS instrument concept: Key parameters 98
Table 8.2. STS SANS/WANS instrument concept: Key parameters 99
Table 8.3. STS horizontal surface reflectometer concept: Key parameters 100
Table 8.4. STS cold neutron chopper spectrometer optimized for small sample area: Key parameters 101
Table 8.5. STS multimodal high magnetic field instrument: Key parameters 104
Table 8.6. STS single crystal diffractometer for small samples: Key parameters 105
Table 8.7. STS diffractometer optimized for magnetic structure studies: Key parameters 106
Table 8.8. STS multiscale engineering beamline: Key parameters 108

Executive Summary

Leadership in materials science underpins future technologies in energy, security, and other applications that drive this nation's economy. Neutron scattering is among the crucial characterization techniques necessary to ensure a world-leading position in materials science for the United States. The Second Target Station (STS) at the Spallation Neutron Source (SNS) will provide transformative new capabilities for the study of a broad range of materials using neutron scattering and will support users in many fields of research—materials science, physics, chemistry, geology, biology, and engineering, among others—and from academia, government laboratories, and industry.

This report describes examples of first experiments to be conducted at the STS in five key science areas: polymers and soft materials, quantum matter, materials synthesis and energy materials, structural materials, and biology and life sciences. These examples serve to illustrate the extraordinary potential of the STS to impact a broad spectrum of scientific fields. When it is fully built out, the capabilities offered by the 22 instruments planned for the STS will complement those of two existing US Department of Energy (DOE) Office of Science neutron scattering user facilities at Oak Ridge National Laboratory (ORNL)—the First Target Station (FTS) of the SNS and the High Flux Isotope Reactor (HFIR)—as well as those of the National Institute for Science and Technology (NIST) Center for Neutron Research (NCNR). The STS has a pivotal role to play in extending the reach of neutron scattering to new transformative opportunities for discovery science, including in particular applications that require time-resolved examination of nonequilibrium processes in dynamic hierarchical systems over greatly increased length, energy, and time scales. It will enable experiments that will not be possible at any other facility in the world.

The STS, which will be pulsed at 15 Hz, will deliver cold neutrons with the highest peak brightness in the world and with a broad range of neutron energies. These capabilities, when combined with advances in neutron optics, instrumentation, and detectors, will sustain the nation's position at the frontier in neutron scattering for decades to come. Specifically, the STS is designed to enable:

- Time-resolved measurements of kinetic processes and beyond-equilibrium matter, including cinematic viewing (i.e., "movies") of materials as they are being synthesized, processed, or self-assembled; chemical processes at interfaces; and formation and function of biological macromolecular complexes
- More intense neutron beams with smaller cross sections to explore smaller samples of newly discovered or synthesized materials under extreme conditions, such as magnetic field, pressure, and temperature
- Simultaneous measurements of hierarchical architectures across an unprecedented range of length scales, from the atomic scale to the micron and beyond, providing new insight into functional materials

With these new capabilities, the STS will provide world-leading resources for the examination of materials over broad ranges of length, energy, and time scales, making it possible for researchers to study the structure, dynamics, properties, and reactions of complex materials that have heterogeneity, interfaces, and disorder and to conduct temporally resolved, in situ and operando studies of materials and chemical processes. In addition, by enabling studies of materials systems across length scales from the atom to the micron and beyond, the STS will reveal how materials self-assemble into hierarchical structures and how proteins interact in living biological cells.

The new scientific opportunities enabled by the STS were defined in consultation with the research community at numerous scientific conferences, workshops, and advisory committee meetings over the

past decade. To illustrate the extraordinary potential of the STS to impact a broad spectrum of scientific fields, this report describes examples of first experiments to be conducted at the STS in five areas of science: Polymers and soft materials, quantum matter, materials synthesis and energy materials, structural materials, and biology and life sciences. Specific advantages of the STS in each of these five areas are summarized below.

- The STS will transform the way neutron scattering is used to provide fundamental knowledge on the synthesis, assembly, structure, and dynamics of **polymers and soft materials**. Specifically, smaller beam sizes with high brightness will allow in situ and operando examination of dynamic processes across broad length scales (0.1–100 nm). Examples of dynamic processes to be studied at the STS include phase transitions, aggregation, crystallization, and processes that occur under the influence of external forces, such as shear. Greater understanding of these processes will provide knowledge needed for the design of new soft materials, such as self-healing polymers, membranes for water purification, and lightweight structural materials, and for addressing the challenge of renewable resourcing, recycling, and upcycling.
- Neutrons are an exquisitely sensitive probe for the study of magnetic properties in materials. The unique capabilities of the STS will make it possible to study **quantum matter** in ways that are not possible at any current neutron source, yielding the knowledge required both to discover new quantum materials and to control quantum states that could lead to future quantum technologies. For example, the small beam size and brightness of the STS will make it possible to conduct inelastic neutron scattering experiments on far smaller samples of new materials (1 mm^3), so that neutron scattering can be employed in the early stages of materials development or when large, high-quality single crystals are not available. Further, these characteristics will facilitate the study of quantum materials using higher field magnets (with smaller bores) and specialized sample environments, such as very high pressure diamond anvil cells. Finally, the STS will enable studies of the dynamics of quantum systems, such as magnetism beyond thermal equilibrium. Such time-resolved studies—for example, pump-probe experiments to study excited-state lifetimes and decay pathways with tight energy resolution and broad momentum coverage—are not possible using other techniques.
- The ability to study dynamic processes with the STS will provide a revolutionary capability for examining **materials synthesis and energy materials** with neutrons, making it possible to probe the structure and morphology of materials in real time and across broad length scales, from the atomic level to millimeters, in situ and operando. This will make it possible to observe materials and even obtain "movies" as materials are being synthesized or processed, for example during 3D printing, or as they are modified during use in materials systems, such as changes in battery electrodes during charge/discharge cycles. The STS will also make it possible to study in real time important chemical processes that occur at interfaces, such as corrosion, dissolution, catalysis, separations, and other dynamic processes that are important to a wide range of energy technologies.
- The STS will provide exciting new capabilities for **structural materials,** because it will provide information at high resolution on specific regions in a material while also examining a material across broad length scales. This will allow simultaneous characterization of microstructures, including nucleation and growth of precipitates, metastable phases in complex alloys and composites, long-range order, and defects. This information will provide a fundamental understanding of how composition and processing affect the structure, properties, and performance of structural materials used in transportation, buildings, and other applications.
- A major advantage of the STS for **biology and life sciences** is the ability to study dynamic systems. Life's processes are never at equilibrium, and unraveling the dynamic processes requires the ability to understand these systems by monitoring them in real time. The STS will enable the study of processes such as the formation and dissociation of protein complexes and the formation of protein aggregates from intrinsically disordered proteins, without the need to repeatedly reconfigure the experiment to

probe all of its aspects. In addition, the STS source characteristics will make it possible to conduct these studies on smaller samples and across broad length scales—from molecules to cells.

The experiments outlined in this report illustrate how the STS will provide wholly new capabilities that both complement and substantially extend this nation's current resources for neutron scattering.

This report also includes descriptions of advances in neutron instrumentation and technologies that can be applied to the STS to make optimal use of the high peak brightness cold neutrons produced by this new source. The STS, which is projected to conduct its first experiments in 2028, will be a transformative new tool for addressing grand challenges at the frontiers of energy and matter.

(Intentionally left blank)

1. INTRODUCTION

Neutron scattering and spectroscopy were initially developed in the 1940s and 1950s, and the 1994 Nobel Prize in Physics was awarded to Clifford G. Shull and Bertram N. Brockhouse for their pioneering efforts [Levi, 1994]. Over the past seven decades, neutron scattering has become a vital tool for studying materials across many scientific fields and applications, including automotive engines, batteries, data storage, geology, polymers, and biomedicine. The exceptional properties of neutrons provide unique insight into the structure and function of materials, as summarized below.

- *Materials structure and dynamics:* Neutrons have a broad range of useful wavelengths, allowing the examination of structures from the atomic level to the size of biological cells. (The achievable wavelength range is dependent on the design of the neutron source and neutron scattering instrument.) Neutron energies span a range that is ideal for studying the individual and collective atomic motions that determine the properties of materials. Differences in neutron energy can be measured to allow the dynamics of atomic and molecular processes to be followed on time scales ranging from fractions of a picosecond to microseconds—corresponding to vibrations in rigid lattices to the slow movements of large macromolecules.
- *Elemental and isotopic sensitivity:* Neutrons are scattered via interactions with atomic nuclei, which makes them sensitive to the identity of both the element and the specific isotope being studied. Hence, unlike other techniques that scatter from the electric charge density in atoms, neutron scattering can readily distinguish between some elements with similar atomic numbers and is sensitive to light elements such as hydrogen, even in the presence of heavy elements. Further, the neutron scattering response of some isotopes can vary, making differentiation of isotopes very distinct. This unique property of neutrons makes it possible to use isotopic substitution—for example, replacing hydrogen with deuterium—to study the role of hydrogen in catalytic processes or the association of water in protein complexes.
- *Magnetism:* Neutrons have a magnetic moment, but no charge. Thus, neutrons provide an exquisitely sensitive probe for the study of magnetic properties and dynamics in materials. This feature has been exceptionally valuable for the study of materials ranging from superconductors and quantum materials to computer storage media.
- *Penetrating power:* Neutrons readily pass through most materials, which makes it possible to study bulk materials and buried interfaces. Further, samples can be studied under realistic conditions, such as in situ and operando studies of catalytic processes in reactors, studies of geological processes under extremes of pressure and temperature, and observations of fuel injector performance in an operating automobile engine.

Today, more than a dozen major neutron scattering facilities exist worldwide, including both reactor-based and accelerator-based neutron sources [*Neutrons for the Nation,* 2018]. The STS will provide new capabilities that ensure US leadership in neutron scattering. In the United States, the Office of Science of the US Department of Energy (DOE) currently supports two major neutron scattering user facilities at Oak Ridge National Laboratory (ORNL): the High Flux Isotope Reactor (HFIR) and the Spallation Neutron Source (SNS) and the US Department of Commerce supports the National Institute of Standards and Technology (NIST) Center for Neutron Research (NCNR). Each year, more than a thousand researchers from nations around the globe use the two DOE neutron sources that are made available by the Office of Science user program ["Number of Users," 2019]. A brief summary of the characteristics of HFIR and SNS and how they compare to other leading neutron sources is presented here.

Operating at 85 MW, HFIR is the highest flux reactor-based source of neutrons for research in the United States, and it provides one of the highest steady-state neutron fluxes of any research reactor in the world. Its thermal neutron flux is similar to that of the high-flux reactor of the Institut Laue-Langevin (ILL), the

premier European reactor-based neutron source, and neutron scattering instruments at HFIR and ILL address similar scientific questions.

The First Target Station (FTS) at SNS is presently the most powerful accelerator-driven neutron source in the world, operating at a power of 1.4 MW. It provides beams of neutrons in short pulses at a repetition rate of 60 Hz with the highest peak brightness in the world. When the 25 Hz pulsed neutron source at the Japan Proton Accelerator Research Complex (J-PARC) reaches its full power capability in in the near future, it will exceed the peak brightness of SNS. In addition, the European Spallation Source (ESS), now under construction in Sweden, will provide similar peak brightness once it begins operating at 2 MW in the mid-2020s, with a future upgrade path to 5 MW. ESS will deliver beams of neutrons in long pulses at 14 Hz, which will provide time-averaged fluxes of both cold and thermal neutrons comparable to those of a reactor-based source. The lower repetition rates of ESS and J-PARC compared to the FTS will allow the use of broader ranges of neutron energies in each pulse. Long-pulse spallation sources, such as the ESS, are highly flexible, and individual instruments can be optimized for experiments that require high peak brightness and a broad range of energies or for high time-averaged flux, essentially bridging between short pulsed sources and continuous neutron sources.

HFIR and the FTS at SNS provide optimized beam characteristics that are used for specific studies of materials. Briefly, HFIR produces continuous beams of either cold or thermal neutrons that are typically monochromatic and are optimized for studies of materials over selectable but narrow ranges of length scale or energy. The FTS produces pulsed beams of neutrons with very short pulses and therefore high energy resolution. Its high (60 Hz) repetition rate allows for a medium bandwidth of neutron energies to be used, because neutrons of different energies are separated by their arrival time at the detector; a longer time between pulses therefore results in a broader energy bandwidth. The FTS is best optimized for thermal neutrons that are ideal for spatial resolutions on the atomic scale and fast dynamics studies of materials.

SNS is currently undergoing a proton power upgrade (PPU) to double its power capability to 2.8 MW. This upgrade, which will be completed in 2024, will deliver 2 MW of proton beam to the FTS, resulting in a significant increase in thermal neutron brightness to enable new capabilities for materials research in the thermal energy (shorter wavelength) range. The PPU will keep the FTS competitive with J-PARC and ESS for experiments that require beams of thermal neutrons with high peak brightness and high energy resolution and will ensure that researchers in the United States continue to have access to world-leading neutron scattering capabilities.

Even with these existing sources, there is a global need for a high-intensity cold neutron source that is able to simultaneously use a broad energy/wavelength range. Such a source would provide the research community with exciting new opportunities to explore a wide range of materials, including in situ and operando studies during synthesis and processing, nonequilibrium phenomena, and dynamics. This need will be partially addressed by ESS in Europe and J-PARC in Japan, as discussed above. The proposed Second Target Station (STS) at SNS will provide the US with a world-leading capability in high-brightness cold neutron beams with broad energy/wavelength ranges. The STS will complement existing US sources to ensure future state-of-the-art capabilities for the US research community.

SNS, which began operating in 2006, was designed with an accelerator capable of generating neutrons not only for the existing FTS, but also for a future second target station. The ongoing PPU project at SNS, described above, is designed to provide 0.7 MW of proton beam to power the STS (in addition to delivering 2 MW to the FTS). Construction of the STS will provide transformative capabilities that allow thousands of users to address grand scientific challenges [Hemminger, 2015], advance energy research [BES Workshop Reports, 2019], and accelerate industrial innovations through the combination of:

- Cold (long-wavelength) neutrons of unprecedented peak brightness (1.5×10^{15} n/s/cm^2/Å/ster at $\lambda = 3$ Å)
- Short pulses containing neutrons with broad ranges of usable wavelength or energy ($\Delta\lambda = 13.2$ Å at 15 Hz at a distance of 20 m from the source)

This unique combination of neutron beam characteristics will open new avenues for examining materials and systems over greatly increased length, energy, and time scales. These characteristics—in combination with a proposed suite of new instruments (capacity of 22 instruments) and sample environments, advances in neutron optics and detectors, and new computational methods—will make it possible to conduct a wide range of experiments that are not now possible anywhere in the world. Specifically, the STS will provide unique capabilities for experiments that require:

- Time-resolved or cinematic (i.e., "movies") measurements of kinetic processes and beyond-equilibrium matter
- Simultaneous measurements of hierarchical architectures across unprecedented length scales, from the atomic scale to the micron and beyond
- Smaller sample and beam sizes needed for characterization of new materials
- Special environments for exploring new frontiers in materials at extreme conditions

The revolutionary increase in cold neutron peak brightness at the STS is made possible by combining recent innovations in neutron production technologies that allow (1) neutron production in a more compact volume by focusing the incident proton beam on a smaller area of the target; (2) using a solid, rotating tungsten target that can accommodate higher proton flux; (3) locating the cold moderators that are used to tune neutron energy as close as possible to the compact neutron production zone; and (4) a compact cold moderator geometry that can increase neutron brightness. These advances, together with proton pulse compression in the existing SNS accumulator ring, will produce sharp, cold neutron pulses with unprecedented peak brightness, as described in Sect. 2.

The experiments outlined in this report serve as examples of how the STS will provide wholly new capabilities that both complement and substantially extend this nation's current resources for neutron scattering. The STS has a pivotal role to play in extending the reach of neutron scattering to new and transformative opportunities for discovery science. These opportunities include studying the structure, dynamics, properties, and reactions of complex materials that have heterogeneity, interfaces, and disorder and conducting temporally resolved, in situ and operando studies of materials and chemical processes. In addition, they include studies of materials systems across larger length scales—from the atomic scale to the micron scale and beyond—revealing how materials self-assemble into hierarchical structures or molecules interact in living biological cells.

As highlighted in the report *Neutrons for the Nation* [2018], the United States is in need of additional neutron scattering facilities, especially at long wavelengths. The STS addresses the research community's need for bright beams of cold neutrons and provides US users with three DOE-sponsored facilities that offer distinctly different capabilities—the STS, the FTS, and HFIR—in addition to other facilities, such as the NCNR. The STS will furnish wholly new experimental capabilities needed to address future critical questions across a wide range of scientific areas and to drive the development of the technologies of tomorrow.

References for Sect. 1

BES Workshop Reports, 2019. Series of reports available at https://science.osti.gov/bes/Community-Resources/Reports (accessed May 30, 2019).

Hemminger, J. C. (chair). *Challenges at the Frontiers of Matter and Energy: Transformative Opportunities for Discovery Science: A Report from the Basic Energy Sciences Advisory Committee,* U.S. Department of Energy, November 2015. Available at https://science.osti.gov/-/media/bes/besac/pdf/Reports/Challenges_at_the_Frontiers_of_Matter_and_Energy_rpt.pdf (accessed June 8, 2019).

Levi, B. G. *Phys. Today* **1994,** *47* (12), 17.

Neutrons for the Nation: Discovery and Applications while Minimizing the Risk of Nuclear Proliferation, American Physical Society, College Park, MD, July 2018.

"Number of Users Reported by BES User Facilities," https://science.osti.gov/-/media/bes/suf/pdf/BES_Facilities_Number_of_Users.pdf (accessed November 19, 2019).

2. OVERVIEW OF STS NEUTRON BEAM PRODUCTION

The proposed Second Target Station (STS) is designed to produce beams of cold (long-wavelength) neutrons in short pulses with high peak brightness. High brightness will be achieved by employing three coupled processes. First, the cross section of the incoming proton beam at the target will be compressed by >50% relative to the First Target Station (FTS) at the Spallation Neutron Source (SNS). Second, the STS will be equipped with a solid rotating tungsten target that can support the higher proton flux. Finally, novel compact moderator designs will be optimally coupled to the target. This source design, coupled with a short proton pulse that produces neutrons in a short period of time, results in world-leading neutron peak brightness. The short proton pulse is made possible by using the existing accumulator ring to compress the train of long pulses produced by the SNS linear accelerator. The STS will receive proton pulses from the accumulator ring at 15 Hz, allowing the use of a very broad range of neutron energies. This section presents an overview of how the STS has been designed to provide the unique beams of neutrons that will enable the experiments described in Sects. 3–7.

2.1 Production of Proton Pulses

A schematic layout of the SNS complex, including the proposed STS, is shown in Fig. 2.1. The accelerator comprises a negative hydrogen (H^-) ion injector (also called the front-end system), a 1 GeV linear accelerator (linac), an accumulator ring, and associated beam transport lines. The injector consists of an H^- ion source, a low-energy beam transport (LEBT) system that provides initial acceleration to 65 keV and electrostatic chopping of the 1 ms pulses that are produced at a rate of 60 Hz, a 402.5 MHz radiofrequency quadrupole (RFQ) that accelerates the beam to 2.5 MeV and imposes the radiofrequency (RF) time structure, and a medium-energy beam transport (MEBT) line. The linac consists of permanent quadrupole magnets in drift tube assemblies that transversely focus the H^- ion beam and superconducting cryomodules that generate RF standing waves that further accelerate the beam to 1 GeV. The ongoing proton power upgrade (PPU) project will install additional superconducting cryomodules and upgrade the RF systems so that the final energy of the beam can be increased to 1.3 GeV. Together with increased H^- ion current output from the front-end system, these changes will increase the power capability of the linac from 1.4 MW to 2.8 MW.

The linac beam is transported via the high-energy beam transport (HEBT) line to the injection point in the accumulator ring, where the electrons are stripped off the H^- ions by passing through a diamond foil, converting the H^- ions to protons. The accumulator ring consists of magnets that circulate the protons during accumulation at a fixed energy. The 1000 “mini-pulses” contained in the 1 ms long pulses of

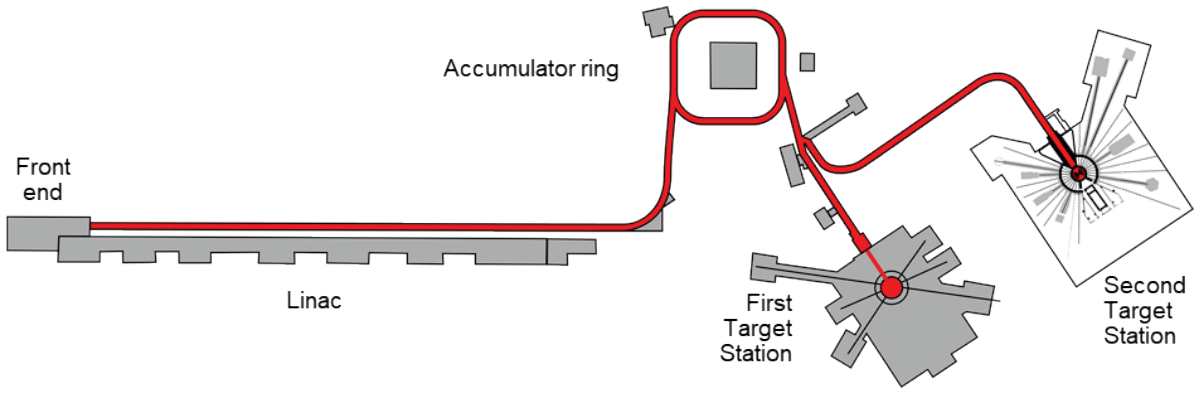

Fig. 2.1. Schematic layout of the SNS complex, including the proposed STS (at right). The beam path is shown in red. Image source: ORNL.

protons are “stacked” (accumulated) on top of one another in the ring to produce a 1 μs pulse, reaching an intensity of 1.5×10^{14} protons per pulse. When accumulation is complete, extraction kicker magnets fire during the 250 ns gap between pulses to remove the accumulated beam in a single turn and direct it into the ring-to-target beam transport (RTBT) line.

To support the STS, the kicker magnets will be programmed to redirect one out of every four proton pulses to a second RTBT line. The STS will therefore operate with a 700 kW beam of proton pulses with a frequency of 15 Hz, whereas the FTS will operate with a 2 MW beam of proton pulses with 45 pulses per second delivered at a frequency of 60 Hz. This design allows both target stations, the FTS and the STS, to be supported by the same accelerator, yet they will operate independently of each other.

In the selection of these operating power and frequency parameters, an important consideration was that the FTS was designed to receive a maximum power of 2 MW. The selected frequency allows the two target stations to use almost all of the power capability (2.8 MW beam power, with 46.7 kJ of energy per proton pulse) of the SNS accelerator after the PPU project has been completed. The lower frequency of the STS compared to the FTS will provide beams of neutrons that have a greater (4×) range of usable wavelengths. This increased wavelength range was an important requirement of the scientific case for STS. Alternative frequencies of 10 Hz and 20 Hz were considered; the recommendation from an external technical review was that 15 Hz provided a sufficiently broad range of neutron wavelengths to satisfy the science case while maximizing the power delivered to the STS target and therefore the neutron flux. In making this decision, the review team took into consideration the fact that operating the STS at 20 Hz would reduce the number of pulses that could be sent to the FTS to 40 per second. This would reduce the operating power of the FTS to below 2 MW. The team also took into consideration the fact that neutron instruments at the STS could be operated at 7.5 Hz by using choppers to remove every second neutron pulse, increasing the range of neutron wavelengths if required. In summary, an operating frequency of 15 Hz offers greatest flexibility while maximizing the power and performance of both the STS and FTS.

2.2 Compact Source Design

The STS neutron source will be designed to produce high-brightness cold neutron beams by employing three coupled processes. First, the incoming proton beam at the target will be compressed in size by more than 50% relative to the FTS to a cross section of ~62 cm^2. Second, a solid rotating tungsten target that can support the higher proton flux will be employed. Finally, novel compact moderator designs will be optimally coupled to the target. This source design, coupled with a short proton pulse that produces neutrons in a short period of time, results in world-leading neutron peak brightness.

The proton pulses transported to the STS from the accumulator ring will impact the outer edge of the rotating tungsten target to spall neutrons that will be directed to instruments (preliminary instrument concepts are described in Sect. 8). The target is approximately 1.1 m in diameter and 6 cm thick. Figure 2.2 shows the STS target and moderator design.

The target consists of 21 separate stainless steel segments, each housing a solid 6 cm thick tungsten block that is encased in a layer of tantalum to protect the tungsten from contact with cooling water. The stainless steel segments are welded to a central hub at the end of a 4 m long shaft that extends above the target monolith. This shaft is connected to a drive system that rotates the target at ~42.9 rpm, so that it completes one rotation every 1.4 s. The target is rotated to spread the power load on the target and therefore simplify the cooling requirements. The target is cooled by water conveyed through the shaft and directed through the stainless steel housings around the tantalum-clad tungsten blocks. This design allows

the incident proton energy to be spread across the 21 target blocks, so that each block receives the equivalent of ~33 kW (700 kW distributed over 21 blocks) of proton beam power. With a stationary target, further segmentation of the tungsten would be needed to allow for greater water cooling; this would reduce the average density of the target material in the neutron production zone and consequently decrease neutron production in the vicinity of the moderators. Thus, the rotating target design enables a brighter neutron source.

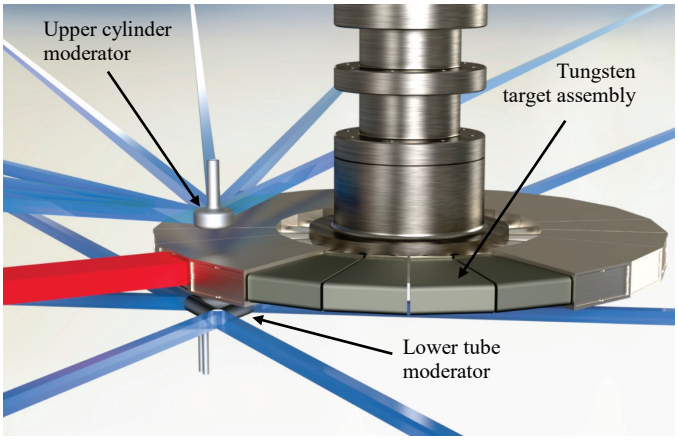

Fig. 2.2. Rotating tungsten target and moderator configuration. The outer diameter of the target assembly is 1.1 m. The red beam illustrates the incident proton beam coming from the accelerator, while the blue beams represent the outgoing neutron beams emitted from the two moderators. The neutron beam size is shown as 3 × 3 cm^2. Image source: ORNL.

The spalled neutrons are then moderated (reduced in energy) by a pair of compact moderators (~30 mm tall), located above and below the target, to optimize the production of high-brightness cold neutrons. Neutrons collide with hydrogen molecules in these moderators, thereby reducing their energy. They are surrounded by 20 mm of light water, which acts as a pre-moderator. The moderators are operated at a temperature of 20 K and with high-purity *para*-hydrogen i.e., molecules of hydrogen with aligned spins.

The upper moderator is a vertical cylinder (3 cm high, 8.2 cm in diameter) that emits neutrons; these neutrons then enter guides and are delivered to 16 instruments (for clarity, only 8 of the 16 emitted neutron beams/instrument paths are shown in Fig. 2.2). This upper moderator has a narrower neutron pulse width for better neutron wavelength resolution. The lower moderator consists of three horizontal tubes (14–16 cm long, 3 cm in diameter) that are connected to form a triangle; the neutrons enter along the length of each tube and are emitted from the 3 cm diameter ends of these tubes to illuminate six beam lines. The lower moderator has the same peak brightness as the upper moderator but produces somewhat broader neutron pulses with a correspondingly higher time-integrated brightness. Instruments that require better resolution will view the upper cylindrical moderator, while those that require lower resolution will view the lower moderator and benefit from receiving more neutrons. Both moderators are far smaller than the 120 mm tall moderators at the FTS; this results in much brighter beams of neutrons, as discussed below.

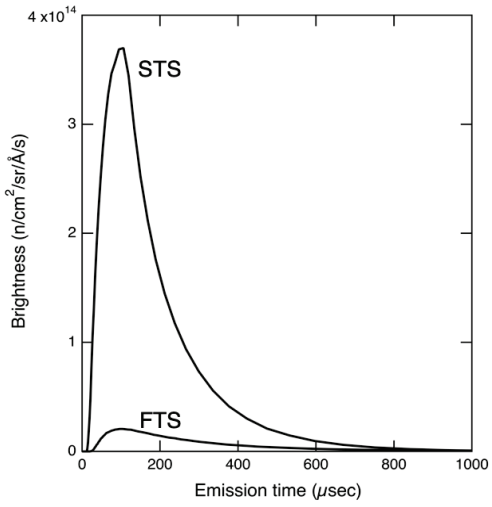

Fig. 2.3. Pulse shapes emitted from FTS and STS cold, coupled moderators at a wavelength of 5 Å (a typical benchmark for cold neutrons). Calculations are for STS operation at 15 proton pulses per second and 700 kW and for FTS operation at 45 proton pulses per second and 2 MW. Image source: ORNL.

Figure 2.3 shows the expected neutron brightness that will be emitted from the STS coupled moderator design, compared to that at the FTS. Here we define the brightness of a beam of neutrons as the number of neutrons of a certain wavelength (i.e., per angstrom) that

pass through an area of 1 cm^2 in 1 s and are traveling in a direction within a solid angle of 1 steradian (i.e., n/s/cm^2/Å/ster). Brightness thus differs from source flux, a quantity that does not depend on the solid angle (divergence) of neutrons within the beam. For many experiments, brightness is a more important beam property than flux because higher brightness directly translates into more neutrons on the sample. This is the foundation for delivering the multiple orders of magnitude gains in instrument performance required to address the science challenges envisioned for the STS.

In Fig. 2.3, the height of the pulse shapes is the peak brightness; the integral under the curve multiplied by the number of proton pulses per second (15 and 45 for the STS and the FTS, respectively) is the time-averaged brightness. Instrument performance scales with peak brightness if the width of the pulse is broad enough to deliver the wavelength resolution desired, which is true for most of the instruments envisioned for the STS. This means that the higher the peak brightness, the better the performance of instruments at the STS.

Figure 2.4 compares the peak brightness and the time-averaged brightness of major current and planned neutron sources; this comparison shows that the STS will provide beams of cold neutrons with the world's highest peak brightness. In Sect. 8, we discuss how these beams will be used to realize new neutron scattering instrument concepts that incorporate additional improvements in neutron optics to provide the transformational capabilities that enable the experiments described in Sects. 3–7.

The FTS will remain the source of choice for many important classes of experiments, especially for experiments requiring thermal neutrons to examine materials on the atomic scale and for fast dynamics of materials.

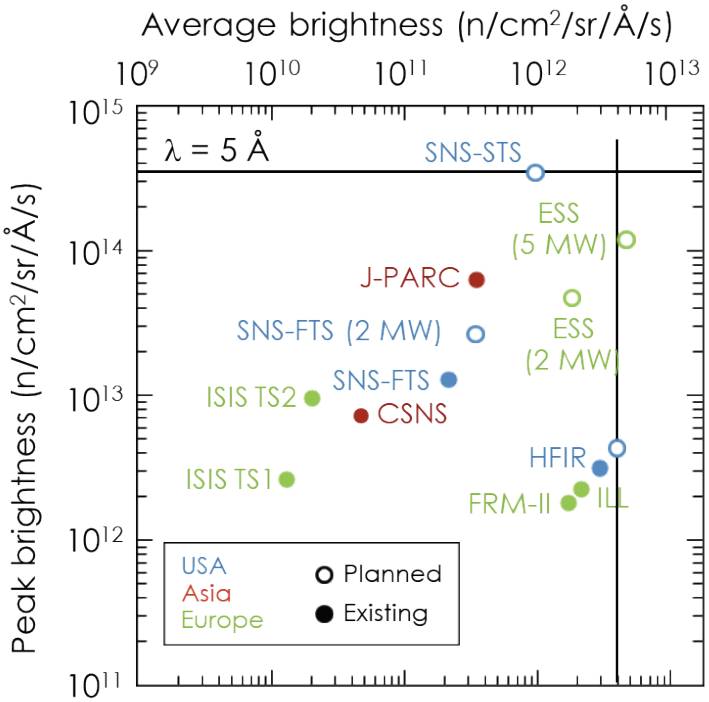

Fig. 2.4. Peak and time-averaged brightness of current (closed circles) and planned (open circles) neutron sources, illustrated at 5 Å. CSNS: China Spallation Neutron Source, China; ESS: European Spallation Source, Sweden; FRM-II: Forschungsreaktor München II, Germany; ILL: Institut Laue-Langevin, France; ISIS: ISIS Neutron and Muon Source, UK (TS: Target Station); J-PARC: Japan Proton Accelerator Research Complex, Japan. Image source: ORNL.

3. POLYMERS AND SOFT MATERIALS

The STS will transform the way neutron scattering is used to provide fundamental knowledge on the synthesis, assembly, structure, and dynamics of soft matter that is currently unobtainable. This transformation will result from the greatly increased peak brightness of STS cold neutrons, which will make it possible to address one of the biggest scientific challenges in soft matter science: understanding how hierarchical structures with desired properties emerge from nonequilibrium processes. Soft matter experiments at the STS are ideal to couple with high-performance computing simulations, including machine learning approaches, to enable full decoding of these complicated processes. Smaller beam sizes with high brightness at the STS will advance the possibilities for spatially resolved in situ, operando, and multiprobe studies. Further, the much broader range of neutron energies accessible simultaneously in a single experiment at the STS will allow researchers to follow changes over the ranges of size and energy scales associated with soft materials with hierarchical architectures—complex fluids, copolymers, hybrids, composites, coacervates, and vitrimers. These new STS experimental capabilities will provide for the development of a predictive time-dependent understanding of soft matter and the ability to master hierarchical architectures for tomorrow's advanced soft materials for energy applications.

3.1 Introduction

Soft condensed matter researchers examine the properties of an incredibly diverse range of materials that are composed primarily of carbon and hydrogen, along with oxygen, nitrogen, or other elements. These materials—which include polymers, liquids, emulsions, gels, colloids, liquid crystals, and biological materials—are made of molecular building blocks that self-assemble by intermolecular (noncovalent) interactions, which are often a thousand times mechanically weaker than those found in conventional solids; nevertheless, they can assemble over long length scales into a wide variety of macroscopic objects, ranging from soft structures such as micelles, which are influenced by thermal fluctuations, to materials with strength and functionality that surpass those of conventional inorganic solids (such as Kevlar).

The physical properties of soft materials at ambient temperature emerge from the delicate balance of weak enthalpic forces between molecules and the entropy of movement of those molecules. In polymers, the situation is further complicated by large molecule architectures and by the existence of hierarchical levels of entropic degrees of freedom. In many cases, materials exist in intermediate or metastable states that are not at thermal equilibrium because the polymer chains are kinetically trapped upon cooling.

Among the biggest scientific challenges in soft matter science is understanding how hierarchical structures with desired properties emerge from **nonequilibrium processes** [Hemminger, 2007, 2015]. This underpins all synthesis and processing of soft matter and is beyond our current experimental and theoretical capabilities. The key to understanding this behavior is to decode the underlying noncovalent intermolecular interactions and kinetic processes, some of which are irreversible and which span a daunting range of length and time scales, in **hierarchically organized structures**. This means characterizing and sampling an enormous number of different metastable states that are separated by very small energy differences, approaching kT. Understanding such complex out-of-equilibrium processes requires new levels of, and approaches to, experimental characterization that probe and capture the underlying temporal and spatial ranges without directly perturbing those processes, accompanied by advances in theory.

Understanding nonequilibrium behavior in soft matter will advance our ability to synthesize and process new materials, such as self-healing polymers, selective membranes, lightweight structural materials, and recyclable polymers, with superior properties and function. The chemical diversity and tunability of soft matter are vast and growing; this creates new opportunities and scientific challenges. Tunable polymer design includes chemical functionality, molecular weight, polydispersity, tacticity, and branching, as well

as the use of block copolymer, graft or multigraft and dendrimeric architectures, or the addition of organic or inorganic fillers or reinforcing fibers to make hybrid composites. The molecular building blocks, such as monomers, polymers or surfactant molecules, may be covalently or noncovalently assembled into hierarchically organized structures with desirable macroscopic properties, resulting in nearly endless versatility for creating materials with specific functionalities by design. As the complexity of these systems grows, so do the challenges for understanding and controlling their fundamental structures and properties.

One such challenge lies in understanding the interplay between assemblies at different length and time scales and using this information to manipulate the processing conditions and chemistry to create materials with prescribed macroscopic material properties. It is important not only to study the static and dynamic behavior of newly designed soft materials, but also to investigate these materials in situ as part of operating devices or under "real world" processing conditions to understand how their structure and properties evolve under external stimuli.

To experimentally investigate the nonequilibrium behavior of soft matter, neutron scattering offers a major advantage in its ability to nondestructively "see" light atoms (C, H, O, and N) and penetrate through reaction vessels, allowing in situ measurements to monitor time-dependent processes, without damaging weak bonds. In addition, neutrons can readily differentiate between hydrogen (H) and deuterium (D) (using H/D contrast experiments) to provide insight into reaction mechanisms, structure, and interfaces. With partial deuteration of specific molecules or sections of larger molecules, such as tails of long polymers, or side chains in branched polymers, for example, it is possible to highlight specific components or regions in complicated multicomponent and hierarchical materials. Deuteration of soft matter requires specialized skills in organic and polymer synthesis; the ORNL Center for Nanophase Materials Sciences (CNMS), which is located near the SNS, has expertise in deuteration for neutron scattering, and researchers can submit user proposals to CNMS for synthesis and characterization of deuterated compounds for use in neutron experiments. This ready access to deuteration promotes optimized labeling strategies to do the best neutron experiment for the highest scientific impact.

Moreover, neutron energies are well matched to those of molecular vibrations, which are ideally captured in neutron spectroscopy. Even more importantly, neutron spectroscopy techniques, such as spin echo, simultaneously give information about both energy (or equivalently time) and size scales of the observed molecular processes, providing a unique avenue to understanding the interplay of structure and dynamics in soft materials. As described in Sect. 3.2, the STS will have significant advantages over current neutron sources in that the beam will be smaller and brighter, which will significantly advance the possibilities for in situ and operando studies, and its short-pulse, low repetition rate will provide simultaneous access to wider ranges of length and time scales, reaching from below picoseconds and angstroms to microseconds and micrometers. At the same time, the brighter beams will enable completion of some measurements in less than a second.

Further, the new capabilities of STS will address knowledge gaps in soft matter research that also arise from the growing mandate for polymeric materials made from renewable sources. Creating these materials requires fundamental understanding of how to develop and process materials derived from sources such as cellulose, corn sugar, or lactic acid into materials with desirable properties that are compostable or biodegradable at the end of life. Likewise, the need to recycle, or better yet upcycle, vast quantities of plastics and elastomers requires a deeper understanding of how to blend thermodynamically incompatible polymers into useful materials through the clever use of block copolymer additives, the development of new reactions and processes to recycle thermosets and deconstruct polymers into monomers or feedstocks, and the development of superior resins intended for recycling.

These emerging trends underscore the need for a foundational understanding of nonequilibrium dynamics and hierarchical structural features on multiple length and time scales in materials that are subjected to diverse and sometimes extreme environments during processing or use. The STS will provide wholly new capabilities for studying the complex interplay of molecular architecture, dynamic hierarchical self-assembly, and emerging macroscopic properties. The bright neutron beams with broad simultaneous energy range at the STS will make it possible to probe these fundamental aspects under conditions found in realistic environments through the application of temperature gradients and shear-flow fields and the creation of extreme chemical environments such as those encountered in batteries and fuel cell membranes. The information obtained is ideal for validating high-performance computing simulations that provide information at different length and time scales. Overall, these capabilities will reveal the synergistic activity and additive properties of soft matter molecules and drive a new paradigm for designing soft materials from a fundamental understanding of molecular and nonequilibrium dynamics.

3.2 New STS Experimental Capabilities for Soft Materials Research

The broad simultaneous range of neutron energies and high peak brightness of cold neutrons at the STS will directly translate into unique experimental capabilities that will create new fundamental understanding and address currently unsolvable challenges in soft matter research. Hierarchical soft matter structures that self-assemble from atom-level interactions up through the nanoscale and mesoscale require techniques that simultaneously cover broad ranges of observable size and time scales. These techniques will be enabled by the STS short-pulse, low-repetition-rate source characteristics and realized in new neutron instruments. Simultaneous observation at multiple scales is crucial because of the nonequilibrium, transient nature of many soft matter systems. This dynamic behavior over multiple concurrent length and time scales that are connected in nontrivial ways through molecular architecture and self-assembly is a key characteristic that makes soft matter research so challenging and interesting.

The most frequently used neutron techniques for studying soft matter structure are small-angle neutron scattering (SANS), which is applied to bulk samples in transmission geometry, and neutron reflectivity (NR), which is applied to film surfaces/interfaces. The unprecedented simultaneous neutron energy bandwidth of the STS in these two techniques translates into broad ranges of measured momentum transfer (also known as scattering vector, **Q**), which in turn means that multiple levels of length scale (0.1–100 nm) are observed at the same time. The STS source characteristics will be especially useful for new experiments—not possible today—that combine, in a single measurement, SANS and wide-angle neutron scattering or diffraction (SANS/WANS, SANS/WAND). In this manner, atomic-level details, such as local solvation around a surfactant headgroup, can be observed concurrently with nanoscale features such as surfactant self-assembly into micelles or microemulsions.

The broad usable energy bandwidth provided by the STS also means that more neutrons will be on the sample at a given time; this speeds up measurement times and provides access to kinetic studies. The ability to perform time-resolved and cinematic studies of kinetic processes and beyond-equilibrium matter is one of the most important transformative advances enabled by the STS. With the STS, measurement times for most techniques will be reduced 100-fold and in some cases by more. For example, a typical NR experiment on a thin film of block copolymer, in which the blocks can be distinguished by selective deuteration, takes roughly 10 to 15 minutes on existing neutron sources. Reducing this to less than 10 seconds opens a window for probing dynamical phenomena associated with surface-driven structural rearrangements as a function of environmental stimuli. In favorable cases, data collection will be possible in less than a second, thereby opening up the possibility of single-shot (i.e., single neutron pulse) experiments. The ability to monitor the nonequilibrium structural and dynamic evolution that follows changes in temperature, shear flow, pressure, and other environmental conditions is crucial for understanding the performance and/or processing of soft materials.

In addition to the time-resolved (kinetic) snapshots of structure provided by NR, SANS, and WANS, individual and collective molecular motion is directly observable by neutron spectroscopy methods. Importantly, these techniques can simultaneously resolve both size scale and time scale by measuring both momentum and energy transfer of the neutron. The very fine energy resolution of neutron spin echo (NSE) spectroscopy provides a powerful tool for measuring the low-energy or "soft" coherent collective dynamics near kT in soft materials that take place from picoseconds to hundreds of nanoseconds. NSE is a dynamic extension of SANS and WANS techniques, and it will profit as SANS does from the STS source characteristics. Just as a SANS/WANS technique at the STS will simultaneously cover atomistic and nanoscale structures, a wide-angle NSE spectrometer will measure molecular motions simultaneously on the scale from angstroms to 100 nanometers. As with SANS and NR, the gains from the increased neutron energy bandwidth will speed up data acquisition for NSE, making it possible to address scientific challenges that were previously out of reach of NSE through dynamics measurements over wide Q-ranges on systems that evolve in tens to hundreds of seconds.

The smaller neutron beam diameters that will be available at the STS, thanks to the delivery of increased flux from compact and brighter cold moderators, will enable new experiments on hierarchical, nonequilibrium systems in several ways: Nonuniform, nonequilibrium systems can be spatially scanned with smaller beams in situ or operando, for example in the case of shear flow in nontrivial geometries. The scope of experiments will be greatly broadened to include such approaches as directing a small-diameter (~0.1 mm) beam at different portions of a specimen subjected to inhomogeneous and time-dependent flow, for example in a melt extruder. If sample size is a limiting factor, then the smaller beam will allow sample volumes 100 times smaller than those needed today. Further, neutrons often enable unique insights into unresolved soft matter questions by providing information complementary to that obtained from other probes, such as optical spectroscopy. Smaller neutron beams and faster sampling times will advance the possibilities for coincident multiprobe experiments. Techniques that lend themselves to this approach include UV-visible, Raman, and IR. This would permit, for example, the simultaneous measurement of the optical and electronic performance of an organic photovoltaic and its structure during annealing to understand structure-performance relationships.

These new STS capabilities will enable studies of nonequilibrium processes, phase transitions, assembly/disassembly, aggregation, interfacial layer formation, and stimuli-induced active motion in soft matter. Indeed, the importance of "spatially and temporally resolved maps of dynamics that allow quantitative predictions of time-dependent material properties" is highlighted in *Challenges at the Frontiers of Matter and Energy* [Hemminger, 2015 (see p. vii)], which identifies the Grand Challenge of "Mastering Hierarchical Architecture and Beyond-Equilibrium Matter."

The new capabilities of the STS also address the four priority research directions defined in the report of the Basic Research Needs Workshop on Innovation and Discovery of Transformative Experimental Tools (Belkacem, 2017):

1. Establish new frontiers in time, space, and energy resolution for characterization and control.
2. Create innovative experimental methods for investigating "real-world" systems.
3. Simultaneously interrogate form and function, bridging time, length, and energy scales.
4. Drive a new paradigm for instrumentation design through integration of experiment, theory, and computation.

The neutron scattering techniques developed for the STS, including SANS, NR, and NSE, will have new capabilities that are enabled by very bright, compact cold neutron moderator sources that deliver neutrons in short pulses at a low repetition rate, maximizing usable neutron energy bandwidth with superb time-of-flight resolution. These capabilities will provide new fundamental knowledge for tackling the

daunting challenges in nonequilibrium polymer dynamics and the evolution of hierarchical structures for design and synthesis of new functional materials for energy, environmental, and societal needs.

3.3 First STS Experiments

3.3.1 Macromolecular Assembly in External Fields

One of the most important questions in soft matter science is how the structure and organization of soft materials evolve over time during synthesis, processing, or aging. These dynamic processes are difficult to study because they can occur over a wide range of time scales, may be irreversible, and take place under extreme environments. With the peak brightness of the STS and the ability to operate in cinematic mode, great strides can be made in probing kinetic processes in soft materials, such as self-assembly, under extreme processing and operating conditions. The brighter beams available at the STS will facilitate the examination of phase transitions, blend formation, aggregation, crystallization, and even in situ synthesis with measurements completed in seconds or less. Key areas of study, in which nonequilibrium dynamics control structural evolution and properties over time, include investigation of thermoplastics under external forces (such as shear), dynamic polymer networks, self-healing polymers, and compatibilization of polymers.

Understanding how the macroscopic rheological behavior of soft matter relates to molecular-level deformations and molecular-scale interactions is critically important because the processing of thermoplastics and many other polymers involves flow under shear and/or extensional deformation in the presence of temperature gradients. The small, bright beams and broad neutron energy bandwidth available at the STS will make it possible to simultaneously study structures at the atomic and macromolecular scale in nontrivial temperature-shear-flow gradient fields. These issues, which are not yet understood even in simple semicrystalline polymers such as polyethylene, are becoming more urgent with the development of new polymers and composites and with advances in three-dimensional (3D) processing methods, which present new challenges and opportunities.

In this context, advances in understanding the evolution of structures and properties under nonequilibrium flow would revolutionize the processing of plastics and the translation of technology to 3D printing methods. For example, in injection molding, polymer pellets are heated above their melting point and pushed through an extrusion nozzle to fill a mold and create a part. Determining the correct mixture and processing conditions (pressure, flow rate, temperature, etc.) to obtain the desired mechanical properties is typically accomplished by trial and error rather than through a fundamental understanding of the structure-property-flow relationships. New insights into the evolution of the structure of the polymer chains in different regions of the extruder and mold would provide new (currently unavailable) insight into controlling materials properties under nonequilibrium conditions. With the small, bright neutron beams at the STS, it will be possible to determine polymer chain structures in different regions of the extruder and mold, particularly if a small percentage of the macromolecules being studied are deuterium labeled in a predominantly hydrogenated bulk (or vice versa), because the individual polymer chain conformation can be observed. SANS/WANS can be used to study the spatially resolved evolution of structure from the atomistic level to the nanoscale (0.1–100 nm), and the results will be coupled to development of new computational models for predictive understanding of nonequilibrium flow of polymer.

Although understanding structural evolution in thermoplastics under flow is challenging, understanding the evolution of structure and properties in polymers that form dynamic bond networks, such as vitrimers (see Fig. 3.1), presents far greater challenges—and opportunities. These macromolecules are opening up a new generation of materials, which could change the landscape of materials science in a variety of applications and lead to the creation of recyclable thermosets [Christensen, 2019]. Mastering reversible

changes in polymers is a key for controlling material structure and properties through the use of local stimuli or changes in the nanoscale environment. Such "dynamic polymers" possess reversible interactions including hydrogen bonds, electrostatic interactions, and dynamic covalent bonds, such as esters, imines, or Diels-Alder adducts.

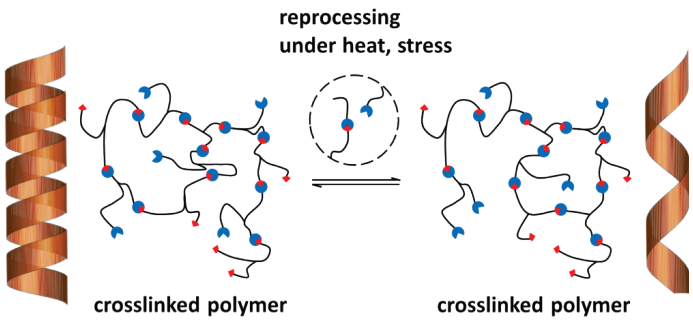

Fig. 3.1. Dynamic exchange reaction of vitrimers. Image source: Adapted from Fortman et al. [2018, Fig. 2]; used with permission of the American Chemical Society].

The key chemistries enabling dynamic behavior are dynamic exchangeable groups or dynamic reversible groups, which enable changes in local chain connectivity without chemical degradation. As a result, these materials can be processed and reprocessed into desired shapes through the breaking and reforming of bonds in response to application of the proper stimulus, but they otherwise remain stable. Understanding and controlling this dynamic process in the solid state and as a function of environmental stimuli is challenging, but by coupling spectroscopy, to follow bond making and breaking, with SANS/WANS, to follow structural evolution, new fundamental understanding can be gleaned. The theoretical aspects of these weakly linked systems require developments in the interplay of quantum mechanics with modern polymer theory; this remains an area in which major advances can be expected.

Self-healing polymers comprise another exciting class of advanced dynamic polymers that can repair damage under specific stimulation via a temporary increase in mobility, which leads to a reflow of the material in the damaged area followed by chemical or physical bonding. The predominant molecular mechanisms involved in the healing processes include dynamic covalent chemistry, thermoreversible physical interactions, or supramolecular chemistry. Challenges arise in understanding stimuli-induced structural and dynamical changes in the polymer on the relevant time and length scales. The SANS/WANS capabilities at the STS enable simultaneous investigation of the evolution of structures from the atomic scale to the nanoscale (0.1–100 nm).

The dynamic behavior of these materials arises from reversible interactions (e.g., hydrogen-bonding, ionic, or even Van der Waals interactions) and drives the self-healing that restores their mechanical performance and original functionalities; this can extend lifetimes, improve performance, and contribute to polymer upcycling. Self-healing polymers are of keen interest for separations membranes, structural composites, sealants, and coatings because of their potential to extend the functional lifetimes of these materials. Understanding the pathways to self-healing will be useful in the development of synthetic polymeric materials that exhibit predictable dynamic behavior with controlled reversible interactions.

One of the challenges in the recycling and upcycling of polymers is the requirement for pure polymer streams. A major step in addressing this challenge would be the development of copolymers that could compatibilize otherwise nonmiscible polymer blends, such as polyethylene and polypropylene, into materials with properties that are as good as (or superior to) those of the starting polymers. The challenge is in understanding the miscibility of the chains at the polymer–polymer interface and the entanglement and dynamics of the polymer chains. Researchers at the STS will study self-assembly from monomer interactions to polymer chain conformation, using SANS/WANS and wide-angle NSE spectroscopy, as a function of chemistry and blend composition. Deuterated polymers will be used to study the polymer–polymer interface. The flux available at the STS will make it possible to perform in situ characterization of these blends while they are subjected to temperature and shear gradients. Moreover, by applying the

small, bright beams of the STS and using millifluidic mixing sample environments, researchers will explore polymer blend phase spaces by continuously varying composition, time after mixing, and environmental conditions such as temperature. This type of spatially resolved kinetic experiment can only be performed at the STS. Although some fundamental theoretical studies of polymer–polymer interfaces have been conducted, many questions remain, including issues associated with interpenetration of dangling ends. These new experiments at the STS will surely induce advances from the theoretical/ computational community.

Owing to its excellent penetrating power and sensitivity to the light elements, neutron scattering is one of few tools for operando characterization of, for example, the morphology and dynamics of membranes used in fuel cells, batteries, or water purification. The unparalleled spatial resolution and flux offered by the STS and the broad Q-range of proposed instruments allow time-resolved measurements of structural changes on length scales from angstroms to a few hundred nanometers during a single experiment. The knowledge gained from these measurements will help to guide the synthesis of next-generation materials with revolutionized properties and stabilities.

3.3.2 Making Hierarchical Structures Using Charged Polymers

The unique structures and properties of polymers arise from a combination of the composition (chemical constitution, size, structure, and cross-linking), noncovalent interactions between the polymer chains, and the method used to process them. While assembly of many synthetic polymers tends to rely on weak van der Waals interactions, biological systems also take advantage of electrostatic interactions and hydrogen bonding. Including these interactions in synthetic polymers adds new diversity to the structure and dynamics of the polymers and creates new opportunities for novel function, such as ion and proton transport, catalytic activity, response to stimuli, and biomimicry.

Charged polymers are particularly challenging because the additional interactions are spatially heterogeneous, ranging from the atomic scale (angstrom) to nanometers and micrometers. The interactions also impact chain dynamics, which changes how the materials assemble and function. Indeed, polyelectrolyte dynamics in polar solvents has hardly been explored even at the theoretical level. Neutron scattering studies can provide key insights into the complex interplay of molecular architecture, dynamic hierarchical self-assembly, and emerging macroscopic properties. The bright neutron beams of the STS that simultaneously provide broad measurements over length scales from atomic to nanoscale will enable studies of these fundamental aspects of charge polymer behavior in situ under a variety of temperatures, pressures, and flows, as well as in various chemical environments.

Polyelectrolytes are synthetic or natural polymers that contain ionizable functional groups that dissociate in aqueous solution, making the polymers charged. Polyelectrolytes are classified as anionic, cationic, or ampholytic, depending on whether the ionized polymer carries negative or positive charges, or both. They can serve as thickening agents, emulsifiers, conditioners, flocculants or dispersants. Polyelectrolytes are responsive to the environment; this enables, for example, a delivery vehicle for specific cargoes, such as ions in batteries (triggered with electric fields) and drugs for medical applications (triggered with changes in pH), as well as robust (strain hardening) or self-healing materials. However, a fundamental understanding of how polyelectrolyte molecules behave in solution remains elusive. For example, in typical aqueous media in the presence of salts, ion condensation on the polymers has been a controversial problem, which requires solution if progress is to be made. Furthermore, as a result of electrostatic repulsion, polyelectrolytes can be strongly correlated both topologically and at the intermolecular level, and numerous experimental variables can be used to control their structure and dynamics. Thus, the description of polyelectrolytes in their liquid and solid states is one of the most challenging issues in chemistry, physics, and the biological sciences.

One class of polyelectrolyte materials now being studied is polymer coacervate complexes, which are mixtures of polyanions and polycations. Coacervates are often used as platforms for encapsulation, particularly in food and personal care products; they also find application in adhesion, deriving and transporting biomaterials, and sensing applications. These systems have broad current and future applications in biomedicine, such as cartilage mimicry, tissue culture scaffolding, and adhesives for wet, biological environments. Coacervate complexes can be formed from both synthetic and biological polyelectrolytes. However, synthetic block copolymers provide an excellent platform around which specific structures and functionalities may be developed and tuned, because the resulting coacervates are highly dependent on the architectures of the polymers and on their concentrations.

A simple example of a synthetic coacervate complex is a polyelectrolyte-rich aqueous solution that results from the electrostatic complexation of oppositely charged macroions, such as poly(styrenesulfonate) and poly(diallyldimethylammonium). The constituents can also be more complex, such as those that form from block copolymers. An example of such a coacervate and the rich phase behavior that can exist is shown in Fig. 3.2. ABA block copolymers with differently charged end groups and a water-soluble, central block form micelles at low concentration. As the concentration increases, the micelles become linked to form a gel that transitions to a well-ordered crystal structure at even higher concentrations [Srivastava, 2017; Krogstad, 2014; Ortony, 2014].

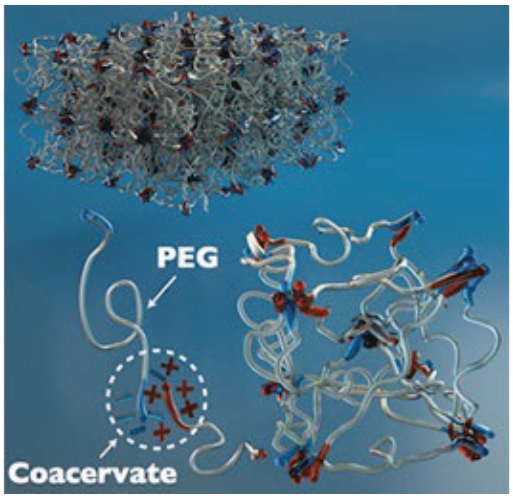

Fig. 3.2. Schematic of an ABA block copolymer complex coacervate. The oppositely charged A blocks (red and blue) create the coacervate (lower left) that forms micelles at low concentration. The coacervate domains are bridged by the neutral B block (here, polyethylene glycol [PEG], shown in grey). The coacervate domains can adopt a loose gel-like structure (top left) that can become very well ordered at the nanoscale if concentrations are high enough [Srivastava, 2017]. Image source: Used with permission of Peter Allen, Institute for Molecular Engineering, University of Chicago.

The process of coacervation is kinetic and is strongly modulated via changes in ionic strength, pH, salt additives, and temperature. How the polymer chains respond during the process of coacervation remains largely unknown but must be determined if the relationship between formation pathways and control of the responsiveness of the solid form of these materials is to be achieved.

Assembling and manipulating the properties of polyelectrolytes on a surface is even more challenging than in solution because the noncovalent polymer–polymer and polymer–surface interactions must be controlled by stimuli such as pH, ionic strength, temperature, and solvent to achieve the desired film. The potential also exists for covalent interactions, such as a polyelectrolyte brush on a surface. The polymer composition (including the nature and density of charged groups), polarity and structure of the polymer backbone, and the polymer morphology all influence the final structure and properties. Neutron scattering methods are well suited for these studies, and the flux and bandwidth provided by the STS will be used to perform experiments that result in unprecedented levels of detail, with time resolution of seconds. These results will engender more attention to these issues from the theoretical community.

For example, multilayer films of poly(methacrylic acid) (PMAA) assembled through hydrogen-bonded layer-by-layer adsorption with poly(vinylpyrrolidone) (PVP) on surfaces can be crosslinked with ethylenediamine (EDA) and the PVP subsequently released at high pH to leave a crosslinked PMAA

hydrogel, which can exhibit dramatic and reversible volume changes under external stimuli [Kozlovskaya, 2013]. However, even for this simple set of polymers, the complex sequence of events that occur during the crosslinking reaction and lead to the hierarchical structures has yet to be fully characterized, and many fundamental questions remain [Kozlovskaya, 2015]. Specifically:

- Are the reactions reversible, and how does that impact the structural evolution?
- How does the ionization of PMAA disrupts the film stability?
- Does the ionic strength of the media impact the final structure?
- Do the reagents penetrate into the film or is the surface crosslinked?

Current NR studies demonstrate that spin-coated multilayer films are highly organized after crosslinking; this implies that reaction must happen on a time scale shorter than or close to the induced ionization by the EDA. To resolve the reaction pathways, a subminute time-resolved NR experiment is needed; this experiment can only be performed at the STS. Answers to these and many other fundamental questions about how polymer coacervates form at surfaces and how they respond to changes in their environment will lay the foundation for guided functional material development.

Although understanding coacervate structure and dynamics in solution is challenging, assembling and manipulating their properties on a surface presents many additional issues because the polymer–polymer and polymer–surface interactions must be controlled by stimuli such as pH, ionic strength, temperature, and solvent. Moreover, as noted, the final structure and properties are influenced by the polymer composition, the polarity and structure of the polymer backbone, and the polymer morphology. The instruments at the STS will enable measurements of coacervation kinetics with a time resolution of seconds because of the intense beams and broad measurement bandwidth. Such measurements are not presently feasible at any neutron source. With the world-leading SANS/WANS and NR instruments that the STS will provide, researchers can finally decode this long-standing mystery and unlock our ability to predictively employ molecular topology; chemical sequence; orthogonal interactions, such as hydrogen bonding; and more complex 3D structures to deliver highly functional coacervate materials.

3.3.3 Watching Polyelectrolytes at Work

While many neutron scattering experiments on polyelectrolytes and their complexes seek to gain new, fundamental knowledge about the physics and chemistry of the materials, a great deal can also be learned about materials during use. One of the great advantages of neutrons over other experimental probes is that they are highly penetrating and nondestructive. As a result, systems can be studied under realistic and operational conditions. In the case of polyelectrolytes, these charged materials can be observed as they interact with other parts of an assembled system, such as a battery or a fuel cell. With the small, bright beams of the STS and the wide dynamic range, a deep understanding of functioning materials can be gained with time resolutions on the order of seconds. Such studies can help drive improvements in device performance and directly impact real-world applications.

For example, polyelectrolytes can be used as membranes in lithium ion and flow batteries, water purification, and ion exchange applications. Solid polymer electrolytes are highly attractive because of their mechanical properties and their low flammability compared to commonly used liquid electrolytes. However, their ionic conductivities are currently an order of magnitude lower than the liquids used in commercial Li^+ ion batteries. Fundamental research in functional devices can be used to help guide advanced materials development, and the performance gains that the STS will provide will be invaluable.

To improve ion conductivity in solid polyelectrolyte batteries, the relationship between ion transport and the structure and dynamics of the polymer must be understood and controlled. In particular, an understanding of how ions interact with the polymer chain is essential. A feature observed in previous

scattering studies of polyelectrolyte membranes is the so-called ionomer peak, which is thought to arise from clustering of ions into "multiplets" or cylindrical micelles in the hydrophobic environment created by polymer backbone. [MacKnight and Lundberg, 1984; Lantman et al., 1988]. Such clustering would invariably impact performance. However, despite recent successes investigating ion clusters in membranes [Schmidt-Rohr and Chen, 2008; Middleton et al., 2016], the relationship of this clustering with the mobility of water, ions and protons in various ionomer membranes has yet to be resolved. The instruments of the STS can provide new information on the structure of the clusters over a wide range of length scales under conditions of applied electric field, while also revealing the dynamics of the clusters under operational conditions, such as in an operational Li^+ ion battery, thereby making it possible to visualize the basis for the differences in ion conductivity.

In fuel cells [Hickner et al., 2004], solar fuel generators [Lewis and Nocera, 2006], and supercapacitors [Simon and Gogotsi, 2008], understanding and controlling proton transport in amphoteric electrolyte membranes is critical. However, the relationship between the dynamics of molecular processes (e.g., hopping and diffusion) and proton conduction remains elusive. Proton hopping is presumed to decouple transport from diffusion and enhance both the fraction of the ionic current carried by the proton (i.e., the transference number) and the overall ionic conductivity [Hoarfrost et al., 2012a, 2012b; Newman and Thomas-Alyea, 2004]. Learning the underlying physical mechanisms that govern proton transport in amphoteric electrolytes as well as in aqueous solutions via the Grotthuss proton tunneling mechanism would constitute a major milestone in alternative energy conversion and storage.

Inelastic neutron scattering can reveal proton dynamics due to the large difference in incoherent scattering cross section between hydrogen and deuterium. With deuterium labeling of just a fraction of the molecules, the hydrogenated protons of interest become selectively "visible" to neutron beams without large changes in the molecular thermodynamic properties. Inelastic neutron scattering is complementary to nuclear magnetic resonance (NMR), since the latter is a purely local probe. In particular, deep insights can be obtained with the proposed wide-angle NSE instrument, a type of instrument that would greatly benefit from the brightness of the STS. This instrument, combined with a hermetic, temperature- and humidity-controlled sample environment for applying an electric field, would have a major impact on the evolution of the understanding of proton and, more generally, ion transport.

3.3.4 Discovering Advanced Soft Matter Composites In Situ

Advances in soft materials for real-world applications will come not only from optimizing the structure and properties of pure compounds, but also from employing polymer mixtures, copolymers, and composites. Soft matter research at the STS will advance our understanding of composite blends of polymers with organic or inorganic additives, metals, nanoparticles, or fibers, created to enhance one or more properties of the bulk material. Because polymer composites can have high strength and stiffness, and are light in weight, corrosion resistant, machinable, and moldable, there has been significant interest in using them for a wide range of applications, from transportation to construction materials to sports equipment. For example, new 3D printing technology has been developed for polymer/carbon-fiber composites. In these polymer matrix composites, the matrix serves as a load distributor by transferring the applied force to the stronger and stiffer fiber. Therefore, strong interfacial interactions between the polymer and the fiber are required to establish an efficient load transfer, which increases the mechanical properties of the composites. This requirement is even more important in nanocomposites, in which nanoparticles are typically <50 nm and have an extremely high surface-to-volume ratio. Polymer nanocomposites with functionalized nanoparticles are of great interest because their properties can be controlled not only by the size and nature of the nanomaterial, but also by its surface functionalization, which helps to increase compatibility with the polymer matrix.

These advances in 3D printing technology are creating a need to understand and characterize the impacts of external processing conditions on the interfacial interactions between the polymer and the matrix, the

influence of the nanoscale particles on the fabrication route, and the final properties of the composite. In most 3D printing techniques, the polymer and nanoparticles or fibers are mixed and deposited by melting and curing in a nonequilibrium process. In a layer-by-layer process, the mechanical strength of the final product largely depends on the strength of the bonding between adjacent layers. It is crucial to understand in real time the extent to which polymer molecules of sequentially deposited layers interdiffuse and to know what degrees of orientation or strain are exhibited by the individual polymer molecules, because these factors are linked to important bulk material properties, including residual stress and layer adhesion. The situation is further complicated by the presence of filler materials used to produce polymer composites.

Overall, a clear understanding of the interplay of molecular interactions and packing, polymer chain conformation, density fluctuations, and filler dispersion and alignment is needed. Through selective deuteration of the polymer matrix and/or the surface coating, the interactions between the matrix and the nanoparticles or fibers can be studied with neutron scattering in real time with subsecond resolution during processing at the STS; these studies can be accomplished only with the STS instruments, which will simultaneously probe the dynamics and the hierarchical structure from the atomic to molecular scale (0.1–100 nm).

In polymer-nanoparticle composites, the nanoparticle can act as a template for the self-assembly of hierarchical structures with unique properties. To understand and control the properties of polymer-nanoparticle composites, it is necessary to identify and characterize the different kinetic phenomena and molecular interactions in the self-assembly and crystallization processes. For example, it has been found that single-wall carbon nanotubes (SWCNTs) can induce self-assembly and crystallization of an amorphous nonlinear polyetherimide in a polymer nanocomposite [Hegde et al., 2013; Hegde et al., 2014; Hegde et al., 2015]. This results in appreciable improvements in thermomechanical properties (Fig. 3.3). However, many fundamental questions regarding this self-assembly process remain elusive: how the CNTs induce crystallization in this high-performance polymer; what initiates and promotes nucleation and growth; what are the crystallization kinetics and what is the morphology of the crystalline domains; and how does crystallization influence the hierarchical structure of the composite? Electron microscopy techniques provide limited information due to the poor contrast between the crystalline polymer and SWCNT, moreover, these measurements observe limited area of the samples. The high flux of cold neutrons and wide *Q*-range SANS instrument at the STS are critical for the in situ experiments where crystal growth as function of time and temperature can be investigated. Simultaneously probing length scales from 0.1 to 100 nm, uniquely enabled by these new STS capabilities will permit investigations of the origins of CNT as well as other nanomaterial induced crystallization and advance the design of novel polymer nanocomposites for both structural and functional applications. Access to the higher flux and brighter beam will be critical for these time-resolved experiments. These experiments will provide new insights into how the interfacial interactions in polymers and matrix controls the structure and properties of polymer composites and provide insights into the design of new materials with superior properties.

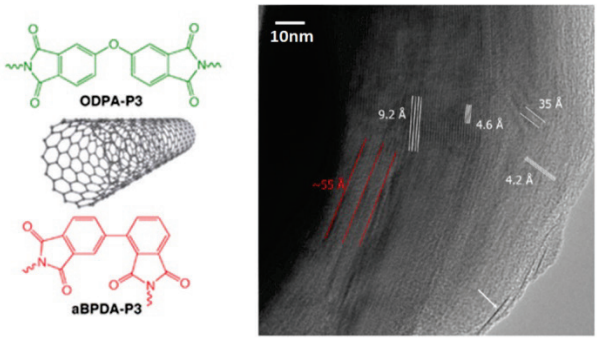

Fig. 3.3. Crystalline domains of ODPA-P3 matrix containing 2.4 vol% SWCNTs. The repeat distances of the crystalline domains are marked, but the microscopy has little contrast [Hegde et al., 2013]. The STS will provide structural information over several length scales for studies of both polymer and nanotube structures. Image source: Reprinted with permission from Hegde et al. [2013, Figs. 2 and 5].

Perhaps one of the greatest opportunities for applying the unique capabilities of STS to soft matter research will arise from correlating soft material composition and processing with the structure and the desired property—and to do so in situ and in real time. Relating the composition of any polymer composite to function is not simple because it involves length scales from angstroms to hundreds of nanometers. Significant fundamental research is required to forge this link. The relationships between composition, degree of polymerization or polydispersity, and miscibility or crystallization, as well as all combinations of these parameters, must be established. The resulting data will be multidimensional, which presents opportunities and challenges. Machine learning methods are an enabling technology for bridging complex experiments with actionable knowledge, and the ORNL Leadership Computing Facility (OLCF) has been leading efforts to apply these methods to a wide variety of problems. The tools and expertise developed in this task will be of great value in developing and validating models that explain the data collected at the STS; leveraging the resources of the OLCF would go a long way toward addressing fundamental challenges identified at a 2016 National Science Foundation workshop held to assess the opportunities and challenges facing the field of polymer science and engineering [Bates, 2016].

Beyond simple composition, processing conditions such as temperature, shear flow, or curing time can be varied in time and integrated with post-fabrication performance characterization to train integrated machine learning such that if a composition is specified, its performance parameters can be predicted based on the processing performed to produce it. Such "in situ discovery of material fabrication" is currently unthinkable but will be feasible by combining STS instrumentation enabled by the available flux and bandwidth with novel sample environments and new approaches to neutron data evaluation aided by machine learning. Applying these methods to renewable polymers and nanocomposites will speed up development of new materials and may reveal ways to achieve heretofore unforeseen properties. Ultimately, the STS and the beamlines that it serves enable these approaches, which are currently not possible due to flux and measurement bandwidth limitations.

3.3.5 Controlling Structure and Flow in Complex Fluids

Complex fluids are integral to many facets of daily life. Shampoo, engine oil, mixed solvents for chemical separations, and fluids for hydraulic fracking to recover oil and natural gas are all examples of complex fluids. The key challenge posed by complex fluids is that synergistic interactions between components may lead to an unpredictable behavior that none of the components exhibits by itself. Further, complex fluids are rarely encountered when they are static. Instead, they are found in constantly changing conditions that alter how they interact with their environment, which creates challenges to understanding how they work and respond. A fundamental understanding of the link between the structure of a complex fluid, its dynamics, and its response to changing conditions, such as temperature, pressure or shear, is lacking. Developing a predictive level of quantitative understanding remains a grand challenge because the scope of the problem—the ranges of length and time scales that are important—is immense. Interactions that take place from the atomic level to hundreds of nanometers represent a regime from which macroscopic behaviors emerge and on which the STS will have a critical impact. The small, bright beams and broad bandwidth provided by the STS will enable rapid, simultaneous measurement of these length scales with time resolution of seconds or faster—which is required for studying materials that are not static (i.e., nonequilibrium phenomena) or uniform, such as are found when complex fluids are flowing in confined spaces.

The solvent mixtures employed in the PUREX process for recovering plutonium and uranium from used nuclear fuel (i.e., nitric acid, water, tri-*n*-butyl phosphate [TBP], and *n*-octane) provide a useful example [Motokawa et al., 2019]. Metal nitrates are coordinated by two TBP molecules (Fig. 3.4). Hydrophobic coordination complexes assemble into well-defined primary clusters, which further assemble into superclusters, resulting in a hierarchical assembly that is vital for the most efficient performance of this separations chemistry of metal ions. If the concentrations of the components of the solvent change, this

system phase separates and fails to perform. Previous studies have used a combination of X-ray spectroscopy and neutron scattering experiments to cover all of the relevant length scales. Instruments at the STS will be able to cover the same length scales with a single measurement in real time, thereby making it possible to correlate the impact of experimental variables, such as temperature, concentration, and pH, with structure and performance. Understanding and controlling the formation of these aggregates will lead to the design of more efficient separations processes.

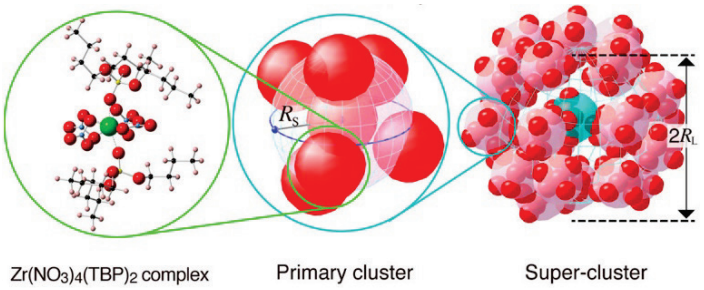

Fig. 3.4. Hierarchical structures in the complex fluid used in the PUREX process. Complexes (left) assemble into clusters (center) that themselves form superclusters (right). Image source: Motokawa et al. [2019, Fig. 2].

Fluids employed in hydraulic fracking are prime examples of complex fluids that are subjected to a variety of changing flow, shear, temperature, and pressure during use. All of the interactions that create the functional structure of the fluid and how it interacts with the surrounding rock and responds to these forces are not fully understood. Many fracking fluids in current use are primarily aqueous based but have additives that improve various aspects of their performance, such as flow through pipe and shale and ability to extract products from the well. As noted in *Basic Research Needs for Energy and Water* [Tirrell, 2017], current technologies require a great deal of water over the lifetime of the well, and the water cannot always be readily recovered or recycled. The development of new hydraulic fracking fluids has the potential to both improve performance and reduce environmental impact.

Nonaqueous foams composed of polymers, nanoparticles, and surfactants, which contain low water content, constitute a proposed replacement for fracking fluid that would greatly reduce water consumption over the lifetime of a well [Middleton et al., 2015] and could be more environmentally friendly than current fluids. The challenge lies in learning how the components assemble into the foam and understanding how the foam changes as it is injected into a well and pressurized to extract oil and gas. During use, these foams will be subjected to pressure, flow and shear, as well as changes in chemical composition. Because neutrons are highly penetrating and uniquely sensitive to light elements, specifically hydrogen and deuterium, neutron scattering is one of the few probes that can study these materials under the conditions that they would experience in an active well. The self-assembled structures (formed at length scales from 1 Å to hundreds of nanometers) that are responsible for the intrinsic physical and chemical properties of the foam and govern its behavior as it transitions from outside the well to inside the fractures that form in the shale can only be probed simultaneously at the STS. By combining the intense beams of the STS with realistic sample environments that can probe foams in situ (i.e., rock) at relevant temperatures and pressures, it will be possible to study the relationship between foam composition, preparation methods, and the resulting structure and properties in real time with time resolution of seconds or faster.

3.4 Conclusion

The STS will enable major breakthroughs in addressing the grand challenges in soft matter science. New fundamental knowledge will be gained in the understanding and control of nonequilibrium processes and resulting hierarchical structures and properties in soft matter; this will have an enormous impact on a wide range of industrial processes, including melt processing of thermoplastics (extrusion, blow molding, co-extrusion, thermoforming); thermoset and adhesive reaction engineering; extruding fiber-reinforced

and nanoparticle polymer composites; and applying self-healing coatings and films. Moreover, emerging technologies in 3D and 4D printing and additive manufacturing of polymeric composite materials require new understanding of polymer flow and self-assembly to bring them closer to competitive and commercial applications. Current knowledge is limited to what can be borrowed from bulk processing and conventional formative manufacturing methods. There is a need to find new materials, such as monomers, additives, and binders; new hierarchical structures; and innovative processes to create soft matter with desired properties for future applications. This requires new fundamental knowledge and understanding and advanced in situ characterization tools, which can be leveraged to advance American competitiveness in the generation of transformational materials and advanced manufacturing processes not easily duplicated by other countries.

The increased peak brightness of cold neutrons and the advances in neutron optics and detector technology at STS will reduce neutron scattering measurement times by two orders of magnitude or more, enabling studies with subsecond time resolution of the interplay between structure and dynamics during nonequilibrium processes that are not possible today. The STS will offer smaller beam sizes for spatially resolved in situ and operando studies and a much broader range of neutron energies that will allow the simultaneous measurement of atomic to nanoscale changes in structures from 0.1 to 100 nm, which is key to understanding the evolution of structure and properties.

These new STS experimental capabilities provide for the development of a predictive time-dependent understanding of the structure and dynamics of soft matter and the ability to master hierarchical architectures, paving the way to innovative and sustainable soft materials for energy applications. The experimental advances gained from the STS also have the potential to stimulate important advances in theory, simulation, and the management and exploitation of increasingly large data sets (see Sect. 8). The development and operation of the STS will equip the scientific community with tools for pursuing many of the priority research directions articulated in the series of workshops and roundtables organized by the U.S. Department of Energy's Office of Basic Energy Sciences over the past two decades [BES Workshop Reports, 2019].

References for Sect. 3

Bates, F. S. (chair). *Frontiers in Polymer Science and Engineering: Report of a 2016 NSF Workshop,* University of Minnesota–Twin Cities, Minneapolis, 2017. Available at http://iprime.umn.edu/sites/g/files/pua2396/f/frontiers_in_polymer_science_and_engineering_2016_nsf_workshop_report.pdf (accessed June 7, 2019).

Belkacem, A. (chair). *Basic Research Needs Workshop on Innovation and Discovery of Transformative Experimental Tools,* U.S. Department of Energy, Washington, DC, 2017. Available at https://science.osti.gov/-/media/bes/pdf/reports/2017/BRNIDTET_rpt_print.pdf (accessed June 7, 2019).

BES Workshop Reports, 2019. Website at https://science.osti.gov/bes/Community-Resources/Reports (accessed May 30, 2019).

Christensen, P. R.; Scheuermann, A. M.; Loeffler, K. E.; Helms, B. A. *Nature Chem.* **2019,** *11,* 442–448.

Fortman, D. J.; Brutman, J. P.; De Hoe, G. X.; Snyder, R. L.; Dichtel, W. R.; Hillmyer, M. A. *ACS Sustainable Chem. Eng.* **2018,** *6,* 11145–11149.

Hegde, M.; Lafont, U.; Norder, B.; Picken, S.J.; Samulski, E.T.; Rubinstein, M.; Dingemans, T. J. *Macromol.* **2013,** *46,* 1492.

Hegde, M.; Lafont, U.; Norder, B.; Samulski, E.T.; Rubinstein, M.; Dingemans, T. J. *Polymer* **2014,** *55,* 3746–3757.

Hegde, M.; Samulski, E. T.; Rubinstein, M.; Dingemans, T. J. *Composites Sci. Technol.* **2015,** *110,* 176–187.

Hemminger, J. C. (chair). Directing Matter and Energy: Five Challenges for Science and the Imagination A Report from the Basic Energy Sciences Advisory Committee, U.S. Department of Energy, December 2007. Available at https://science.osti.gov/-/media/bes/pdf/reports/files/Directing_Matter_and_Energy_rpt.pdf (accessed June 7, 2019).

Hemminger, J. C. (chair). Challenges at the Frontiers of Matter and Energy: Transformative Opportunities for Discovery Science: A Report from the Basic Energy Sciences Advisory Committee, U.S. Department of Energy, Washington, DC, November 2015. Available at https://science.osti.gov/-/media/bes/besac/pdf/Reports/Challenges_at_the_Frontiers_of_Matter_and_Energy_rpt.pdf (accessed June 7, 2019).

Hickner, M. A.; Ghassemi, H.; Kim, Y. S.; Einsla, B. R.; McGrath, J. E. *Chemical Rev.* **2004,** *104,* 4587.

Hoarfrost, M. L.; Tyagi, M.; Segalman, R. A.; Reimer, J. A. *J. Phys. Chem. B* **116,** 8201 (2012)

Hoarfrost, M. L.; Tyagi, M.; Segalman, R. A.; Reimer, J. A. *Macromol.* **45,** 3112 (2012)

Kozlovskaya, V.; Zavgorodnya, O.; Wang, Y.; Ankner, J. F.; Kharlampieva, E. *ACS Macro Lett.* **2013,** *2,* 226–229.

Kozlovskaya, V.; Zavgorodnya, O.; Ankner, J. F.; Kharlampieva, E. *Macromol.* **2015,** *48,* 8585–8593.

Krogstad, D. V.; Choi, S-H.; Lynd, N. A.; Audus, D. J.; Perry, S. L.; Gopez, J. D.; Hawker, C. J.; Kramer, E. J.; Tirrell, M. V. *J. Phys. Chem. B* **2014,** *118,* 13011–13018.

Lantman, C. W.; MacKnight, W. J.; Higgins, J. S.; Peiffer, D. G.; Sinha, S. K.; Lundberg, R. D. *Macromol.* **1988,** *21,* 1339–1343.

Lewis, N. S.; Nocera, D. G. *Proc. Natl. Acad. Sci.* **2006,** *103,* 15729.

MacKnight, W. J.; Lundberg, R. D. *Rubber Chem. Tech.* **1984,** *57,* 652–663.

Middleton, R. S.; Carey, J. W.; Currier, R. P.; Hyman, J. D.; Kang, Q.; Karra, S.; Jiménez-Martínez, J.; Porter, M. L.; Viswanathan, H. S. *Appl. Energy* **2015,** *147,* 500–509.

Middleton, L. R.; Tarver, J. D.; Cordaro, J.; Tyagi, M.; Soles, C. L.; Frischknecht, A. L.; Winey, K. I. *Macromol.* **2016,** *49,* 9176–9185.

Motokawa, R.; Kobayashi, T.; Endo, H.; Mu, J.; Williams, C. D.; Masters, A. J.; Antonio, M. R.; Heller, W. T.; Nagao, M. *ACS Cent. Sci.* **2019,** *5,* 85–96.

Newman, J.; Thomas-Alyea, K. E. *Electrochemical Systems,* 3rd ed., John Wiley & Sons, Inc., Hoboken, NJ, 2004.

Ortony, J. H.; Choi, S.-H.; Spruell, J. M.; Hunt, J. N.; Lynd, N. A.; Krogstad, D. V.; Urban, V. S.; Hawker, C. J.; Kramer, E. J.; Han, S. *Chem. Sci.* **2014,** *5,* 58–67.

Simon, P.; Gogotsi, Y. *Nature Mater.* **2008,** *7,* 845.

Schmidt-Rohr, K.; Chen, Q. *Nature Mater.* **2008,** *7,* 7583.

Srivastava, S.; Andreev, M.; Levi, A. E.; Goldfeld, D. J.; Mao, J.: Heller, W. T.: Prabhu, V. M.: de Pablo, J. J.; Tirrell, M. V. *Nature Commun.* **2017,** *8,* 14131.

Tirrell, M. (chair). *Basic Research Needs for Energy and Water,* U.S. Department of Energy, 2017. Available at https://science.osti.gov/-/media/bes/pdf/reports/2017/BRN_Energy_Water_rpt.pdf (accessed June 7, 2019).

4. QUANTUM MATTER

The STS will make it possible to explore quantum phenomena in ways that are not possible on any current neutron source in the world. The increased peak brightness of neutrons at the STS, in combination with advances in neutron optics, will make it possible to exploit the neutron's exquisite sensitivity to magnetism and low-energy excitations for studies of quantum materials at the very earliest stages of materials discovery—long before large crystals are available. This will provide researchers with the ability to test theoretical predictions as soon as new materials are synthesized, with the potential to significantly accelerate the discovery of quantum materials. In fact, the STS will enable the reduction of the sample size required for inelastic neutron scattering by at least two orders of magnitude, ultimately enabling timely studies of artificially layered materials, epitaxial interfaces, or layers of nanoparticles. In addition, the characteristics of the STS will lead to groundbreaking advances in studying the response of quantum materials to extreme external conditions, such as magnetic fields and applied pressure.

4.1 Introduction

Quantum properties in materials have transformed our society: silicon, the material that underpins much of today's technology, is a semiconductor whose electrons and holes make our phones smart, power the internet, and make energy from sunlight. Nearly everything we do is affected by how these charge carriers move around at the atomic scale. The Silicon Age came about as a result of new ideas about the quantum behavior of electrons, combined with ingenuity as to how these ideas could be used to do things that were formerly impossible. Another transformation is now in progress, driven by the discovery of new kinds of quantum states in real materials and the exploitation of their remarkable properties and behavior

In many ways, silicon is not fully a quantum material; its charge carriers only come about because of quantum rules that exclude electrons from sharing states, but one thing is missing: entanglement. Entangling independent particles means putting them into a combined quantum state that can transport, process, and convert energy and information in new ways. For example, harnessing entanglement is at the heart of unbreakable encryption, teleportation, and quantum computation. It is only very recently that the principles behind the formation of highly entangled states in materials were proposed and that methods were developed to exploit the ability of these materials to generate charge carriers. The key to this breakthrough is the recognition that topology, the mathematics of how to classify different types of knots, for example, could act as a guide to finding new quantum states that could become the full quantum replacement for silicon.

An explosion in discoveries has begun with new types of quasiparticles, from Dirac and Weyl fermions in topological quantum materials to magnetic monopoles and Majorana fermions in spin liquids being proposed and even in some cases seen. Magnetism is central in quantum materials research because it provides a way of controlling the quantum states; frequently, the states themselves have magnetic constituents. Neutrons are vital to making progress not only because they are both able to unravel the magnetism in solids but also because, as a quantum probe, they give irreplaceable information on quantum states at the atomic scale.

Neutron scattering provides a unique view of the magnetic structure and dynamics of quantum materials. As a recent example, inelastic neutron scattering (INS) has provided essential information needed to understand the exotic Kitaev quantum spin liquid state proposed to exist in α-$RuCl_3$ [Banerjee et al., 2016]. Many exotic quantum behaviors have been predicted, some of which require extreme conditions of temperature, magnetic field, and pressure. Current neutron sources have limited access to this parameter space, making experimental verification challenging or impossible.

The quantum materials revolution is just beginning, and the discoveries and understanding that will only be made possible by the leap forward in neutron capabilities provided by the STS will keep the United States at the forefront of the new science and technology. The extraordinary properties of quantum materials will have far-reaching impact, with the promise of transformative properties in energy storage, conversion, and transmission and in new types of computing involving low-power electronics, spin-based processing, or quantum computing and storage.

4.2 New STS Experimental Capabilities for Quantum Materials

As recommended in the report on the Basic Research Needs Workshop on Quantum Materials for Energy Relevant Technology [Broholm, 2016], a detailed understanding of complex quantum materials, including their fundamental structures and quasiparticle excitations, will require new experimental tools. Many of the exotic properties exhibited by quantum materials are mediated by quantum fluctuations, where the energy scale of the associated quasiparticles is low. This requires probes optimized to explore these energies and measurements at very low temperatures. Furthermore, the complexity of these materials requires measurements over a range of length scales from atomic to mesoscale. These characteristic energies and length scales make the high peak brightness beams of cold neutrons provided by the STS ideal for exploring the fundamental properties of quantum materials.

The intense interest in quantum materials is leading to the discovery of new materials at a rapid pace. These materials are often complex, and crystal growth requires different approaches including techniques such as high-pressure synthesis that only yield small quantities. The high peak brightness of cold neutrons combined with focusing optics will enable INS measurements on samples ~100 times smaller than is possible today.

Sample environment equipment used to provide extreme conditions, such as pressure cells or high-field magnets, often limits sample sizes and results in a restricted detector view. Time-of-flight (TOF) neutron scattering can enable neutron diffraction and INS under such restricted conditions, and the accessible range of *d*-spacing and energy transfer is directly coupled to the available neutron bandwidth. The broad range of wavelengths delivered within a single pulse of the STS will enable simultaneous mapping of wide regions of the energy-momentum landscape. Combining this bandwidth with the unrivaled brightness of the STS and focusing optics will enable neutron scattering measurements in regimes of pressure, field, and temperature. These unique source characteristics, together with advances in diamond anvil cell design, will allow neutron diffraction measurements at pressures up to 100 GPa and INS beyond 10 GPa.

Similarly, the bandwidth and peak brightness of the STS open new possibilities for neutron scattering in high magnetic fields. High-temperature superconductors can now be used in ultrahigh-field magnets for neutron scattering with a maximum field exceeding 35 T. Such magnets (similar to those at the National High Magnetic Field Laboratory) require substantial infrastructure and would necessitate a dedicated installation with an optimized neutron scattering instrument built around the magnet. The scale of the magnet infrastructure, in combination with the need to avoid stray field impacts on neighboring instruments, would require positioning this magnet relatively far from the source. In a TOF neutron scattering instrument, the available neutron bandwidth is reduced at larger distances from the source due to overlap with subsequent pulses. With the distance restriction imposed by such a high-field magnet, the 15 Hz operation of the STS is required to provide the necessary neutron bandwidth to enable both elastic neutron scattering and INS under these extreme conditions. Further, the magnet bore size will restrict the available sample volume; consequently, the high peak brightness and focusing optics that will be available at the STS are essential, particularly for INS. Together, these characteristics of the STS will provide an unprecedented ability to comprehensively study magnetic structure and dynamics of quantum materials in fields above 35 T.

As informative as conventional unpolarized neutron scattering is, polarized neutrons provide even greater specificity. Such measurements enable separation of competing and intertwined orders and detailed studies of chiral states in topological materials; they may hold the key to quantitatively understanding quantum entanglement. Polarized neutron scattering over a broad range of energy-momentum space is technically challenging and has only been possible in recent years. Despite progress in polarizing neutron optics, these methods are still subject to intensity limitations, making such measurements for both elastic neutron scattering and INS possible only for large samples and large magnetic scattering cross sections. The STS provides the peak brightness and bandwidth to overcome these limitations and will deliver critical information that can be uniquely obtained from polarized neutron scattering when it is needed most: for small, high-quality samples with quantum spins.

In summary, the next-generation neutron scattering capabilities provided by the STS are ideally suited to probe quantum materials across relevant length and time scales, simultaneously, both in and out of equilibrium. The broad impact of the STS in this area of research is described through a series of specific examples in Sect. 4.3.

4.3 First STS Experiments

4.3.1 Revealing the Fundamental Interactions in Quantum Disordered Materials

Conventional magnetic materials undergo a symmetry-breaking phase transition to spin or valence bond order upon cooling below the characteristic interaction energy scale, *J.* In some quantum materials, quantum fluctuations suppress this phase transition to temperatures far below *J,* opening a temperature regime with exotic emergent quasiparticles such as spinons, visons, skyrmions, and monopoles, which may persist to the absolute zero temperature analogous to superfluid helium. Gaining a deeper understanding of quantum materials and their potential technological applications requires detailed measurements of their emergent quasiparticle excitations and of the fundamental magnetic interactions that define them. The STS will provide transformative insight into quantum materials to accelerate progress.

A prototypical quantum state of matter is the quantum spin liquid (QSL). The defining property of the QSL state is quantum entanglement, which can result in topologically protected quasiparticles [Savary and Balents, 2017]. Examples include spinons, which are fractionalized magnons; Majorana fermions; and visons [Kitaev, 2006]. Neutron scattering can provide unique insight into candidate QSL materials; neutron diffraction can identify potential long-range magnetic order and INS can map the diffuse spectrum characteristic of fractionalized excitations (see Fig. 4.1). As these phenomena are driven by quantum fluctuations, the resulting energy scale of the excitations is typically low (often well below 10 meV, as in the case of α-$RuCl_3$ shown in Fig. 4.1), and measurements must be performed at low temperatures. Detecting such low energy excitations requires cold neutrons. The high peak brightness of the STS, coupled with advances in polarized neutron techniques and extreme sample environments as described in Sect. 8, will transform our ability to understand and design materials governed by strong quantum fluctuations and entanglement.

The number of QSL candidate systems has grown substantially in recent years, in part because of an expanded materials space resulting from the realization that effective spin-1/2 systems exist in 4*d*/5*d* electron materials (e.g., Ir^{4+}, Ru^{3+}) and certain rare earth magnets with ground state doublets (e.g., Yb^{3+}). Candidate QSL systems identified recently include Na_2IrO_3 [Chun et al., 2015], α-$RuCl_3$ [Banerjee et al., 2016], $YbMgGaO_4$ [Paddison, 2017], Zn-doped brochantite ($ZnCu_3SO_4(OH)_6$) [Li et al., 2014], Zn-doped

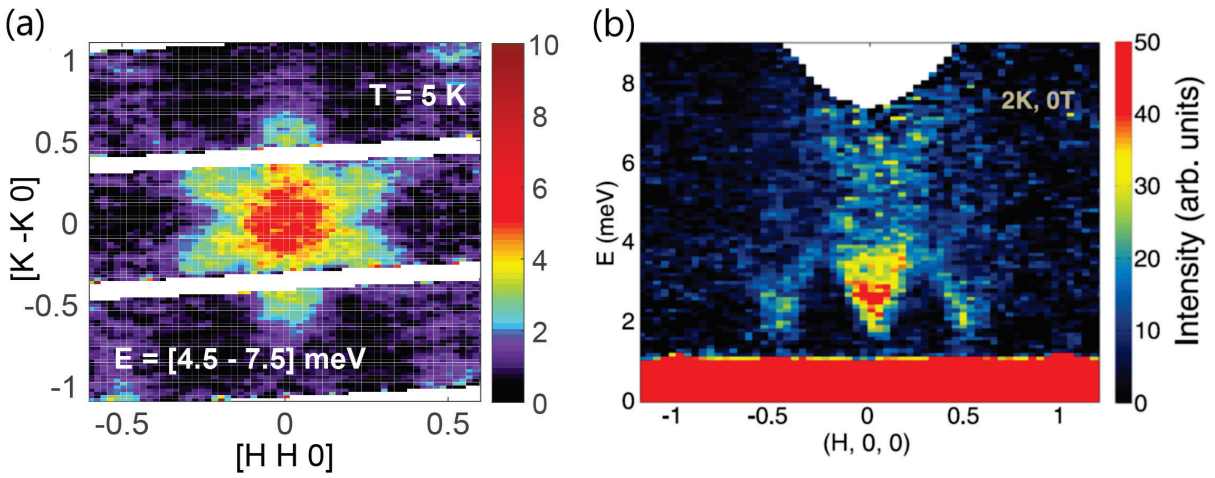

Fig. 4.1. Fractionalized excitations in candidate QSL materials result in a diffuse response in INS experiments. A recent example is the wave vector and energy response of the excitation spectrum in the Kitaev candidate material α-$RuCl_3$ [Banerjee et al., 2017, 2018]. These measurements were enabled by two modern time-of-flight spectrometers at SNS: (a) SEQUOIA and (b) HYSPEC. The STS will enable similar measurements on much smaller samples than those required today, making it possible to obtain such information earlier in the materials discovery cycle. Image source: (a) Reprinted with permission of the American Assocation for the Advancement of Science from Banerjee et al. [2017, Fig. 2]; (b) Banerjee et al. [2018, Fig. 2].

averievite $Cu_{5-x}Zn_xV_2O_{10}(CsCl)$ [Botana et al., 2018], β-Li_2IrO_3 [Takayama et al., 2015] and $H_3LiIr_2O_6$ [Kitagawa et al., 2018]. As INS provides crucial information on fractionalization required to identify a QSL, it is critical to make such measurements more routine and integral to the materials discovery cycle.

Current INS capabilities impose limits on sample size that often preclude the most interesting experiments on small samples with quantum spins. The peak brightness of the STS will enable detailed INS measurements on much smaller samples, perhaps as small as ~1 mm^3 single crystals. This reduces the demands on crystal synthesis, making it possible to perform crucial experiments using INS earlier in the materials development process. For example, the intensity gains at the STS will enable INS measurements on crystals synthesized by techniques that limit sample mass, such as electrochemical and high-pressure methods. One long-standing example is the organic QSL candidate material κ-$(BEDT\text{-}TTF)_2Cu_2(CN)_3$ [Shimizu, 2003] (see Fig. 4.2). Only small single crystals of this compound can be obtained because of limitations of the electrochemical growth process. Thus, INS measurements of these types of samples have not yet been possible and, consequently, fractionalized excitations have not been observed. The broader family of these organic magnets exhibits a wealth of correlated magnetic phenomena, including metal-insulator transitions, superconductivity, and strong spin-lattice coupling, about which INS can provide important fundamental information. By substantially reducing the size of the sample needed, the STS will dramatically broaden the applicability and impact of INS in quantum materials and beyond.

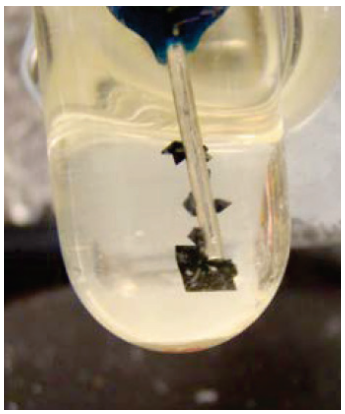

Fig. 4.2. Single crystals of the organic superconductor κ−$(BEDT\text{-}TTF)_2Cu[N(CN)_2]Br$. Typical crystal dimensions in this synthesis are submillimeter. Other members of this family of compounds, including the QSL candidate κ-$(BEDT\text{-}TTF)_2Cu_2(CN)_3$, are synthesized using the same electrochemical process. Photo source: Used with permission of J. A. Schlueter, Argonne National Laboratory.

Detailed features of the spectrum of magnetic excitations in a proposed QSL candidate can help to elucidate the nature of the ground state. As these are often low-energy features requiring microelectron-volt energy resolution, the high brightness of cold neutrons at the STS can provide essential information. For example, in materials proposed to be realizations of the Kitaev model on a honeycomb lattice, the so-called vison mode is predicted [Knolle et al., 2014] to have a signature in the form of a characteristic peak, visible at energies that are small compared with the broader spectrum of excitations. The compound Na_2IrO_3 is predicted to be a realization of a Kitaev QSL [Chun et al., 2015]. However, the weak magnetic signals and the neutron absorption cross section of iridium have precluded successful single-crystal neutron measurements, even with today's best instruments. INS measurements of this family of materials—and others in which synthesis limitations or neutron absorption restricts the crystal size—will finally become possible; the observation of the vison at millikelvin temperatures will establish a key signature of Kitaev physics in QSLs.

Key to the interplay between theory and experiment is knowledge of the interactions and anisotropies that define the spin Hamiltonian of a given material. This quantitative information can be obtained using INS by using high magnetic fields. As spinons form bound states in high fields, fractionalized excitations are replaced by spin wave excitations, whose dispersion relations directly reflect the fundamental magnetic interactions. One example of this approach is a study of Cs_2CuCl_4 [Coldea et al., 2002], for which a 12 T field was sufficient to saturate the magnetization and allow the underlying interactions to be determined from INS measurements. The STS will facilitate the use of extreme sample environments, such as higher field magnets, as its intense neutron pulses and broad dynamic range of energy and wave vector transfers enable both diffraction and INS measurements despite restrictions imposed by the magnet geometries. With current neutron sources, the field limit for INS experiments is typically ~15 T, the practical limit of split bore magnets employing low-temperature superconductors. This severely limits the number of materials that can be driven to magnetic saturation for determination of their interactions with INS. The STS will enable INS at 35 T and beyond, so this method can be applied to quantum magnets with 2–3 times higher energy scales, including perhaps α-$RuCl_3$ [Yadav, 2016]. A model-free determination of the relevant exchange constants and anisotropies in α-$RuCl_3$ and related compounds would be an important step in the process of realizing the Kitaev spin liquid and probing its anticipated Majorana fermions.

Theoretical efforts to understand quantum materials are leading to new concepts; for instance, entanglement entropy may be the key to classifying QSL states. How to experimentally study entanglement entropy remains an important open question [Islam et al., 2015; Jiang et al., 2012; Hauke et al., 2016]. The STS will enable mapping $S(\mathbf{Q},\omega)$ over a wide range of $\mathbf{Q}$-ω space with excellent energy resolution, and advanced polarized neutron techniques will allow separate access to each component of the full tensor, $S^{\alpha\beta}(\mathbf{Q},\omega)$. Such measurements may hold the key [Hauke et al., 2016] to experimentally determining entanglement entropy. The peak brightness of the STS will enable fully polarized INS for a much wider range of quantum materials.

Finally, the diffuse neutron scattering characteristic of quantum disordered states requires advances in modeling to facilitate interpretation. Machine learning approaches to understand such data are being developed using the instruments at the FTS and the leadership-class supercomputing resources at ORNL. Such approaches can help to understand a range of quantum materials, from QSLs to topological semimetals and frustrated magnets. Figure 4.3 shows a three-dimensional (3D) diffuse scattering data set collected on a spin liquid material using the CORELLI diffractometer at the FTS. Machine learning was used to train a neural network to interpret the data and identify the experimental features and phases over five independent dimensions of model interactions/parameters [Samarakoon et al., 2019]. This example demonstrates how new science that goes beyond current theory and analysis can be realized utilizing such

new approaches. The high peak brightness and broad neutron bandwidth of the STS will result in larger, multi-dimensional data sets with unique information on the fundamental properties of materials. Machine learning approaches can greatly accelerate the extraction of scientific knowledge from such data sets to advance understanding and the potential for applications for a wide range of quantum material. See Sect. 8.5 for further discussion of the promise of leveraging big neutron data through machine learning.

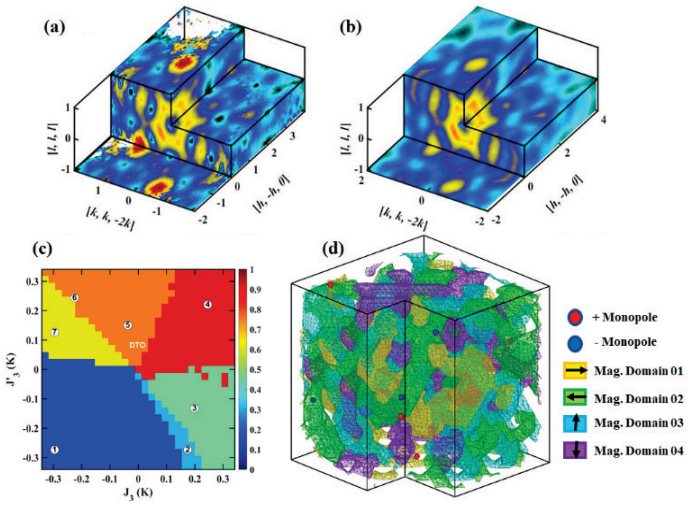

Fig. 4.3. Machine learning using neural networks leading to visualization of glass formation in a cooled spin liquid. (a) Rendering of a 3D diffuse scattering measurement of spin correlations in the gauge spin liquid $Dy_2Ti_2O_7$ measured on CORELLI. (b) Results of machine learning, which denoises and removes experimental artifacts and directly optimizes model parameters from the 3D data set. (c) Slice through a five-dimensional parameter space where machine learning has identified distinct physical behaviors (phases) and features. (d) Visualization of the model in real space, showing monopole localization and intertwined order formation that constitutes the emergent low-temperature glass phase. Image source: Samarakoon et al. [2019]; used with author's permission.

4.3.2 Exploring Magnetism Beyond Thermal Equilibrium

While neutron scattering provides unique information about magnetic structure and excitations in thermal equilibrium, new quantum-based applications raise fundamental questions that cannot be addressed with traditional methods at existing neutron sources: How do materials approach thermal equilibrium? How fast can a quantum material transition between degenerate states? In a system where entropy decreases with increasing internal energy—a phenomenon that is statistically equivalent to having a negative temperature—is the structure of matter fundamentally different? The STS will provide an atomic-scale view of materials beyond thermal equilibrium under conditions that are technologically relevant and scientifically revealing, as outlined below.

As the timing resolution of a neutron scattering experiment is intensity limited, the unrivaled peak brightness of the STS will dramatically expand our ability to probe time-dependent processes in materials. For measurements on time scales of seconds or longer, the additional intensity will permit faster measurements and better time resolution. More advanced stroboscopic methods will enable measurements on the microsecond to millisecond time scale [Granroth et al., 2018]. It will be possible to excite samples with pulsed extreme conditions and to follow the subsequent thermalization with momentum and energy resolution. Examples described below involve stimulating quantum magnets with pulses of terahertz radiation at low temperatures. In such cases, the STS will enable time-dependent neutron scattering (diffraction, INS, SANS, or reflectometry) while stimulating the sample. New regimes of fields and current densities can be employed to follow quench dynamics of strongly interacting quantum systems at the atomic scale. Because these experiments will provide new information about unfamiliar and technologically relevant regimes of materials, the potential for impact and discovery is high.

Time-resolved neutron scattering offers new insight into the nature of quantum materials that are dynamic at low temperature when competing interactions and quantum fluctuations frustrate the formation of conventional static orders. An example is the Coulomb phase of quantum spin ice formed by ferro-

magnetically interacting spins on a lattice of corner-sharing tetrahedra (Fig. 4.4) [Kimura et al., 2013]. In the Coulomb phase, spins fractionalize into pairs of monopoles with opposite magnetic charges and Coulomb interactions. To understand and perhaps develop applications of the Coulomb liquid, we look to experiments that expose the quantum dynamics of monopoles, including their creation, quantum coherent motion, and pair annihilation. The intense pulsed neutrons provided by the STS, combined with terahertz electromagnetic radiation, will be able to provide information on monopole dynamics that is currently inaccessible.

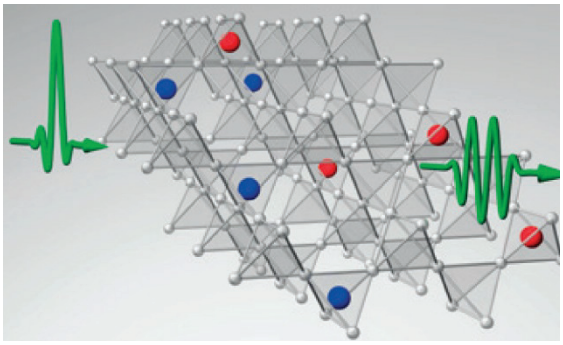

Fig. 4.4. Schematic of a pyrochlore Ising ferromagnet. Monopoles of opposite signs (red and blue spheres) can be created with pulsed radiation (green), and the subsequent quantum dynamics and pair annihilation probed with intense pulsed neutrons. Image source: Reprinted with permission from Pan et al. [2016, Fig. 1].

Additional possibilities for nonequilibrium measurements can be illustrated with a specific example. Molecular magnets contain complex molecules of strongly interacting transition metal ions, where intramolecular magnetic interactions far exceed intermolecular interactions (inset, Fig. 4.5). Time-resolved inelastic neutron scattering on these systems is already feasible in some instances; for example, it has been applied to examine magnetic relaxation in the Mn_{12}ac system [Waldmann et al., 2006]. Depending on the temperature the relevant time scales in Mn_{12}ac can span seconds to years; the experiments of Waldmann et al. achieved time resolutions better than 2 minutes. The STS will enable a more interesting class of experiments—for example, measuring normally forbidden transition with inelastic scattering. Molecular magnets exhibit a tower of discrete excited states that can have long lifetimes and might be employed as qubits for quantum computing (Fig. 4.5). While neutron scattering can probe the excitation spectrum and eigenstates, selection rules preclude access to all but a few excited states from the ground state. Rather than working from a thermal ensemble at elevated temperatures, a pump-probe experiment establishes a specific excited state as the initial state with pulsed microwaves before probing excitations from that state with a synchronized pulse of neutrons. Such time-dependent neutron scattering experiments are greatly advanced by the high peak brightness of the STS. Through the time dependence of the scattering cross section, such pump-probe experiments will provide unique information, including excited state lifetimes and decay pathways, which are important for applications in quantum computation and inaccessible through other techniques.

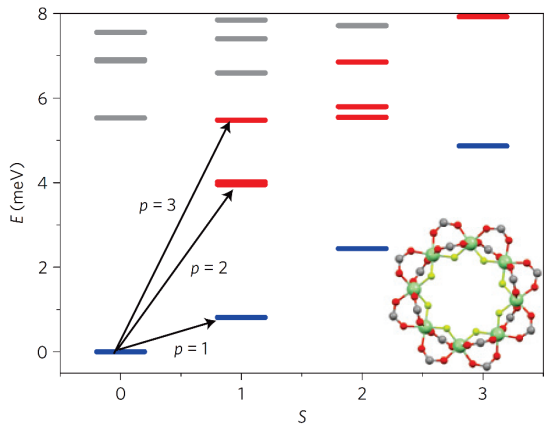

Fig. 4.5. Energy level scheme for the chromium-8 molecule. Blue and red symbols indicate L- and E-band states, respectively; grey symbols indicate states not belonging to these bands. The states are classified by total spin *S,* and only the indicated states are accessible from the ground state. By creating a population inversion of low-energy $S = 1$ states with pulses of terahertz radiation, states with $S = 2$ become accessible to INS. Inset: Schematic of Cr_8 molecule ($C_{80}Cr_8F_8D_{144}O_{32}$). Image source: Reprinted with permission from Baker et al. [2012, Fig. 1(a)].

4.3.3 Understanding Structure and Dynamics of Topological Quantum Matter

Topology classifies the geometrical properties of an object, which are invariant under continuous deformations. A series of theoretical discoveries, some recognized by the 2016 Nobel Prize in physics, have revealed the importance of topology in materials. Beyond symmetry, the topology of the electronic wave function has profound impacts on electronic structure and transport properties in solids. Extensive research has predicted and, in some cases, realized multiple types of topological materials, including interacting and noninteracting topological insulators, topological superconductors, correlated topological matter, and topological magnets and spin liquids. The intense interest in topological quantum materials is in part driven by their potential for diverse applications ranging from quantum computing [Kitaev, 2003; Das Sarma et al., 2015; Nayak et al., 2008] to spintronics [Heremans et al., 2017] and thermoelectrics [Heremans et al., 2017].

Throughout much of the solid-state electronics revolution, the impacts of topology on electronic transport went largely unnoticed and unutilized [Xiao et al., 2010]. In 1984, Berry showed that an eigenstate can acquire a unique phase shift (the Berry phase) when Hamiltonian parameters traverse a closed trajectory [Berry, 1984]. As an example, electrons moving through a noncollinear spin structure acquire a Berry phase shift equivalent to that associated with motion in an extremely large magnetic field (see Fig. 4.6). Indeed, the effective field strengths can approach the field strength within a neutron star! This leads to strong coupling of charge and spin currents to topologically protected spin order with great potential for technological applications [Nagaosa and Tokura, 2013]. These effects enable efficient manipulation of spin structures by charge and spin currents, and vice versa.

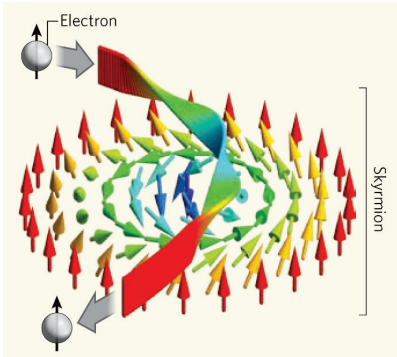

Fig. 4.6. Emergent electrodynamics of topological spin structures: deflection of an electron when passing through a skyrmion. Image source: Reprinted with permission from Pfleiderer and Rosch [2010, Fig. 1].

Magnetic skyrmion lattices—topological spin structures first observed experimentally in chiral magnets using neutron scattering [Mühlbauer et al., 2009] and later confirmed through microscopy [Yu et al., 2010b]—provide rich opportunities to explore the emergent electrodynamics associated with Berry curvature. A wide variety of materials can form topological spin textures. Of importance is understanding the precise topological character of complex spin structures, comprising incommensurate forms of spin, orbital and charge order. Some topological spin structures are predicted to exist at zero magnetic field but may also be stabilized under large magnetic fields up to many tens of tesla [Morin and Schmitt, 1980; Amara and Morin, 1995; Martin and Batista, 2008; Kamiya and Batista, 2014; Leonov and Mostovoy, 2015; Wang et al., 2015]. High-resolution neutron diffraction, small-angle scattering and spectroscopy using high-brightness cold neutron beams are required to reveal topological spin textures, particularly when only small quantities of materials can be accessed. Polarized neutron scattering is of critical importance to expose these complex incommensurate magnetic structures and their chiral nature. Combined with the ability to tune the magnetic structure with magnetic field and pressure, the STS will transform our ability to understand and exploit topological spin structures and their profound effects on quantum behaviors.

Correlated topological materials represent another exciting class of materials. It is important to understand both the band structure and the magnetic properties of these materials. Angle-resolved photoemission spectroscopy is a powerful tool here, but it does have limitations. Neutron scattering can provide essential complementary energy and momentum sensitivity and spin-polarized specificity to understand both the bulk band structure and magnetism in such materials. Importantly, neutron scattering experiments can be

conducted under the extreme conditions of pressure, temperature, and magnetic field required to access distinct phases induced by electronic correlations.

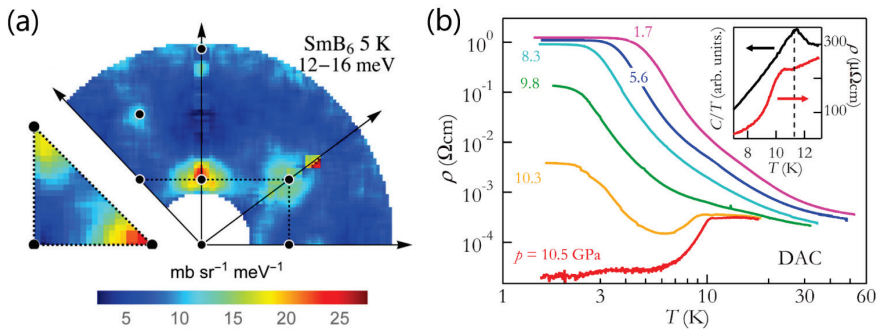

Fig. 4.7. Exploring the properties of SmB_6. (a) Wave vector dependence of energy-integrated magnetic neutron scattering from SmB_6. Image source: Reprinted with permission from Fuhrman et al. [2015, Fig. 1]. (b) Temperature dependence of the electrical resistivity ρ of SmB_6 vs hydrostatic pressure. The plateau at low temperature and pressure is a result of topologically protected surface transport [Wolgast et al., 2013]. Pressure induces a transition from topological Kondo insulator to a bulk conducting state about which little is known. Image source: Reprinted with permission from Derr et al. [2008, Fig. 1].

As an example, the topological Kondo insulator SmB_6 defied understanding and classification for decades because knowledge of its underlying topology is needed to understand the effects of its electronic correlations. The data shown in Fig. 4.7(a), acquired on the SEQUOIA instrument at the FTS, show the wave vector dependence of magnetic neutron scattering from SmB_6 at ambient pressure, reflecting the electronic band structure and therefore the topology of this material [Fuhrman et al., 2015]. However, Fig. 4.7(b) shows that pressure in the range of 10 GPa induces an insulator to metal transition [Derr et al., 2008; Sun and Wu, 2016]. It is not currently possible to perform INS at these pressures, and therefore little is known about band structure and topology in the high-pressure phase.

The high brightness and focused beams of the STS will make it possible to perform these measurements at pressures beyond 10 GPa, yielding detailed information about electronic correlations in each of the topologically distinct phases. This information will significantly advance our understanding of the interplay between correlations and topology and move us closer to controlling and applying their effects.

4.3.4 Tuning Emergent Quantum States of Matter

The phase diagrams of many quantum materials are complex, resulting from strong interplay among the relevant degrees of freedom. As magnetism is a natural consequence of electronic correlations, the sensitivity of neutron scattering to magnetic degrees of freedom makes it an indispensable tool in the study of competing and intertwined order. The STS will enable measurements of both structure and dynamics in magnetic fields beyond 35 T. Additionally, inelastic measurements will be possible at pressures exceeding 10 GPa, and diffraction studies will be possible beyond 100 GPa. Thus, the STS will greatly expand capabilities for exploring phase diagrams with neutron scattering. An illustrative example is superconductors, which often exhibit multiple magnetic and electronic phases, some that compete and others that coexist.

An applied magnetic field is ideal for tuning novel phases in quantum materials. In superconductors, high fields can stabilize the underlying normal state for study. Such an approach can be used to understand the pseudogap phase in high-T_c cuprate superconductors, which represents a long-standing scientific challenge. The superconducting phase induced by hole doping in layered cuprates intersects several other phase boundaries (see Fig. 4.8), including the pseudogap phase, where some electronic states on the nominal Fermi surface appear coherent, while others are incoherent and partially gapped [Keimer et al., 2015]. With doping, the pseudogap phase boundary tends toward a quantum critical point (QCP), which

is hidden beneath the superconducting dome [Tallon and Loram, 2001]. There are tantalizing indications of a profound restructuring of the Fermi surface near the apparent QCP [Badoux et al., 2016].

Theoretical proposals for various electronic orders seek to explain the pseudogap phase, with the order ending in a QCP under the superconducting dome, though the question remains whether one of these orders disappears at the QCP. To answer this question, it is necessary to suppress superconductivity with a large magnetic field (>30 T) and probe the structure and dynamics of the resulting normal state. The peak brightness and bandwidth of neutrons provided by the STS will enable both elastic and inelastic studies in the presence of a sufficiently high magnetic field, allowing for understanding of the magnetic and charge orders in the resulting normal state and providing definitive information about the nature of the controversial pseudogap phase.

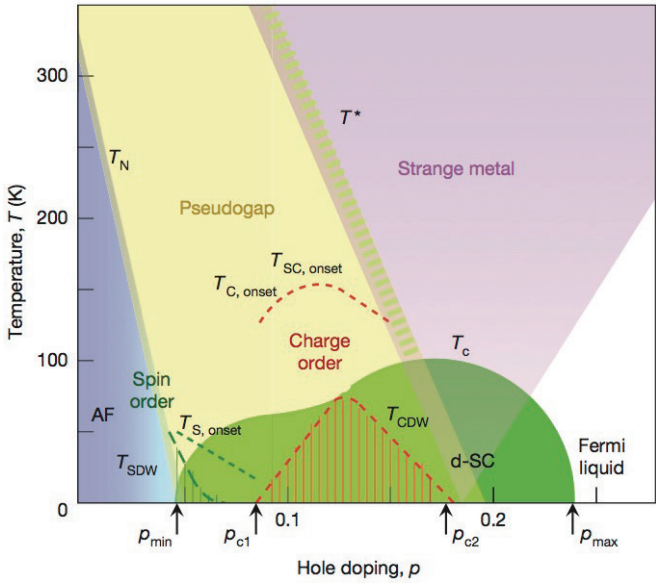

Fig. 4.8. Representative phase diagram of a cuprate superconductor as a function of temperature and hole doping. Phases include superconductivity (green), anti-ferromagnetism (blue), pseudogap (yellow), charge-density-wave order (red stripes), and strange metal (violet). Image source: Reprinted with permission from Keimer et al. [2015, Fig. 2].

Because superconductivity and magnetism are sensitive to small structural distortions, hydrostatic pressure is an ideal tool for modifying these properties. Pressure often mimics the effects of chemical doping but has the advantage that measurements can be performed without changes in the amount of disorder; thus, pressure is often referred to as a "clean" tuning mechanism. Neutron scattering provides unique insights into the structural aspects, including the nature of competing ordered phases, and can be used to explore lattice and magnetic excitations. The high-brightness, focused beams of the STS will enable expansion of the available pressure range for neutron scattering to more than 10 GPa for inelastic measurements and ~100 GPa for elastic measurements.

As an example, FeSe is a superconductor at ambient pressure with a structural distortion associated with magnetic correlations, though magnetic order does not occur [Hsu et al., 2008]. The rich pressure-temperature phase diagram is shown in Fig. 4.9(a). Under hydrostatic pressure, the structural transition is gradually suppressed while the material is tuned into a magnetically ordered state that coexists with superconductivity. Furthermore, the superconducting transition temperature increases from 8 K to near 40 K under a pressure of ~6 GPa [Medvedev et al., 2009]. With existing capabilities, it is impossible to use neutron scattering to follow the evolution of spin excitations with pressure. It is also desirable to simultaneously use magnetic field to suppress superconductivity, so as to probe the pressure dependence of the normal state from which superconductivity develops. The high pressure and high magnetic field capabilities enabled by the high brightness of the STS will offer unique opportunities to systematically study this problem. Elastic and inelastic neutron scattering under high pressure will enable detailed understanding of the evolution of both the structure and excitation spectrum of FeSe, which can be compared to other families of iron-based superconductors [Dai, 2015]. The availability of high pressure and field at the STS to simultaneously probe lattice, charge, and spin degrees of freedom will provide new

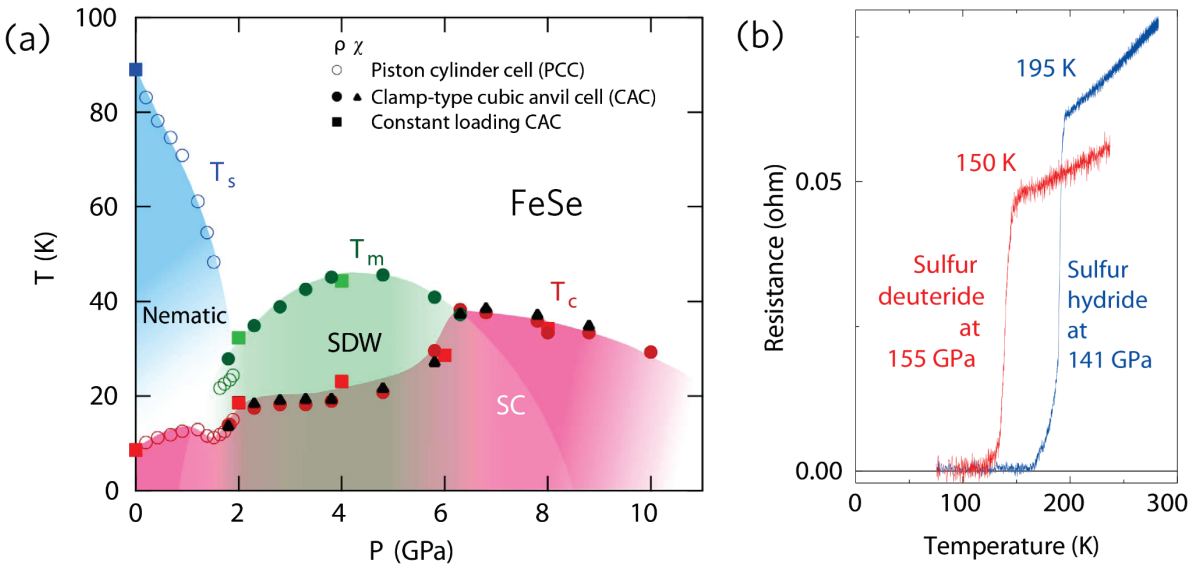

Fig. 4.9. Pressure as a parameter for tuning superconductivity. (a) Pressure-temperature phase diagram for the Fe-based superconductor FeSe. Image source: Sun et al. [2016, Fig. 1]. (b) Resistivity curves for protonated and deuterated sulfur hydride, indicating superconductivity below 200 K at pressures of ~140 GPa. Image source: Reprinted with permission from Drozdov et al. [2015, Fig. 2].

understanding of unconventional superconductors, opening the way to predicting and designing novel materials with desirable properties.

Superconductors such as the cuprate and iron pnictides represented a significant leap forward and led to the conclusion that "unconventional" mechanisms are required to achieve the highest transition temperatures. Nonetheless, it has long been posited that systems composed of light elements, specifically hydrogen, even within the framework of conventional BCS theory could result in greatly increased transition temperatures [Ashcroft, 1968, 2004]. This was recently realized in sulfur hydride with the remarkable observation of superconductivity at ~200 K at very high pressures (~150 GPa) (see Fig. 4.9(b)) [Drozdov et al., 2015] and followed by even higher transition temperatures of >250 K (at ~200 GPa) in lanthanum hydride [Somayazulu et al., 2019; Drozdov et al., 2019]. Despite the extremely high transition temperatures, it is believed that these materials are conventional phonon-mediated superconductors. However, this has not yet been verified because of the inherent difficulty in measuring the structural information at such high pressures. X-ray measurements have been attempted to determine the crystal structure of these materials [Einaga et al., 2016; Gordon et al., 2016], but the insensitivity of X-rays to hydrogen makes the results imprecise. It is crucial to know the detailed structural properties, and neutron diffraction can provide this critical information because of the inherent sensitivity of neutrons to hydrogen. The high brightness of the STS will enable diffraction measurements on smaller samples than are currently possible today. This will allow for structural determination at pressures above 100 GPa, providing fundamental information to understand these and other hydrogen-based metallic alloys that host high-temperature superconductivity.

4.3.5 Exploiting Advances in Heterostructure Fabrication for Applications of Quantum Matter

Interfaces can break inversion symmetry and, if magnetic, time reversal symmetry. As such, interfaces provide a nexus for the emergence of quantum matter. For example, the interface between a ferromagnet and a ferroelectric enables the wave functions of each phase to mix, allowing control of ferroelectricity by

magnetic fields or magnetism by electric field [Ramesh and Spaldin, 2007]. Similarly, the interface between a superconductor and a topological insulator may host Majorana fermions [Linder et al., 2010].

Heterostructures composed of dissimilar materials joined at planar or curved interfaces often yield new material properties that cannot be found in the constituent materials. Examples of interface-mediated physics include superconductivity [Logvenov et al., 2009], two-dimensional electron gases [Ohtomo and Hwang, 2004], magnetism [Nichols et al., 2016], spin transport [Brinkman et al., 2007; Myoung et al., 2016], thermoelectric properties [Choi et al., 2014] and topological phases [Qi et al., 2008]. Interfaces offer unprecedented opportunities to manipulate the interplay between charge, spin, orbital and lattice order parameters. One way to manipulate the interplay involves synthesizing structures of 3*d,* 4*d*, and 5*d* transition metal oxides in ways that take advantage of combinations of Coulomb interactions and spin-orbit coupling. For example, heterostructures of $SrMnO_3$, an antiferromagnetic insulator, and $SrIrO_3$, a paramagnetic metal, yield ferromagnetic interfaces exhibiting strong anomalous Hall effects that are absent in the parent compounds [Nichols et al., 2016]. Numerous other examples exist in which combinations of atomic reconstruction [Moon et al., 2014], orbital reconstruction [Yu et al., 2010a], charge transfer [Grutter et al., 2013], polar discontinuity [Ohtomo et al., 2004] and strain [Lee et al., 2010] across interfaces lead to exotic properties. The opportunities appear so numerous and the physics so intriguing that integration of computational modeling with experiment is essential to focus paths of research and to provide insight into the complexity of multiple interacting degrees of freedom.

Interfaces spatially confine matter, and spatial confinement—particularly at nanometer length scales—implies quantization of properties. For sufficiently small dimensions, quantization may be observed at modest temperatures and magnetic fields [Bertaina et al., 2008]. One effect of spatial confinement is to truncate the density of states. Confinement of phonon and spin waves in proximity to interfaces will alter the dispersion of these waves, and the coupling of interface dispersion to that of the bulk can be used to control physical properties. Phonon and spin wave dispersion at interfaces is unexplored territory, waiting for advances in neutron scattering capabilities and sample growth. The STS will enable the study of interface dynamics in samples containing 1 mg or more of interfaces, which can now be produced, as discussed below.

The dynamics of disordered regions in materials are fundamental to a myriad of materials properties. The disordered regions are separated from the bulk by interfaces. One example is electromechanical coupling in relaxor-based ferroelectrics [Manley et al., 2014]. The motion of small disordered regions in such a material in response to mechanical force (and concomitant changes in electronic properties) has enabled high-resolution 3D medical ultrasound imaging used for everything from detecting a life-threatening blood clot to imaging a fetus in utero. Other examples include strain-induced changes of magnetic coercivity due to disorder associated with phase coexistence [de la Venta et al., 2014], dynamics of spins and conductivity [Dhakal et al., 2007], and interfacial disruption in thermoelectrics [Choi et al., 2014].

The dynamics of bulk materials have been extensively investigated by neutron scattering, and this technique has provided important insight into structure–property relationships. Yet despite the importance of novel functions arising from spatial confinement and interfaces, we have relatively little experimental data about dynamics of atoms or spins in and near interfaces. Such data are needed to guide development of predictive theories for nano- and mesoscale materials. By performing INS experiments on systematically grown materials with large quantities of well-defined interfaces, we may understand how excitations of atoms and spins at or near interfaces differ from the bulk and how these excitations control function at the mesoscale.

The combination of high peak brightness neutrons at the STS and neutron optics with techniques to grow unprecedented quantities of interfaces will enable the use of INS to study the dynamics of atoms and spins at interfaces. An illustrative example involves testing the Haldane effect vs disorder. Haldane

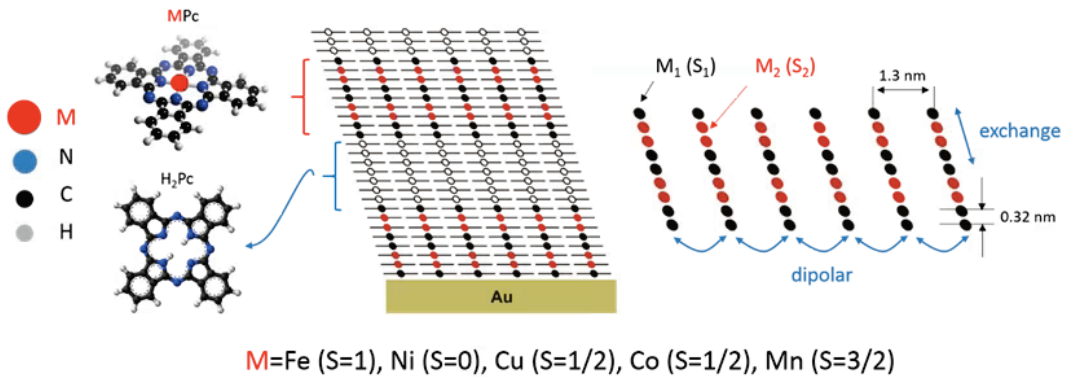

Fig. 4.10. An organic superlattice consisting of 1D pthalocyanine chains can be used to generate custom, variable spin, 1D chains. Image source: C. Monton and I. K. Schuller (unpublished; used with author's permission).

showed that there is a gap in the magnetic excitation spectrum of a Heisenberg chain of integer spin with antiferromagnetic interactions, whereas the half-integer spin chain is gapless [Haldane, 1983]. The Haldane effect and the importance of finite size quantization and disorder can be explored by growing superlattices of one-dimensional (1D) chains of pthalocyanine (see Fig. 4.10). Perfectly ordered pthalocyanine superlattices, 2 cm by 2 cm by 1 μm thick, can be grown with complete control of characteristics including chain length, spacing, and integer or half-integer spin species. Notably, photoactive elements can be systematically introduced anywhere along the chain, making it possible to sever the chain on demand. Disorder can be produced or removed reversibly in the chains with light [Qu et al., 2015]. With the peak brightness of the STS, we will be able to probe spatially confined 1D spin chains, for example, to test the robustness of topologically protected edge states against varying degrees of disorder—a critically important concern for development of devices that rely on topologically protected states. Specifically, spectrometers at the STS could be used to measure the spin wave dispersion in pthalocyanine superlattices. This experimental protocol provides a robust test of a fundamental tenet of topological protection: that topological protection is impervious to disorder.

Interfaces represent another kind of disorder. Recent advances in far-from-equilibrium sample synthesis have made it possible to grow samples containing milligram masses of interfaces, such as so-called nanotrees [Lee et al., 2017], which enable exploration of the dynamics of disorder (of atoms or spins). As shown in Fig. 4.11, nanotrees are single crystal structures ~20 nm in diameter by ~1 μm tall. Each tree is single crystalline, has the same orientation, can be grown alternately with another material to create interfacial materials such as superlattices. This technique can be applied to grow various types of

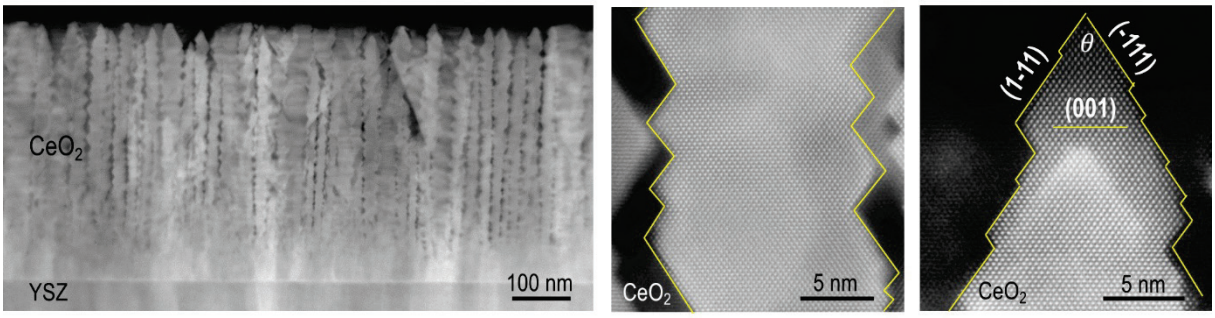

Fig. 4.11. CeO_2 nanotrees. Such arrangements allow the creation of up to ~1 mg of interfaces, opening new avenues for exploration of interfacial effects using neutron scattering. Image source: Reprinted with permission from Lee et al. [2017, Fig. 1].

materials [Fan et al., 2017]. With the high peak brightness of the STS, the dispersion of phonons and magnons at interfaces could be measured for the first time using such samples.

A particularly intriguing example of interfacial effects is the enhanced superconducting critical temperature of FeSe on $SrTiO_3$ (STO; see Sect. 4.3.4). It has been attributed to electron-phonon coupling across the FeSe/STO interface [Rademaker et al., 2016]. High-sensitivity, high-resolution INS could be used to explore this hypothesis through measurements of interfacial phonon line widths. As INS will be possible with milligram quantities of material at the STS, nanotrees consisting of FeSe/STO interfaces will enable such studies, and similar structures have already been grown epitaxially (see Fig. 4.11). Structures such as these, containing a large number of interfaces, will enable the study of other topics, such as the influence of interface disorder on acoustic modes, including ballistic modes (relevant to thermoelectric response) or spin waves (relevant to magnetocaloric or spin Seebeck response) from heterostructures grown with the nanotree architecture.

A similarly challenging task is clarifying the origin of thermal transport across interfaces. Measurements of an epitaxial oxide superlattice indicate a transition from incoherent to coherent phonon scattering with decreasing layer thickness [Ravichandran et al., 2014]. The onset of coherence occurs when the layer thickness is reduced to the coherence length of the phonons. When this happens, it is also expected that coherence will result in standing wave phonons between the layers, which would appear as discontinuities in the phonon dispersion curves at wave vectors corresponding to the layer thicknesses. Standing waves transport no thermal energy. Such size-dependent coherence effects can only be observed in samples containing milligram quantities of a material consisting primarily of interfaces—and epitaxial nanotrees, such as those in Fig. 4.11, with a regular layer thickness. Such information, combined with theory, may enable optimization of the thermoelectric figure of merit, with impacts on the development of efficient thermoelectric devices, which are critically needed to recover waste heat and mitigate challenges of the water-energy-land nexus [Water-Energy Tech Team, 2014].

Presently, INS experiments can be performed with 100 mg samples at the FTS. In fact, the existing CNCS has successfully measured magnetic excitations from $S = 1/2$ samples with masses of 150 mg [Perren et al., 2015]. It is anticipated that a similar spectrometer at the STS will show intensity increases by factors up to 200. With the increase in performance enabled by the STS, and a demonstrated ability to generate samples containing >1 mg of interfaces (which can be expected to improve in the future), INS experiments on interfaces will be possible for the first time.

4.4 Conclusion

The discovery and understanding of new quantum materials is a rapidly evolving field, and these materials have the potential to revolutionize the energy and information technologies on which society now depends. Quantum materials challenge our traditional understanding of materials with exotic physical properties driven by quantum mechanical effects. Harnessing their potential will require a deeper understanding of exotic ground states and the resulting quasiparticles and the development of insight into the role of quantum coherence and entanglement in solids. Achieving this understanding requires new experimental tools to enable measurements that are not possible today. The STS, with its ability to provide cold neutron beams of unprecedented brightness and broad wavelength spread, represents such a tool.

The spectrum of neutrons provided by the STS is ideally suited to investigate a range of quantum materials. The combination of high brightness and broad bandwidth enables neutron scattering in extremes of pressure and magnetic fields. For instance, high-pressure neutron scattering at the STS will advance our understanding of topological correlated materials and the structure and dynamics of superconductors. Elastic and inelastic neutron scattering will be possible in magnetic fields beyond 35 T.

This world-leading capability can be used to determine the fundamental magnetic interactions underlying quantum materials and provide access to the static and dynamic electronic correlations underlying the pseudogap phase of the cuprates. The STS will make polarized neutron scattering a versatile probe of quantum materials, providing access to topological spin textures and possibly even quantum entanglement. STS neutron beams will enable INS measurements on small, high quality crystals and on interfaces in artificial heterostructures. Overall, the STS represents a next-generation characterization tool optimized for quantum materials research, with the potential to transform our understanding of a broad range of these materials.

References for Sect. 4

Amara, M.; Morin, P. *Physica B* **1995,** *205,* 379–392.

Ashcroft, N. W. *Phys. Rev. Lett.* **1968,** *21,* 1748– 1749.

Ashcroft, N. W. *Phys. Rev. Lett.* **2004,** *92,* 1–4.

Badoux, S.; Tabis, W.; Laliberté, F.; Grissonnanche, G.; Vignolle, B.; Vignolles, D.; Béard, J.; Bonn, D. A.; Hardy, W. N.; Liang, R.; Doiron-Leyraud, N.; Taillefer, L.; Proust, C. *Nature* **2016,** *531,* 210–214.

Baker, M. L.; Guidi, T.; Carretta, S.; Ollivier, J.; Mutka, H.; Güdel, H. U.; Timco, G. A.; McInnes, E. J. L.; Amoretti, G.; Winpenny, R. E. P.; Santini, P. *Nature Phys.* **2012,** 8, 906–911.

Banerjee, A.; Bridges, C. A.; Yan, J.-Q.; Aczel, A. A.; Li, L.; Stone, M. B.; Granroth, G. E.; Lumsden, M. D.; Yiu, Y.; Knolle, J.; Bhattacharjee, S.; Kovrizhin, D. L.; Moessner, R.; Tennant, D. A.; Mandrus, D. G.; Nagler, S. E. *Nature Mater.* **2016,** *15,* 733–740.

Banerjee, A.; Yan, J.-Q.; Knolle, J.; Bridges, C. A.; Stone, M. B.; Lumsden, M. D.; Mandrus, D. G.; Tennant, D. A.; Moessner, R.; Nagler, S. E. *Science* **2017,** *356,* 1055–1059.

Banerjee, A.; Lampen-Kelley, P.; Knolle, J.; Balz, C.; Aczel, A. A.; Winn, B.; Liu, Y.; Pajerowski, D.; Yan, J.; Bridges, C. A.; Savici, A. T.; Chakoumakos, B. C.; Lumsden, M. D.; Tennant, D. A.; Moessner, R.; Mandrus, D. G.; Nagler, S. E. *npj Quantum Materials* **2018,** *3,* 8.

Berry, M. V. Proc. R. Soc. London, Ser. A **1984,** 392, 45–57.

Bertaina, S.; Gambarelli, S.; Mitra, T.; Tsukerblat, B.; Müller, A.; Barbara, B. *Nature* **2008,** *453,* 06962.

Botana, A. S.; Zheng, H.; Lapidus, S. H.; Mitchell, J. F.; M. R. Norman. *Phys. Rev. B* **2018,** *98,* 054421.

Brinkman, A.; Huijben, M.; van Zalk, M.; Huijben, J.; Zeitler, U.; Maan, J. C.; van der Wiel, W. G.; Rijnders, G.; Blank, D. H. A.; Hilgenkamp, H. *Nature Mater.* **2007,** *6,* 493.

Broholm, C. (chair). *Quantum Materials for Energy Relevant Technology: Report of the Office of Basic Energy Sciences Workshop on Quantum Materials,* U.S. Department of Energy, Washington, DC, 2016, https://science.osti.gov/-/media/bes/pdf/reports/2016/BRNQM_rpt_Final_12-09-2016.pdf (accessed May 31, 2019).

Choi, W. S.; Ohta, H.; Lee, H. N.; *Adv. Mater.* **2014,** *26,* 6701.

Chun, S. H.; Kim, J-W.; Kim, J.; Zheng, H.; Stoumpos, C. C.; Malliakas, C. D.; Mitchell, J. F.; Mehlawat, K.; Singh, Y.; Choi, Y.; Gog, T.; Al-Zein, A.; Moretti Sala, M.; Krisch, M.; Chaloupka, J.; Jackeli, G.; Khaliullin, G.; Kim, B. J. *Nature Phys.* **2015,** *11,* 462–466.

Coldea, R.; Tennant, D. A.; Habicht, K.; Smeibidl, P.; Wolters, C.; Tylczynski, Z. *Phys. Rev. Lett.* **2002,** *88,* 137203 (2002).

Dai, P. *Rev. Mod. Phys.* **2015,** *87,* 85596.

Das Sarma, S.; Freedman, M.; Nayak, C. *npj Quantum Inf.* **2015,** *1,* 15001.

de la Venta, J.; Wang, S.; Saerbeck, T.; Ramírez, J. G.; Valmianski, I.; Schuller, I. K. *Appl. Phys. Lett.* **2014,** *104,* 062410.

Derr, J.; Knebel, G.; Braithwaite, D.; Salce, B.; Flouquet, J.; Flachbart, K.; Gabáni, S.; Shitsevalova, N. *Phys. Rev. B* **2008,** *77,* 193107.

Dhakal, T.; Tosado, J.; Biswas, A. *Phys. Rev. B* **2007,** *75,* 092404.

Drozdov, A. P.; Eremets, M. I.; Troyan, I. A.; Ksenofontov, V.; Shylin, S. I. *Nature* **2015,** *525,* 73.

Drozdov, A. P.; Kong, P. P.; Minkov, V. S.; Besedin, S. P.; Kuzovnikov, M. A.; Mozaffari, S.; Balicas, L.; Balakirev, F.; Graf, D.; Prakapenka, V. B.; Greenberg, E.; Knyazev, D. A.; Tkacz, M.; Eremets, M. I. *Nature* **2019,** *569,* 528–531.

Einaga, M.; Sakata, M.; Ishikawa, T.; Shimizu, K.; Eremets, M. I.; Drozdov, A. P.; Troyan, I. A.; Hirao, N.; Ohishi, Y. *Nature Phys.* **2016,** *12,* 835.

Fan, L.; Gao, X.; Lee, D.; Guo, E. J.; Lee, S.; Snijders, P. C.; Ward, T. Z.; Eres, G.; Chisholm, M. F.; Lee, H. N. *Adv. Sci. (Weinh.)* **2017,** *4,* 1700045.

Fuhrman, W. T.; Leiner, J.; Nikolić, P.; Granroth, G. E.; Stone, M. B.; Lumsden, M. D.; DeBeer-Schmitt, L.; Alekseev, P. A.; Mignot, J-M.; Koohpayeh, S. M.; Cottingham, P.; Phelan, W. A.; Schoop, L.; McQueen, T. M.; Broholm, C. *Phys. Rev. Lett.* **2015,** *114,* 036401.

Gordon, E. E.; Xu, K.; Xiang, H.; Bussmann-Holder, A.; Kremer, R. K.; Simon, A.; Köhler, J.; Whangbo, M-H.; *Angew. Chem. Int. Ed.* **2016,** *128,* 3746–3748.

Granroth, G. E.; An, K.; Smith, H. L.; Whitfield, P.; Neuefeind, J. C.; Lee, J.; Zhou, W.; Sedov, V. N.; Peterson, P. F.; Parizzi, A.; Skorpenske, H.; Hartman, S. M.; Huq, A.; Abernathy, D. L. *J. Appl. Crystallogr.* **2018,** *51,* 616–629.

Grutter, A. J.; Yang, H.; Kirby, B. J.; Fitzsimmons, M. R.; Aguiar, J. A.; Browning, N. D.; Jenkins, C. A.; Arenholz, E.; Mehta, V. V.; Alaan, U. S.; Suzuki, Y. *Phys. Rev. Lett.* **2013,** *111,* 087202.

Haldane, F. D. *Phys. Rev. Lett.* **1983,** *50,* 1153.

Hauke, P.; Heyl, M.; Tagliacozzo, L.; Zoller, P. *Nature Phys.* **2016,** *12,* 778–782 (2016).

Heremans, J. P.; Cava, R. J.; Samarth, N. *Nature Rev. Mater.* **2017,** *2,* 17049.

Hsu, F.C.; Luo, J. Y.; Yeh, K. W.; Chen, T. K.; Huang, T. W.; Wu, P. M.; Lee, Y. C.; Huang, Y. L.; Chu, Y. Y.; Yan, D. C.; Wu, M. K. *Proc. Nat. Acad. Sci.* **2008,** *105,* 14262.

Islam, R.; Ma, R.; Preiss, P. M.; Tai, M. E.; Lukin, A.; Rispoli, M.; Greiner, M. *Nature* **2012,** *528,* 77–83.

Jiang, H-C.; Wang, Z.; Balents, L. *Nature Phys.* **2012,** *8,* 902–905.

Kamiya, Y.; Batista, C. D. *Phys. Rev. X* **2014,** *4,* 011023.

Keimer, B.; Kivelson, S. A.; Norman, M. R.; Uchida, S.; Zaanen, J. *Nature* **2015,** *518,* 179–186.

Kimura, K.; Nakatsuji, S.; Wen, J-J.; Broholm, C.; Stone, M. B.; Nishibori, E.; Sawa, H. *Nature Commun.* **2013,** *4,* 1934.

Kitaev, A. Y. *Ann. Phys.* **2003,** *303,* 2–30.

Kitaev, A. Y.; *Ann. Phys.* **2006,** *321,* 2–111.

Kitagawa, K.; Takayama, T.; Matsumoto, Y.; Kato, A.; Takano, R.; Kishimoto, Y.; Bette, S.; Dinnebier, R.; Jackeli, G.; Takagi, H. *Nature* **2018,** *554,* 341–345.

Knolle, J.; Kovrizhin, D.L.; Chalker, J.T.; Moessner, R. *Phys. Rev. Lett.* **2014**, *112*, 207203.

Lee, D.; Gao, X.; Fan, L.; Guo, E-J.; Farmer, T. F.; Heller, W. T.; Ward, T. Z.; Eres, G.; Fitzsimmons, M. R.; Chisholm, M. F.; Lee, H. N. *Adv. Mater. Interfaces* **2017,** *4,* 1601034 (2017).

Lee, J. H.; Fang, L.; Vlahos, E.; Ke, X.; Jung, Y. W.; Kourkoutis, L.F.; Kim, J-W.; Ryan, P. J.; Heeg, T.; Roeckerath, M.; Goian, V.; Bernhagen, M.; Uecker, R.; Hammel, P.C.; Rabe, K. M.; Kamba, S.; Schubert, J.; Freeland, J. W.; Muller, D. A.; Fennie, C. J.; Schiffer, P.; Gopalan, V.; Johnston-Halperin, E.; Schlom, D. G. *Nature* **2010,** *466,* 954.

Leonov, A. O.; Mostovoy, M. *Nature Commun.* **2015,** *6,* 8275.

Li, Y.; Pan, B.; Li, S.; Tong, W.; Ling, L.; Yang, Z.; Wang, J.; Chen, Z.; Wu, Z.; Zhang, Q. *New J. Phys.* **2014,** *16,* 093011.

Linder, J.; Tanaka, Y.; Yokoyama, T.; Sudbø, A.; Nagaosa, N.; *Phys. Rev. Lett.* **2010,** *104,* 067001.

Logvenov, G.; Gozar, A.; Bozovic, I. *Science* **2009,** *326,* 699–702.

Manley, M. E.; Lynn, J. W.; Abernathy, D. L.; Specht, E. D.; Delaire, O.; Bishop, A. R.; Sahul, R.; Budai, J. D. *Nature Commun.* **2014,** *5,* 3683.

Martin, I.; Batista, C. D. *Phys. Rev. Lett.* **2008,** *101,* 156402.

Medvedev, S.; McQueen, T. M.; Troyan, I. A.; Palasyuk, T.; Eremets, M. I.; Cava, R. J.; Naghavi, S.; Casper, F.; Ksenofontov, V.; Wortmann, G.; Felser, C. *Nature Mater.* **2009,** *8,* 630.

Moon, E. J.; Colby, R.; Wang, Q.; Karapetrova, E.; Schlepütz, C. M.; Fitzsimmons, M. R.; May, S. J. *Nature Commun.* **2014,** *5,* 5710.

Morin, P.; Schmitt, D. *J. Magn. Magn. Mater.* **1980,** *21,* 243–256.

Mühlbauer, S.; Binz, B.; Jonietz, F.; Pfleiderer, C.; Rosch, A.; Neubauer, A.; Georgii, R.; Böni, P. *Science* **2009,** *323,* 915–919.

Myoung, N.; Park, H. C.; Lee, S. J. *Sci. Rep.* **2016,** *6,* 25253.

Nagaosa, N.; Tokura, Y. *Nature Nanotechnol.* **2013,** *8,* 899–911, and references therein.

Nayak, C.; Simon, S. H.; Stern, A.; Freedman, M.; Das Sarma, S. *Rev. Mod. Phys.* **2003,** *80,* 1083–1159.

Nichols, J.; Gao, X.; Lee, S.; Meyer, T. L.; Freeland, J. W.; Lauter, V.; Yi, D.; Liu, J.; Haskel, D.; Petrie, J. R.; Guo, E-J.; Herklotz, A.; Lee, D.; Ward, T. Z.; Eres, G.; Fitzsimmons, M. R.; Lee, H. N. *Nature Commun.* **2016,** *7,* 12721.

Ohtomo, A.; Hwang, H. Y. *Nature* **2004,** *427,* 423.

Paddison, J. A. M.; Daum, M.; Dun, Z.; Ehlers, G.; Liu, Y.; Stone, M. B.; Zhou, H.; Mourigal, M. *Nature Phys.* **2017,** *13,* 117–122.

Pan, L. D.; Laurita, N. J.; Ross, K. A.; Gaulin, B. D.; Armitage, N. P. *Nature Phys.* **2016,** *12,* 361–366.

Pfleiderer, C.; Rosch, A. *Nature* **2010,** *465,* 880–881.

Perren, G.; Moller, J. S.; Huvonen, D.; Podlesnyak, A. A.; Zheludev, A. *Phys. Rev. B.* **2015**, *92,* 054413.

Qi, X-L.; Hughes, T. L.; Zhang, S-C. *Phys. Rev. B* **2008,** *78,* 195424.

Qu, D-H.; Wang, Q-C.; Zhang, Q. W.; Ma, X.; Tian, H. *ACS Chem. Rev.* **2015,** *115,* 7543.

Rademaker, L.; Wang, Y.; Berlijn, T.; Johnston, S. *New J. Phys.* **2016,** *18,* 022001.

Ramesh, R.; Spaldin, N. A. *Nature Mater.* **2007,** *6,* 21.

Ravichandran, J.; Yadav, A. K.; Cheaito, R.; Rossen, P. B.; Soukiassian, A.; Suresha, S. J.; Duda, J. C.; Foley, B. M.; Lee, C-H.; Zhu, Y.; Lichtenberger, A. W.; Moore, J. E.; Muller, D. A.; Schlom, D. G.; Hopkins, P. E.; Majumdar, A.; Ramesh, R.; Zurbuchen, M. A. *Nature Mater.* **2014,** *13,* 168.

Samarakoon, A. M., Barros, K.; Li, Y. W.; Eisenbach, M.; Zhang, Q.; Ye, F.; Dun, Z. L.; Zhou, H.; Grigera, S. A.; Batista, C. D.; Tennant, D. A. Machine Learning Assisted Insight to Spin Ice $Dy_2Ti_2O_7$. *Nature Commun.,* submitted for publication, 2019.

Savary, L.; Balents, L. *Rep. Prog. Phys.* **2017,** *80,* 016502.

Shimizu, Y.; Miyagawa, K.; Kanoda, K.: Maesato, M.; Saito, G. *Phys. Rev. Lett.* **2003,** *91,* 107001.

Somayazulu, M.; Ahart, M.; Mishra, A. K.; Geballe, Z. M.; Baldini, M.; Meng, Y.; Struzhkin, V. V.; Hemley, R. J. *Phys. Rev. Lett.* **122,** 027001.

Sun, J. P.; Matsuura, K.; Ye, G. Z.; Mizukami, Y.; Shimozawa, M.; Matsubayashi, K.; Yamashita, M.; Watashige, T.; Kasahara, S.; Matsuda, Y.; Yan, J-Q.; Sales, B. C.; Uwatoko, Y.; Cheng, J-G.; Shibauchi, T. *Nature Commun.* **2016,** *7,* 12146.

Sun, L.; Wu, Q. *Rep. Prog. Phys.* **2016,** *79,* 084503.

Takayama, T.; Kato, A.; Dinnebier, R.; Nuss, J.; Kono, H.; Veiga, L. S. I.; Fabbris, G.; Haskel, D.; Takagi, H. *Phys. Rev. Lett.* **2015,** *114,* 077202.

Tallon, J. L.; Loram, J. W. *Physica C* **2001,** *349,* 53.

Waldmann, O.; Carver, G.; Dobe, C.; Biner, D.; Sieber, A.; Güdel, H.U.; Mutka, H.; Ollivier, J.; Chakov, N. E. *Appl. Phys. Lett.* **2006,** *88*, 042507.

Wang, Z.; Kamiya, Y.; Nevidomskyy, A. H.; Batista, C. D. *Phys. Rev. Lett.* **2015,** *115,* 107201.

Water-Energy Tech Team, *The Water-Energy Nexus: Challenges and Opportunities*, U.S. Department of Energy, Washington, DC, June 2014; online at https://www.energy.gov/downloads/water-energy-nexus-challenges-and-opportunities (accessed June 1, 2019).

Wolgast, S.; Kurdak, Ç.; Sun, K.; Allen, J. W.; Kim, D.-J.; Fisk, Z. *Phys. Rev. B* **2013,** *88,* 180405(R).

Xiao, D.; Chang, M-C.; Niu, Q. *Rev. Mod. Phys.* **2010,** *82,* 1959–2007.

Yadav, R.; Bogdanov, N. A.; Katukuri, V. M.; Nishimoto, S.; van den Brink, J.; Hozoi, l. *Sci. Rep.* **2016,** *6,* 37925.

Yu, P.; Lee, J.-S.; Okamoto, S.; Rossell, M. D.; Huijben, M.; Yang, C-H.; He, Q.; Zhang, J. X.; Yang, S. Y.; Lee, M. J.; Ramasse, Q. M.; Erni, R.; Chu, Y.-H.; Arena, D. A.; Kao, C-C.; Martin, L. W.; Ramesh, R. *Phys. Rev. Lett.* **2010a,** *105,* 027201.

Yu, X. Z.; Onose, Y.; Kanazawa, N.; Park, J. H.; Han, J. H.; Matsui, Y.; Nagaosa, N.; Tokura, Y. *Nature* **2010b,** *465,* 901.

5. MATERIALS SYNTHESIS AND ENERGY MATERIALS

The study of materials synthesis and of the behavior of energy materials under operating conditions requires methods to probe the structure and morphology of materials in real time, often on time scales of seconds or minutes, and the ability to probe length scales ranging from the atomic to the mesoscale. Current neutron sources have already enabled breakthroughs in many areas of energy-related materials research because of the neutron's sensitivity to a wide range of elements and its penetrating power, which have enabled the use of complex and realistic sample environments. However, it is only with the STS that experiments providing cinematic details will be possible—observing samples over wide ranges of length scales under realistic operando conditions at the relevant time scales of materials synthesis, battery charging and discharging, pressure-induced transformations, and other processes. The knowledge gained will accelerate the realization of a new generation of energy technologies, such as safer, longer-lasting batteries and inexpensive solar cells.

5.1 Introduction

Progress in human capacity to create and use materials has long been a measure of our civilization: we have progressed from the Stone Age to the Bronze Age, the Iron Age, and ultimately to our current abilities to harvest and store energy, collect and analyze information, and use complex chemistry and materials in a myriad of applications that define our daily life. Advances in our ability to understand and create new materials and structures often underpin new technological breakthroughs. Hierarchical architectures—i.e., structures in which different parts of the assembly perform specific roles at dissimilar length scales (from atomic to mesoscale) and time scales (from minutes to hours)—are at the heart of systems used to store or harvest energy. These include fuel cells, supercapacitors, and batteries for energy storage, and approaches to convert energy from the sun, geothermal sources, or waste heat and spurious mechanical vibrations for energy harvesting. Moreover, it is being increasingly recognized that hierarchical architectures and self-assembly are commonplace during the formation of both natural and engineered materials. Understanding how networks of atomic-scale chemical reactions synergistically influence and/or determine larger-scale structures and material properties is a grand challenge that often defies current capabilities.

Their unique physical properties make high-intensity neutron beams an important tool for the discovery, characterization, and application of new materials and chemical reactivity, complementing the capabilities of electrons and photons [Crabtree and Parise, 2014]. The ability of the neutron to nondestructively penetrate real samples and materials under functional conditions, its sensitivity to hydrogen and light elements, and its ability to probe modes and dynamics over wide length and time scales make it an extremely powerful probe. Moreover, the weak interaction and attendant simplicity of the neutron scattering cross section offer critical complementarity to computational modeling probes, and classical and ab initio calculations have emerged as powerful tools to predict formation and stability, to simulate the structures and behavior of materials, and to probe the effects of chemical reactivity. Modeling has proven valuable in interpreting and rationalizing experimental outcomes and has served to accelerate improved performance in many advanced materials. Continued progress in high-performance computing and modeling algorithms, exemplified by capabilities at the Oak Ridge Leadership Computing Facility (OLCF), can be combined with the results of experiments conducted using the high-intensity neutron beams of the STS to realize a synergistic program in materials synthesis and discovery and in control of chemical reactivity.

5.2 New STS Experimental Capabilities for Materials Synthesis and Energy Materials

The STS offers opportunities to propel critical advances in instrumentation methodologies with beamlines that can combine multiple techniques such as diffraction, small-angle scattering and spectroscopy. New instrument suites with higher flux, wider momentum transfer (**Q**) range, unique detector layouts, improved focusing optics, and integrated advanced sample environments (see Sect. 8) will **provide high temporal resolution over a broad range of length scales in situ**. This will improve capabilities to **probe small sample volumes** to understand complexities and variations in, for example, chemistries and macro-/microstructure that typically control essential materials properties such as (ion) transport and durability and ultimately functional performance and reliability.

Neutrons are essential for acquiring a detailed understanding of materials characteristics and behaviors, including the role of disorder and defects; fluid flow and reactivity in glasses and liquids; kinetics studies, exploration of materials growth and synthesis, and exploration of materials in nonequilibrium conditions and also in extreme conditions far from equilibrium; and for understanding how components and integrated materials in devices function under realistic in situ/in operando conditions. Obtaining this information is a prerequisite for developing the next generation of energy technologies and understanding hierarchical and heterogeneous structures from the atomic scale to real-world components and systems [Wadsworth, 2007; Alivisatos and Buchanan, 2010; Crabtree et al., 2010; Hemminger, 2010].

To transition the knowledge of the properties of these hierarchical materials to practical applications necessitates an integrated understanding of synthesis at the nano-, meso-, and macroscale. It is now possible to envision an integrated model that considers precursor materials, process design (including tuning of reaction kinetics and pathways), and property predictions. The interplay between these elements is becoming increasingly important in the endeavor to fully understand and develop new materials with advanced functionality. The challenge of tracking potentially rapid changes at multiple length scales requires a new generation of instrumentation, as envisaged for the STS—incorporating multiple modalities, not only by combining different neutron scattering analyses made simultaneously on a single sample, but also by combining neutron measurements with concurrent measurements of materials properties using other analytical tools.

The ability to combine sophisticated synthesis and processing with highly configurable instrument layouts, tunable optics, and other analytical tools will allow for studies not previously possible at neutron sources. The results of these experiments will be compared to predictions from high-speed computational studies that provide direct guidance for the design of experiments. The STS thus enables the concept of a beamline as a laboratory to explore new horizons in matter under controlled perturbations such as combinations of deformation, pressure, temperature, or photon irradiation, and simulating synthesis, processing, and service conditions. The power and adaptability of the proposed STS beamlines will allow a significant advance in the ability to conduct complex experiments in situ and in real time, probing these processes with a temporal resolution of minutes.

Another area in which the STS will excel, thanks to its wide bandwidth, is understanding and probing nanoscale interfacial structure. The STS will make it possible to develop neutron reflectometry that provides a high-time-resolution, real-time view to elucidate complex mechanisms occurring at the interface and to develop innovative ways to control the moving interface. The broad wavelength bandwidth delivered by STS, coupled with its unparalleled peak brightness, will enable the observation of interfacial structure at a single instrument setting (like a camera) in exposures on the order of a few seconds, enabling cinematic experiments. This novel capability will be transformative, because it will no longer be necessary to collect data for tens of minutes for a system that is known to change many times

over in that timeframe. All the richness and varieties of chemical reactivity and mass transport will be on view in real time.

The strengths of these new experimental capabilities are illustrated in the form of three experiments described in Sect. 5.3.

5.3 First STS Experiments

5.3.1 Mastering Hierarchical Assembly and Crystallization from Complex Solutions

The high data collection rates offered by the STS will open the possibility of observing in detail reactions occurring on the scale of minutes to hours under real-world conditions; current neutron sources require much longer data acquisition times to capture the full information. Thermal decomposition reactions, solid-state reactions, rearrangements, etc., are amenable to this treatment, as are investigation of catalysts under reaction conditions with realistic gas pressures and gas adsorption and separation processes. The expanded length scales accessible in a single measurement at the STS—simultaneously spanning from the atomic scale to the mesoscale—will enable us to link atomic-scale structures to nano- and macroscopic properties, such as hierarchical assembly. This capability will revolutionize our ability to control matter and chemical reactivity through the design of new synthesis strategies, allowing for the tailored design of complex functional materials.

Materials with hierarchical architectures have the potential to transform the generation, storage, and use of energy [Hemminger, 2015]. By their very nature, these complex materials challenge our established frameworks for understanding and characterizing their structure and associated chemical processes, which have typically targeted specific length or time scales. Because neither the formation nor the function of hierarchical assemblies can be understood without first understanding the interplay across these scales—which extend over many orders of magnitude—entirely new approaches are needed to advance the development and eventual deployment of these structures and materials.

Understanding the formation of such hierarchical assemblies presents a daunting challenge, because multiple processes are involved which must be studied simultaneously across broad length and time scales. No single technique can span all time scales involved in synthesis, from picoseconds to hours. Some experiments, such as vibrational spectroscopy to provide access to the timescales of atomic processes, are ideally suited for the capabilities of the FTS. However, at the time scales of the coarsening of nanostructures and the evolution of hierarchical assemblies, i.e., at minutes and hours, real-time observations will become possible at STS, coupled with an ability to investigate length scales from the atomic (through diffraction) to micrometers or larger (through small-angle scattering). Only by understanding the totality of these assembly processes can we control synthesis processes and direct their assembly to realize desired functionalities. Currently, uncertainties in the chemical reaction mechanisms that occur during the nucleation and growth of solid phases from liquid solutes, and the subsequent (self-) assembly of nanoscale structures into macroscopic aggregates, hinder our ability to predict and control crystallization phenomena.

In the past decade, numerous potential mechanisms have been identified by which crystallization might occur (see Fig. 5.1). However, we still lack the ability to identify which mechanism is dominant under an arbitrary solution condition, and which solute or solvation properties are driving that mechanism. This information is essential for providing the knowledge needed to formulate a quantitative predictive theory that can be used to guide new synthesis methods. The prototypical example is that of biomineralization: organisms can create inorganic structures and inorganic/organic composites of complexity far beyond what is possible to synthesize. Organisms do this by manipulating the nucleation processes, and their locale, that control the precipitation reactions and resultant atomic structure of solid phases that affect

particle morphology and assembly of nanoparticles. By focusing on a wide range of length scales, the STS will allow us to examine the interplay of atomic-level chemical reactions that drive assembly of nanoparticles and their macroscopic properties. Harnessing these reactions and processes could enable dramatic new synthesis strategies and device efficiencies. Examples range from the hierarchical assembly of nanodevices for increased efficiency during solar energy conversion, to controlling defect density as a way of tailoring device properties (such as band-gap or reactive surface site density), tailoring catalyst morphologies to favor a specific ensemble of chemical reactions (e.g., converting CO_2 to a specific liquid multi-carbon chemical), utilizing confinement effects on adsorbents to develop new efficient and selective separation methods (e.g., critical materials such as adjacent lanthanides that are difficult to separate), or relieving rate-limiting reactions while designing crystallization methods to deal with contaminants or other undesirable species.

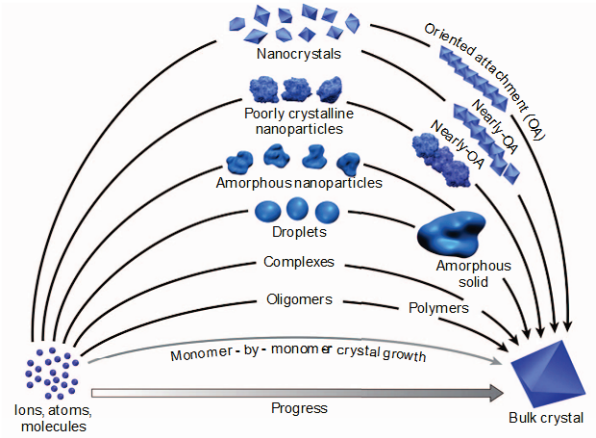

Fig. 5.1. Mechanisms of crystallization from aqueous solutions. The STS will allow us to identify which mechanism is important under a given solution condition, identify why that mechanism is occurring, and conduct quantification that will lead to predictive capabilities far beyond existing theories, all accelerated by integration with high-performance computing simulations. Image source: Reprinted with permission of the American Association for the Advancement of Science from De Yoreo et al. [2015, Fig. 1].

Simultaneously observing these types of systems across time and length scales will provide detailed insight into crystallite or amorphous phase formation and morphological changes, together with elucidation of solvation structures of dissolved species. A recent publication shows how even with the current capabilities the addition of neutron data can be invaluable in understanding the structure within solutions [Semrouni et al, 2019]. Even in static cases (thermodynamic equilibrium), **the combination of SANS with diffraction and total scattering (WANS)** can provide a remarkably complete picture. However, to gain a quantitative and mechanistic understanding of how the kinetics of nanoparticle assembly and crystallization are influenced by the atomic-scale structure of the liquids from which they are formed, such measurements must be performed in one experiment (see Fig. 5.2), covering the length scales from ~0.3 Å to ~300 nm, and on a time scale that is relevant to these assembly processes, i.e., minutes rather than hours.

The design features of the STS will enable entirely new types of neutron experiments that will provide unprecedented insight into these important processes:

- The combination of the increase in cold neutron peak brightness with the broad range of usable wavelengths in each pulse will enable simultaneous observations across this entire relevant length scale, by SANS and WANS, with one instrument (SANS/WANS).
- The increase of cold neutron brightness will allow researchers to conduct **measurements on materials that have a far lower solubility** or behave differently at lower concentration compared with what is currently feasible, opening up these experiments to many more scientifically and technologically relevant material and chemical systems.

The revolutionary insight that these novel data sets provide will challenge our current understanding of associated processes across length and time scales. This will clearly require a tight integration with high-

performance computing capabilities that have become available for simulations of the contributions of atomic-scale structure and dynamics to macroscopic properties, such as the morphology and rheology of a material.

Experiment details: This experiment aims at linking atomic-scale solution structure and ion association to precipitation, aggregation and crystallization reactions. Within a single time-resolved in situ measurement, it will be possible to monitor simultaneously the extended solvation structures of dissolved species, their reactivity, and the morphologies of precipitates resulting from crystallization reactions. Such measurements will target not just the atomic-scale structure of complex aqueous solutions, but also the ionic and molecular association reactions that create polynuclear clusters, the aggregation of those clusters into amorphous nanomaterials or incipient nuclei, and finally the crystallization into bulk-like materials.

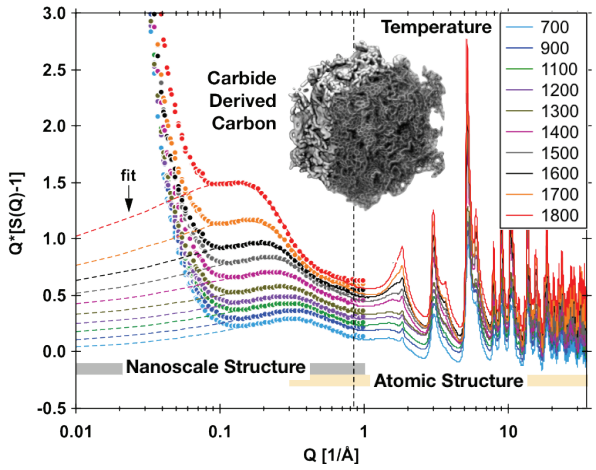

Fig. 5.2. Simulated neutron scattering data. Ex situ measurements of nanoscale (small-angle) and atomic structure (structure factor for pair distribution function analysis) of carbide-derived carbon (model in inset), stitched together to create a single data set spanning the relevant length scale range, as will be possible in a single in situ experiment on STS instruments. Such a capability will make time-resolved in situ measurements of coarsening, aggregation, and crystallization a reality. Curves are displayed for samples annealed at different temperatures (ºC). Image source: Data from H-W. Wang, personal communication; inset image: Zhan et al. [2017].

This experiment at the STS will probe SiO_2 and $CaCO_3$ crystallization to link the atomic-scale hydration structure of an aqueous solution to its precipitation, aggregation, and crystallization behavior. Neutron data is essential to gain a complete picture of the solvation structure, since some correlations can only be characterized via neutron data even when high quality X-ray synchrotron data is available [Semrouni et al., 2019]. Despite the significant prior work on these systems, we currently lack the ability to quantitatively link specific atomic-scale solvation structures in solution to their reaction pathways during liquid-solid transitions, and then to specific nanoscale morphologies, aggregation behavior, and their ultimate macroscopic crystal form. This is despite the fact that their rich liquid-solid transition chemistry—via which isolated ions in solution associate to form clusters, amorphous hydrated nanomaterials, and ultimately well-crystallized macroscopic crystals [Cartwright et al., 2012; Belton et al., 2012]—has long been recognized. Because of this rich reactivity and their use as biominerals by organisms, these materials are often thought of as candidates for the synthesis of bio-inspired devices, the goal of which is to control hierarchical assembly and crystallization reactions to tailor specific properties or material morphologies. Without the ability to link the relevant reaction and assembly mechanisms across length scales, a crystallization strategy must be developed through phenomenological discoveries and not as a rational design process.

Performing simultaneous SANS/WANS experiments at the STS will allow us to break through this bottle-neck by linking atomic-scale solvation structures to ion and molecule association reactions, to the aggregation behavior of nanomaterial solids, and to the ultimate crystallization outcome. Coupling the results to simulations will allow us to generate quantitative, predictive theories of hierarchical assembly during precipitation that are currently lacking, thus enabling the creation of a rational-design workflow for bio-inspired materials. This in turn will have benefits with scientific impacts beyond materials synthesis and aqueous solution reaction chemistries, extending to many processes in which complex aqueous solutions, or other environments, are involved.

This same type of approach can be applied to more complex systems for explorations such as examining how confinement affects ion adsorption, aggregation, and precipitation within a porous medium, including reaction dynamics, and phase selection. In all of these cases, combining advances in high-performance computing capabilities with cutting-edge advances in coarse-graining and upscaling methods in reverse Monte Carlo (RMC) and other simulations could provide a comprehensive model to fit the scattering data across the four decades of length scales measured at the STS. Such models can then be used to predict macroscopic properties of the solution, such as rheology, and to predict the morphologies of the synthesized material quantitatively.

The new STS capabilities and the time-resolved approach, spanning an extraordinary range of length scales that can currently be covered only by combining measurements performed in different configurations or with different instruments, represent a powerful tool to observe complex materials in their native/operating environments, which will have broad scientific impact. Neutron diffraction and spectroscopy measurements will provide critically needed quantitative data that complement additional characterization measurements—some of which will eventually be carried out concurrently on multi-modal instruments. This will allow researchers to uncover, with unprecedented detail, how atoms come together through irreversible and transient processes to form materials at solid-solid, solid-liquid, and solid-gas interfaces, informing computation and the rational synthesis of new and more efficient materials. This ability is currently lacking in many use cases, inhibiting our ability to create specific structure-function relationships. This in turn would establish quantitatively how a given synthesis method, structure, or reaction environment favors a specific ensemble of atomic-scale reactions. It is precisely these interactions and sequences that impact larger-scale properties, ultimately determining the function-ality or efficiency of the macroscopic product or device.

5.3.2 Discovery and Synthesis of Functional Materials via High Pressure

The STS, through the increase in peak brightness for cold neutrons and characteristics that can exploit advanced focusing optics, will overcome many obstacles currently faced during the study of exotic materials. These exotic states exist (far) away from equilibrium within a material's energy landscape and are usually accessed via extreme conditions such as high pressures, high temperatures, or nonlinear conditions present during irradiation. Specifically, STS instruments will provide orders of magnitude increases in measurement of signal and minimized background, while allowing for small beam sizes suitable for such experiments, which are usually conducted within the constraints of a confining sample environment.

The application of extreme conditions allows for the synthesis of novel materials with revolutionary functionality that cannot be accessed any other way. Indeed, such synthesis may alter the properties of materials well established in their technological uses through improvement of a particular characteristic. Neutron scattering is a critical tool for understanding the dynamics and properties of novel exotic materials. A prime example for useful new synthesis pathways via high pressure is found in the many exotic allotropes of the elemental semiconductor silicon. Silicon has enabled technological revolutions through its many wide-ranging applications, from computer chips to solar power conversion. The main advantages of silicon lie in its wide abundance and nontoxicity rather than its band gap structure. High-end semiconductor applications require more suitable band gap characteristics—for example, the direct band gap of ~1.42 eV found in gallium arsenide for improved solar power conversion. Such materials are, however, expensive, often toxic, and not easily scalable to industrial needs. These issues could be over-come if different allotropes of silicon with improved band gap characteristics were used.

Several structures of silicon synthesized via high pressure can be recovered to ambient conditions [Haberl et al., 2016]. Under strain application or in the form of hydrogenated nanoparticles, these polymorphs are expected to be hugely advantageous for inexpensive, Si-based solar power conversion [Haberl et al., 2016; Wippermann et al., 2016; Taylor, 2016; Beekman, 2015]. Furthermore, a 2015 study has reported

the high-pressure synthesis of a novel allotrope of silicon, Si_{24}, from a NaSi clathrate as precursor (see Fig. 5.3) [Kim et al., 2015]. Application of sufficient strain or pressure may turn the quasi-direct band gap of Si_{24} into a direct band gap close to the ideal range for solar power conversion. To facilitate such strain-induced tuning of the band gap, a full understanding of Si_{24}'s phonons is necessary. This understanding can only be obtained with inelastic neutron scattering under pressure such as afforded through the brightness of the STS with advanced focusing optics.

This powerful capability of inelastic neutron scattering under pressure could have equal impact on high pressure synthesis from silicon's sister element carbon. The energy landscape of carbon is particularly amenable to searches for new synthesis pathways, since many metastable carbon allotropes already exist and are often synthesized under extreme conditions [Hirsch, 2010; Bovenkerk et al., 1959; Bundy et al., 1955; Kasper and Wentorf, 1977; McKenzie, 1996; Robertson, 1986; Fitzgibbons et al., 2015] with diamond [Bovenkerk et al., 1959; Bundy et al., 1955] being the prime example.

One of these novel super-strong carbon allotropes was first discovered through neutron scattering at the FTS [Fitzgibbons et al., 2015]. Furthermore, many new functional carbon phases have been predicted in this highly active field [Clark et al., 1995; Yin, 1984; Hoffmann et al., 2016]. A key focus thereby lies on carbon allotropes that exhibit a hardness higher than that of diamond [Clark et al., 1995; Yin, 1984; Pan et al., 2009]. Such a material clearly would have a transformative impact on major industries, ranging from mining to reactor safety.

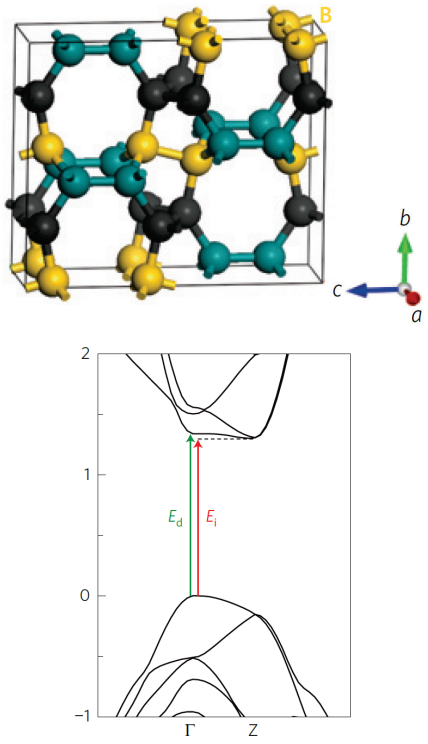

Fig. 5.3. Details of the new phase of silicon. Top: The unit cell of Si_{24}, exhibiting three crystallographically unique positions in each color. The open channels in this unit cell are obtained through "leaching" Na from the parent NaSi clathrate. (b) The quasi-direct band gap in Si_{24}, calculated to be 1.30 eV, making it a potentially highly useful material for solar power conversion. Image source: Reprinted with permission from Kim et al. [2015, Figs. 1 and 3].

Synthesis of these predicted new materials is often unsuccessful because the application of extremes to crystalline precursors is insufficient to overcome the strong kinetic barriers in the carbon energy landscape. This issue can be overcome through the use of disordered precursors, which are inherently metastable. Recent work thereby demonstrates the synthesis of hexagonal-diamond/lonsdaleite carbon from glassy carbon, a disordered sp^2 bonded carbon [Shiell et al., 2016]. Hexagonal-diamond is predicted to exhibit higher hardness than diamond [Pan et al., 2009]. The transition process from sp^2 bonded glassy carbon to the fully sp^3 bonded crystalline hexagonal diamond/lonsdaleite is not understood. To understand this transition—and apply new knowledge to the synthesis of other carbon materials—it is crucial to investigate and understand the changes that occur in the disordered material under pressure prior to crystallization and phase transition.

Neutron scattering is an invaluable tool for such amorphous structure determination, specifically when inelastic and elastic data are combined. Although high Q resolution is not usually necessary for studying amorphous materials, the broad wavelength capabilities of STS confers major advantages. The combination of elastic and inelastic data enables the creation of advanced models that elucidate structural

changes as they occur under compression in ways impossible with either data set alone. The formation of hexagonal diamond and of other desirable carbon allotropes will, however, require pressures beyond current capabilities at the FTS for elastic data, and even more so for inelastic data.

Experimental details: The inelastic pressure experiment will be performed inside a diamond anvil cell (DAC) specifically developed at ORNL for neutron measurements [Boehler et al., 2017, Haberl et al., 2018]. This DAC, in combination with the increased flux of neutrons and advances in neutron optics at the STS, will enable **in situ inelastic neutron scattering (INS) to unprecedented pressures**. Although INS of ~1 mm^3 size samples pressurized to 10 GPa is possible now on the VISION instrument at the FTS, this technique can be used only with materials that contain significant percentages of hydrogen. A small sample of a relatively poor scatterer, such as silicon, or a small sample of a disordered material such as the glassy carbon precursors cannot be observed inside a pressure cell. Even if prohibitively long exposure times were to be used, the sample signal would remain beneath parasitic scatter from the surrounding pressure cell. Indeed, no neutron spectrometer in the world is currently capable of obtaining useful inelastic scattering from Si samples or disordered carbon samples small enough to allow for pressures well in excess of 10 GPa.

With significantly increased brightness, advances in collimation, and beams focused to optimized sizes for DACs, the STS will overcome this limitation, offering world-leading instruments for high-pressure INS. This capability at the STS will allow in situ observation of the pressure dependence of phonons and the band gap of Si_{24} during compression to ~10 GPa. Such data will give new insights into the formation of superhard allotropes and will be used to identify the next functional silicon or carbon.

5.3.3 In Situ Examination of Dynamic Interfaces in Batteries and Supercapacitors

Within a relatively short amount of time, the markets for—and opportunities with—personal electronics were transformed by the introduction of lithium-ion batteries. The next advances in electrical energy storage could lead to similarly revolutionary changes in transportation, grid-scale renewable energy harvesting and storage, and distributed power, or in wearable devices and deployed sensors powered by energy efficiently harvested and stored at the point of use. For most of these applications, today's batteries are not good enough—they are too big, too heavy, too expensive, and often too dangerous.

Electrical energy storage relies on the coordinated motion of electrons and ions through a material that is undergoing atomic-scale rearrangements mediating voltage and cyclability. Our scientific understanding of these processes is challenged by the complexity of the motion of atoms and molecules through and in the hierarchical architectures of electrode/electrolyte interfaces, embedded nanoparticles, and materials containing a variety of vacancies and voids that are needed to facilitate the transport. To advance our understanding of these processes, and thus to ultimately discover and develop the next generation of energy storage mechanisms, requires an approach that integrates in situ and operando experiments with computational models, design concepts, synthesis, and characterization [Crabtree, 2017]. Real-time characterization of operating batteries needs to probe their behavior from the nano- to the mesoscale.

Neutron studies of materials for electrical energy storage include a variety of needed techniques and methods, and the different neutron sources at ORNL and across the world provide complementary capabilities for these investigations. Powder diffraction on this class of materials, for example, will best be performed at the FTS due to its optimized performance for thermal neutrons, the medium range of neutron energies, and the high energy resolution. In contrast, the STS provides a unique opportunity for the study of interfaces using neutron reflectometry (NR), for which the **broad range of neutron energies will enable the needed cinematic experiments**, i.e., studies in which the evolution of an interface can be probed over time and under realistic operating conditions.

Understanding interfaces in energy materials is crucial: Energy generation, storage, and conversion technologies depend on high rates of transfer of heat, mass, ions, and electrons that result in highly heterogeneous interfaces and associated chemical and physical processes that are far from equilibrium.

For example, energy storage processes involve the transport of ions, electrons, and molecules through complex chemical environments at the interface with electrode surfaces. The poorly understood interfacial structure between two dissimilar materials in liquid or solid electrolytes is confounded further because this interface continually changes and relaxes during charge/discharge cycles, with currents producing significant atom rearrangement on the time scale of seconds [Hemminger, 2007]. Correlating interfacial structure and relaxation with electrical and mechanical response is a prerequisite to realizing next-generation energy technologies. It is impossible to make a predictive assessment of how to best optimize the facile transport of ions, mass, and heat across and along these interfaces without a full understanding of the complex, dynamic interfacial environments and the involved chemical and physical processes, such as:

- the structure, kinetics, and dynamics of atom segregation and cascades that form at solid-solid, solid-polymer, and solid-liquid interfaces with external modifiers like heat, electrical potential, and mechanical load;
- phonon coupling across nonepitaxial interfaces during ion motion or heat transfer;
- transport of ions and atoms at and across grain boundaries; and
- the contact formed between disparate materials during fabrication and its relation to adhesion strength, ion motion, and heat conduction.

All of these issues involve dynamic processes that occur far from equilibrium or in transient states over length scales from nanometers to microns; exploring them requires nondestructive, real-time characterization, with specificity to light elements, and without perturbing the processes of interest. Ion transport across a solid-solid interface is a particularly intriguing challenge, as applications in electrical energy storage require current densities of almost 10^{19} ions/s·cm^2. Currently, we do not know how materials and interfaces accommodate this massive flux, or how collective ion transport in the bulk correlates to ion transport through an interface. A full understanding of how mass is transported through and along interfaces is a significant bottleneck in the advancement of these energy technologies.

NR can provide much-needed insight into interfacial structure at the nanoscale. In addition, this tool is sensitive to different isotopes of light elements and is able to penetrate solid substrates to view buried interfaces. The evolution of such interfaces during chemical changes or other operando conditions is of paramount importance. A combination of specular and off-specular reflectivity can reveal structure both normal and parallel to a planar interface. However, observing transient phenomena in real time with today's NR capabilities is hindered by the length of time required to collect a complete specular reflectivity curve in a single instrument setting, typically restricting measurements to a "semi-equilibrium" state with 1-hour increments [Veith, 2017].

Instrumentation proposed for the STS will overcome this limitation by taking advantage of unprecedented peak brightness distributed over a large wavelength bandwidth. High STS flux delivered into a broad wavelength bandwidth will enable the observation of interfacial structure in a single instrument setting on time scales able to capture transient processes. This powerful and efficient way of collecting data observes the sample but does not interfere with the operando environment. As shown in Fig. 5.4, refinable specular reflectivity data will be available in as little as a few seconds. Thus, the STS will provide a revolutionary capability to examine interfacial systems in real time and provide insight into time-dependent phenomena (e.g., temperature, electrochemical, magnetic, or chemical alteration).

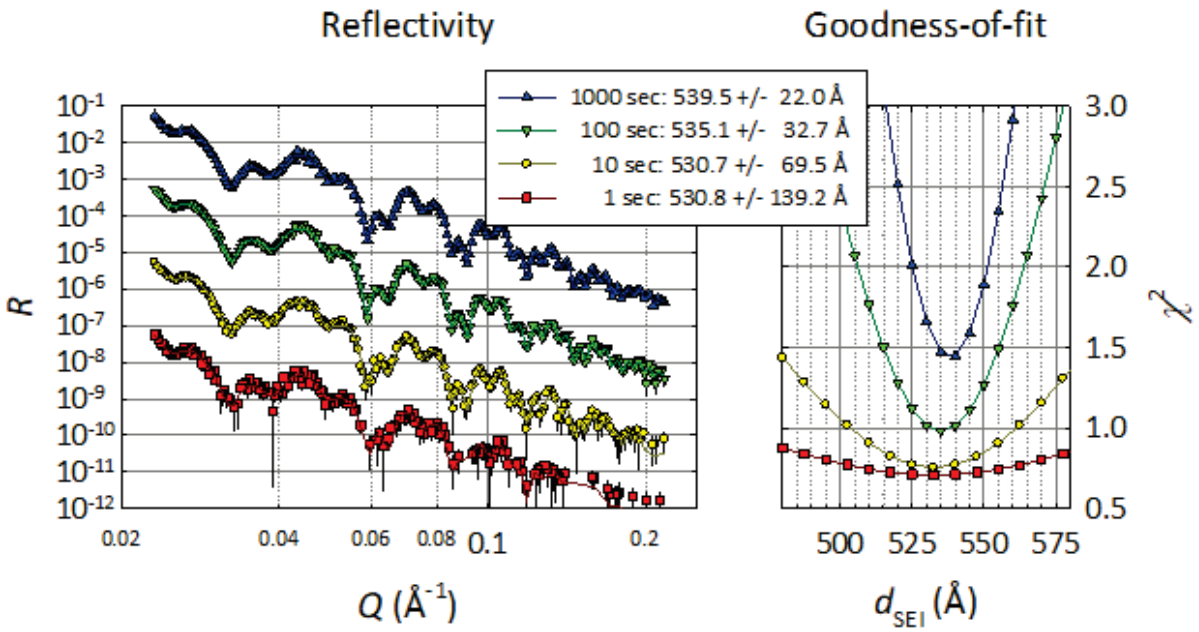

Fig. 5.4. Simulated performance of a reflectometer designed for the STS, derived from fitted reflectivity data obtained on the FTS Liquids Reflectometer. Reflectivity profiles (left) were generated by exposing a sample to simulated STS flux for 1, 10, 100, and 1000 seconds. The evolution of an interfacial layer and the variation of its fitted value are shown at right as a function of counting time. A 100 s exposure yields equivalent goodness of fit to that of the 40 min (2400 s) data set from the current instrument, a 24-fold improvement. Image source: Courtesy of John Ankner, ORNL.

Experiment details: In energy devices, the interfaces often constitute a dynamic boundary where large amounts of mass are rapidly added or removed. Control of nucleation and growth processes is critical to maintaining the desired interface and phase distribution required for optimal and reliable device operation. At a solid-liquid interface, porous and dendritic structures may form; at a buried solid-solid interface, however, observation and control are more challenging to observe and difficult to predict, particularly at high rates of mass flow. Nominally ideal layers may in fact exhibit a complex morphology, with pores, dendrites, inclusions, cracks, and delamination. Interruption for slow or ex situ characterization gives the structure time to anneal and redistribute, obscuring information about critical processes, without modifying the system.

It is thus critical to explore these processes as they occur in situ and operando. A specific case in point is solid-state electrolytes, which are essential for the next generation of energy storage technologies because they eliminate the necessity of organic and potentially flammable liquids. However, the dynamics of atomic and structural rearrangements in solid electrolytes remain unknown. Initial studies will explore the lithium-metal/glassy-electrolyte lithium phosphate oxynitride (Lipon) interface during lithium plating. This system is currently the only solid electrolyte that is compatible with elemental lithium electrodes. To date, it has not been possible to study the dynamics of this interface because lithium has a weak X-ray atomic form factor, and current neutron-based instrumentation lacks the time resolution necessary to capture the dynamics of these interface processes.

As mentioned above, the **STS will make it possible to develop a reflectometry instrument to provide a high–time-resolution, real-time view to elucidate complex mechanisms occurring at the interface and to evaluate innovative ways to control the moving interface.** All the richness and varieties of redox reactions and mass transport will be in view in real time. Because neutrons can penetrate most structural materials, this approach will enable the operando study of these dynamic processes, with a time

resolution of seconds to minutes, which will enable elucidation of the processes involved in the initiation and transient growth of lithium metal at a solid-solid interface in a working battery. Further insight will be afforded using isotope contrast techniques. In this case, real-time observations of heterostructures of plated ^{6}Li and then ^{7}Li (isotopes distinguishable by neutrons) will be used to yield fundamental insight into these diffusion and reorientation processes. With such insight, we will examine, in real time, the effect of applying static or dynamic loads or variation in electrical current or temperature as likely factors that may influence the structure of moving interfaces—something that has never been observed before.

5.4 Conclusion

STS will offer transformative opportunities for capturing the structure and dynamics of complex systems in situ, in real time, and in industrially relevant settings. Researchers will be able to follow self-assembly and other reaction networks at the atomic/molecular level through to aggregation/crystal growth of particles toward targeted architectures and functionalities. Quantitative validation of theories on eutectic compositions, solute-solvent interactions, and deviation from ideality will impact the rational control of biological and geological systems, electrical energy storage systems, catalysis processes, separations science, and more. Linking reactivity, stereoselectivity, chemoselectivity, and kinetics toward reactions with macroscopic device or product efficiencies, under realistic conditions of temperature and pressure, will have a broad impact on many industries and position us for future applications in energy efficiency, production, and storage, and in extreme environments.

Extreme environments provide a prime example for the impact of the STS. Such environments inherently require a sample to be measured within a confining space, often made of nontransparent materials. Neutrons can be an ideal nondestructive probe because they penetrate many materials easily. Furthermore, the application of extreme conditions typically requires small samples, since extreme pressures or temperatures, for example, typically cannot be maintained uniformly across large areas or volumes. To date, this has prevented studies of materials with INS at pressures above 10 GPa and of materials with elastic neutron scattering at pressures above 100 GPa. Access to these pressures is, however, critical to understand the formation of many new materials, such as superhard carbon allotropes or new functional semiconductor allotropes; it is equally important in planetary sciences and even in the understanding of new superconducting superhydrides such as the lanthanum hydrides.

With regard to the study and control of interfaces, the STS, with its unprecedented peak brightness and broad range of usable wavelengths, will present the opportunity to observe numerous chemical processes, under environmental control, in real time as they happen, for example inside an energy storage cell during electrochemical reactions under current-voltage control. The ability to make such observations offers unprecedented opportunities. Beyond electrochemical energy storage, the importance of observations of solid-solid or solid-liquid interfaces is far reaching. Interfaces operating under extreme conditions play a key role in systems such as concentrating solar power plants, nuclear reactors, and turbines. The ability to perform studies of corrosion, dissolution, rearrangements, and other processes dynamically using the new capabilities available at the STS will clearly be transformational for a broad range of applications in which the time evolution of a chemically active interface, or an interface exposed to extreme chemical constraints, is important, as well as in areas of polymer films and coatings, synthetic or biological membranes, and liquid-liquid interfaces.

The STS will have a tremendous impact overall on DOE mission space, but it will be particularly useful in aiding us in the design and synthesis of new energy materials, through better understanding of their chemical reactivity and other processes. These breakthroughs will be achieved by using the enhanced bandwidth and brilliance of the STS to conduct the required cinematic experiments, where structures of samples are observed over wide ranges of length scale with enhanced time resolution under realistic

operando conditions, i.e., at the relevant time scales of materials synthesis, battery charging and discharging, pressure-induced transformations, etc.

References for Sect. 5

Alivisatos, P.; Buchanan, M. V. (co-chairs), *Basic Research Needs for Carbon Capture: Beyond 2020*, U.S. Department of Energy, Washington, DC, 2010. Available at https://science.osti.gov/-/media/bes/pdf/reports/files/ Basic_Research_Needs_for_Carbon_Capture_rpt.pdf (accessed June 8, 2019).

Beekman, M.; *Mater. Today* **2015,** *18,* 304–305.

Belton, D.; Deschaume, J. O.; Perry, C. C. *FEBS J.* **2012,** *279,* 1710–1720.

Boehler, R.; Molaison, J. J.; Haberl, B. *Rev. Sci. Instrum.* **2017,** *88,* 083905.

Bovenkerk, H. P.; Bundy, F. P.; Hall, H. T.; Strong, H. M.; Wentorf, R. H., Jr., *Nature* **1959,** *184,* 1094.

Bundy, F. P.; Hall, H. T.; Strong, H. M.; Wentorf, R. H., Jr., *Nature* **1955,** *176,* 51 (1955).

Cartwright, J. H.; Checa, A. G.; Gale, J. D.; Gebauer, D.; Sainz-Díaz, C. I. *Angew. Chem. Int. Ed. Engl.* **2012,** *51,* 11960–11970.

Clark, S. J.; Ackland, G. J.; Crain, J. *Phys. Rev. B* **1995,** ***52,*** 15035.

Crabtree, G. (chair). *Basic Research Needs for Next Generation Electrical Energy Storage,* U.S. Department of Energy, Washington, DC, 2017. Available at https://science.osti.gov/-/media/bes/pdf/reports/2017/BRN_NGEES_rpt.pdf (accessed June 8, 2019).

Crabtree, G.; Glotzer, S.; McCurdy, B.; Roberto, J. (co-chairs). *Computational Materials Science and Chemistry: Accelerating Discovery and Innovation through Simulation-Based Engineering and Science,* U.S. Department of Energy, Washington, DC, 2010. Available at https://science.osti.gov/-/media/bes/pdf/reports/files/ https://science.osti.gov/-/media/bes/pdf/reports/files/ Computational_Materials_Science_and_Chemistry_rpt.pdf (accessed June 8, 2019).

Crabtree, G., Parise, J. (organizers), *Frontiers in Materials Discovery, Characterization and Application: Workshop Report,* UT-Battelle, LLC, Oak Ridge, Tennessee, 2014. Available at https://neutrons.ornl.gov/sites/default/files/CEMD Workshop Report Draft Oct19v4_Chicago.pdf (accessed June 8, 2019).

De Yoreo, J. J.; Gilbert, P. U. P. A.; Sommerdijk, N. A. J. M.; Penn, R. L., Whitelam, S.; Joester, D.; Zhang, H.; Rimer; J. D.; Navrotsky, A.; Banfield, J. F.; Wallace, A. F.; Michel, F. M.; Meldrum, F. C.; Cölfen, H.; Dove, P. M. *Science* **2015,** *349,* 6760.

Fitzgibbons, T. C.; Guthrie, M.; Xu, E.; Crespi, V. H.; Davidowski, S. K.; Cody, G. D.; Alem, N.; Badding, J. V. *Nature Mater.* **2015,** *14,* 43.

Haberl, B.; Strobel, T. A.; Bradby, J. E. Appl. Phys. Rev. **2016,** *3,* 040808.

Haberl, B.; Dissanayake, S.; Wu, Y.; Myles, D. A.; dos Santos, A. M.; Loguillo, M. J.; Rucker, G.; Armitage, D.; Cochran, M. J.; Andrews, K. M.; Hoffmann, C.; Cao, H. B.; Matsuda, M.; Meilleur, F.; Ye, F.; Molaison, J. J.; Boehler, R. *Rev. Sci. Instrum.* **2018,** *89,* 092902.

Hemminger, J. C. (chair). *Directing Matter and Energy: Five Challenges for Science and the Imagination: A Report from the Basic Energy Sciences Advisory Committee,* U.S. Department of Energy, Washington, DC, December 2007. Available at https://science.osti.gov/-/media/bes/pdf/reports/ files/Directing_Matter_and_Energy_rpt.pdf (accessed June 7, 2019).

Hemminger, J. C. (chair). *Science for Energy Technology: Strengthening the Link between Basic Research and Industry*, U.S. Department of Energy, Washington, DC, August 2010. Available at https://science.osti.gov/-/media/bes/pdf/reports/files/Science_for_Energy_Technology_rpt.pdf (accessed June 8, 2019).

Hemminger, J. C. (chair). *Challenges at the Frontiers of Matter and Energy: Transformative Opportunities for Discovery Science: A Report from the Basic Energy Sciences Advisory Committee,* U.S. Department of Energy, Washington, DC, November 2015. Available at https://science.osti.gov/-/media/bes/besac/pdf/Reports/Challenges_at_the_Frontiers_of_Matter_ and_Energy_rpt.pdf (accessed June 8, 2019).

Hirsch, A. *Nature Mater.* **2010,** *9,* 868.

Hoffmann, R.; Kabanov, A. A.; Golov, A. A.; Proserpio, D. M. *Angew. Chem. Int. Ed.* **2016,** *55,* 10962–10976.

Kasper, J. S.; Wentorf, R. H., Jr., *Science* **1977,** *197,* 599.

Kim, D. Y.; Stefanoski, S.; Kurakevych, O. O.; Strobel, T. A. *Nature Materials* **2015,** *14,* 169.

McKenzie, D. R. *Rep. Prog. Phys.* **1996,** *59,* 1611.

Pan, Z.; Sun, H.; Zhang, Y.; Chen, C. *Phys, Rev. Lett.* **2009,** *102,* 055503.

Robertson, J. *Adv. Phys.* **1986,** *35,* 317–374.

Semrouni, D.; Wang, H-W.; Clark, S. B.; Pearce, C. I.; Page, K.; Schenter, G.; Wesolowski, D. J.; Stack, A. G. *Phys. Chem. Chem. Phys.* **2019**, *21*, 6828.

Shiell, T. B.; McCulloch, D. G.; Bradby, J. E.; Haberl, B.; Boehler, R.; McKenzie, D. R. *Sci. Rep.* **2016,** *6,* 37232.

Taylor, P. C. *Phys. Today* **2016,** *69,* 34.

Veith, G. M.; Doucet, M.; Sacci, R. L.; Vacaliuc, B.; Baldwin, J. K. S.; Browning, J. F. *Sci. Rep*. **2017,** *7,* 6326.

Wadsworth, J. (chair). *Basic Research Needs for Materials Under Extreme Environments*, U.S. Department of Energy, Washington, DC Available at https://science.osti.gov/-/media/bes/pdf/reports/files/Materials_under_Extreme_Environments_rpt.pdf (accessed June 8, 2019).

Wippermann, Y.; He, M.; Vörös, G. G. *Appl. Phys. Rev.* **2016,** *3,* 040807.

Yin, M. T. *Phys. Rev. B* **1984,** *30,* 1773–1776.

Zhan, C.; Lian, C.; Zhang, Y.; Thompson, M. W.; Xie, Y.; Wu, J.; Kent, P. R. C.; Cummings, P. T.; Jiang, D. E.; Wesolowski, D. J. *Adv. Sci.* **2017,** *4,* 1700059.

6. STRUCTURAL MATERIALS

The higher brightness of long-wavelength neutrons at the STS, combined with advances in neutron optics, will be transformative for neutron scattering investigations of structural materials. In particular, the STS will significantly shorten the time needed for measurements and allow smaller beam sizes with higher brightness to be targeted on specific regions of interest for real-time, in situ, time-dependent, and location-specific characterization of complex materials during synthesis (e.g., additive manufacturing), processing (e.g., metamorphic manufacturing), mechanical testing, and environmental exposure (e.g., corrosion and irradiation) of specimens of realistic size. The higher intensity of STS instruments will enable subsecond time-resolved measurements of structural changes in complex materials. Additionally, the availability of a much wider range of neutron wavelengths will allow simultaneous characterization of microstructures and phenomena across multiple length scales, including nucleation and growth of precipitates, metastable and intermediate phases in complex alloys and composite materials, long-range order, and defects. These new capabilities of the STS will have enormous impact on advancing the fundamental understanding of how composition and processing affect the structure, properties, and performance of structural materials.

6.1 Introduction

Structural materials are, and will remain, critical to broad swaths of the economy, from energy, transportation, security, aerospace, and health to manufacturing and infrastructure. New materials are needed to withstand increasingly demanding conditions, such as extremes in temperature, stress, and chemical environments. For example, new alloys are needed to reduce the weight of vehicles while maintaining or enhancing stiffness, strength, and energy absorption during crashes. Materials for more efficient engines and turbines, and for advanced hypersonic applications, require fail-safe operation at higher temperatures and stresses. Increasing demand for "green" materials that are energy efficient and environmentally friendly drives the search for new low-cost recyclable structural materials. New materials are also needed to realize next-generation terrestrial and space nuclear reactors that will experience extremes of radiation and temperature and exposure to corrosive coolants such as molten salts and liquid metals. Safe long-term storage of nuclear waste is a longstanding problem for which new materials solutions are critically required. Cheaper, lighter, and tougher cryogenic materials are needed for a range of applications from the everyday (e.g., transoceanic transport of liquified natural gas) to the exotic (e.g., colonization of Mars and mining of asteroids). In short, structural materials perform a myriad of functions that impact our lives, and they will remain at the heart of technologies, devices, and societal infrastructure into the future.

Most materials currently used for structural applications have reached, or are close to reaching, their performance limits. In order to accelerate the development of next-generation advanced structural materials to meet future needs, broad scientific principles that can guide alloy design are needed. Unfortunately, our understanding of the "materials pentahedron," where composition, structure, processing, properties, and performance comprise the five corners, is limited in several fundamental ways. Arguably, the biggest gap in our understanding is: how exactly do structure and properties evolve during synthesis, processing and service? This is important because these aspects of structural materials (structure and properties) are not state variables that depend only on the initial and final states; rather they are path-dependent (i.e., they depend on the precise route taken to reach the final state). Therefore, postmortem evaluations can only provide a limited view (or are extremely tedious if multiple ex situ tests must be interrupted for subsequent characterization), making in situ characterization invaluable.

In this respect, the introduction of in situ testing capabilities in electron microscopes and X-ray and neutron beamlines was a significant development, because it made possible the study of the evolution of structure and (some) properties in a single specimen. Among these techniques, in situ neutron scattering

offers benefits accruing from the unique physical properties of neutrons that complement the capabilities of electrons and photons [Crabtree and Parise, 2014]. The neutron's ability to nondestructively penetrate real components and materials under operational conditions, its sensitivity to hydrogen and light elements, and its ability to investigate modes and dynamics over virtually all practical length and time scales make it an extremely powerful probe. Collimation of intense neutron beams enables the measurement to be defined from a small (~1 mm^3) scattering volume within a comparatively large bulk sample, thereby enabling mapping of critical microstructural features such as phase fractions, orientations, elastic strains, and dislocation densities. Beyond conventional time-resolved measurements, stroboscopic techniques enable much finer time resolutions than are intrinsic to the source pulse rate. Structural evolution in response to a cyclically applied perturbation can be resolved to time scales as short as the neutron pulse width—on the order of tens of microseconds.

Notwithstanding these past successes, it is important to articulate what cannot be done, either easily or at all, at the FTS. Because the peak brightness occurs at short wavelengths (0.1 nm), investigations requiring longer wavelengths (e.g., measurement of the *d*-spacings of complex crystal structures and composites) are difficult to perform because of the rapid drop-off in flux with increasing wavelength. This reduction in intensity also makes the FTS ill-suited for complementary (and simultaneous) transmission-based measurements, such as SANS.

Similarly, the temporal resolution at current facilities is significantly lower than is desirable for following time-dependent phenomena in near-real time. Critical limitations restrict our understanding of the evolution of structure and properties during synthesis, processing, and service—which, as noted, represents a key gap in our understanding of the behavior of structural materials. The challenge of tracking potentially rapid changes at multiple length scales under complex mechanical, electromagnetic, and thermal conditions requires a new generation of neutron facilities that support multiple measurements and analyses simultaneously from a single bulk sample in near-real time under realistic conditions (stress, strain, temperature, environment, etc.). A detailed understanding of how structure and properties evolve during synthesis and processing across multiple length scales, from subnanometer to microns, represents a crucial step in advancing scientific understanding of materials' performance. Such understanding can then be integrated into future models that also consider precursor materials and process variables (including reaction kinetics and pathways).

The interplay between these elements and property predictions is becoming increasingly important in the endeavor to fully understand and develop new materials with advanced functionality. The STS will combine sophisticated synthesis, processing, and analytical tools with highly configurable instrument layouts, tunable optics, and high-speed computational tools, which will allow studies not previously possible.

6.2 New STS Experimental Capabilities for Structural Materials

The STS offers opportunities to propel critical advances in characterization methodologies with beamlines combining multiple techniques such as diffraction, spectroscopy, and imaging. New instrument suites with higher flux, better resolution, wider *Q* range, unique detector layouts, improved focusing optics and integrated advanced sample environments will provide high temporal and spatial resolutions for in situ characterization. This will improve capabilities to probe even smaller sample volumes to understand complexities and variations in chemistries and macro-/microstructure that typically control essential materials properties such as (ion) transport under corrosion conditions, strength, and ultimate functional performance and reliability. With the existing suite of neutron scattering instruments, there are measurements that simply cannot be done today.

An integrated understanding of synthesis and processing at multiple length scales (from <1 nm to a few nanometers, through micrometers, to millimeters and beyond) represents a crucial step beyond (static) structure-based prediction of materials properties. The STS will incorporate multiple modalities, combining different neutron scattering analyses simultaneously from the same sample as well as combining neutron measurements with parallel measurement of materials properties and high-speed computational tools. The STS thus enables designing a beamline as a laboratory to explore matter under controlled perturbations such as combinations of deformation, pressure, temperature, or irradiation, with simulation of synthesis, processing, and service conditions.

The power and adaptability of the proposed STS instruments will allow a significant advance in the ability to conduct complex experiments in situ and in near-real time. At current neutron sources, a series of experiments is needed to study the features of materials via separate diffraction, SANS, imaging, and/or spectroscopy measurements. The multimodality potential of the new instruments built around the STS opens entirely new capabilities for materials science experiments, so that the measurements are made on the same volume of the same sample at the same time.

The next generation of advanced alloys will be increasingly complex and even hierarchically structured materials. The macroscopic properties of these materials result from multiscale interactions among features from the atomic scale to the microscale. Thus, probes are needed to simultaneously examine those features across those length scales as a function of time. The new capabilities at the STS will enable neutron diffraction, SANS, and Bragg edge imaging data collection and allow the observation of microstructural changes, such as changes in precipitate density and morphology, from the same sample volume. This capability will eliminate the ambiguity of comparing measurements taken with different techniques on different samples. The ability to simultaneously observe these phenomena on relevant time scales is essential to advance our understanding of how complex materials respond to realistic external stimuli. These insights into structure-property relationships will aid materials design; improve the reliability of critical structural materials; and provide new opportunities for the study of time-resolved phenomena and kinetics associated with processing, additive manufacturing (3D printing), and the development of new alloys to meet future needs in energy technologies, national security, and a wide range of manufacturing applications.

The new capabilities provided by the STS (i.e., high-intensity neutron beams over an extended energy range in energy) will greatly expand the opportunity to develop a synergistic program in materials synthesis and discovery. Historically, scaling up from the laboratory to the “real world” has been a major challenge. STS neutron instruments will leverage the high penetration depth to precisely probe small volumes buried in intact large-scale components, with a range of energies that will resolve microstructural details over a considerable length scale (i.e., from angstroms to microns), with high brightness enabling time-resolved studies. The STS will enable transformative strides in probing transient, time-dependent, and nonequilibrium processes in structural materials by simultaneously providing

- high brightness to enable rapid collection of data to capture structural evolution during processing or operation, and real-time capability to resolve interfacial structure and chemistry;
- high neutron flux at longer wavelengths to enable investigations of complex and low-symmetry materials; and
- new multimodal instrument concepts enabled by the wide bandwidth at the STS to permit simultaneous characterization of microstructural and crystallographic features across multiple length scales.

6.3 First STS Experiments

6.3.1 Understanding How to Overcome the Strength-Ductility Trade-off

The quest for materials with ever higher strengths that do not sacrifice other essential properties such as ductility and toughness is endless [Morris, 2017]. Since dislocations are the main carriers of plastic deformation in crystalline materials, putting obstacles in their path is a surefire way to increase strength. Unfortunately, this almost always degrades ductility and toughness [Ritchie, 2011]. There are, however, notable exceptions that defeat the strength-ductility trade-off [Gludovatz et al., 2014; Li et al., 2016]. Interfaces lie at the heart of their exceptional behavior; in particular, the dynamic generation of certain types of interfaces during deformation. Alternative approaches of enhancing strength have taken advantage of certain types of precipitates [Jiang et al., 2017] or nanoscale ordered interstitial complexes [Lei et al., 2018], although in those cases the ductility either decreased or stayed roughly constant. A key difference between these two sets of approaches is that the density of obstacles in the former (twin or phase boundaries) increases with strain, whereas in the latter, the density of precipitates and nano-complexes is fixed before deformation after which it does not change. Another difference is that, broadly speaking, the former approach is better suited to enhance ductility whereas the latter is better suited for improving strength. A combination of both approaches is therefore needed to maximize strength and ductility: that is, a high density of coherent, closely spaced precipitates in a metastable matrix that undergoes twinning and/or phase transformation under an applied stress. Furthermore, to maximize the strengthening due to precipitates, they should be ordered (to increase their resistance to cutting by dislocations).

While the broad outlines of how to accomplish the above goals are known, fundamental scientific questions need to be answered in order to develop a sound basis for alloy design. One important question addresses twin and phase boundaries: do they act merely to provide a steady (or even increasing) source of work hardening and thus delay the onset of necking instability in materials whose ductility is limited by premature necking, or do they also provide additional deformation modes to accommodate the applied strain and thus enhance ductility? Other central questions include the following:

- How do the crystal structures of the parent and transformed phases and any attendant volume changes affect strength and ductility?
- What are the effects of external constraints (e.g., those exerted by grain boundaries or precipitates) on the activation barriers for twinning and stress-induced phase transformations?
- Are there any synergies to be exploited between hardening due to increased dislocation storage on the one hand and generation of deformation-induced twin and phase boundaries on the other? (For example, one could envision delaying as much as possible the strain at which the processes of twinning and phase transformation are exhausted, which would allow maximum dislocation hardening to take place in the interim.)
- How can we control the metastability of the pretransformed matrix phase, and the volume fractions, morphologies, and sizes of the strengthening precipitates, to obtain the highest combination of strength and ductility?

Answering all of these questions will require in situ neutron diffraction experiments at the STS so that we can study the evolution of relevant microstructural features as a function of strain and temperature. In cases where one (or more) of the phases involved is ferromagnetic, performing the experiments in a high magnetic field may produce certain preferred morphologies during transformation whose effects on strength and ductility are currently unknown.

For the first STS experiments, we envision designing model alloys using computational thermodynamics approaches specifically tailored to answer one or more of the above questions. For example, alloys can be

designed so that their matrices are either face-centered cubic (fcc) or body-centered cubic (bcc) at elevated temperatures, with a tendency to transform to bcc or hexagonal close-packed (hcp) at low temperatures. The thermodynamic driving force for such phase transformations can be tuned by adjusting the alloy composition to enable complete (thermal) transformation during cooling at one extreme, or zero transformation at the other extreme, with various transient states in between where the structure is metastable. These metastable states can then transform during deformation under the influence of the additional driving force provided by stress. Metastability can be further tuned by constraining the transformation through the introduction of nanoscale ordered precipitates in the matrix that also serve to strengthen. In fcc alloys, the activation barriers for twinning and fcc-hcp transformation are closely related and depend on the stacking fault energy, which can be calculated reasonably well from first principles and therefore will help in the interpretation of the experimental results. In situ straining experiments will be performed as a function of temperature to determine the evolution of different phases with strain to understand quantitatively the relationship between phase transformations and work hardening rates (Fig. 6.1). Texture evolution with strain will be evaluated to distinguish between ordinary dislocation plasticity and twinning. Load shedding from one phase to another, which can be determined from their respective elastic strains, will help us understand how the global applied stress is partitioned among the different constituents, which in turn will shed light on potential stress-relief mechanisms that contribute to ductility. Small-angle neutron scattering will provide information on the precipitate distribution (size and volume fraction), which in combination with the phase analyses will allow a deeper understanding of how they interfere with both thermal and deformation-induced phase transformations. Correlative transmission electron microscopy (TEM) performed at the Center for Nanophase Materials Sciences will provide additional details of the precipitate structure, coherency, and chemistry, as well as dislocation cutting mechanisms. Together, these results will help in the development of broadly applicable scientific principles that can be used to design future generations of stronger and tougher alloys.

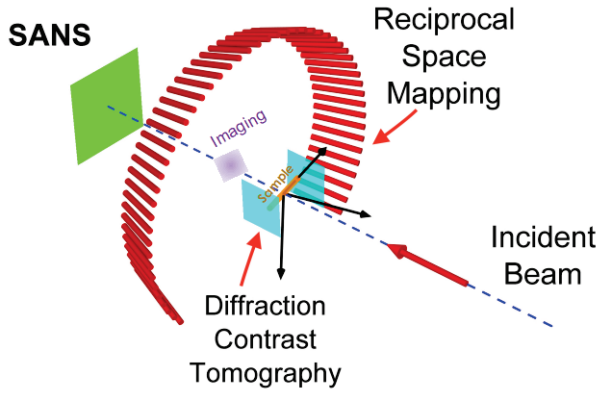

Fig. 6.1. Schematic of real-time in situ multimodal experiments at the STS. Multidirectional lattice strain, phase transformation, precipitation, texture, etc., can be measured by diffraction, diffraction contrast tomography [Wu et al., 2018], SANS, and imaging. Image source: ORNL.

In connection with the in situ mechanical tests outlined above, the STS offers unique capabilities that are not currently available elsewhere. It provides high flux at longer wavelengths, which enables multiscale analysis of microstructural features over the wide length scales of interest in phase transformations, from nanometer to millimeter, by using simultaneous scattering and transmission measurements. The high flux at longer wavelengths also allows the larger *d*-spacings of ordered superlattices (strengthening precipitates) to be determined; this is currently difficult to accomplish because the flux is high enough only at shorter wavelengths, where unfortunately there is considerable overlap of the fundamental diffraction lines. Because of the unique detector geometry planned, simultaneous measurement along three orthogonal directions will be possible. The high brightness of the STS will allow continuous data collection while the specimens are being strained, as opposed to experiments on complex materials with current beamlines, on which the straining must be stopped for a long enough time (on the order of many minutes) to collect sufficient data during which stress relaxation processes occur in the material, greatly complicating interpretation of results (especially if bidirectional transformations occur, as recently reported by Lu et al. [2018]).

6.3.2 Exploring the Fundamentals of Additive and Metamorphic Manufacturing

As previously mentioned, a key gap in our understanding of structural materials is what happens during processing. In situ processing of bulk specimens will enable a deeper understanding of the elementary steps that make up the overall process and of microstructural changes as they occur. Both are difficult (and sometimes impossible) to deduce after the fact. Synthesis of materials is a process that is well suited for in situ investigation at the STS; here we discuss its application to structural materials.

Among the various synthesis routes available for structural materials, additive manufacturing (AM) has the greatest potential to revolutionize how parts and structures will be built in the future. AM uses powder or wire feedstock that is heated with focused, computer-controlled laser or electron beams to build 3D structures layer by layer (Fig. 6.2). Among the advantages of AM are increased energy efficiency, lower environmental impact, the ability to produce parts on demand, and the ability to manufacture complicated shapes, which enables innovative designs [Frazier, 2014; DebRoy et al., 2018]. AM can also produce gradients in composition and, therefore, gradients in microstructure and properties [Dobbelstein et al., 2019].

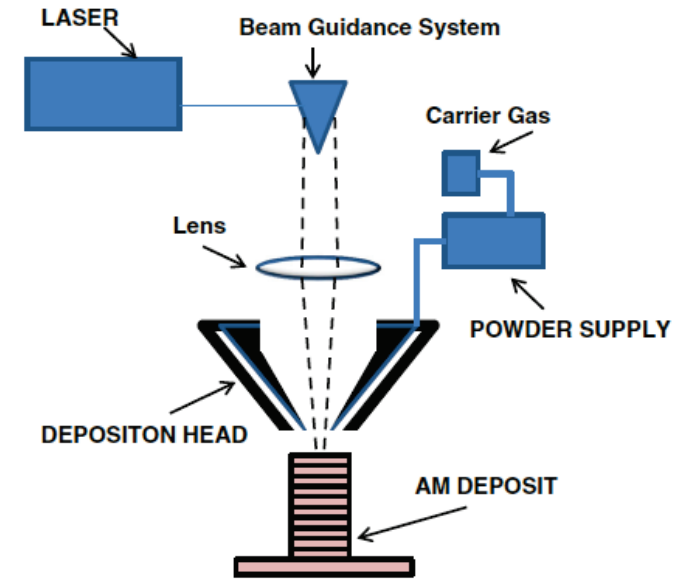

Fig. 6.2. Schematic of powder-fed additive manufacturing setup with a scanning focused laser beam for heating. Image source: Reprinted with permission from Frazier [2014, Fig. 2].

There are significant differences between materials synthesized by AM and those produced conventionally—for example, residual stress distribution, microstructural anisotropy [DebRoy et al., 2018], and the formation of certain defects such as pores, spatter, and denuded zones [Khairallah et al., 2016]. Many of these affect mechanical properties and can make it difficult to predict how AM materials will behave based on existing knowledge of conventionally processed materials. Moreover, the differences vary from alloy to alloy, and a detailed understanding of the responsible mechanisms is lacking. Without this understanding, predictability suffers, and each individual part and material must be developed by trial and error. A more thorough understanding of the relationships among process variables, microstructure, properties, and performance is therefore necessary. In general terms, from prior work on solidification and welding, it is known that the temperature gradient and the velocity of the solid-liquid interface affect its morphology, for example, whether it is planar, cellular, or dendritic, and the resulting microstructures (e.g., dendritic or equiaxed). The thermophysical properties of the melt and solid combined with the process variables such as heat input and cooling rate determine some of the defects that form during solidification. However, the discrete nature of the powder feedstock used in AM introduces complications that need to be accounted for. Sophisticated model simulations have proven successful in reproducing several critical defects that form during laser-based AM [Khairallah et al., 2016]. Experimental validation is challenging because it requires monitoring the process with precise spatial and temporal resolution. In situ studies using neutron diffraction/ absorption in conjunction with high-speed IR cameras will greatly advance understanding by bridging these gaps.

The third wave of digital manufacturing, after computer numerical controlled (CNC) machining and AM, is metamorphic manufacturing (MM), which has been referred to as "robotic blacksmithing" [TMS, 2019]. MM is still in its infancy, but the basic idea is to combine sensors, thermal control, incremental mechanical deformation, robotic manipulators, and real-time computational tools to make complex shapes in which the microstructures and properties can be controlled at specific locations. MM has the potential to overcome the biggest limitation of AM: its inability (by and large) to control local microstructure and properties. Therefore, MM working together with AM (i.e., thermomechanical processing integrated into the AM build process) has the potential to enable the control of composition, microstructure, and properties on demand, in a location-specific way, in complex shapes.

Many challenges (both engineering and scientific) must be overcome before MM can be widely deployed [TMS, 2017]; given that AM has been under development for almost three decades, a similar time scale can be assumed for MM. From a materials standpoint, we lack a quantitative, predictive understanding of processing-structure-property-performance relationships, especially when AM and MM are combined. Characterization is typically performed after the process is completed; in both AM and MM, however, in-process characterization of continuous change in structure and properties is needed to reveal how process variables affect performance. The various analysis methods that will become available at the STS, along with the uniquely large sample volume afforded by the high-brightness source, will enable in situ measurements of materials structure and mechanical properties during the build process, which cannot be done anywhere else.

We envision the first STS experiments to be performed on high-melting-point refractory metals that maintain strength at high temperatures and are resistant to attack in harsh environments, such as liquid metals. They are difficult to synthesize using conventional processes but can be produced by AM [Dobbelstein et al., 2018, 2019; Li et al., 2019]. For decades, their poor ductility has remained stubbornly intractable, but recent results have shown that the ductility of certain refractory metals can be significantly enhanced by the so-called high-entropy approach of combining four of more principal elements in high concentrations [Senkov and Semiatin, 2015], while the strength-ductility combination can be maintained at a high level by adding a light element in low concentrations [Lei et al., 2018]. The poor ductility of refractory metals is generally ascribed to an insufficient density of mobile dislocations. MM can be utilized to controllably introduce mobile dislocations above the ductile-brittle transition temperature during the AM process, thereby enhancing ductility. Additionally, the complex microstructures enabled by AM have recently been shown to defeat the strength-ductility trade-off in a conventional stainless steel [Wang et al., 2018], which offers the hope that it might be possible to employ AM and improve mechanical properties in other materials, such as refractory metals, if the responsible mechanisms are understood. The Achilles heel of refractory metals is their poor oxidation resistance. Compositionally graded structures produced by AM have the potential to overcome this problem by creating an oxidation-resistant surface layer.

Introducing a vacuum chamber with a pulsed laser source and powder feeding mechanism into the beam will enable operando analyses of the AM process. By using premixed powders whose chemical compositions can be controlled on the fly, chemical gradients can be produced within the solidified part to achieve corresponding gradients in microstructure. Such gradients will produce gradients in physical, mechanical, and chemical properties. Chemical gradients in combination with applied external fields can be used to tune phase stability and, in turn, the microstructures that form in the material. While the anticipated temporal resolution of the neutron scattering experiments (~30 ms) cannot capture all of the phenomena of interest in AM, it is likely sufficient for the processes of interest in MM. Simultaneous characterization with high-speed cameras (30 μs) will get us most of the way to capturing many of the other phenomena of interest, such as changes in temperature gradients, recoil of molten particles, and denudation of powder particles. The fundamental mechanisms and principles uncovered through such

experiments will be indispensable in formulating new alloy design approaches for next-generation materials for extreme conditions.

6.3.3 Understanding Fundamental Corrosion Mechanisms

The economic cost of corrosion is estimated to be 3 to 4% of the gross domestic product of industrialized nations [Wood and Clarke, 2017; Wood et al., 2018]. On metal surfaces, the corrosion process is complex and involves oxides, hydroxides, and other thin films [Wood and Clarke, 2017]. In addition to time, environmental conditions such as stress, temperature, or radiation can alter the rates of corrosion processes. In spite of decades of corrosion research, the nature of passive films on metals remains poorly understood. In addition to passive films, conversion coatings and inhibitors are widely used for corrosion protection of metals. Although protective structures of some type must exist, interfacial structure has proven difficult to characterize. The problem is that conventional techniques are not able to resolve both the chemical and physical characteristics of nanometer-scale films. Current understanding of protection and failure, therefore, is largely based on indirect methods. In order to advance corrosion science, in situ methods to gain understanding of the fundamental relationship between process, structure, and performance are needed to allow investigation on time and length scales not possible today.

Neutron reflectometry has been extensively used to reveal interfacial structure and has been successfully used as a characterization tool in corrosion science, revealing changes of film composition, thickness, and roughness under corrosive environments [Hu et al., 2013; Hu et al., 2015]. Dong et al. [2011] were able to reveal the structure and morphology of a trivalent chromium process-coated aluminum surface in an aqueous solution under pitting conditions, while Wang et al. [2010] determined that vanadate-based inhibitor film forms a bilayer structure on the surface of an aluminum alloy, forming an effective water barrier. Welbourn et al. [2017] used neutron reflectometry, along with X-ray photoelectron spectroscopy (XPS), to characterize the inhibiting function of surfactant on copper and successfully demonstrated reflectometry's ability to distinguish adsorbed layers from an underlying oxide layer. An important advantage of neutron reflectometry for corrosion research is that it permits a greater range of sample environments, for instance, in vacuum, allowing for studies in well-controlled atmospheres as well as in aqueous environments, allowing for precision control of salinity, for example [Wood et al., 2018]. Neutron reflectometry also offers superior quantitative analysis not offered by conventional techniques. However, a limiting factor for the role of neutron reflectometry in corrosion research is the time required to acquire useful data for investigating kinetic behavior at the environment/surface interface.

Current neutron reflectometers typically require tens of minutes, at best, to acquire useful data due to lack of neutron brightness and broad wavelength flux; thus, quasi-static experiments are employed. The STS, with its high brightness and broad wavelength bandwidth afforded by its 15 Hz operation, will enable the acquisition of statistically significant neutron reflectivity data in real time, making it possible to investigate corrosion phenomena on time scales not available today. For instance, pit nucleation can occur in much less time than is required for anion diffusion across a passive barrier, on the order of seconds in some cases [Wood et al., 2018].

The new capability provided by the STS will allow the determination of the origin, evolution, and failure of passive oxide surfaces on stainless steels. Knowledge will be gained that is complementary to that gained by X-ray methods. Building on techniques perfected in investigations of corrosive behavior using the Liquids Reflectometer at the FTS, we will use neutron reflectometry to determine the film density and composition profile for pure iron and Fe-Cr-Mo alloys prepared by magnetron sputtering. Passive films will then be grown anodically while being continuously monitored with the neutron beam. The response of the film can then be observed under increasingly aggressive environments by performing neutron reflectivity measurements in a split liquid cell under electrochemical potential control (Fig. 6.3). The films will be monitored for the formation of pits and/or cracks in the surface and the subsequent progress of corrosive species formation on the surface as a function of time. It has been shown that effective

corrosion inhibitors preferentially absorb to a surface and can displace destructive corrosion species [Nut, 1970]. Addition of an inhibitor to the electrochemical system can then be monitored to determine rates of adsorption of inhibiting species and their underlying ability to mitigate the corrosive process.

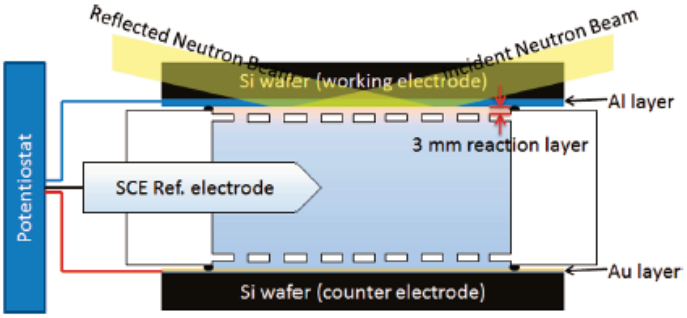

Fig. 6.3. Schematic of an electrochemical split cell for in situ neutron reflectometry measurements. Image source: Reprinted with permission from Dong et al. [2011, Fig. 2].

6.4 Conclusion

The STS will enable heretofore impossible studies of the evolution of the structure and properties of advanced structural materials during synthesis, processing, and service (operation). The knowledge gained will be critical to developing broad scientific guidelines for the design of next-generation structural materials. The key features of the STS that will make such advances possible are the high flux at longer wavelengths, the significantly shorter time needed for measurements, the smaller beam sizes with higher brightness that can be focused on regions of interest, and the large sample environment chambers in which multiple characterization techniques can be applied simultaneously.

References for Sect. 6

Crabtree, G.; Parise, J. (organizers), *Frontiers in Materials Discovery, Characterization and Application: Workshop Report,* UT-Battelle, LLC, Oak Ridge, Tennessee, 2014. Available at https://neutrons.ornl.gov/sites/default/files/CEMD Workshop Report Draft Oct19v4_Chicago.pdf (accessed June 8, 2019).

DebRoy, T.; Wei, H. L.; Zuback, J. S.; Mukherjee, T.; Elmer, J. W.; Milewski, J. O.; Beese, A. M.; Wilson-Heid, A.; De, A.; Zhang, W. *Prog. Mater. Sci*. **2018,** *92,* 112–224.

Dobbelstein, H.; Gurevich, E. L.; George, E. P.; Ostendorf, A.; Laplanche, G. *Addit. Manuf.* **2018,** *24,* 386–390.

Dobbelstein, H.; Gurevich, E. L.; George, E. P.; Ostendorf, A.; Laplanche, G. *Addit. Manuf.* **2019,** *25,* 252–262 (2019).

Dong, X. C.; Argekar, S.; Wang, P.; Schaefer, D. W. *ACS Appl. Mater. Interfaces* **2011,** *3*, 4206–4214.

Frazier, W. E. *J. Mater. Eng. Perf.* **2014,** *23,* 1917–1928.

Gludovatz, B.; Hohenwarter, A.; Catoor, D.; Chang, E. H.; George, E. P.; Ritchie, R. O. *Science* **2014,** *345,* 1153–1158.

Hu, N. P.; Dong, X. C.; He, X. Y.; Argekar, S.; Zhang, Y.; Browning, J. F.; Schaefer, D. W. *J. Appl. Crystallogr.* **2013,** *46*, 1386–1396.

Hu, N. P.; Dong, X. C.; He, X. Y.; Browning, J. F.; Schaefer, D. W. *Corros. Sci.* **2015,** *97*, 17–24.

Jiang, S. H.; Wang, H.; Wu, Y.; Liu, X. J.; Chen, H. H.; Yao, M. J.; Gault, B.; Ponge, D.; Raabe, D.; Hirata, A.; Chen, M. W.; Wang, Y. D.; Lu, Z. P. *Nature* **2017,** *544,* 460–464.

Khairallah, S. A.; Anderson, A. T.; Rubenchik, A.; King, W. E. *Acta Mater*. **2016,** *108,* 36–45.

Lei, Z. F.; Liu, X. J.; Wu, Y.; Wang, H.; Jiang, S. H.; Wang, S. D.; Hui, X. D.; Wu, Y. D.; Gault, B.; Kontis, P.; Raabe, D.; Gu, L.; Zhang, Q. H.; Chen, H. W.; Wang, H. T.; Liu, J. B.; An, K.; Zeng, Q. S.; Nieh, T. G.; Lu, Z. P. *Nature* **2018,** *563,* 546–550 (2018).

Li, Y.; Lin, X.; Hu, Y.; Kang, N.; Gao, X.; Dong, H.; Huang, W. *J. Alloys Cmpd*. **2019,** *783,* 66–76.

Li, Z.; Pradeep, K. G.; Deng, Y.; Raabe, D.; Tasan, C. C. *Nature* **2016,** *534,* 227–230.

Lu, W.; Liebscher, C. H.; Dehm, G.; Raabe, D.; Li, Z. *Adv. Mater.* **2018,** *30,* 1804727.

Morris, J. W., Jr., *Nature Mater*. **2017,** *16,* 787–789.

Nut, K. *Corros. Sci.* **1970,** *10* (8), 12.

Ritchie, R. O. *Nature Mater*. **2011,** *10,* 817–822.

Senkov, O. N.; Semiatin, S. L. *J. Alloys Cmpd*. **2015,** *649,* 1110–1123.

TMS (The Minerals, Metals & Materials Society), *Metamorphic Manufacturing: Shaping the Future of On-Demand Components*, TMS, Pittsburgh, PA, 2019. Electronic copies available at www.tms.org/metamorphicmanufacturing.

Wang, P.; Dong, X. C.; Schaefer, D. W. *Corros. Sci.* **2010,** *52,* 943–949.

Wang, Y. M.; Voisin, T.; McKeown, J. T.; Ye, J. C.; Calta, N. P.; Li, Z.; Zeng, Z.; Zhang, Y.; Chen, W.; Roehling, T. T.; Ott, R. T.; Santala, M. K.; Depond, P. J.; Mathews, M. J.; Hamza, A. V.; Zhu, T. *Nature Mater*. **2018,** *17,* 63–71.

Welbourn, R. J. L.; Truscott, C. L.; Skoda, M. W. A.; Zarbakhsh, A.; Clarke, S. M. *Corros. Sci.* **2017,** *115*, 68–77.

Wood, M. H.; Clarke, S. M. *Metals* **2017,** *7* (8).

Wood, M. H.; Wood, T. J.; Welbourn, R. J. L.; Poon, J.; Madden, D. C.; Clarke, S. M. *Langmuir* **2018,** *34*, 5990–6002.

Wu, W.; Stoica, A. D.; Berry, K. D.; Frost, M.; Skorpenske, H. D.; An, K. *Appl. Phys. Lett.* **2018**, *112*, 253501.

7. BIOLOGY AND LIFE SCIENCES

A fundamental principle of complex biological systems is dynamic hierarchical organization. These systems—including metabolic and signaling pathways, organelles, cells, organisms or ecosystems—are made of simpler, interconnected building blocks. However, even the simplest of systems, comprising a few distinct molecules, are a challenge to analyze. This is because these systems are dynamic, with component molecules catalyzing reactions through quantum mechanical proton and electron movements, making and breaking associations with other molecules and even changing their shapes (conformations) in response to stimuli. As described in a recent report on grand challenges for biological and environmental research, "The capacity to quantitatively predict functions in biological systems is not limited to static snapshots. To enable accurate understanding of dynamic processes, tools are needed to precisely probe systems in temporally or spatially controlled ways" [Stacey, 2017].

The unprecedented peak brightness and broader energy range of neutrons at the STS, together with associated advances in neutron optics and detectors, will transform neutron scattering capabilities for biological research. The brightness and energy range provided by the STS will make it possible to observe changes in biological systems in real time, using smaller samples, and across the multiple length scales relevant to biological systems, from quantum biological phenomena up to cellular scales. By combining the new capabilities of the STS with precision deuterium labeling, multimodal experimental environments (or techniques), and state-of-the-art high performance computing, time-resolved measurements will become possible, providing "movies" of collective motions in biomolecular systems and of cellular components as they interact in real time, forming functional complexes and higher-order hierarchical assemblies that span the organizational levels of the cell. Thus, development of a dynamic understanding of the function of complex, hierarchical biological systems will become possible, enabling advances in areas such as artificial photosynthesis, biocatalysis, and biopharmaceuticals.

7.1 Introduction

Natural systems demonstrate a mastery of physical laws and engineering principles against which the best artificial systems look primitive. Examples of this are highly selective catalytic processes, efficient energy conversion, and optimized materials synthesis. Biological systems are self-organizing, self-healing, highly specialized, adaptive and robust. Such emergent properties are the key to the complex, higher-order functions performed by cells—such as sensing, communication, transport, reproduction, adaptation, self-repair, movement, and memory.

A major goal of biological research is to elucidate the molecular basis of these remarkable processes, with the grand challenge of gaining a predictive understanding of the designs and mechanisms that underpin them [Alberts, 2011]. This knowledge will allow us to mimic the architectures and processes of living systems to create new biomaterials and bio-inspired technologies and will also provide detailed molecular and personalized descriptions of human biology and disease that will enable us to protect and repair physiological systems. The quest for such a predictive understanding has taken centuries and passed remarkable milestones, such as Mendelian genetics, the atomic structures of DNA and proteins, the first complete genome sequences, and recent gene editing technologies. However, much remains to be done.

Over the next decade, progress will continue at an increasing pace in determining the detailed atomic-resolution structures of biological molecules, such as proteins, using X-ray crystallography at advanced light source user facilities. High throughput -omic sciences (e.g., genomics, transcriptomics, proteomics, and metabolomics) combined with new gene-editing technologies (such as CRISPR/Cas) will increase our ability to manipulate biological systems and to improve our understanding of the relationship between gene and function—a grand challenge for biological and environmental research [Stacey, 2017].

Emerging techniques such as cryo-electron microscopy (cryo-EM) and free electron lasers will continue to be improved so that they have increasing impact, particularly in their ability to visualize larger protein complexes and assemblies that cannot be crystallized.

Harder to obtain will be an integrated view and a predictive understanding of the dynamic function of cellular components and molecular complexes within the living cell, and of how they are organized in time and space. Further, some key biological systems will remain recalcitrant to crystallographic and electron-based experimental techniques, including systems such as lipid membranes and intrinsically disordered proteins. This is where the application of neutron scattering will be most powerful, and the next decade is the time frame for the STS beginning operations with transformative new capabilities.

A major advantage of neutrons for the study of biological systems is that they interact directly with an atom's nucleus rather than its electrons. As such, they are highly sensitive to hydrogen (H), so they can locate important H atoms that are nearly impossible to detect with X-rays or electrons, even in atomically resolved structures. Moreover, neutrons are sensitive to motions of molecular systems and are nondestructive to delicate biological materials. Further, neutrons can readily distinguish H from its stable isotope deuterium (D), enabling a powerful experimental technique, unique to neutrons, called isotopic contrast variation [Jacrot, 1976]. Through the judicious substitution of D for H, contrast can be increased or eliminated, such that specific parts of a multicomponent biological system are either contrasted sharply or made invisible to neutrons. Isotopic contrast variation can also be applied within a single molecule, or even to an entire living cell (Fig. 7.1). These properties, combined with the nondestructive nature of neutrons, have made neutron scattering an important tool in biological sciences. Researchers use techniques such as small-angle neutron scattering (SANS), neutron macromolecular crystallography (NMC), reflectometry, neutron spin echo (NSE), and quasielastic neutron scattering (QENS) to study the structure and dynamics of biological systems, but their fields of application have been limited by the relatively low flux of available cold neutron beams [Ashkar et al., 2018]. The unprecedented peak brightness and broader energy range of neutrons at the STS will remove these limitations.

The structural basis of quantum biological processes involving proton and electron transfer has been difficult to see directly using standard crystallographic techniques. In contrast, neutron crystallography can locate protons at different stages of their pathways through proteins, thus definitively identifying reaction pathways and quantum chemical mechanisms, but the need for long collection times has limited the application of this technique to only a few biological systems. The higher brightness of STS will open up a world of biological enzymes and channels for this type of unambiguous study.

The STS will also begin operation in a remarkable era of biological research, characterized by the converging top-down synthetic simplification of known organisms approaching the minimum blueprint for life (including *Mycoplasma mycoides* JCVI-syn3.0 [Hutchison, 2016]) and the bottom-up construction of artificial cells (proto-cells) of increasing complexity and functionality [Blain and Szostak, 2014; Buddingh' and Van Hest, 2017]. A minimal form of the bacterium *Bacillus subtilis* has been proposed and will likely be created over the next few years [Reuß et al., 2016]. Complementary to these advances,

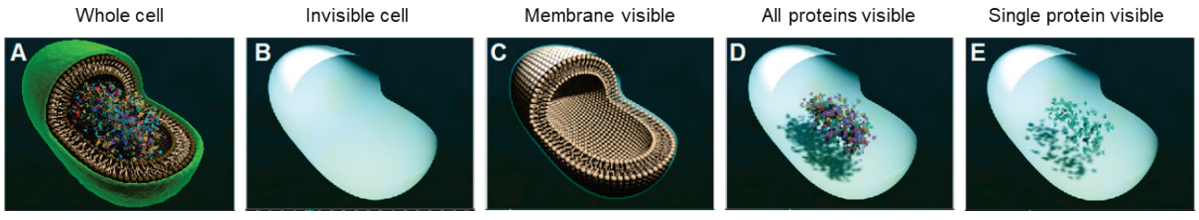

Fig. 7.1. Application of deuterium labeling and contrast matching. These techniques can highlight or mask the diffraction signal for certain members of a multi-component system. Image source: ORNL.

in 2017, at the FTS, a *B. subtilis* cell system enabled in-beam detection of raft-like domains in membranes of living cells, creating a new neutron-based observatory for in vivo analysis of biological structure and function [Nickels et al., 2017]. The STS will transform this observatory to real time, enabling the mapping of dynamics and kinetics of cellular processes in space and time. Subcompartments, reminiscent of organelles, have also been proposed and created, and it is potentially feasible to power artificial cells with light [Steinberg-Yfrach et al., 1998; Choi and Montemagno, 2005] or simple food molecules [Jewett and Swartz, 2004]. The STS will provide detailed characterization of these natural, composite, and hybrid materials across relevant length and time scales, enabling the principles and properties of biological organization, assembly, and cooperative response to be translated and incorporated into new functional biomaterials with tailored behaviors and biomimetic properties. As the STS comes on line, allowing researchers to experimentally characterize cellular processes, capabilities in exascale computing will enable simulation of these processes, allowing the mechanistic basis of physiological processes to be understood.

The examples illustrated in this section represent just some of the many outstanding biological challenges for which neutron science can elucidate key mechanisms. Processes such as photosynthesis, membrane signaling, the formation of organelles with membranes, and DNA repair combine mechanisms including catalysis, recognition, self-assembly, and self-organization across length scales from the atomic to the mesoscale, and across wide time scales. Uncovering the mysteries of these processes holds the key to new energy technologies, medical breakthroughs, superior materials, and novel devices. The STS dramatically extends the capabilities of neutron scattering to meet the challenges of this new frontier, delivering orders of magnitude gains in neutron brightness and capabilities that will enable us to watch biological events unfold in time on scales from the atomic and molecular to the cellular level.

7.2 New STS Experimental Capabilities for Biological Function

Through the new capabilities described below, the STS will lead the way toward widespread use of neutron techniques in biological research. It will enable new communities of researchers to address major challenges that cannot now be approached. The net result will be both broader use of neutrons and fuller realization of the potential of neutrons to produce unique insights in structural biology. The promise of the STS for biological research is to **make difficult and exotic experiments routine, and now-impossible experiments possible.** The STS will provide new ways to investigate how cellular components interact in real time, both with each other, and within the higher-order functional complexes and hierarchical assemblies that span the organizational levels of the cell and beyond. This will be accomplished through time-resolved spectroscopy, the characterization of biological structure across scales, and labeling and contrast matching schemes. When combined, these techniques offer unparalleled insights into dynamic biological phenomena from catalytic cleavage of covalent bonds to soil transport processes.

STS offers unprecedented peak brightness and a broader energy range for each incident neutron pulse, as well as much greater overall flux at the longer wavelengths that are essential for biological studies. Further, innovations in neutron optics and other technologies, such as dynamic nuclear polarization, will provide instrument performance gains of two orders of magnitude or more. Together, these improvements will result in a dramatic reduction in data collection times while also allowing the use of smaller samples, an important consideration because some biological samples are difficult to obtain. Specific new capabilities enabled by STS include:

Time-resolved measurements of kinetic processes and beyond-equilibrium matter. Understanding biological systems requires more than static pictures of individual molecular components—it demands "movies," or cinematic measurements, that show the dynamic behavior of these components in action. At present, neutron scattering has mastered the "still photo" level of analysis. Using isotopic contrast

variation, it is now possible to study the overall size and shape of stable multimolecular complexes and the individual molecules within them. However, much of the relevant dynamic behavior is too fast to resolve because of insufficient time resolution due to the relatively weak flux of available neutron beams. The increased intensity at the STS will enable researchers to pass this threshold and gain access to the movies, resolved at minutes or seconds, that are required to follow biological processes in real time. Such time-resolved experiments have been much in demand but are not feasible at any current neutron facility. The ability to perform time-resolved studies is one of the most important transformative advances enabled by the STS. With the STS, measurement times for most techniques will be reduced by 100-fold and in some cases by more.

Simultaneous measurements of hierarchical architectures across unprecedented length scales, from the atomic scale to the micron scale and beyond. The STS band structure is ideally suited for biological study, as it will enable simultaneous measurements of hierarchical architectures across a broad range of length scales. This is important because biological processes are inherently multiscale, ranging from proton transfer and ligand binding on the molecular scale to cellular processes on the mesoscale.

Smaller sample and beam sizes that allow characterization of new biological systems. These characteristics are particularly important for biological systems. The increased flux of the STS creates new opportunities for probing smaller samples, which will expand by several-fold the number and classes of biological problems that can be investigated. Small sample sizes are key to spectroscopic measurements on proteins that are difficult to express, to scattering of dilute solutions, and to diffraction studies using small-crystal volumes. It is expected that net gains for neutron crystallography will be transformative, allowing precision analysis of much larger molecular complexes than currently possible, and with far smaller crystals.

Simultaneous examination of broad ranges of length, energy, and time scales for studying biological dynamics. Inelastic neutron spectroscopy techniques are powerful tools for measuring functional collective dynamics in biological materials. The wide wavelength energy range offered at the STS will revolutionize these techniques by improving the dynamic range covered. The potential gains in simultaneous wavevector and Fourier time coverage for NSE (see Sect. 8) will make it possible to address important scientific challenges that have previously been out of reach of NSE through dynamics measurements over wide Q-ranges and to 6 orders of magnitude in time, on systems that evolve from picoseconds to hundreds of nanoseconds. This direct measurement of global molecular dynamics is unique to neutrons and will be complemented by time-resolved structural studies using SANS over broad wavelength ranges corresponding to 1 nm to hundreds of nanometers in length scale. These STS experiments will provide data suitable for verification of many classical and quantum mechanical dynamics simulations.

Labeling and contrast variation in multicomponent systems. The unique way in which neutrons interact with matter can provide information about complex biological and environmental systems that can be difficult to obtain with other techniques. For example, because neutrons interact directly with atomic nuclei, hydrogen atoms are easily detected and can be readily distinguished from deuterium. This feature enables isotopic contrast variation, which can reveal the individual components within a multicomponent system. Moreover, their energies make neutrons ideal probes of motions in complex systems.

While deuterium labeling and contrast matching are not new capabilities, they will play critical roles in maximizing the value of the new STS instruments. Selective deuterium labeling allows some elements of a multicomponent system to become more visible, while contrast matching renders other elements invisible. Different classes of biomolecules, such as lipids, proteins, and DNA, have different elemental compositions and hence intrinsically different scattering length densities (SLDs). When the SLD of a

biomolecule matches that of the surrounding water, it is contrast-matched and invisible to neutrons (Fig. 7.2). Deuteration increases SLD, as shown by the arrow, allowing experimentalists to control contrast through deuteration of water and biomolecules. In 42% D_2O, ordinary proteins disappear, and only deuterated proteins are visible. Their structure and properties can then be studied in the context of partner proteins, which are present but invisible, as illustrated in Fig. 7.2. The increased STS neutron intensity will enhance the ability to distinguish between and contrast-match different classes of biomolecules.

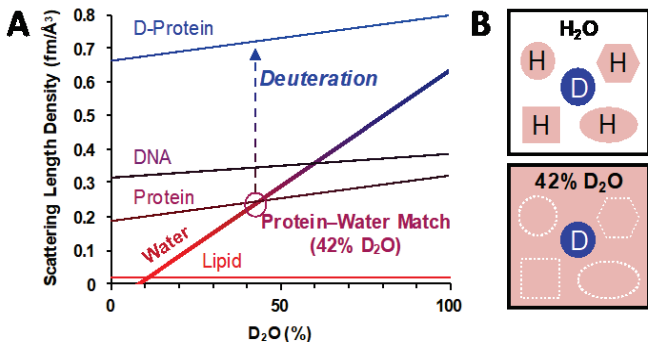

Fig. 7.2. Isotopic contrast variation. (A) SLD increases with deuteration, as shown by the arrow, allowing experimenters to control contrast through selective deuteration of water and biomolecules. (B) Contrast variation is illustrated with several species of interacting proteins, represented as different shapes. In H_2O (top), ordinary and deuterated proteins are contrasted from each other and the solvent; in 42% D_2O (bottom), only the deuterated protein is visible. Image source: ORNL.

7.3 First STS Experiments

7.3.1 Time-Resolved Disorder in Amyotrophic Lateral Sclerosis

Many proteins, such as enzymes, have well-defined three-dimensional (3D) architectures that allow them to be crystallized and permit analysis of their structures at atomic resolution. Intrinsically disordered proteins (IDPs) represent a completely different structural paradigm. They are highly dynamic and do not by themselves fold into well-defined structures. However, they are essential for many biological processes, and, indeed, 50% of all human proteins are either wholly or partially disordered. However, disordered does not mean disorganized, and IDPs are in fact prominent organizing features in many protein interaction networks, particularly signaling and regulatory pathways, where they may fold as a result of specific interactions or remain flexible and disordered in "fuzzy" complexes [van der Lee et al., 2014]. Networks of IDPs can even grow large enough to form distinct fluid phases within the cell, where they are referred to as membrane-less organelles [Mitrea and Kriwacki, 2016].

Establishing relationships between disorder and function is a major challenge. Neutrons can make substantial contributions to overcoming this challenge because of their unique ability to probe the heterogeneous conformations of disordered systems in solution. With the enhanced time resolution and extended spatial range and resolution of neutron scattering instruments at the STS, the advances in structural knowledge of IDPs and their complexes will provide a framework for understanding the molecular basis of neurodegenerative and other diseases, while providing insights for innovative therapeutics. Because many uncharacterized genes encode for IDPs, uncovering the genetic basis of plant and microbial phenotypes will be aided by understanding the structural mechanisms utilized by IDPs in recognizing their binding partners. In addition, disordered regions of otherwise ordered proteins, such as glycosylated linkers in cellulases that bind dynamically to cellulose, can have important biological functions.

Experiment description: The dynamic assembly of IDPs into important hierarchical structures with various pathologies provides a particularly important example of the need to understand the mechanisms of protein aggregation. Amyotrophic lateral sclerosis (ALS), also known as Lou Gehrig's disease, is an incurable neurodegenerative disorder that results in loss of voluntary muscle movement and, in most

cases, death within a few years of diagnosis. Recently, the misregulation of membrane-less organelles (phase-separated fluid regions in cells that arise where proteins and nucleic acids condense into dense liquid-like or hydrogel-like structures termed "stress granules" [Mitrea et al., 2016; Hyman et al., 2014; Weber and Brangwynne, 2012]) has been shown to be involved in this disease. In addition, mutations in a protein called FUS, an IDP, are linked to ALS and are thought to promote irreversible conversion of the protein from a functional, liquid-like state into pathological fibers (Fig. 7.3). The formation and aging of the liquid-like state in FUS have only recently been emulated in the laboratory [Molliex et al. 2015; Patel et al. 2015]. Physical changes are observed using fluorescence techniques over the course of seconds to minutes, but the underlying changes in molecular structure remain unknown. Understanding the formation and architecture of membrane-less organelles and FUS fibers will permit the molecular mechanism of the disease to be determined and pave the way for new therapeutic approaches.

SANS techniques can probe the architecture of networks within nucleoli and other membrane-less organelles, including those altered in neurodegenerative disorders such as ALS. Contrast matching techniques, in which selective deuterium labeling is employed, will make it possible to observe the individual components within multimolecular complexes and isolate the signal from FUS within membrane-less organelles. The high flux and broad dynamic range available at the STS SANS instrument will further facilitate time-resolved studies of the structural transitions in FUS that occur over seconds or minutes, providing insight into the molecular-level details of these dynamic processes. Further, the STS will permit direct structural observations of these transitions on relevant timescales and without the unwanted changes caused by exogeneous labels such as fluorescent dyes. These studies will provide new insight into the molecular mechanism underlying the formation of membrane-less organelles and FUS fibers and will allow researchers to conceive of ways of disrupting their formation. For example, if the shapes and locations of FUS are known, then computer simulations deriving the driving forces for aggregation can be used to predict the action of potential therapeutics and the design of new drugs.

The success of these studies will also enable new discoveries in the mechanism of action of amyloid proteins, another class of IDPs that can form aggregates, fibrils, and plaques, which are hallmarks of diseases such as Alzheimer's, Parkinson's, and Huntington's. While the exact mechanisms of pathogenesis are unknown, it is believed that conformational transitions in the disordered amyloid proteins lead to the formation of soluble aggregates that are toxic to cells long before they precipitate and become visible under the microscope. Mapping out the early steps in protein aggregation pathways, by

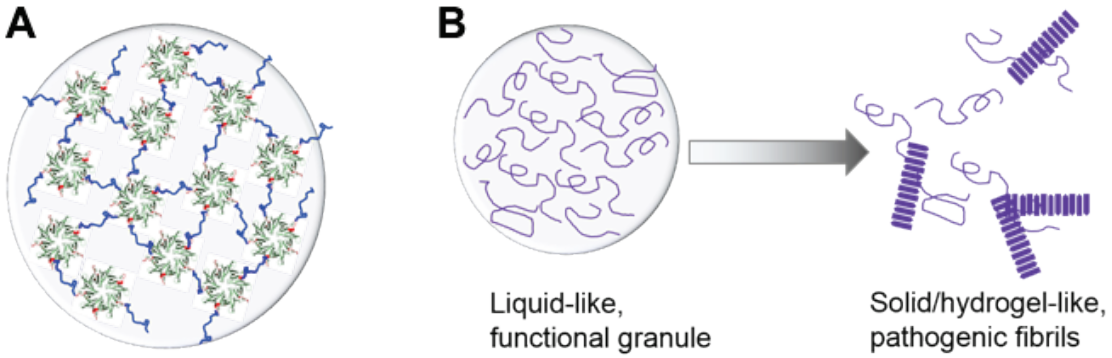

Fig. 7.3. Hijacking membrane-less organelles in ALS. Aging of ribonucleoprotein granules in neurodegenerative disease can be studied using high-flux, time-resolved SANS at the STS. (A) Schematic representation of protein-protein interactions leading to molecular assembly within liquid-like droplets. (B) Schematic of structural changes responsible for conversion of liquid-like ribonucleoprotein granules into pathogenic amyloid fibers associated with ALS. Image source: Courtesy of Diana Mitrea and Richard Kriwacki, St. Jude Children's Research Hospital.

identifying the various precursor structures and mechanisms of assembly, is critical to establishing their underlying roles in disease.

SANS has distinct advantages for studying amyloid proteins. It can detect conformational changes in individual molecules and then report on the formation of larger ensembles or aggregates under physiologically relevant conditions in solution. For example, time-resolved SANS at the FTS and HFIR provided new structural information on huntingtin, the protein responsible for Huntington's disease, and on how an abnormally expanded polyglutamine sequence in mutant huntingtin makes it highly susceptible to aggregation [Stanley et al., 2011]. However, structural information about the early events of aggregation is missing because of the limited neutron flux available.

The STS will overcome this limitation and provide, for the first time, the ability to obtain critical details about early events, over seconds to minutes, in the formation of aggregates in amyloidosis that cannot now be observed. With the use of selective deuterium labeling of the polyglutamine regions that are known to modulate the aggregation properties of huntingtin, the STS also will enable new time-resolved SANS contrast matching experiments to determine how the sequence context of huntingtin impacts internal structural changes across the entire aggregation reaction. Acquiring such key structural information is essential toward designing effective therapeutics to combat Huntington's disease and related amyloid disorders.

7.3.2 Understanding the Structure, Dynamics, and Function of the Microbial Cell Envelope

A major challenge for the next decades is to achieve an understanding of the structure, dynamics, and function of the microbial cell envelope at atomic detail. Information on the compositions of microbial envelopes is rapidly becoming available, and, for example, the lipid compositions of microbial membranes and many structures of membrane-associated proteins have been (and are being) determined. The time is therefore approaching where near-complete descriptions of the compositions of the cell envelopes of both Gram-positive and Gram-negative bacteria will be available. The challenge will then be to transform this compositional data into full 3D descriptions of functional microbial cell envelope structure and dynamics (see Fig. 7.4).

Neutrons will play a pivotal role in achieving this goal. Neutrons are a valuable tool for studying membranes because some membrane lipids are sensitive and easily damaged by X-rays or electrons, but not by neutrons. Moreover, membrane lipids are the most hydrogen-rich class of biomolecules and are thus ideally suited for H/D isotopic contrast variation. In addition, membranes are intrinsically dynamic, fluid structures. Neutrons have energies well matched to those of the relevant molecular motions, and inelastic neutron scattering techniques such as NSE can detect small transfers of energy between neutrons and molecules and thereby sense the collective motions and nanoscale diffusion of lipids or proteins in the membrane. Such dynamic measurements can then be connected with physical properties of the membrane, such as mechanical moduli. These themes, which apply universally across all biological systems, will drive neutron-based biomembrane research at the STS.

With the aid of selective deuteration of membrane components, experiments using SANS, reflectometry, and NSE will link composition to structure and structure to dynamics. Neutron scattering from microbial membranes will link these properties to function. Neutron experiments will also serve to benchmark the molecular simulations, specifically by refining their force fields, thus unleashing the predictive power of computation for the study of complex biological problems. Exascale supercomputing will provide simulation models of complete microbial membranes to synergize with and interpret neutron experiments.

Experiment description: How cell membranes are organized, both laterally and transversely, is of great importance to biology. In particular, the spatial organization of lipids and proteins in biological membranes has a functional role in the life of a cell. Experimental evidence now supports the participation of *nanoscopic lipid domains* in membrane processes including protein sorting, vesicular transport, and cell signaling. However, despite intense interest, the fundamental mechanisms controlling the emergence of lipid domains and their size have remained elusive. An obstacle that has prevented us from gaining an insight into these mechanisms is the lack of techniques capable of interrogating biomaterials at the nanoscale.

The high peak brightness of cold neutrons at the STS, in combination with advances in neutron optics, will result in much shorter data collection times. This will enable time-resolved studies capable of probing the response of H/D-labeled membrane components in vivo to environmental factors such as temperature, pH, and solute concentrations. Structural properties determined by SANS will be coupled with dynamic neutron scattering measurements using NSE, which provides detailed information of the membrane's mechanical properties. These studies will provide a molecular-level understanding of membrane organization, overcoming the current bottleneck in transforming compositional information into fully fledged envelope structure and function.

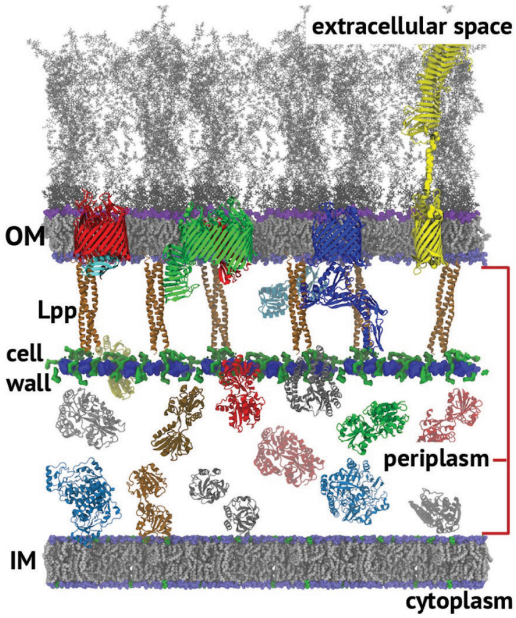

Fig. 7.4. Computer model of the cell envelope of a Gram-negative bacterium. Understanding the structure, mechanics, dynamics, and function of systems such as this at atomic detail will require integrating a range of STS experiments with computer simulations and specific labeling experiments. (OM: outer membrane; Lpp: lipoprotein; IM: inner membrane.) Image source: Reprinted with permission from Hwang et al. [2018, Fig. 1].

The STS will enable structural studies of biological membranes made of heterogeneous mixtures of lipids and other molecules in order to probe their functional aspects. In addition, it will be possible to access the relevant time scales to determine how membrane structure and dynamics impart function to membrane-embedded and peripheral proteins, and how local lipid composition affects their functionality. It is possible that in vivo, active processes such as protein/cytoskeletal interactions [Yethiraj and Weisshaar, 2007] or rapid lipid turnover [Turner et al., 2005] may prevent equilibrium conditions from being reached. Accordingly, measurements of live cells will be needed. However, these questions cannot be addressed with current instrumentation because of the inherently weak signals of overall dilute specific components such as membrane proteins and specific membrane domains in the context of in vivo studies, which result from limited neutron brightness. With the increased neutron brightness and longer wavelength neutrons of the STS, resolution of these central questions in membrane biology, which can be addressed only with neutrons, will become a reality.

The societal benefits of understanding microbial envelope function at the molecular level will be enormous. They can include the rational design of antimicrobial drugs that penetrate or disrupt envelopes of pathogenic microbes, the design of functional biomimetic membranes, the development of a predictive understanding of first-line microbial responses to external environmental perturbations, and the engineering of microbial membranes to improve their tolerance to the stressful conditions associated with biofuel/bioproduct formation.

7.3.3 Photosystem II: The Light-Activated Water-Splitting Enzyme

The photo-induced oxidation of water (H_2O) to oxygen gas (O_2) is one of the most abundant proton transfer processes in nature. Most of the oxygen in the atmosphere is generated by plants, algae, and cyanobacteria through this reaction. In photosynthetic organisms, the reaction is catalyzed by the multisubunit membrane protein, Photosystem II. At the center of this system is the oxygen-evolving complex (OEC), a small metal ion cluster (Mn_4CaO_5) that catalyzes the oxidation of H_2O, forming an oxygen-oxygen bond in a chemical reaction that is unique in nature. Artificial systems able to mimic photosynthesis would efficiently produce fuels, such as in photo-induced hydrogen production.

Experiment description: Pump-probe neutron diffraction, combined with the ability of neutrons to resolve hydrogen atoms, offers a unique tool for studying water splitting by photons in Photosystem II. With the new capabilities of the STS (i.e., the ability to collect data sets quickly and on small crystal sizes), it will be possible to obtain a detailed picture of the water environment of the catalytic site, allowing insight into the vital role of light-induced changes in the hydrogen bonding network and protonation around the active site. When H_2O is oxidized, it produces O_2 and protons and sequentially releases four electrons in an oxygen atom. This light-induced reaction is thought to involve different stable illuminated states in the five-state kinetic model for photosynthetic oxygen evolution originally proposed by Kok et al. [1970]. This model consists of four (meta)stable intermediates (S_0 to S_3) and a transient S_4 state, which precedes the formation of dioxygen. The oxidation state of the manganese atoms within the OEC cluster alters during the reaction, which illustrates the importance of using a probe that does not influence the oxidation states [Yano, 2005]; neutrons are thus ideally suited to follow the Kok cycle (see Fig. 7.5). The final stages of the cycle, which involve the transient S_4 state, are highly debated, largely owing to the inability of experimental techniques to capture this short-lived intermediate. Taking advantage of the proton location information contained within the neutron structures of the S_0–S_3 intermediate states, quantum mechanics/molecular mechanics (QM/MM) simulations will be used to model the transient S_4 state to complete a detailed understanding of proton transfer in the Kok cycle.

In this first experiment, diffraction data will be collected on the stable intermediates S_2, S_3, and S_0 of protein photosystem II, each generated by laser pumping, and entirely recorded before decay to the dark state (S_1) begins. Scaling preliminary low-resolution diffraction data collected at the FTS by the gains in brightness provided by the STS allows us to project that the diffraction resolution can be increased

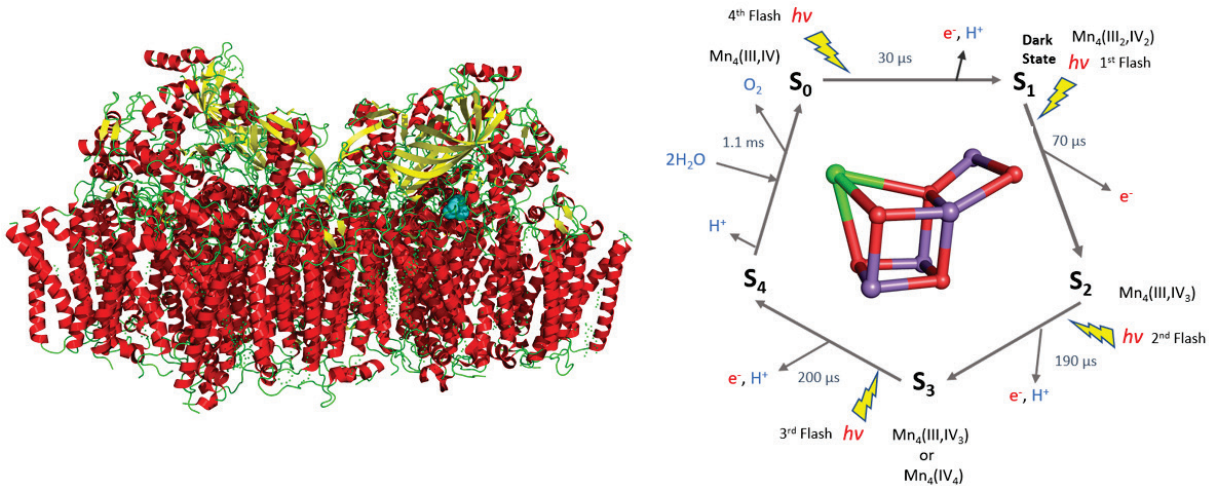

Fig. 7.5. Photosystem II and the Kok cycle. At left, the structure of the multisubunit photosystem II complex. At right, the classical Kok cycle with its five kinetic states (S_0 to S_4); a structural model of the OEC, an unusual metal cluster formed of manganese, calcium, and oxygen, is superimposed. The oxidation of H_2O is catalyzed via a series of light-induced transitions between the five kinetic states of the Kok cycle. Image source: ORNL.

sufficiently to visualize protons that are coupled with the electron transfer processes involved in water splitting. At existing neutron facilities, in order to visualize protons in a biological macromolecule, a neutron crystallographic structure is determined by collecting diffraction data from a crystal in several orientations—typically 20 to 30. At each orientation, the crystal is exposed for several hours to obtain sufficient diffraction signals. This approach makes time-resolved or parametric studies impossible. The high peak brightness and broad energy range of cold neutrons at the STS will enable visualization of crystal structures of macromolecules in relatively short periods of time with just one neutron exposure; the broad energy range will allow a large enough volume of reciprocal space to be simultaneously surveyed in a single crystal orientation; and the high peak brightness will enable measurements in a shorter time. This represents a transformative new capability to study proton transfer processes in biology.

The ability to rapidly acquire data throughout the Photosystem II reaction cycle will enable an analysis of the neutron scattering density from each data set and allow the proton transfer pathways to be mapped, providing critical insight into the full range of chemical mechanisms employed by Photosystem II to split water using photons. This vital information will accelerate the development of bio-inspired catalysts with impacts on areas ranging from fuel cells and solar cells to carbon capture technologies.

7.3.4 Harnessing the Catalytic Power of a Versatile Family of Enzymes

This experiment and the experiment described in Sect. 7.3.3 use neutron crystallography to study proton transfer, a process underlying many biological functions. For example, proton transfer is the foundation for almost all chemical reactions catalyzed by enzymes; is involved in many transmembrane-associated processes; and is also the chemical basis of photosynthesis, one of the most critical reactions in nature. Because protons are light particles, their transfer processes are inherently quantum mechanical, and biological proton transfer is an important element of quantum biology. Tracking the exact pathway taken by protons during these chemical reactions is therefore essential for gaining insight into fundamental biological processes at the quantum level. Because neutrons are highly sensitive to light elements and readily differentiate hydrogen from deuterium, neutron crystallography can be used to elucidate proton transfer processes at different stages of a chemical reaction. Further, neutrons probe biological samples without inducing radiation damage artifacts, such as altered oxidation states of catalytic metal centers [Yano et al., 2014].

Enzymes operate in water near neutral pH and ambient temperature, have exquisite substrate selectivity, and achieve remarkable rate accelerations. By coordinating the action of weak acids (proton donors) and weak bases (proton acceptors), enzymes can facilitate proton-transfer reactions that otherwise require extremes of temperature or pressure. Moreover, the design of strong inhibitors or biomimetic catalysts requires a knowledge of the reaction mechanisms of the enzymes and therefore the precise locations of active site hydrogen atoms. Neutron crystallography is unrivaled in its ability to provide detailed 3D structural information on proton locations in enzyme active sites.

Experiment description: We will utilize neutron crystallography to study a class of enzymes that modulate the catalytic activity of pyridoxal-5′-phosphate (PLP), a vitamin B6 derivative co-factor (see Fig. 7.6). Remarkably, PLP-dependent enzymes are capable of catalyzing more than 140 chemical reactions, such as transamination, racemization, decarboxylation, retro-aldol cleavage, etc., using a single PLP catalytic center. These enzymes are involved in neurotransmitter synthesis, amino-acid metabolism, and myriad other physiological pathways. Furthermore, pathogens such as *Mycobacterium tuberculosis* and *Plasmodium* and many other microorganisms depend on the action of PLP enzymes for their survival.

Our goal is to answer a fundamental question: how do PLP-dependent enzymes catalyze so many disparate biochemical transformations using just a single co-factor? The PLP co-factor is incredibly catalytically versatile. Which of the many possible reaction pathways is actually taken by any given PLP-dependent enzyme depends on the specific 3D protein environment in which the co-factor is embedded.

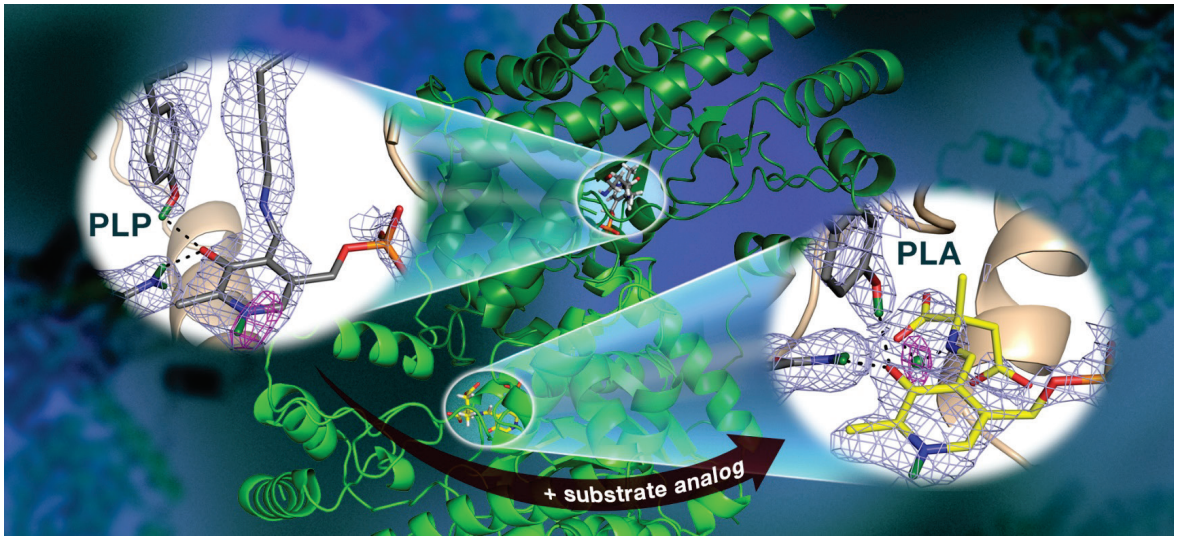

Fig. 7.6. The dimeric aspartate aminotransferase (AAT) enzyme and two active sites. The active site labeled PLP is the reactant state, while the site labeled PLA is the intermediate product state generated by addition of a substrate analog. Within the AAT crystal both states are obtained, as the chemical reaction occurs only in one active site (Dajnowicz et al., 2017). Image source: ORNL/Jill Hemman and Andrey Kovalevsky.

The electrostatic field of the protein determines the protonation states of groups on PLP during different steps of any given reaction, associated with intricate hydrogen-bonding networks, and this in turn corrals the enzyme along the specific reaction pathway. This makes PLP-dependent systems ideal for detailed study with macromolecular neutron crystallography. However, the limited flux on existing neutron crystallography instruments means that only one or two of these enzymes can be practically studied, and this is insufficient to derive the principles determining the highly variable reactions. The STS will enable much faster data collection from much smaller crystals to encompass a vast space of catalytic mechanisms without compromising on the details that need to be learned about the reaction pathways. These studies will explain how these enzymes catalyze so many disparate biological transformations.

This first experiment will focus on mapping reaction pathways catalyzed by the four families of PLP-dependent enzymes, distinguished by different 3D folds, from *Mycobacterium tuberculosis,* including the α-family (Fold I), the β-family (Fold II), the alanine racemase family (Fold III), and the D-amino acid, or branched chain amino acid, aminotransferase family (Fold IV). Fold I serine hydroxymethyl transferase is the major source of carbon atoms needed for synthesis of thymidine, necessary for DNA synthesis. Fold II O-acetylserine sulfhydrylase makes cysteine, an essential amino acid. Fold III alanine racemase makes D-alanine, which is required for bacterial cell wall maturation. Fold IV branched chain amino acid aminotransferase is needed for synthesis of essential amino acids, valine, leucine, and isoleucine.

Neutron structures of the active enzymes with the PLP co-factor bound (the internal aldimine state), with an enzyme-specific substrate bound (the external aldimine state), and with substrate analogs that allow trapping different stages of catalysis will be obtained. The hydrogen atom positions and hydrogen bonding interactions will be mapped along the reaction pathways in order to elucidate catalytic mechanisms and devise rules for substrate specificity of the four selected PLP-dependent enzymes. This first experiment will also make it possible to determine the hydrogen positions in complexes of the enzymes with the drug cycloserine, which targets alanine racemase. The understanding of a unique natural catalytic steering system gained from this first experiment will pave the way to similarly tuned biomimetic systems.

7.4 Conclusion

Neutron scattering can address frontier challenges in biological research by providing crucial elusive information that cannot be obtained using any other experimental method. The STS will dramatically extend the capabilities of neutron scattering, delivering orders of magnitude gains in neutron flux, and capabilities that will enable us to watch molecular events unfold in time. These advances will enable the use of neutrons in a transformative way, integrating structural and dynamical descriptions of biological systems, most notably in linking the atomic scale and mesoscale of cellular organization. For instance, the dynamic assembly of many biological complexes involves networks of competing inter-actions, which constantly assemble and disassemble in response to their cellular environment. Examples include large dynamic multicomponent complexes, some of which can act as molecular machines; multidomain proteins connected by flexible linkers; protein folding; intrinsically disordered proteins; transmembrane and membrane-associated complex systems; and even entire organelles and living cells. Breakthroughs in these areas will provide researchers with opportunities to improve the conversion of biomass to fuels and increase drought resistance in crops; to deliver vital information needed for the development of more effective treatments for cancer, drug-resistant infections, and neurodegenerative diseases; and to synthesize bio-inspired materials such as targeted drug delivery systems and biosensors.

The unique information provided by the STS will complement and extend information obtained from other user facilities utilizing techniques employing, for example, photons or electrons. The nondestructive nature of neutron scattering and its ability to use deuteration to highlight specific components position the STS as a forefront facility for the analysis of complex biological systems, both in vitro and in situ. It stands poised to make unique and timely scientific contributions that will accelerate the convergence—of natural with artificial, of physical with virtual, and of molecular with cellular—on which a predictive understanding of biology depends.

References for Sect. 7

Ahmed, M. A.; Kroener, E.; Benard, P.; Zarebanadkouki, M.; Kaestner, A.; Carminati, A. *Plant Soil* **2016,** *407,* 161–171.

Alberts, B. *Science* **2011,** *333,* 1200.

Amundson, R. Annu. Rev. Earth Planet Sci. 2001, 29, 535–562.

Ashkar, R.; Bilheux, H. Z.; Bordallo, H.; Briber, R.; Callaway, D. J. E.; Cheng, X.; Chu, X.; Curtis, J. E.; Dadmun, M.; Fenimore, P.; Fushman, D.; Gabel, F.; Gupta, K.; Heberle, F.; Heinrich, F.; Hong, L.; Katsaras, J.; Kelman, Z.; Kharlampieva, E.; Kneller, G. R.; Kovalevsky, A.; Krueger, S.; Langan, P.; Lieberman, R.; Liu, Y.; Losche, M.; Lyman, E.; Mao, Y.; Marino, J.; Mattos, C.; Meilleur, F.; Moody, P.; Nickels, J. D.; O'Dell, W. B.; O'Neill, H.; Perez-Salas, U.; Peters, J.; Petridis, L.; Sokolov, A. P.; Stanley, C.; Wagner, N.; Weinrich, M.; Weiss, K.; Wymore, T.; Zhang, Y.; Smith, J. C. *Acta Crystallogr.* **2018,** *D74,* 1129–1168.

Blain, J. C.; Szostak, J. W. *Annu. Rev. Biochem.* **2014,** *83,* 615–640 (2014).

Buddingh', B. C.; van Hest, J. C. M. *Acc. Chem. Res.* **2017,** *50,* 769–777.

Carminati, A.; Moradi, A. B.; Vetterlein, D.; Vontodel, P.; Lehmann, E.; Weller, E.; Vogel, H-J.; Oswald, S. E. *Plant Soil* **2010,** *332,* 163–176.

Carminati, A.; Schneider, C. L.; Moradi, A. B.; Zarebanadkouki, M.; Vetterlein, D.; Vogel, H-J.; Hildebrandt, A.; Weller, U.; Schuler, L.; Oswald, S. E. *Vadose Zone J.* **2011,** *10,* 988–998.

Carminati, A.; Vetterlein, D. *Ann. Botany* **2013,** *112,* 277–290.

Carminati, A.; Zarebanadkouki, M.; Kroener, E.; Ahmed, M. A.; Holz, M. *Ann. Botany* **2016,** *118,* 561–571.

Choi, H. J.; Montemagno, C. D. *Nano Lett.* **2005,** *5,* 2538–2542.

Dajnowicz, S.; Johnston, R.C.; Parks, J. M.; Blakeley, M. P.; Keen, D. A.; Weiss, K. L.; Gerlits, O.; Kovalevsky, A.; Mueser, T. C. *Nature Commun.* **2017,** *8,* 955.

Dhiman, I.; Bilheux, H.; DeCarlo, K.; Painter, S. L.; Santodonato, L.; Warren, J. M. *Plant Soil* **2017,** *417,* 1–17.

Hwang, H.; Paracini, N.; Parks, J. M.; Lakey, J. H.; Gumbart, J. C. *Biochim. Biophys. Acta, Biomembr.* **2018,** *1860,* 2566–2575.

Hyman, A. A.; Weber, C. A.; Jülicher, F. *Annu. Rev. Cell Dev. Biol.* **2014,** *30*, 39–58.

Hutchison, C. A., III; Chuang, R.; Noskov, V. N.; Assad-Garcia, N.; Deerinck, T. J.; Ellisman, M. H.; Gill, J.; Kannan, K.; Karas, B. J.; Ma, L.; Pelletier, J. F.; Qi, Z.; Richter, R. A.; Strychalski, E. A.; Sun, L.; Suzuki, Y.; Tsvetanova, B.; Wise, K. S.; Smith, H. O.; Glass, J. I.; Merryman, C,; Gibson, D. G.; Venter, J. C. *Science* **2016,** *351,* aad6253.

Jacrot, B. *Rep. Prog. Phys.* **1976,** *39,* 911–953.

Jewett, M. C.; Swartz, J. R. *Biotechnol. Prog.* **2004,** *20,* 102–109.

Kok, B.; Forbush, B.; McGloin, M. *Photochem. Photobiol.* **1970,** *11,* 467–475.

Labbé, J.; Jorge, V.; Kohler, A.; Vion, P.; Marçais, B.; Bastien, C.; Tuskan, G. A.; Martin, F.; Le Tacon, F. *Tree Genet. Genomes* **2010**, *7,* 617–627.

Lal, R. *Energy Environ. Sci.* **2008,** *1,* 86–100.

Mitrea, D. M.; Kriwacki, R. W. *Cell Commun. Signal.* **2016,** *14* (1), DOI: 10.1186/s12964-015-0125-7.

Mitrea, D. M.; Cika, J. A.; Guy, C. S.; Ban, D.; Banerjee, P. R.; Stanley, C. B.; Nourse, A.; Deniz, A. A.; Kriwacki, R. W. *eLife* **2016,** *5,* e13571.

Molliex, A.; Temirov, J.; Lee, J.; Coughlin, M.; Kanagaraj, A. P.; Kim, H. J.; Mittag, T.; Taylor, J. P. *Cell* **2015,** *163,* 123–133.

Moradi, A.B.; Carmina, A.; Vetterlein, D.; Vontobel, P.; Lehmann, E.; Weller, U.; Hopmans, J. W.; Vogel, H-J.; Oswald, S. E. *New Phytol.* **2011,** 192, 653–663.

Moradi A. B.; Carminati, A.; Lamparter, A.; Woche, S. K.; Bachmann, J.; Vetterlein, D.; Vogel, H-J.; Oswald, S. E. *Vadose Zone J.* **2012,** *11* (3), vzj2011.0120.

Nickels, J. D.; Chatterjee, S.; Stanley, C. B.; Qian, S.; Cheng, X.; Myles, D. A. A.; Standaert, R. F.; Elkins, J. G.; Katsaras, J. *PloS Biol.* **2017,** *15,* e2002214.

Patel, A.; Lee, H. O.; Jawerth, L.; Maharana, S.; Jahnel, M.; Hein, M. Y.; Stoynov, S.; Mahamid, J.; Saha, S.; Franzmann, T. M.; Pozniakovski, A.; Poser, I.; Maghelli, N.; Royer, L. A.; Weigert, M.; Myers, E. W.; Grill, S.; Drechsel, D.; Hyman, A. A.; Alberti, S. *Cell* **2015,** *162,* 1066–1077.

Reuß, D. R.; Commichau, F. M.; Gundlach, J.; Zhu, B.; Stülke, J. *Microbiol. Mol. Biol. Rev.* **2016,** *80,* 955– 987.

Schmidt, M. W.; Torn, M. S.; Abiven, S.; Dittmar, T.; Guggenberger, G.; Janssens, I. A.; Kleber, M.; Kögel-Knabner, I.; Lehmann, J.; Manning, D. A.; Nannipieri, P.; Rasse, D. P.; Weiner, S.; Trumbore, S. E. *Nature* (2011), *478* (7367), 49–56.

Stacey, G. (chair). *Grand Challenges for Biological and Environmental Research: Progress and Future Vision; A Report from the Biological and Environmental Research Advisory Committee,* DOE/SC-0190, U.S. Department of Energy, Washington, DC, 2017. Available at https://www.berstructuralbioportal.org/wp-content/uploads/2017/12/BERAC_Grand_Challenges_121117.pdf (accessed June 10, 2019).

Stanley, C. B.; Perevozchikova, T.; Berthelier, V. *Biophys. J.* **2011,** *100.* 2504– 2512.

Steinberg-Yfrach, G.; Rigaud, J. L.; Durantini, E. N.; Moore, A. L.; Gust, D.; Moore, T. A. *Nature* **1998,** *392,* 479–482.

Strobl, M.; Grünzweig, C.; Hilger, A.; Manke, I.; Kardjilov, N.; David, C.; Pfeiffer, F. *Phys. Rev. Lett.* **2008,** *101,* 123902.

Strobl, M.; Betz, B.; Harti, R. P.; Hilger, A.; Kardjilov, N.: Manke, I.; Grünzweig, C. (2016). *J. Appl. Crystallogr.* **2016,** *49,* 569–573.

Strobl, M.; Harti, R. P.; Gruenzweig, C.; Woracek, R.; Plomp, J. (2017). *J. Imaging* **2017**, *3,* 64.

Turner, M. S.; Sens, P.; Socci, N. D. *Phys. Rev. Lett.* **2005,** *95*, 168301.

van der Lee, R.; Buljan, M.; Lang, B.; Weatheritt, R. J.; Daughdrill, G. W.; Dunker, A. K.; Fuxreiter, M.; Gough, J.; Gsponer, J.; Jones, D. T.; Kim, P. M.; Kriwacki, R. W.; Oldfield, C. J.; Pappu, R. V; Tompa, P.; Uversky, V. N.; Wright, P. E.; Babu, M. M. *Chem. Rev.* **2014,** *114,* 6589–6631.

Warren, J.M.; Bilheux, H.; Kang, M.; Voisin, S.; Cheng, C-L.; Horita, J.; Perfect, E. *Plant Soil* **2013,** *366,* 683–693.

Weber, S. C.; Brangwynne, C. P. *Cell* **2012,** *149,* 1188–1191.

Yano, J.; Kern, J.; Irrgang, K.; Latimer, M. J.; Bergmann, U.; Glatzel, P.; Pushkar, Y.; Biesiadka, J.; Loll, B.; Sauer, K.; Messinger, J.; Zouni, A.; Yachandra, V. K. *Proc. Natl. Acad. Sci.* **2005,** *102,* 12047–12052.

Yano, J.; Yachandra, V. *Chem. Rev.* **2014,** *1148,* 4175–4205.

Yethiraj, A.; Weisshaar; J. C. *Biophys J.* **2007**, *93*, 3113–3119.

Zarebanadkouki, M.; Kim, Y. X.; Carminati, A. *New Phytol.* **2013,** *199,* 1034–1044.

8. APPLYING ADVANCES IN NEUTRON INSTRUMENTATION AND TECHNOLOGIES TO THE STS

The proposed Second Target Station (STS) at the Spallation Neutron Source (SNS) will incorporate advances in neutron instrumentation and technologies to provide enhancements in instrument performance of two orders of magnitude or more. These enhancements will enable scientific experiments that cannot now be conducted at any existing neutron facility worldwide. Advances in the technology that transports neutrons from the source to the sample position will enable fine control over the neutron beam characteristics to provide smaller, focused beams with selectable angular divergence. The need for polarized neutrons in quantum materials research has been clearly articulated (see, e.g., Sect. 4.3), and polarized neutron techniques underpin advanced methods such as Larmor (neutron spin precession) methods. Developments in the production and manipulation of polarized neutrons are facilitated by the cold neutron beams that are a key strength of the STS. The broad wavelength bandwidth of the STS enables new approaches to the design of neutron scattering instruments; instruments with the dynamic range needed to simultaneously measure changes in samples across all relevant length scales will be feasible, while the STS high neutron brightness will make it possible to make these measurements more rapidly, enabling time-resolved experiments that probe transient phenomena.

8.1 Introduction

The new science enabled by the unique characteristics of the STS source will be amplified by a suite of next-generation neutron scattering instruments, neutron optics, and computational tools to support the user community. Neutron optics transport neutrons from the source to the instrument and are used to tailor the characteristics of the neutrons that illuminate the samples. The capability to focus neutron beams to smaller samples while controlling their angular divergence will be enabled by novel mirror-optics designs incorporated into specific STS instrument concepts. Once neutrons scatter from the sample, neutron detectors must record the position and time at which the neutron is detected. New concepts for neutron detector technologies will be explored to meet the demands of neutron scattering instruments at the STS.

An important aspect of the development of next-generation neutron scattering instrumentation at the STS will be the integration of high-performance computing (HPC), coupled with the use of artificial intelligence (AI) and machine learning. While computational tools for analyzing and modeling neutron scattering data already exist, critical steps in data reduction and traditional analysis and parametrization often require direct manual and often iterative input and control by the researcher. This human factor frequently becomes the limiting step in exploiting the full scientific value of the data generated by neutron scattering, and this problem will be especially challenging at the STS. Recent developments in AI hold great promise to enhance our ability both to analyze neutron scattering data sets and to recognize scientifically relevant features that may have been hidden or difficult to identify with traditional methods—and even to provide new ways to design and execute experiments. Deep learning is a rapidly developing technology that has great potential to maximize the science impact derived from these data.

Advances in neutron scattering instruments, neutron optics, and computational data are all key to delivering next-generation experimental capabilities at the STS, including:

- Time-of-flight methods that support recording of individual detected neutrons, enabling an experiment to be “replayed” one detected neutron after another and correlated with changes in the sample environment or conditions
- Time-resolved and cinematic measurements of kinetic processes and beyond-equilibrium matter

- Smaller sample and beam sizes that support measurements in extreme fields or of limited sample quantities
- Simultaneous measurements across broad length scales to observe hierarchical organization in complex materials

8.2 Neutron Optics

The field of neutron optics includes techniques to transport, focus, monochromatize, polarize, or otherwise manipulate the state of a neutron beam. Neutron guides typically consist of a rectangular tube whose interior surfaces are coated with a neutron-reflective material. The neutron beam is then confined within the guide by total external reflection and is guided from the neutron source to the sample position in a manner analogous to how light is guided with a fiber optic. The neutron refractive index n for most materials varies only slightly from 1.0, the value for vacuum or air, so that $1 - n \approx 10^{-6}$. This means that the critical angle for total external reflection is very small, less than 0.1°/Å—the value it achieves for a nickel coating. A neutron with wavelength 1 Å has a critical angle of only 0.1°, while a 2 Å neutron has a critical angle of 0.2° for a nickel-coated surface. Neutrons that arrive at the reflecting surface at an angle greater than the critical angle are not reflected and are "lost." Nickel was one of the original materials used for coating the reflecting surfaces of the guide; the critical angle for other materials is often expressed relative to the value for nickel as a reflective index m. A coating with a reflective index of $m = 1$ would be equivalent to nickel, and a coating with a reflective index of $m = 2$ would have a critical angle twice that of nickel for a given neutron wavelength.

Supermirrors extend the reflective index of guide coatings to $m = 7$ and beyond by combining refraction with diffraction from a graded multilayer coating. Even so, the critical angles are limited to no more than a few degrees, which in turn severely limits the set of optical techniques available for neutrons. However, the combination of the high-brightness/long-wavelength moderators planned for the STS and the availability of high-quality high-index ($m > 7$) supermirror coatings will enable the use of more sophisticated neutron optics than has been feasible in the past and opens up new possibilities for neutron transport.

8.2.1 Neutron Beam Transport

An important consideration in neutron scattering instrument design is determining the neutron phase space requirements for a given instrument and designing the optics of that beamline to deliver only what is needed as efficiently as possible. These requirements include the range of neutron wavelengths desired, the range and distribution of vertical and horizontal neutron beam angles, the size of the beam at the sample position, and a spin variable if the instrument uses polarized neutrons.

In analyzing neutron transport, it is useful to represent the neutron in a six-dimensional phase space representation that uses three conjugate momenta and three canonical position coordinates. The neutron beam is an ensemble average of the individual neutrons that it comprises. The neutrons in the beam can be conditioned for optimal transport by undergoing only one or two reflections at the entrance to the transport optics and then reshaped for scattering, diffraction, or imaging at the far end. To increase the neutron flux (the number of neutrons per area per second) reaching the sample, previous-generation neutron guides that were illuminated by large, less "bright" moderators frequently delivered beams that were larger than the sample and required apertures near the sample to define the beam spot size; however, these additional neutrons have the potential to raise the background near the sample position and decrease the overall signal-to-noise ratio. As a result of the high brightness and compact size of the STS moderators, coupled with the use of high-index supermirrors, more phase space volume can be captured at the entrance of the neutron transport system simply because there are more neutrons within the wavelength range and solid angle that the optics can accept. Consequently, much greater control of the

phase space transport is possible, resulting in a much-improved signal-to-noise ratio for experiments and a reduction in the need for beam apertures near the sample position.

8.2.2 Neutron Focusing/Imaging Optics

Several important techniques first developed for X-ray optics can now be implemented effectively on neutron scattering beamlines because of advances in neutron guide coatings. When combined with the high-brightness STS moderators, these techniques will enable more efficient beam transport and control over the neutron phase space, which is particularly important to create the small beam spots that are a signature of many proposed STS instruments. Examples include axial-symmetric focusing techniques such as Wolter mirrors [Liu et al., 2013a, 2013b] and off-axis imaging techniques such as Kirkpatrick-Baez (KB) mirrors [Ice et al., 2010; Meilleur et al., 2013].

Techniques that image the entrance aperture onto the sample position are generally more constrained than focusing optics in both wavelength bandwidth and beam divergence, but they offer the possibility of controlling the size and shape of the beam cross section at the sample position without significant change in the flux or angular divergence by employing an adjustable aperture far upstream rather than near the sample. In addition to KB mirrors and Wolter optics, techniques that can now be implemented using the high-brightness moderators at the STS include plane grating monochromators, twin parabolic mirrors, ellipsoidal mirrors, polycapillary focusing, various types of one- and two-dimensional gratings, and Fresnel zone plates.

8.2.3 Polarizing Supermirrors

In conjunction with the development of high-index supermirrors, high-quality, high-*m* polarizing neutron mirrors are also now available. Polarized neutron scattering, which can be used to distinguish magnetic from nuclear scattering, is an exquisite probe of magnetic structure and dynamics in materials. Polarized neutrons also enable neutron spin precession methods such as neutron spin echo. In addition to polarizing ^{3}He spin filters and field gradient–type polarizers, a neutron beam can be polarized by diffraction from a monochromator or by reflection from a mirror that has a different scattering cross section for the two neutron spin states. Polarizing neutron mirrors are advantageous because they are less expensive and more readily available than older technologies such as Heusler, ^{57}Fe, and FeCo monochromator crystals, and they are far less complicated and more user friendly than ^{3}He spin filter setups. Their application is particularly attractive for the polarization of cold neutrons because the critical angle of reflection increases linearly with neutron wavelength, enabling the transport of more highly divergent neutron beams.

Among the most impressive implementations to date is on the WASP high-intensity spin-echo spectrometer now being commissioned at the Institut Laue-Langevin (ILL), where the mirrors are used to analyze the polarization of the scattered neutron beam across a wide angle [Bigault et al., 2014]. At the STS, mirrors of this type, in combination with the high-brightness, long-wavelength spectrum of the moderators, will enable highly efficient manipulation of the polarization of the neutron beams.

8.3 Polarized Neutrons and Larmor Methods

Many of the latest innovations in neutron techniques and instrumentation use polarized neutrons either as a probe of magnetic structure and phenomena (identified as a key capability of several STS instrument concepts, such as the cold neutron chopper spectrometer and the versatile magnetic diffractometer) or for spin precession (Larmor) methods to access long length or slow dynamics, as required for many experiments in soft matter (Sects. 3.3.1 and 3.3.3) and biological science (Sect. 7.3.2). The STS provides an ideal environment for these experiments because its beams of cold neutrons will enable access to the slowest dynamics and longest length scales.

With Larmor methods, the main objective is to significantly enhance the experimental resolution in a particular scattering variable (such as energy transfer ħω or momentum transfer Q) by encoding this variable in the neutron spin precession angle and measuring the beam polarization. The resolution gain thus achieved can be much greater than with a conventional approach in which the beam is made either more monochromatic or less divergent (or both). Critically, the resolution gain is also largely decoupled from the intensity loss resulting from a conventional approach to improving the resolution; however, this gain is not "free" as it costs neutron flux to polarize a beam, and it is more difficult and time-consuming to measure polarization in addition to the scattered neutron intensity. Most importantly, however, the fundamental limit for the resolution gain is a function of the amplitude and homogeneity of the magnetic field that is involved. Fundamentally, Larmor methods are the only current approaches that break the inverse relationship between improving the resolution in a scattering variable and losing intensity.

Larmor methods have generally been developed using monochromatic neutron beams because neutron polarizing devices have traditionally performed best in a narrow wavelength band. Advances in broad wavelength devices, such as the polarizing supermirrors described in Sect. 8.2.3, combined with the greatly increased cold neutron brightness of the STS open the door to much greater and far more effective use of these methods at a time-of-flight (TOF) neutron source that uses a broad wavelength band. Two examples that illustrate advantages that could be achieved at the STS are described below.

Wide-angle neutron spin echo: A wide-angle neutron spin echo (NSE) instrument at the STS would provide an entirely new capability to the scientific community to study coherent dynamics of materials. Conventional NSE measures the intermediate scattering function $S(Q,t)$ by scanning the wave vector Q and the Fourier time independently and sequentially. Recent advances in NSE techniques incorporate the use of a large bank of detectors to cover a wide Q-range (for example, WASP at ILL, Grenoble) [Fouquet et al., 2007].

A TOF wide-angle NSE instrument at the STS would take advantage of a wide wavelength bandwidth (approximately 4.5 Å) and the high flux of cold neutrons to measure wide Q and Fourier time ranges simultaneously, for the first time, as illustrated in Fig. 8.1. This instrument will not reach the ultimate correlation time (Fourier time) of a high-resolution, solenoidal NSE because of the magnetic field geometry it employs, but will reach a realistic upper limit of ~100 ns. The STS wide-angle NSE instrument will be optimized for studying diffusion of atoms and spin excitations on atomic and molecular length scales (0.1–10 nm) with typical counting times for individual spectra estimated at minutes, enabling time-resolved dynamic studies in soft materials or in situ investigations of time-dependent molecular dynamics. Typical applications include studies of the motion of biological functional groups, dynamics in molecular magnets, dynamics of 1D and 2D confined molecules, and understanding systems near the glass transition (as illustrated in Fig. 8.1). In addition, the high count rate estimated for this instrument will enable studies of small samples. Adding an operational mode as a polarized beam chopper spectrometer (with one additional neutron chopper) would expand the dynamic range of the instrument by two orders of magnitude toward short correlation times.

Angular resolved spin echo: The use of Larmor precession in small-angle scattering and reflectometry experiments is an emerging field. In this application, Larmor precession is used to encode the neutron scattering angle in the phase of the neutron spin [Bouwman et al., 2008]. This allows neutron scattering techniques to measure very small scattering angles without extreme collimation of the beam and the commensurate loss in flux on sample and neutron count rate. These methods may be considered either for a dedicated STS instrument or as "add-ons" to more conventional neutron scattering instruments.

One approach that could be incorporated at a traditional SANS instrument is spin-echo-modulated SANS (SEMSANS) [Strobl et al., 2012]. This approach does not compromise the performance of the instrument. An instrument incorporating a SEMSANS option is operating at the European Spallation Source (ESS)

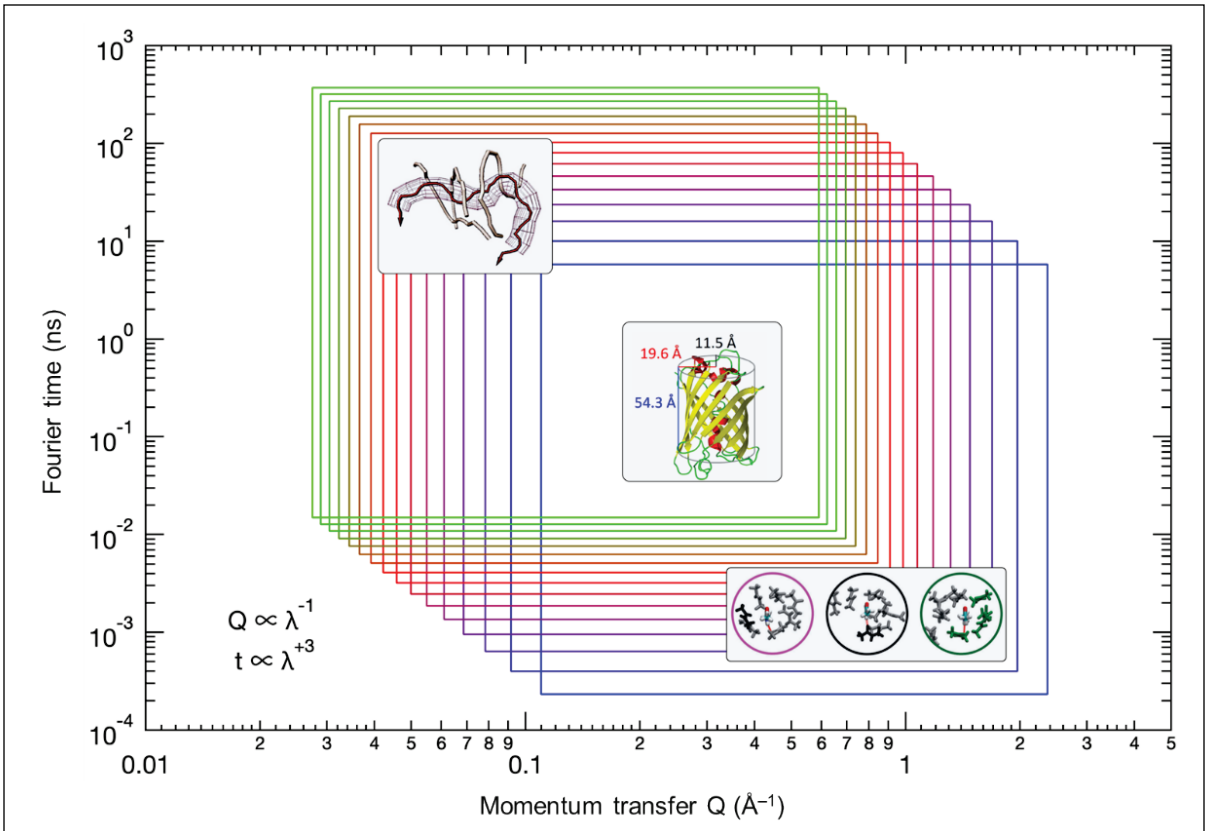

Fig. 8.1. Illustration of the range of Fourier time and momentum transfer measured by a wide-angle NSE at the STS. Neutron wavelengths are color-coded from 5 Å (blue) to 20 Å (green) in steps of 1 Å. Each neutron wavelength probes motions within its rectangular box. At a reasonable instrument length, a range of 4.5 Å within 2–20 Å can be used simultaneously when the instrument is operated at 15 Hz, or twice this in pulse-skipping mode. Slower motions occurring on larger length scales are measured to the upper left of this domain space, while faster motions on smaller length scales are sampled to the lower right. The insets illustrate the types of motions that could be characterized in the indicated region of the graph: at upper left, polymer diffusion [Polymer Reptation, 2019]; in the center, range of motions in a protein [Perticaroli et al., 2017a]; and at lower right, single molecule dynamics and the glass transition [Perticaroli et al., 2017b]. Image source: ORNL; insets reprinted with permission.

[Kusmin et al., 2017]. Incorporating such an option into a SANS and/or SANS/WANS instrument at the STS would extend the maximum length scale to at least 10 μm with a reasonable development goal to reach a length scale of 50 μm.

8.4 Neutron Detectors

Although neutron detector technology has advanced rapidly over the past 10 years, the smaller, brighter neutron beams of the STS will require new detectors with higher spatial resolution (smaller pixels) that are capable of higher neutron count rates than current technologies can support. Instrument types that are particularly demanding include SANS, SANS/WANS, reflectometers, and single-crystal diffractometers, all of which are represented in the instrument concepts described in Sect. 8.7.

Recent developments at ORNL in scintillator-based technologies are leading the way to meeting the requirements of these instrument types. Anger logic technology uses an array of sensors to measure the cone of light emitted from a scintillator upon neutron absorption and then triangulates to the spot where

the event occurred. Recent advances in this technology using silicon photomultipliers (SiPMs) as light sensors have demonstrated 0.7 mm FWHM spatial resolution (see Fig. 8.2), which is adequate for use on the FTS and HFIR neutron scattering instruments; however, continued development will be needed to reach the 0.3 mm requirement of the STS single crystal diffractometer (see Sect. 8.7.6). The STS reflectometer will require a detector with the highest linearity and highest small-area count rate, ~100 $n \cdot mm^{-1} \cdot s^{-1}$ (100 times the requirement for the SANS instruments) over a local area approaching 100 mm^2 within a total 400 cm^2 detection area to support its cinematic mode of operation.

ORNL is in the early stages of developing a new pixelated, scintillator-based detector with the potential to meet these requirements, but further development will be required. As recent developments in support of the ESS reflectometers mature [Mauri et al., 2018], they will also be considered for use on the STS instrument.

Other instrument concepts described in Sect. 8.7 rely on large-area arrays of detectors (up to tens of square meters). Traditionally, these instruments would often have used large numbers of ^{3}He-filled tubes to measure the scattered neutrons. ^{3}He-based detectors have desirable characteristics for many neutron scattering applications, including low gamma sensitivity, high uniformity of response, and high neutron counting efficiency; they represent a mature and robust technology.

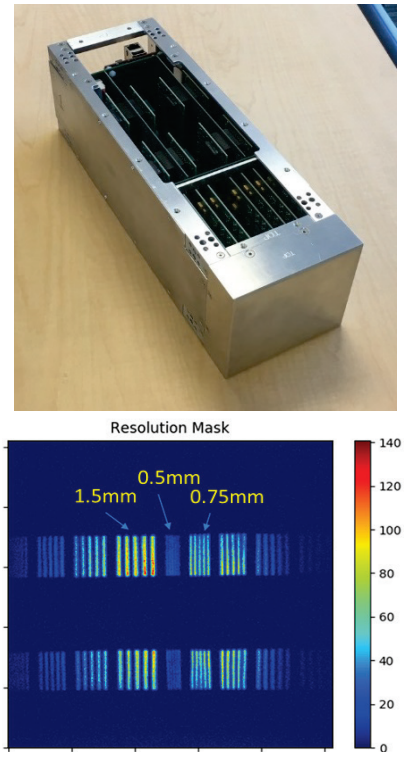

Fig. 8.2. Scintillator Anger camera detector technology. Top: The first production SNS scintillator-SiPM Anger camera; for scale, the front face is 120 × 120 mm. Bottom: Resolution mask image collected on prototype SiPM Anger camera, demonstrating 0.7 mm FWHM spatial resolution. Image source: ORNL.

Four of the eight STS instrument concepts require relatively low spatial resolution (≥ 6 mm) and low per-pixel line count rates (generally ≤ 6000 $n \cdot s^{-1}$), which are well satisfied by current commercially available ^{3}He tube array technology. The highest anticipated per-tube count rate for an STS instrument is ~15,000 $n \cdot s^{-1}$, which is close to the acceptable limit for this technology when used for diffraction. Because of the high cost and recent limited availability of ^{3}He, alternative $^{10}B^4C$-based technologies have been developed, especially for use as large detector arrays on powder diffractometers and direct geometry inelastic spectrometers [Lacy et al., 2011; Anastasopoulos et al., 2017]. When ^{3}He detector technology meets the requirements (speed and pixel size) of a neutron scattering instrument, it is usually the detector technology of choice. As alternative technologies continue to mature and demonstrate their capabilities in large installations, they may become the detector of choice for some STS instruments. Particularly for large detector arrays, cost can become a significant consideration.

In addition to ^{3}He tube arrays for measuring diffraction, the materials engineering instrument concept will require a very high spatial resolution (50 micron pixel size) imaging detector. This detector requirement can be met by ^{10}B/Gd-microchannel plate (MCP) Quad-Timepix detector technology [Tremsin et al., 2011, 2015]. ORNL has several years of operational experience with this type of detector, both at SNS and at the higher neutron flux imaging station at HFIR. Staff in ORNL's Neutron Sciences Directorate are developing in-house design and production capabilities (see Fig. 8.3) to meet increasing demands for this type of detector at HFIR and the FTS today and at the STS in the future. This detector has the potential to reach a spatial resolution of ~10 μm.

As the concepts for the STS instrument suite are developed, advances will continue to be made in new technologies and materials for neutron detection that could enhance the performance of these instruments. For example, new scintillator materials and scintillator morphologies could increase neutron counting efficiency and reduce the gamma sensitivity of current materials.

8.5 Data and Computing

The scientific impact of data collected in a neutron scattering experiment is realized only in its analysis, interpretation through modeling and simulation (mod-sim), and ultimately its communication and publication. Data and computing will therefore have an essential role in realizing the scientific potential of the STS. Our vision is to operate neutron facilities with smart beamlines for experimental design, control, and data reduction and analysis, with these instruments integrated into a comprehensive computing and data management infrastructure that allows rapid and transparent access to advanced computing and data analytics capabilities.

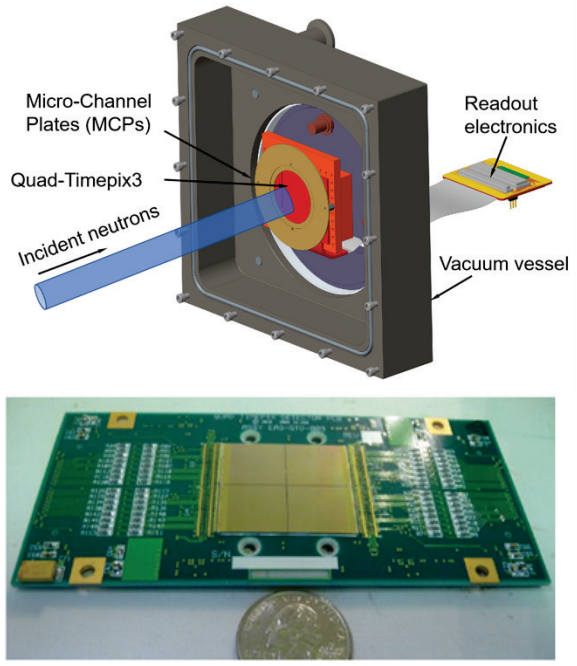

Fig. 8.3. Advancing detector technology. Top: Engineering schematic of SNS ^{10}B/Gd MCP Timepix3 detector. Bottom: Prior generation Timepix2 component module. Image source: ORNL.

Our major activities in data and computing for SNS and HFIR at present include making the specialized software capabilities for data reduction and analysis more robust, exploring better integration with ORNL's world-leading HPC capabilities, developing more powerful approaches to modeling and simulating data for comparison with experimental data, and exploiting artificial intelligence (AI) and machine learning (ML) to improve almost every aspect of the data life cycle. They also include developing computing on the stream and workflow management, particularly multisite interoperable workflows.

The STS will require further advances in data and computing to manage and fully exploit larger data collection rates, larger and more complex information content of data, and new types of experiments. Some STS instruments will have data acquisition rates two orders of magnitude greater than those of existing instruments. STS instruments will also enable new types of experiments, such as the ability to measure kinetic processes in real time or the ability to simultaneously measure samples with hierarchical architectures across much larger ranges of energy and momentum than are possible today. Several other communities, such as high energy and nuclear physics and light sources, face similar data challenges, and the STS will leverage the knowledge base of those communities. In this section we describe approaches that are being formulated at ORNL to prepare for these new challenges, focusing on future rather than ongoing activities.

Data analysis at SNS and HFIR today is largely dependent on traditional mod-sim approaches to comparing calculated neutron data with reduced data. This involves multiple transfers of data between instruments, instrument control computers, clusters, local storage, and centralized storage in a sequential way during and after the experiment. When required, access to HPC is through allocation awards and batch queues with centralized file systems. This approach is vulnerable to interruptions in data transfer, slow data transfer rates of large data sets, and unreliable access to remote resources. Despite these

vulnerabilities, we have already prototyped live data reduction on the event stream, and this novel method of data reduction will continue to be fully deployed to enable workflows that allow real-time visualization and analysis at the STS. Much tighter integration with computing, including HPC, will be required at the STS, and this tighter integration will be achieved through a comprehensive data architecture that will cover all stages of computing and data. This architecture is a foundation for support for both operational and scientific workflows, a converged ecosystem of federated smart neutron scattering instruments, and support for advanced uses of data. The approaches discussed in this section leverage recent advances and future possibilities in computing and data managements that are being driven by ORNL.

8.5.1 Comprehensive Data Architecture

A data architecture is a blueprint for development of optimal and efficient structures, systems, and operations in support of the data-centric mission and operations. The STS requires a comprehensive data architecture because, unlike a traditional single-purpose system, this architecture needs to integrate support for:

- all dynamic characteristics of data (streaming and static),
- multistage computing (from edge and instruments to the data center, with support for graceful and efficient restarts),
- metadata and data management for effective scientific discovery, and
- support for both modeling and simulation and AI-oriented scientific computing.

A disciplined approach to data management and the application of best practices result in the values that manifest themselves in more than one domain. In the case of STS data architecture, this approach will support both operational needs, such as efficient running of experiments, scheduling, and tracking of resources, and the primary research mission of scientific discovery from data.

The operational mission will be supported by recording, tracking, analyzing, and reporting of all elements of operations. In other words, it will be used for instrumentation of the operations of the facility, and consequent optimizations. From a scientific point of view, and keeping in mind the pivot to data-intensive science, the STS data architecture will promote productive, efficient, and scientific discovery experience through best practices in metadata and data management, including management of AI-specific data such as labeled training data, consequently accelerating both human-intensive and machine-supported processes of scientific discovery (e.g., making phenomena in data more easily discoverable by using best practices in labeling machine-readable data and storing the comprehensive metadata that will facilitate the research essential search and discovery functions).

8.5.2 Smart Neutron Scattering Instruments in a Converged Data and Computing Ecosystem

We propose to push data analytics closer to the source of data generation, the neutron scattering instruments, to achieve more robust, faster, and easier communication between these instruments and the advanced data and computing services at ORNL. Each instrument will have local computing and micro data centers and sensors (detectors, motor controls, sample environments, etc.). This approach has similarities to edge computing and has similar benefits. We refer to instruments that are enabled in this way as “smart” instruments. Continued improvements in decentralized accelerated node technologies will further improve communications between smart instruments that communicate with each other and other federated data and computing services at ORNL in higher tiers, such as midrange servers, clusters, and data centers. The benefits of this approach will include reduced completion times, remote facility use, and an environment that enables AI knowledge learning and inference for instrument control, design of experiments, and online learning.

We further propose to enable sophisticated data management solutions in data sharing, data publishing, rich metadata management, efficient search and discovery of data and new knowledge pathways, and making data available for AI, through a graph network approach. This approach federates the extracted and derived information, *"metadata knowledge indexes,"* from smart instruments and other computing services and links and correlates them in novel ways, toward the scalable searching, sharing, and publishing of millions of datasets and the discovery of new knowledge pathways.

A necessary first step to realizing this graph network is the creation of metadata knowledge indexes through the automatic extraction of information from the STS resource fabric (millions of data sets, storage system stat information, tens of thousands of sample environments, users, millions of reduction and analysis jobs and the systems they run on, experiment proposals, and publications). By federating the rich resource information, we will build a neutron science relationship graph network as an overlay atop the STS resource fabric. Each node in the graph represents an object of a particular entity type (e.g., user, data set, experiment, sample environment, analysis job, papers), with metadata about it represented as properties, and the edges representing the relationships between objects. Such a graph structure can elegantly capture the many-to-one and many-to-many relationships between these entities. The science graph network will use the federated metadata knowledge to automatically and intelligently build associations between the resource entities (e.g., discover and suggest similar data sets based on an overlap in the model/process used).

Beyond associations, more profound levels of knowledge discovery can only be unraveled with deep mining and analytics techniques. Deep search techniques can also enable *automatic data analytics,* e.g., the identification of a key artifact (such as a crystal structure) in a data set, which if annotated in the graph via a tag can automatically trigger further analysis on similar data sets. Using a graph as a basic construct to represent a scientific collaboration will foster relationships, enable scalable data discovery, address future challenges in sharing and publishing, find new knowledge pathways, strengthen AI-based analysis, and accelerate scientific discovery.

8.5.3 Advanced Data Reduction and Analysis

New experimental capabilities at the STS—such as time-resolved studies and studies across broad ranges of length, energy and time scales—will create an absolute requirement for real-time data visualization, reduction, and comparison to calculations for real-time feedback. This in turn will require further development of workflows that allow real-time comparison of mod-sim with reduced data and therefore experiment steering. It will also require further development of approaches to start processing data on the live stream, which have been prototyped at the FTS. The expanded use of the stream will allow for more complex counting criteria (e.g., counting to a statistical measure of a model fit or peak width).

Ongoing developments that are synergistic to this approach include advances in the use of AI and machine learning (ML) for data reduction and analysis, including the use of clustering to identify phase transition in materials and the clustering and training of neural networks to improve the reduction of diffraction data, to recognize features in complex SANS data sets, and to identify features in neutron tomography. Clustering algorithms are a class of tools that allow data sets with similar features to be grouped. Such algorithms have recently been shown to reveal the presence of different phases of materials and also can be used to alert the experiment team or facility staff of unexpected changes in conditions during an experiment [Peterson et al., 2018]. We will implement these routines so that they can be routinely employed on STS instruments.

Neural networks have been used for scientific data analysis for several years. Today, the field of ML is quite large and has applications in both the sciences and the community at large. Several ML packages are targeted to chemistry and materials science, integrating with existing databases of material structures. Their applications cover a wide field, from studying material properties to predicting crystal structures of

new materials [Mueller et al., 2016; Butler et al., 2018]. ORNL has already used ML for diffraction, diffuse scattering, and small-angle neutron data.

ML systems can identify patterns in data recognized from a training set. The process of defining the ML model, training it, and assessing its performance can be difficult; a simplified process is needed to support users at the STS. Two types of problems can be defined for consideration. The first type concerns models that are developed once and then used to address, for example, issues related to running the instruments, such as diagnostics and calibration.

The second type of problems concerns more specific, smaller-scale data analysis issues. For such cases, an ML model may be required to recognize deviations in the shape of diffraction peaks, or a model must be trained to recognize certain atomic structures from patterns on the detector. To enable users to tackle such problems efficiently and more organically, without having to turn to ML experts every time, an ML framework for neutron data analysis will be developed. Such a framework would lower the threshold for scientists to use the power of ML.

ML is a good tool for recognizing known features in data sets and completing tasks such as classifying peaks or assigning theoretical models to reduced data sets. Using such an approach can be of great help in interpreting the data, especially when the measured data is complex or when it comprises features that are not directly related to the material under study. However, ML can also be used to streamline data acquisition. We can envisage three types of processes to help the experiment progress more efficiently: alignment processes used to prepare data acquisition, diagnostics process to assess data quality, and analysis processes to help decide if enough data has been collected and where to measure next.

Instruments with a large number of motors can have an intricate alignment process. For instance, reflectometers use an iterative alignment process that involves beams reflected from a standard sample. Guided alignment processes have already been implemented at the FTS for the Liquids Reflectometer. Such processes still depend on the user, who needs to carefully follow instructions as the system proceeds with several alignment scans. The user must recognize when each of those scans has succeeded before proceeding to the next. Given that the scan data is fairly simple, applying ML to the alignment process could automate a crucial process that often requires instrument staff. The alignment system would proceed like a standard guided procedure, where ML would help determine success.

By processing the instrument data and metadata during acquisition, we can envisage a live diagnostics process that can assess data quality and inform the experiment group when there are problems with the instrument. Training the ML process with standard-looking projections of the data should make it possible to determine whether the acquisition is proceeding as it should. Again, taking the example of reflectometry, it should be possible to determine whether the acquisition requires attention by looking at the TOF distribution as a function of time and the distribution of events on the detector. Such a diagnostic process could be extended to recognize patterns in the data, such as peak location and shape. This could be used to help determine when a new feature appears in the data and when to proceed to the next run. Such a process would require input and would be part of experiment planning. For instance, if an experiment is trying to test a model that would produce a detectable phase transition during acquisition, giving enough input for the computer to recognize such a transition should be possible. Once detected, the program would help us decide when enough data has been accumulated to move on to the next measurement. In this scenario, we would develop an experiment planning tool that takes inputs such as the type of signal to look for and the level of statistics needed to proceed to the subsequent analysis.

8.6 STS Experimental Approaches

This section describes experimental approaches used for various measurements at the STS, focusing on the neutron beams. For most neutron scattering experiments, sample environment equipment, including extremes in temperature, applied fields, pressure and chemical environments, is an essential component of the research. Design and procurement of state-of-the-art sample environment equipment will be an integral part of the STS project, and community input will be sought as part of this process. Thus, a detailed description of these sample environments is beyond the scope of this document.

8.6.1 Time-of-Flight Experimental Approaches

Pulses of neutrons from the STS target will travel from the moderators along beamlines to a specific neutron scattering instrument, where they interact with a sample. As they travel along a beamline, the neutrons spread out in time as lower energy neutrons fall behind faster, higher energy neutrons. Time-of-flight (TOF) methods require knowledge of both the start time and the arrival time of the neutron; the difference in flight time across a known distance defines the neutron velocity. Without further definition, slow neutrons from one pulse can be overtaken by fast neutrons from the next pulse, masking the true start time. The wavelength range of neutrons that can be used without overlap for a source operating at frequency f is $\Delta\lambda = 3956/(Lf)$ for a total flight path of length L (in meters). On an inelastic neutron scattering instrument, L is the distance from the moderator to the sample; for other instrument types, it is the sum of the distances from the moderator to the sample and from the sample to the detector.

To prevent this overlap problem, neutrons can be removed (chopped) from the beam to define this wavelength range. As the pulse frequency decreases (i.e., longer time between pulses), a wider wavelength or energy range of neutrons can illuminate the sample. Because the STS is based on a proton pulse frequency of 15 Hz, neutrons with a very broad range of wavelengths will illuminate the sample, even for the longest flight paths (about 90 m at the STS). The range of neutron energies at the STS can be extended even further by using a technique called "pulse skipping," which effectively halves the frequency to 7.5 Hz by chopping alternate incoming proton pulses. Because the energy of a neutron is proportional to the inverse square of its wavelength, maintaining the necessary energy bandwidth for cold neutron spectroscopy requires a broader $\Delta\lambda$ than is needed for thermal neutron spectroscopy.

At the STS, data will be collected in "event mode"—that is, each detection event, including the location where the neutron is detected and its time of arrival, will be recorded individually along with other associated information. This allows for sophisticated post–data collection processing such as filtering, flexible binning, and time-slicing data [Granroth et al., 2018]. TOF event-mode data collection, in combination with the broad energy range of neutrons at the STS, will enable experimental approaches that simultaneously measure events across huge volumes of energy-momentum (and spin) space, without the need to reorient the sample or reconfigure the neutron scattering instrument. Driven by the world-leading peak brightness of the STS, this ability to survey large four-dimensional (4D) volumes of energy-momentum space and record large data sets of individual events that can be processed in different ways opens up the possibility of completely new types of experiments, some of which are discussed below.

8.6.2 Time-Resolved and Cinematic Measurements of Kinetic Processes and Beyond-Equilibrium Matter

A unique aspect of the STS is the ability to make time-resolved and "cinematic" measurements of materials as they undergo changes across broad ranges of length or energy scales. These measurements are required to characterize kinetic processes, such as those that take place during formation of hierarchical structures in self-assembly of polymers and assembly of protein complexes in biology, and to characterize changes in materials in situ and operando where the sample may evolve in time and/or under the influence of an applied field, changing chemical environment, or during processing. Here we use the

term “time-resolved” to refer to the ability to collect data at a rate that is fast enough to observe changes in the sample with time. The length of time needed to collect data of sufficient quality to determine the scientifically relevant parameter (e.g., a phase transition, radius of gyration, or order parameter) is the time resolution of the experiment. We use the term “cinematic” to refer to continuous collection of data that may be correlated either with time or with changes in an extrinsic sample condition, such as pressure, magnetic field, or pH. These measurements essentially create a recording of the neutrons as they arrive at the detector that can be recombined (histogrammed or sorted) post-experiment in a flexible way determined by the researcher. This post-experiment processing is only possible due to TOF data collection in event mode.

Time-resolved and cinematic experiments will be enabled on all types of STS instruments (neutron scattering, reflectometry, spectroscopy, and diffraction). However, the direct benefits of the high peak brightness and broad energy range of neutrons at the STS for these experiments are most directly illustrated in the case of reflectometry. Figure 8.4 compares the capability of the existing Liquids Reflectometer at the FTS to that of a horizontal surface reflectometer concept under development for the STS. The *y*-axis is proportional to the effective neutron flux on sample (normalized by the reflectivity of the sample).

From this comparison the following observations can be made: (1) If the structure of the sample can be characterized with a specular reflectivity curve using neutron wavelengths up to ~6 Å, then either the FTS or the STS instrument could be used, although the higher flux at the STS would allow better time resolution. (2) If the sample response is more extended in Q and requires neutron wavelengths up to ~14 Å, then this experiment can only be done without changing the instrument configuration at the STS. The FTS instrument could be reconfigured to access longer wavelengths, but the experiment would have to be repeated, making it impossible to characterize the sample in a time-resolved or cinematic fashion simultaneously across all required length scales. (3) If the sample response is even more extended in Q, requiring neutron wavelengths up to ~25 Å, as is the typical case for reflectometry, then the STS instrument could be used in pulse-skipping mode (7.5 Hz). In this case, however, the neutron flux received over the first half of the dynamic range, to neutron wavelengths up to ~14 Å, is reduced compared to STS operation at the higher (15 Hz) frequency. STS instruments can typically accommodate either mode of operation, trading higher flux over a more limited wavelength band for lower flux over a broader wavelength band when required.

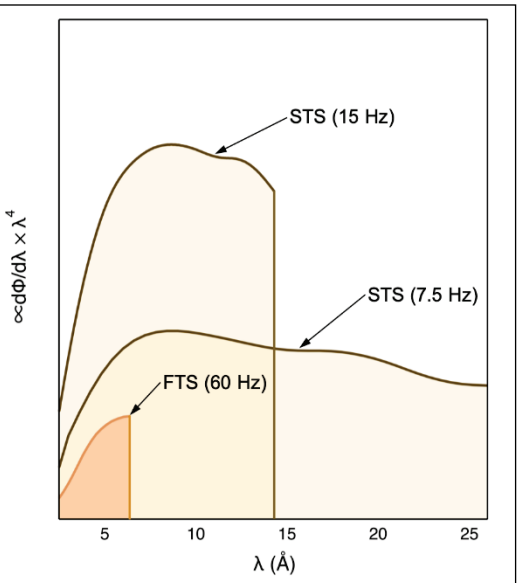

Fig. 8.4. Illustration of the power of cinematic data collection. The effective neutron flux on sample (normalized by reflectivity of the sample) as a function of neutron wavelength is shown for the 15 m Liquids Reflectometer at the FTS and for a 20 m horizontal surface reflectometer concept for the STS in both normal (15 Hz) and pulse-skipping (7.5 Hz) mode. Image source: ORNL.

In summary, the ability to collect complete specular reflectivity curves across a broad dynamic range in momentum transfer (Q_{max}/Q_{min} = 11.5) with time resolutions of seconds or less would be truly transformative for studying kinetic processes and the structure, dynamics, and reactions of complex hierarchical materials that have heterogeneity, interfaces, and disorder. These types of gains, associated with extended bandwidth and the ability to measure kinetic processes, are characteristic of many STS instruments. However, as indicated in Fig. 8.4, counting times may be

dominated by only a small part of the wavelength band (in the case of the reflectometer, at the shortest wavelengths and highest momentum transfers where the signal is weak).

8.6.3 Smaller Sample and Beam Sizes

In many cases, limited sample availability (due to limits in materials synthesis or isolation from biological systems) restricts the applicability of neutron scattering techniques, especially for weakly scattering samples. The one to two orders of magnitude higher neutron flux at the STS instruments will enable studies of materials beyond the reach of the best instruments available today. At the same time, advances in neutron optics technology (see Sect. 8.2.2) are leading to better and more efficient control of neutron transport; this will reduce background by preventing unwanted neutrons from reaching the sample area and improve the signal-to-noise ratio, which is a key requirement for measuring smaller samples.

The high-brightness, focused cold neutron beams of the STS will also facilitate the study of materials under extreme environments, such as high pressure, temperature, and applied fields. Extreme environments can reveal new physical and chemical phenomena, create materials that are not stable at ambient conditions, and mimic the harsh environments in which real-world materials must operate. For example, extreme high-pressure experiments are conducted in diamond anvil cells, requiring focused neutron beams with controlled size and beam divergence. In this case, decreasing the sample volume increases the pressure that can be applied, so focusing beams into smaller volumes makes it possible to cross new thresholds in maximum pressure.

In the case of studying materials under extreme magnetic fields, the high-field magnet is bulky, limiting access to the sample for neutron beams and obstructing desired paths to detectors. Figure 8.5 illustrates the limited vertical access that an extreme high-field magnet might impose on flight paths that scattered neutrons can take to detectors. Wedges in the horizontal plane are also necessary in order to provide mechanical support to keep the upper and lower coils of the magnet separated. In such a case, the wide range of wavelengths available in a single STS pulse provides continuous coverage of momentum transfer in the scattering plane while maximizing the range of momentum transfers that can be accessed within the limited vertical angular access afforded by the magnet.

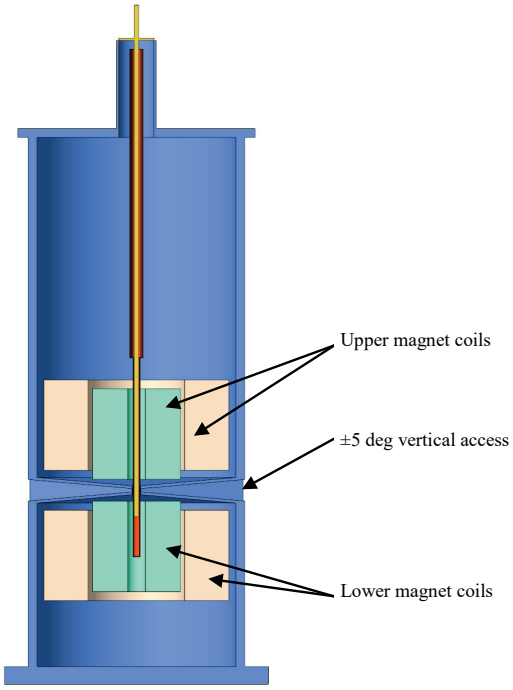

Fig. 8.5. Cartoon of extreme high field magnet, illustrating limited access to the sample location. Image source: ORNL.

8.6.4 Simultaneous Measurements Across Unprecedented Length Scales

In the case of hierarchical materials, at existing neutron sources it is often not possible to simultaneously access the required broad ranges of length or energy scales with sufficient signal-to-noise ratio using just one instrument configuration or sample orientation. The wide range of neutron wavelengths available within a single STS source pulse supports simultaneous measurements across wide regions of reciprocal space, facilitating the study of complex, multiscale matter. STS instrument concepts use this broad wavelength band to provide continuous coverage in momentum transfers over an unparalleled dynamic range

(Q_{max}/Q_{min}) up to four orders of magnitude, from subangstrom to hundreds of nanometers in the case of the combined small-angle and wide-angle neutron scattering (SANS/WANS) instrument (see Sect. 8.7.2). At the same time, the high neutron brightness of the STS makes the measurement faster. The ability to simultaneously observe the evolution of structure on this range of length scales is essential; recent developments open the door to greatly extend the upper bound of this range by combining neutron Larmor methods (e.g., SEMSANS, as described in Sect. 8.3) that measure real-space correlation functions with these reciprocal space methods.

8.7 STS Instrument Concepts

The full complement of 22 beamlines at the STS will support a suite of neutron scattering instruments that provide wholly new capabilities to the US research community. As part of the STS project, an initial suite of eight instruments will be built; for each instrument, this includes (1) the infrastructure to transport the neutrons from the moderators to the sample position and to shape, manipulate, and shield the neutron beam as required along the incident flight path; (2) the instrument end station and its associated shielding, mechanical components, neutron detectors, and an initial suite of sample environment equipment; and (3) the data management infrastructure and scientific software required to reduce and analyze data.

The research community will be engaged in an instrument selection process early in the preliminary design phase of the STS project to select the initial suite of instruments. A 2015 user community workshop [Eskildsen and Khaykovich, 2015] reviewed a number of proposed STS instrument concepts. Figure 8.6 shows 16 of these notional instrument concepts, distributed around the STS target monolith. Eight of these instruments were identified as high priorities for detailed concept development to support preparation of the STS Conceptual Design Report, and brief descriptions of these instrument concepts are presented in this section. These instruments are subject to refinement, additions, or changes based on future community input. Instrument performances have been calculated with detailed Monte Carlo

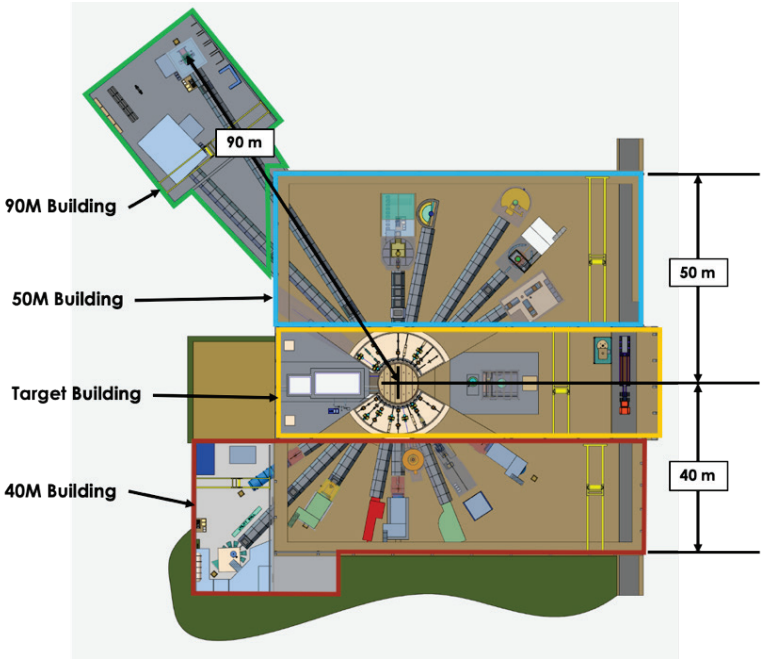

Fig. 8.6. Schematic view of the STS target building and experiment halls, showing 16 of the 22 instruments that will be part of the STS when it is fully outfitted. For clarity, some beamlines have been left unoccupied. Image source: ORNL.

simulations and show gains of up to three orders of magnitude compared to existing instruments, with the potential to deliver extraordinary new capabilities for the scientific user community.

8.7.1 SANS Instrument

Small-angle neutron scattering (SANS) will benefit from combining the high brightness of STS with next-generation detector technology to probe real-time nanoscale changes in materials that are inaccessible today. This will provide new opportunities to study time-resolved phenomena and kinetics associated with materials processing, 3D printing, or the assembly of complex polymers or biological complexes, domain wall and topological defect dynamics in magnets and ferroelectrics, and synthesis of nanomaterials and quantum materials.

For example, SANS at the STS will provide insight into the substructures of cell membranes (see Sect. 7.3.2) and as a tool for revealing the structure of membrane-less organelles associated with diseases such as amyotrophic lateral sclerosis (see Sect. 7.3.1) without inducing damage to the sample during time-resolved studies. This proposed instrument will be used to characterize the structure of materials from 0.4 nm to hundreds of nanometers across a very broad range of science.

Building on recent success at SNS with advances in neutron chopper technology, the proposed instrument will incorporate a high-speed statistical chopper that enables discrimination of elastic (desired signal) from inelastic (background) scattering, improving the signal-to-noise ratio and resolving a long-standing complication in the operation of TOF SANS instruments. The instrument will use stepped arrays of 30 × 30 cm^2 silicon photomultiplier (SiPM) Anger camera detector modules to support the high anticipated data rates of the instrument, as illustrated in Fig. 8.7. The three detector arrays coupled with the broad wavelength band at the STS mean that the instrument can collect data simultaneously across a broad dynamic range of momentum transfers (Q_{max}/Q_{min}) of about 300–800, depending on the selection of wavelength band. Figure 8.8 shows a Monte Carlo simulation demonstrating the resolution of the instrument using a pseudo-sample that produces a sequence of sharp peaks that are logarithmically spaced in momentum transfer [Lefmann and Nielsen, 1999]. Key instrument parameters are listed in Table 8.1.

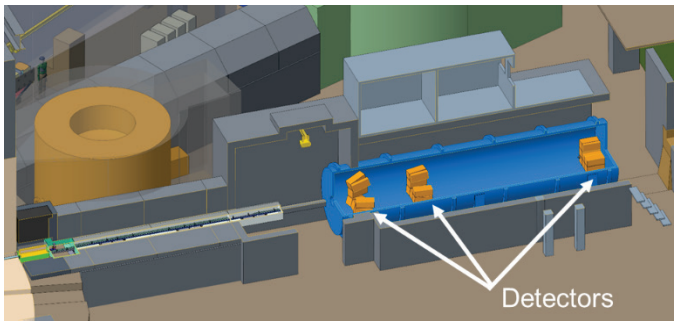

Fig. 8.7. Arrangement of stepped arrays of Anger camera detector modules for the STS SANS instrument. Image source: ORNL.

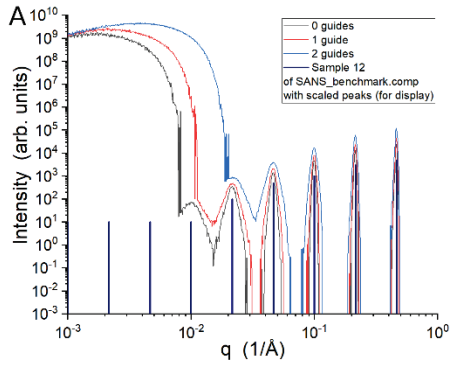

Fig. 8.8. Simulated scattering patterns for the STS SANS instrument. The very sharp diffraction peaks demonstrate the resolution of the instrument. Image source: ORNL.

Table 8.1. STS SANS instrument concept: Key parameters

Parameter	Description
Moderator	Horizontal tube moderator
Beam size	30 × 30 mm^2 guide dimension, nominal 1 cm diameter sample size
Moderator-sample distance	25.2 m (nominal)
Sample-detector distance	1.111 m, 3.333 m, 10.0 m
Detector	Arrays of 30 × 30 cm^2 SiPM Anger camera detectors with 3 × 3 mm^2 pixels for mid-and high-angle banks, as low as 1 × 1 mm^2 pixels for low-Q bank
Q-range (high collimation setting)	0.0017 $Å^{-1} < Q < 1.4668$ $Å^{-1}$ at 2.0 Å < λ < 9.49 Å (15 Hz)
	0.0009 $Å^{-1} < Q < 0.2933$ $Å^{-1}$ at 10.0 Å < λ < 17.49 Å (15 Hz)
	0.0009 $Å^{-1} < Q < 1.4668$ $Å^{-1}$ at 2.0 Å < λ < 16.98 Å (7.5 Hz)

8.7.2 Simultaneous SANS/WANS Instrument

Simultaneous SANS/wide-angle neutron scattering (WANS) will bridge the gap in length scales between those measured on conventional diffractometers and SANS instruments to simultaneously study the evolution of structure from the subangstrom scale to ≈300 nm. The instrument exploits the wide bandwidth of the STS to provide continuous coverage across this range of length scales, at which interactions govern the properties and function of many complex hierarchical materials, such as high-entropy alloys and polymers. This approach of combining SANS with wide-angle diffraction capabilities has been implemented on the TAIKAN instrument at the Japan Proton Accelerator Research Complex (J-PARC) [Takata et al., 2010], but the wide bandwidth at the STS will make such an instrument feasible for the first time at a US neutron source.

The neutron scattering capabilities of this SANS/WANS combination will be further enhanced with additional in situ characterization tools, such as spectroscopic measurements, to build a more complete, time-resolved picture of sample response to changing environmental conditions. The instrument will simultaneously measure structures across a dynamic range (Q_{max}/Q_{min}) approaching four orders of magnitude. The high brightness of the STS will enable time-resolved measurements of materials in action or as they are being processed. These capabilities will have an immediate impact on the understanding of soft matter systems under real-world processing conditions, for example. Early studies that can be anticipated include real-time spatially resolved measurements of polymer mixtures in millifluidic sample environments (see Sect. 3.3.1), elucidating the mechanism of self-assembly, and crystallization of polymers induced by single-wall carbon nanotubes (see Sect. 3.3.4). The large dynamic range will be particularly effective for measuring systems exhibiting hierarchical structures and crystallization from complex solutions, which can occur in flowing complex fluids such as those used in fracking and various industrial processes (see, e.g., Sects. 3.3.5 and 5.3.1).

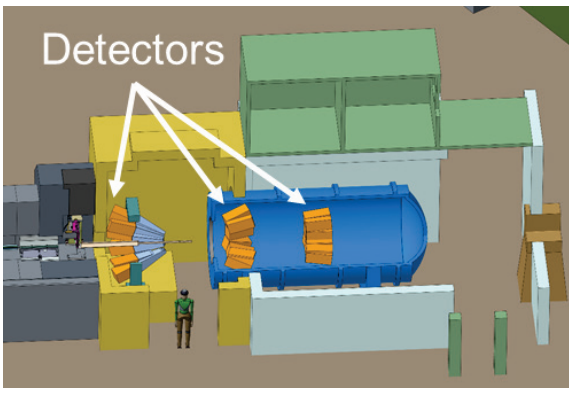

Fig. 8.9. Detector configuration for STS SANS/WANS instrument concept. Image source: ORNL.

Three arrays of 30 × 30 cm^2 SiPM Anger camera detector modules will be used to support the high data rates of this instrument (see Fig. 8.9). The detector locations have been chosen to support a flat sample geometry consistent with low-angle SANS and backscattering diffraction. The detector arrangement provides continuous coverage in

momentum transfer at 15 Hz when configured for a minimum wavelength of less than 2 Å. Continuous coverage is maintained to a minimum incident wavelength of 4 Å when the instrument is operated at 7.5 Hz in frame-skipping mode. As with the SANS instrument concept, inclusion of a correlation chopper is under consideration. Table 8.2 lists key parameters for this proposed instrument.

Table 8.2. STS SANS/WANS instrument concept: Key parameters

Parameter	Description
Moderator	Vertical cylinder moderator
Beam size	20×20 mm^2 guide dimension, nominal 1 cm diameter sample size
Moderator-sample distance	30.25 m (nominal)
Sample-detector distance	–1.25 m (backscattering), 1 m (mid-angle), 3 m (low-angle)
Detector	Arrays of 30×30 cm^2 SiPM Anger camera detectors with 3×3 mm^2 pixels
Q-range	0.00373 Å^{-1} < Q < 24.918 Å^{-1} at 0.5 Å < λ < 8.4 Å (15 Hz)
	0.00316 Å^{-1} < Q < 6.229 Å^{-1} at 2.0 Å < λ < 9.9 Å (15 Hz)
	0.00158 Å^{-1} < Q < 3.115 Å^{-1} at 4.0 Å < λ < 19. 8 Å (7.5 Hz)

8.7.3 Neutron Reflectometer with Horizontal Sample Surface

A neutron reflectometer with a horizontal sample surface will enable real-time studies of interfaces including free liquids and the transport of atoms, molecules, or charge across interfaces. Many advanced properties sought through materials by design will only be realized in new materials having at least one nanoscale dimension where new functionality can arise from surface-dominated forces and interactions. New insights unlocked by this instrument will be key to enabling the creation of next-generation batteries, environmentally responsive coatings, drug delivery systems, and sensors.

Early experiments will utilize this brightness to investigate previously inaccessible regimes of real-time structural change on surfaces and interfaces. These experiments will be particularly relevant to new technologies for energy storage devices—for example, reaction pathways for the structural evolution of polyelectrolytes on surfaces (see Sect. 3.3.2) or various interfaces in batteries, including solid-solid or solid-liquid (see Sect. 5.3.3). This instrument will enable real-time studies of surface corrosion under various in situ conditions (see Sect. 6.3.3) and will have enough intensity to permit detailed studies of heterogeneous mixtures of lipids and other molecules that form biological membranes (see Sect. 7.3.2).

The increased bandwidth of the STS instrument makes it possible to collect complete specular reflectivity curves using a single instrument setting, enabling cinematic operation with continuous observation of the sample as it evolves in time or in response to external stimuli. Samples in time-dependent environments (e.g., temperature, electrochemical, magnetic, or chemical alteration) will be observed in real time, as fast as 1 Hz in favorable cases, such as that shown in Fig. 8.10, which illustrates the ability of the STS reflectometer concept to measure the kinetics of the crosslinking reaction of a polyelectrolyte hydrogel. The engineering concept for this instrument is shown in Fig. 8.11.

To measure reflectivity from samples that must be held horizontal, such as a liquid surface, the neutron beam must be inclined at a small angle, up to approximately 2.5°, relative to the horizontal. Some samples, such as free liquid interfaces where there is a gaseous atmosphere above the liquid, require the neutron beam to reach the interface from above. In this case, the neutron beam is inclined downward from the horizontal. In other cases, such as some liquid-liquid interfaces or when using specialized sample environments such as a rheometer, the neutron beam must reach the interface from below. In this case the neutron beam is inclined upward from the horizontal. This beam line provides both neutron beam geometries with a lower station using a downward-directed beam and an upper station using an upward-directed beam. The two end stations can operate independently and simultaneously support two

independent experiments at the same time, each using a different neutron beam geometry, as indicated in Fig. 8.11. Table 8.3 lists the key parameters of this instrument.

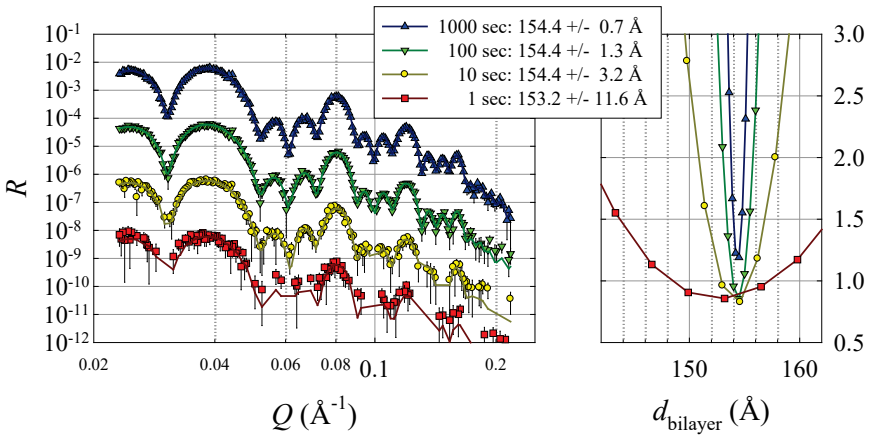

Fig. 8.10. Kinetics of the crosslinking reaction of a polyelectrolyte hydrogel. Left: Simulated 7.5 Hz reflectivity data from a polyelectrolyte multilayer for several collection times at a single incident beam angle of 2.5º. Right: dependence of χ_2 for the fitted value of the marker-layer spacing. Image source: ORNL.

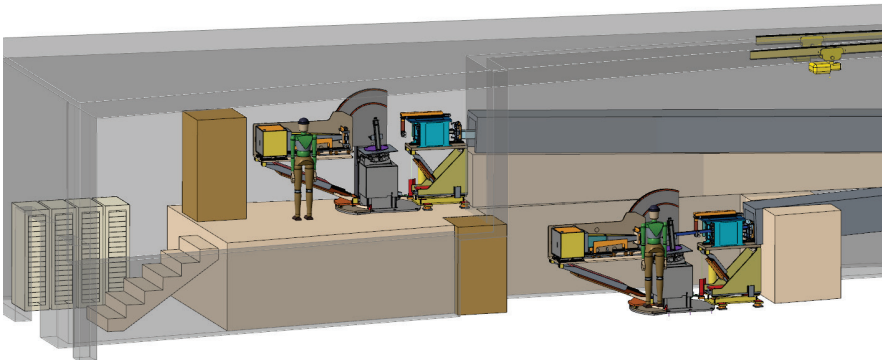

Fig. 8.11. Schematic view of the STS horizontal surface reflectometer concept. The two end stations enable the neutron beam to reflect from below the sample surface (upper) and from above the sample surface (lower). Image source: ORNL.

Table 8.3. STS horizontal surface reflectometer concept: Key parameters

Parameter	Description
Moderator	Vertical cylinder moderator
Beam size	20 × 30 mm^2, delivered by a horizontally curved, vertically tapered guide
Moderator-sample distance	20 m (lower end station)
Sample-detector distance	1.5 m (nominal)
Detector	SiPM pixelated scintillator detector, 40 × 20 cm^2, with 2 × 2 mm^2 pixels (inclined detector gives effective 1 × 2 mm^2 pixels)
Q-range	0.009 Å^{-1} < Q < 0.088 Å^{-1} at 1.0° incident angle
	0.023 Å^{-1} < Q < 0.219 Å^{-1} at 2.5° incident angle
	0.037 Å^{-1} < Q < 0.351 Å^{-1} at 4.0° incident angle

8.7.4 Cold Neutron Chopper Spectrometer

A direct geometry inelastic spectrometer can be designed to probe the weak signals intrinsic to small cross sections (e.g., small magnetic moments) or the limited sample sizes often available for new materials or associated with extreme sample environments, such as high pressure. This instrument will be optimized for the study of quantum and functional materials, but its broad dynamic range is also well matched to measuring diffusion and excitations in soft and biological matter. It will have the ability to simultaneously measure dynamic processes over a wide energy range, as indicated in Table 8.4, making it the spectrometer of choice for first measurements of new materials. This instrument will support a polarized neutron beam and polarization analysis to separate nuclear from magnetic scattering and coherent from incoherent scattering processes in hydrogenous materials.

Table 8.4. STS cold neutron chopper spectrometer optimized for small sample area: Key parameters

Parameter	Description
Moderator	Horizontal tube moderator
Beam size	10×10 mm^2
Moderator-sample distance	29.5 m
Sample-detector distance	2.5 m
Detector	25 mm diameter linear position-sensitive detector (PSD), ^{3}He
E_i range	0.5 meV < E_i < 25 meV; with repetition rate multiplication, the source pulse will be subdivided to 5–10 incident energies across a bandwidth of 7–8 Å
ħω resolution	Flexible, $\Delta\hbar\omega$ =2–5% E_i at the elastic line

This instrument will have an immediate impact on research in quantum materials, revolutionizing the energy-momentum resolved spectroscopy in highly entangled systems such as quantum spin liquids (see Sect. 4.3.1). The huge intensity will enable pump-probe experiments to investigate out-of-equilibrium quantum dynamics in many systems, one prototypical example being the behavior of magnetic monopoles in "spin ice" following a pulse of terahertz radiation (see Sect. 4.3.2). The high brightness and large bandwidth of the STS will be utilized for novel investigations of dynamics in quantum materials under extreme pressure, expanding our understanding of phenomena such as topological transformations (see Sect. 4.3.3) or emergent collective ground states such as pressure-induced superconductivity (see Sect. 4.3.4). This instrument will be equally useful for understanding new functional materials that can only be synthesized at high pressures (see Sect. 5.3.2). The high brightness will allow investigations of excitations in small-volume systems, including artificial heterostructures (see Sect. 4.3.5) and small single crystals.

This instrument will use repetition rate multiplication methods to utilize multiple incident neutron energies sequentially within a single 15 Hz pulse of the STS, making it well suited to perform survey and discovery experiments. Figure 8.12 illustrates this mode of operation with the primary source pulse at 15 Hz subdivided into six incident neutron energies. This ability to simultaneously measure dynamic processes over a wide energy range makes this spectrometer uniquely valuable for surveying materials with excitations covering a large dynamic range where different values of incident energy are needed to provide full coverage at appropriate resolutions. This method is implemented on spectrometers at J-PARC [Nakamura et al., 2009] and has been proposed on a similar instrument concept developed for the ESS [Vickery and Deen, 2014]. In Fig. 8.13, the performance of the STS and FTS chopper spectrometers is compared, illustrating the power of repetition rate multiplication to effectively survey reciprocal space and zoom in on smaller regions with higher resolution when needed [Sala, 2018]. The key parameters of this instrument are listed in Table 8.4.

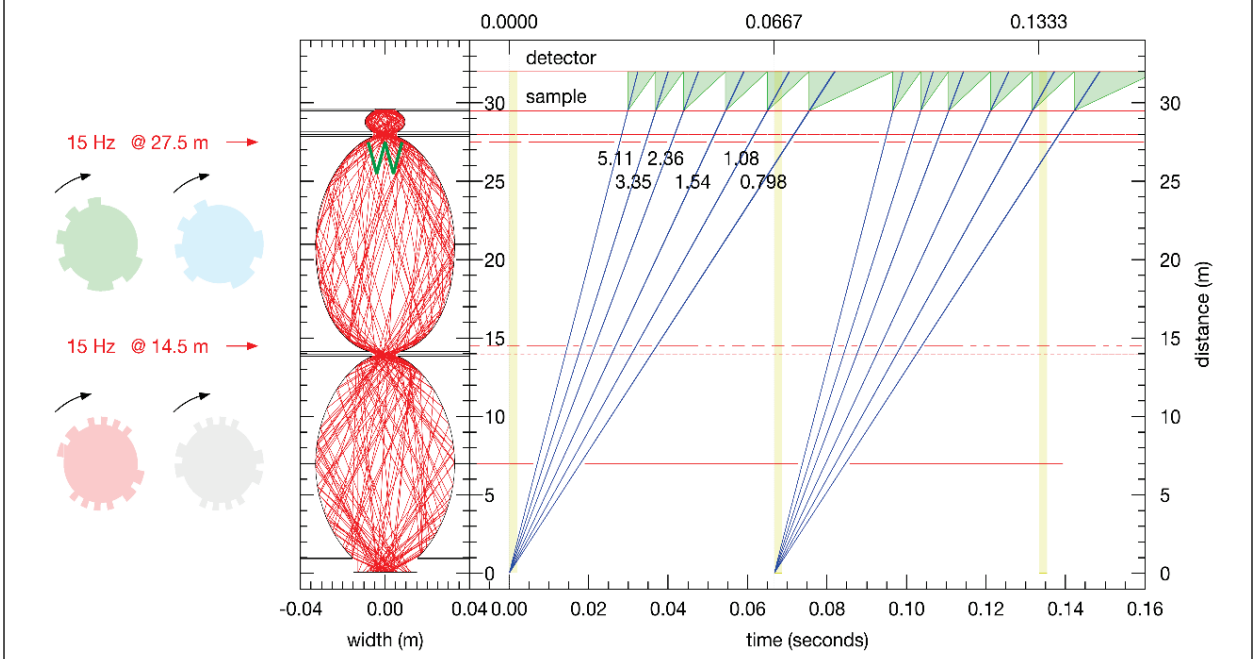

Fig. 8.12. Functional layout of the STS cold neutron chopper spectrometer concept. The time-distance diagram at right illustrates the neutron paths through the guide system (red) and the location of critical components to sort mini-pulses arising from repetition rate multiplication. The incident energies available in a single source pulse are shown for one configuration of the instrument. Image source: ORNL.

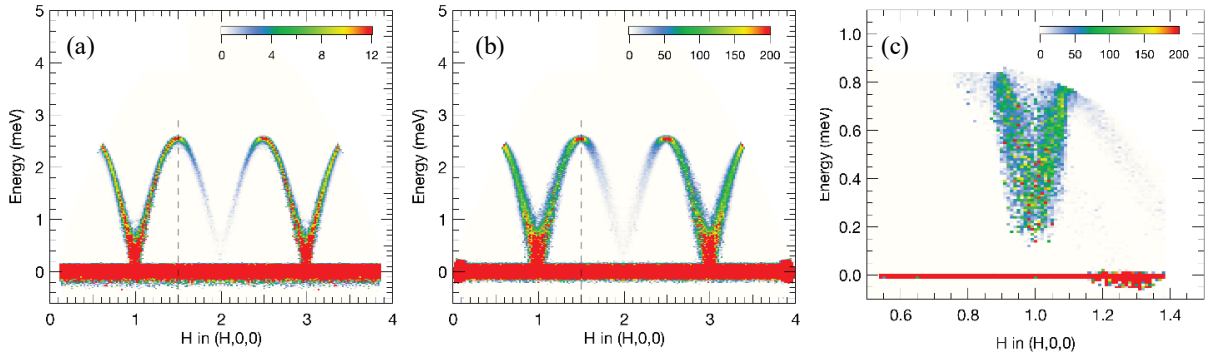

Fig. 8.13. Performance of the FTS and STS cold neutron chopper spectrometers. Spectra calculated for a 1 g sample of $K_2V_3O_8$ for (a) the FTS chopper spectrometer and (b) the STS cold neutron chopper spectrometer at incident neutron energy of 5.1 meV. The intensity is indicated by the color scale at the top of the figures. (c) Benefit of repetition rate multiplication using the 1.08 meV incident energy simultaneously available within a single source pulse to provide higher energy resolution. Image source: ORNL.

8.7.5 Multimodal Instrument for Studies at High Magnetic Field

A multimodal instrument for studies at high magnetic field is designed to collect both indirect geometry spectroscopy and single-crystal diffraction data. This instrument will offer unmatched opportunities to elucidate the structure and dynamics of quantum materials at extremes of magnetic field and low temperatures. A dedicated magnet installation is required to achieve the highest steady-state magnetic fields, similar to the approach taken for the EXED instrument at the Helmholtz Zentrum Berlin BER II

reactor [Smeibidl et al., 2010]. Recent advances in composite conductors using high-temperature superconductors provide a pathway to fields as high as 35 T or beyond in a vertical geometry that is best suited for neutron scattering [Hahn et al., 2019]. The high-brightness, focused cold neutron beams of the STS are ideally matched to illuminate the small sample area intrinsic to achieving the highest magnetic field. This multimodal instrument will open new frontiers in the study of quantum critical phenomena, entangled quantum states, and competing magnetic interactions.

Inelastic neutron scattering under extreme magnetic fields provides detailed quantitative access to the spin Hamiltonian of frustrated magnetic materials by measuring the magnon spectrum in the fully polarized high-field state (see Sect. 4.3.1). The Hamiltonian embodies all relevant information needed to develop a theory of lower field collective properties. The proposed instrument, with its extreme high magnetic field, will greatly expand the materials to which this technique can be successfully applied by crossing new thresholds in the minimum field required to saturate the magnetization. The capacity for unprecedented exploration of both structure and dynamics in phases appearing as a result of field-induced quantum critical points will enable progress on a variety of problems; a classic example is the pseudogap phase hidden beneath the dome in unconventional cuprate superconductors (see Sect. 4.3.4).

Extreme high magnetic fields impose severe limitations on the neutron scattered beam geometry, greatly restricting the vertical and horizontal angular ranges that can be accessed. The proposed instrument will use the broad range of wavelengths available in a single pulse to make the best use of the limited detector view of the sample afforded by an ultrahigh-field magnet. The concept for this instrument has eight arms spaced around the magnet in the horizontal scattering plane, providing access to the sample for incident, transmitted, and scattered neutron beams, as illustrated in Fig. 8.14. These arms will be equipped either with diffraction detectors or with a set of sequential crystal analyzers to enable spectroscopy. The multiple analyzer crystals in each spectroscopy arm, combined with the broad range of incident neutron energies within each STS source pulse, enable the instrument to sweep broad ranges of Q-ω space simultaneously [Groitl et al., 2016]. Figure 8.15 illustrates the range of energy and momentum transfers that can be simultaneously accessed by the inelastic arms using both the (002) and (004) reflections of pyrolytic graphite analyzers at 15 Hz when the instrument is configured to use incident neutron wavelengths of 1 to 5 Å. Table 8.5 lists the key parameters of this instrument.

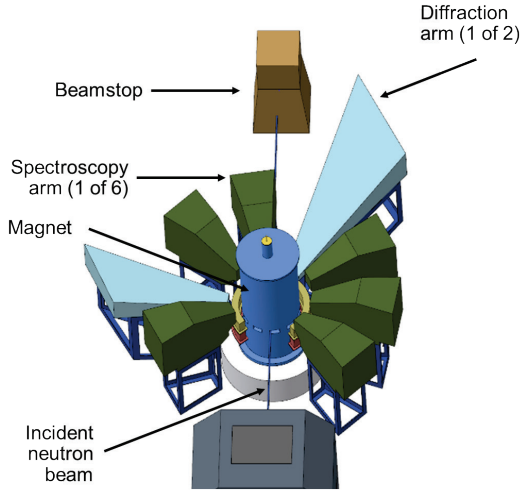

Fig. 8.14. Spectrometer and diffraction arms surrounding the magnet of the multimodal instrument concept. Image source: ORNL.

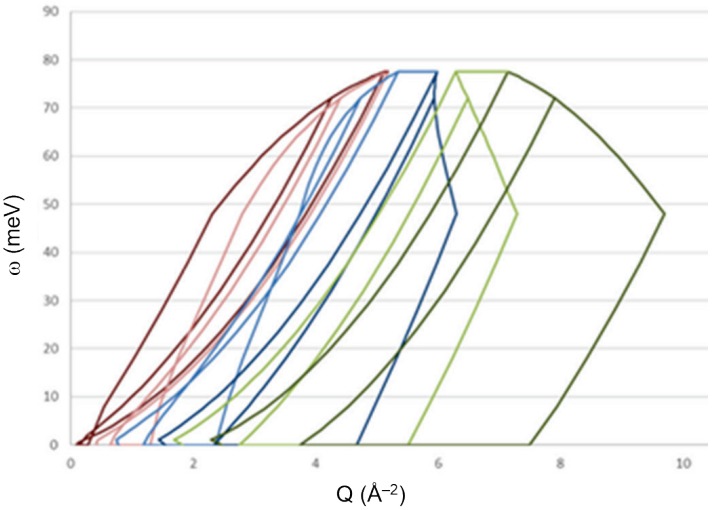

Fig. 8.15. Range of energy and momentum transfer simultaneously accessed by the analyzer arms of the multimodal instrument concept for a single instrument configuration. Image source: ORNL.

Table 8.5. STS multimodal high magnetic field instrument: Key parameters

Parameter	Description
Moderator	Vertical cylinder moderator
Beam size	15 × 15 mm^2
Moderator-sample distance	55 m
Sample-detector distance	3.5 m to diffraction detectors, varied for analyzer arms
Detector	8 mm diameter linear PSD, ^3He
E_i range	3.3 meV < E_i < 80 meV (15 Hz operation, low λ range)
ħω resolution	Δħω =3–8% E_i at the elastic line
Q-range (diffraction arms)	0.4 $Å^{-1}$ < Q < 8.9 $Å^{-1}$ (15 Hz operation, high λ range)

8.7.6 Single-Crystal Diffractometer for Small Samples

A single-crystal diffractometer for small samples will be optimized for collecting Bragg diffraction data from crystal volumes below 0.01 mm^3 with unit cell edges between 10 and 300 Å. The broad wavelength range available in a single STS pulse coupled with the high detector angular coverage of this instrument will enable complete data sets to be collected rapidly, in some cases with only a single orientation of the single-crystal sample. This diffractometer will cross a new threshold in minimum sample crystal sizes, bringing the hydrogen sensitivity of neutrons to new systems, with implications for developing improved drugs to fight multi-drug-resistant viruses and bacteria, understanding enzyme mechanisms, and exploiting the regulation of metabolic pathways for synthetic biology, such as capturing solar energy by mimicking plant photosynthesis. Early experiments will include a crystallographic investigation of PLP-dependent enzymes that should explain how these proteins catalyze so many disparate biological enzyme reactions (see Sect. 7.3.4). The high brightness will also enable detailed crystallographic characterization of the photosynthesis process in the membrane protein known as photosystem II, which proceeds via a specific set of intermediate states (see Sect. 7.3.3).

This proposed instrument features a sophisticated optics system designed for precise control over the neutron phase space delivered to the sample position, as illustrated in Fig. 8.16 [Coates and Robertson, 2017]. The primary slit defining the view of the STS moderator is demagnified by a factor of 30 to produce a beam size at the sample of 1 to 0.001 mm^2. Initial calculations demonstrate that this optics system delivers about twice as many desired neutrons to the sample area as a conventional elliptical guide and about 1000× fewer undesired neutrons to the vicinity of the sample. Monte Carlo simulation shows a very homogeneous neutron distribution at the sample position with flux of 7.64×10^6 n/s/mm^2 integrated over the 15 Hz operating wavelength band from 1.5 to 4.5 Å. Table 8.6 lists key parameters of the instrument.

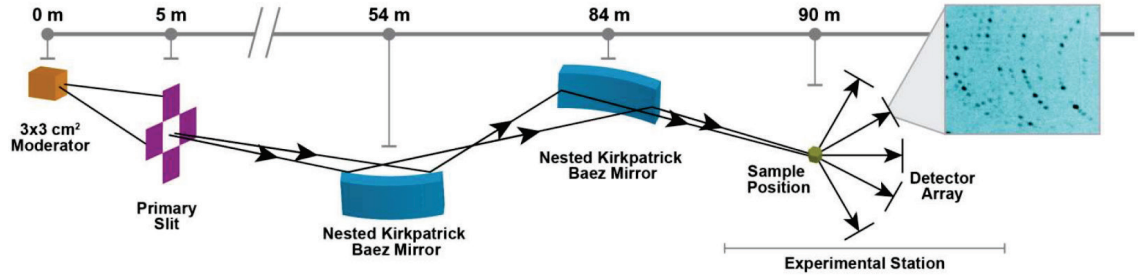

Fig. 8.16. Schematic of the optics design for STS single-crystal diffractometer for small samples. Image source: Coates and Robertson [2017, Fig. 2].

Table 8.6. STS single crystal diffractometer for small samples: Key parameters

Parameter	Description
Moderator	Vertical cylinder moderator
Beam size	Variable from 1–0.001 mm^2; controlled by primary slit
Moderator-sample distance	90 m
Sample-detector distance	0.3 m
Detector	(37–116) × 116 mm^2 SiPM Anger cameras with 0.3 × 0.3 mm^2 pixels
d-spacing range	d_{min} = 0.6 Å

8.7.7 Versatile Diffractometer for Magnetic Structure Studies

A versatile diffractometer for magnetic structure studies at the STS will be world-leading for diffraction studies of magnetism in powders and single crystals, allowing routine measurements of milligram-size samples, small magnetic moment compounds, and diffuse signals. This instrument will probe magnetic local and long-range ordering in quantum materials that exhibit emergent properties arising from collective behavior. These experiments are expected to reveal fundamental behavior in quantum magnets that will help drive development and understanding of the next generation of quantum materials, which have the potential to transform computers and data storage and raise the efficiency of energy storage and transmission.

This diffractometer will be equipped with full polarization capability and will be optimized for studies under extreme conditions of temperature, pressure, and magnetic field. Its unique use of polarized neutrons to isolate the magnetic signature in the measured data will enable detailed insight into local magnetic ordering. Planned early applications include polarized diffraction studies of complex topological structures, such as those in noncollinear magnetic systems exhibiting topological spin structures, including skyrmions (see Sect. 4.3.3). The instrument will also enable previously unfeasible

measurements of the full crystal structure of the high-pressure metal hydride superconductors, including hydrogen positions.

This proposed instrument uses a mirror optics system to flexibly deliver either high resolution (low beam divergence) or high flux and includes an option to polarize the incident neutron beam. The instrument will use a curved supermirror analyzer to provide full polarization capability. The detector layout will be a logarithmic spiral, similar to that employed on the POWGEN diffractometer at the FTS, to preserve the required resolution at low Q by increasing the distance from the sample to the low-angle detectors, as illustrated in Fig. 8.17.

At present, the Wish instrument at ISIS Target Station 2 (ISIS-TS2) is widely considered the world-leading powder diffractometer for magnetic studies. The operating frequencies of ISIS-TS2 (10 Hz) and the STS (15 Hz) are similar; however, the peak brightness at the STS will be more than an order of magnitude larger, and the instrument will receive 50% more pulses than Wish. Table 8.7 lists key parameters of the instrument.

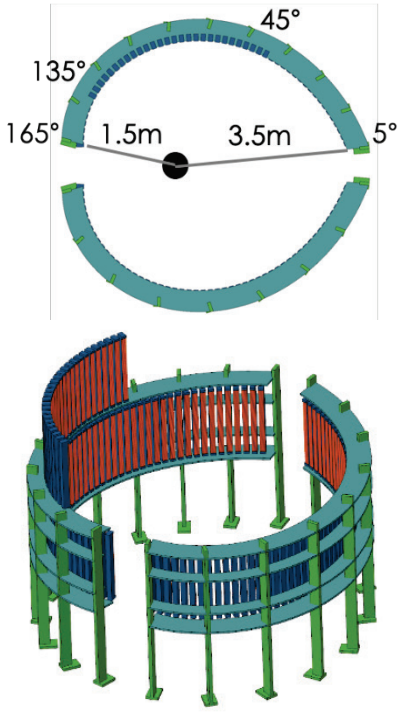

Fig. 8.17. Detector layout for STS diffractometer optimized for magnetic structure studies. Top: View of detector array from above. Bottom: 3D view of detector array. The distance from sample to detector has been selected to preserve the resolution at low Q required for magnetic studies. Image source: ORNL.

Table 8.7. STS diffractometer optimized for magnetic structure studies: Key parameters

Parameter	Description
Moderator	Vertical cylinder moderator
Beam size	Variable from 3 × 3 mm^2 (single crystal) to 10 × 20 mm^2 (powders); controlled by primary slit
Moderator-sample distance	40 m
Sample-detector distance	1.5 m to 3.5 m (detectors arranged in logarithmic spiral)
Detector	^{3}He linear PSDs (1 m long, 10 mm in diameter), 1792 tubes
Q-range	0.1 Å^{-1} < Q < 12.5 Å^{-1} at 1 Å < λ < 6.75 Å (15 Hz, first frame operation)
Q resolution	$\Delta Q/Q \approx 0.3\%$

8.7.8 Versatile Multiscale Materials Engineering Beamline

A versatile multiscale materials engineering beamline at the STS will be a transformational high-flux instrument with unique capabilities for the study of low-symmetry, complex materials. It will support both fundamental and applied materials science and engineering research in a broad range of fields, including advanced alloy design, energy storage and conversion, nuclear energy, aerospace, transportation, and civil infrastructure. This instrument will combine unprecedented long-wavelength neutron flux and high detector coverage to enable real-time studies of complex structural and functional materials

behavior under mechanical, thermal, electrical and magnetic fields. It will incorporate SANS and imaging capabilities to extend its sensitivity to larger length scales and higher spatial resolution. First experiments are expected to include studies of model alloys exhibiting phase transitions proceeding via metastable states (see Sect. 6.3.1) as a function of temperature and strain, with simultaneous measurements of both atomic (i.e., crystal) and microstructural features, as well as texture. Another initial application will be to characterize the real-time structural changes occurring during processing of materials, for example during additive manufacturing (see Sect. 6.3.2).

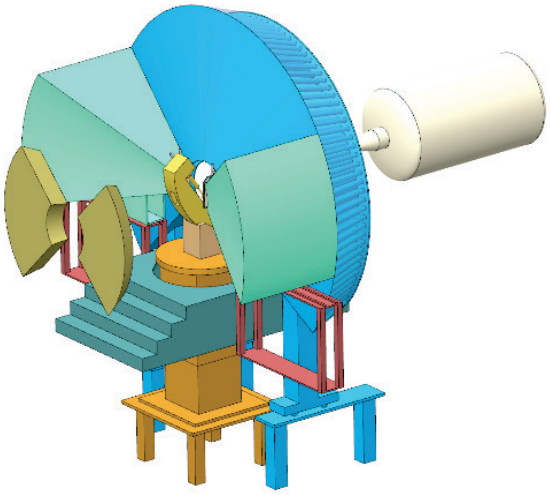

Fig. 8.18. Detector layout for the STS engineering materials instrument. At right, ~5 m from the sample, is a SANS detector. Two detector banks positioned at ~90° are shown in light green, while detector banks that are particularly useful for measuring orientational data are shown in blue. The remaining detector bank, shown in dark tan, provides high-resolution backscattering measurements. Image source: ORNL.

As is the case for the other two STS diffractometer concepts, this proposed instrument will use a mirror optics system to flexibly deliver the desired neutron phase space to the sample location. The unique detector geometry illustrated in Fig. 8.18 provides the capability to measure noncoplanar components of strain and complete orientation distributions for textured samples with a minimum number of simple sample rotations about a single axis. Figure 8.19 compares the performance of this instrument with the FTS engineering diffractometer VULCAN for measurement of diffraction peaks in a Ni_3Al superalloy with a superlattice structure (note the difference in vertical axis scale). The optimized cold neutron moderator at the STS, coupled with advanced neutron optics, will deliver a cold neutron flux to the sample up to three orders of magnitude higher than VULCAN at wavelengths greater than about 5 Å. VULCAN views a thermal moderator and was optimized for thermal neutron performance using neutron wavelengths from about 0.5 Å to 3 Å. In contrast, the STS instrument has been optimized to use neutron wavelengths from 2 Å to 10 Å. Figure 8.19 shows the additional weighting given to long *d*-spacings by the cold spectrum relative to the thermal spectrum of VULCAN. The STS instrument will complement the strengths of VULCAN, which uses the high-wavelength resolution of thermal neutrons available on

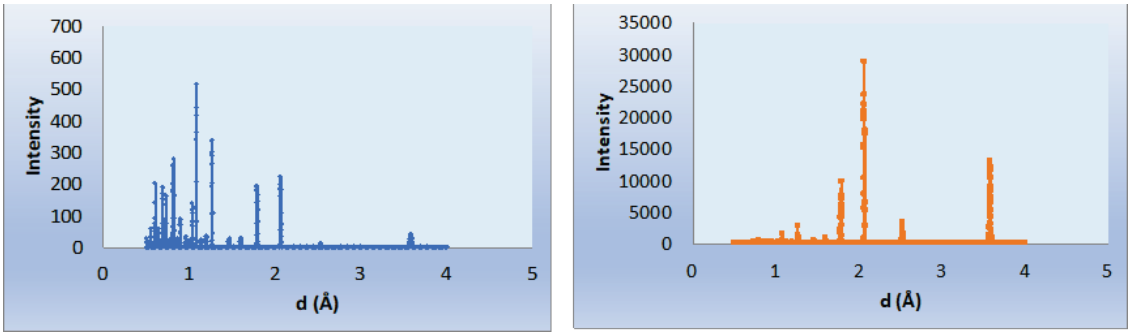

Fig. 8.19. Simulated diffraction data from VULCAN at the FTS (left) and the engineering diffractometer at the STS. Identical gauge volumes and counting time were used in the simulations. Note difference in vertical axis scale. Image source: ORNL.

the FTS to study high-symmetry crystal structures. Table 8.8 lists key parameters of the proposed instrument.

Table 8.8. STS multiscale engineering beamline: Key parameters

Parameter	Description
Moderator	Vertical cylinder moderator
Beam size	1–10 mm^2 in high-intensity mode; up to 1 cm^2 in high-resolution mode
Moderator-sample distance	72 m
Sample-detector distance	Variable depending on detector bank; up to 5 m for SANS
Detector	^{3}He linear PSDs (0.7 m and 1 m long, 8 mm in diameter); B/Gd-doped microchannel coupled to Timepix readout
d-spacing range	0.5 Å < d_{min} < 7.9 Å in 7.5 Hz frame-skipping mode

References for Sect. 8

Anastasopoulos, M.; Bebb, R.; Berry, K.; Birch, J.; Brys, T.; Buffet, J. C.; Clergeau, J. F.; Deen, P. P.; Ehlers, G.; van Esch, P.; Everett, S. M.; Guerard, B.; Hall-Wilton, R.; Herwig, K.; Hultman, L.; Hoglund, C.; Iruretagoiena, I.; Issa, F.; Jensen, J.; Khaplanov, A.; Kirstein, O.; Higuera, I. L.; Piscitelli, F.; Robinson, L.; Schmidt, S.; Stefanescu, I. *J. Instrum.* **2017,** *12,* P04030.

Bigault, T.; Delphin, G.; Vittoz, A.; Gaignon, V.; Courtois, P.; *J. Phys. Conf. Ser.* **2014,** *528,* 012017.

Birch, J.; Buffet, J. C.; Correa, J.; van Esch, P.; Guérard, B.; Hall-Wilton, R.; Höglund, C.; Hultman, L.; Khaplanov, A.; Piscitelli, F. *IEEE Trans. Nucl. Sci.* **2013,** *60,* 871–878.

Bouwman, W. G.; Plomp, J.; Duif, C. P.; Kraan, W. H.; Rekveldt, M. T. *Neutron News* **2008,** *19,* 19–21.

Butler, K. T.; Davies, D. W.; Cartwright, H.; Isayev, O.; Walsh, A. *Nature* **2018,** *559* (7715), 547–555.

Carini, G.; Denes, P.; Gruner, S. (organizers). *Neutron and X-Ray Detectors: Report of the Basic Energy Sciences Workshop,* U.S. Department of Energy, Washington, DC, 2012. Available at https://science.osti.gov/-/media/bes/pdf/reports/files/Neutron_and_X-ray_Detectors_rpt.pdf (accessed June 24, 2019).

Coates, L.; Robertson, L. *J. Appl. Crystallogr.* **2017,** *50,* 1174–1178.

Eskildsen, M. R..; Khaykovich, B. (co-chairs). *Second Target Station Workshop Report,* UT-Battelle, LLC, Oak Ridge, TN, 2015. Available at https://neutrons.ornl.gov/sites/default/files/STS Workshop Report.pdf (accessed June 13, 2019).

Fouquet, P.; Ehlers, G.; Farago, B.; Pappas, C.; Mezei, F. *J. Neutron Res.* **2007,** *15,* 39.

Granroth, G. E.; An, K.; Smith, H. L.; Whitfield, P.; Neuefeind, J. C.; Lee, J.; Zhou, W.; Sedov, V. N.; Peterson, P. F.; Parizzi, A.; Skorpenske, H.; Hartman, S. M.; Huq, A.; Abernathy, D. L. *J. Appl. Crystallogr.* **2018,** *51,* 616–629.

Groitl, F.; Graf, D.; Birk, J. O.; Markó, M.; Bartkowiak, M.; Filges, U.; Niedermayer, C.; Rüegg, C.; Rønnow, H. M. *Rev. Sci. Instrum.* **2016,** *87,* 035109.

Hahn, S.; Kim, K.; Kim, K.; Hu, X.; Painter, T.; Dixon, I.; Kim, S.; Bhattari, K. R.; Noguchi, S.; Jaroszynski, J.; Larbalestier, D. C. *Nature* **2019,** *570,* 496–499.

Ice, G. E.; Choi, J.-Y.; Takacs, P. Z.; Khounsary, A.; Puzyrev, Y.; Molaison, J. J.; Tulk, C. A.; Andersen, K. H.; Bigault, T. *Appl. Phys. A* **2010,** *99*, 635–639.

Kusmin, A.; Bouwman, W. G.; van Well, A. A.; Pappas, C. *Nucl. Instrum. Methods A* **2017,** *856,* 119–132 (2017).

Lacy, J. L.; Athanasiades, A.; Sun, L.; Martin, C. S.; Lyons, T. D.; Foss, M. A.; Haygood, H. B. *Nucl. Instrum. Methods A* **2011,** *652,* 359–363.

Lefmann, K.; Nielsen, K. *Neutron News* **1999,** *10,* 20.

Liu, D.; Hussey, D.; Gubraev, M. V.; Ramsey, B. D.; Jacobson, D.; Arif, M.; Moncton, D. E.; Khaykovich, B. *Appl. Phys. Lett.* **2013,** *102,* 183508.

Liu, D.; Khaykovich, B.; Gubarev, M. V.; Robertson, J. L.; Crow, L.; Ramsey, B. D.; Moncton, D. E. *Nature Commun.* **2013,** *4,* 2556.

Mauri, G.; Messi, F.; Anastasopoulos, M.; Arnold, T.; Glavic, A.; Höglund, C.; Ilves, T.; Lopez Higuera, I.; Pazmandi, P.; Raspino, D.; Robinson, L.; Schmidt, S.; Svensson, P.; Varga, D.; Hall-Wilton, R.; Piscitelli, F. *Proc. R. Soc. A* **2018,** *474,* 20180266.

Meilleur, F.; Munshi, P.; Robertson, L.; Stoica, A. D.; Crow, L.; Kovalevsky, A.; Korisanszky, T.; Chakoumakos, B. C.; Blessing, R.; Myles, D. A. A. *Acta Crystallogr. D* **2013,** *69,* 2157–2160.

Miao, H.; Panna, A.; Gomella, A. A.; Bennett, E. E.; Znati, S.; Chen, L.; Wen, H. *Nature Phys.* **2016,** *12,* 830.

Mueller, T.; Kusne, A. G.; Ramprasad, R. *Rev. Comput. Chem.* **2016,** *29,* 186–273.

Nakamura, M.; Kajimoto, R.; Inamura, Y.; Mizuno, F.; Fujita, M.; Yokoo, T.; Arai, M. *J. Phys. Soc. Japan* **2009,** *78,* 093002.

Perticaroli, S.; Ehlers. G.; Stanley, C. B.; Mamontov, E.; O'Neill, H.; Zhang, Q.; Cheng, X.; Myles, D. A. A.; Katsaras, J.; Nickels, J. D. *J. Am. Chem. Soc.* **2017a,** *139,* 1098–1105.

Perticaroli, S.; Mostofian, B.; Ehlers, G.; Neuefeind, J. C.; Diallo, S. O.; Stanley, C. B.; Daemen, L.; Egami, T.; Katsaras, J.; Cheng, X.; Nickels, J. D. *Phys. Chem. Chem. Phys.* **2017,** *19,* 25859–25869.

Peterson, P. F.; Olds, D.; Savici, A. T.; Zhou, W. D. *Rev. Sci. Instrum.* **2018**, *89,* 093001.

Polymer Reptation. https://www.ill.eu/users/instruments/instruments-list/in15/examples/polymer-reptation/ (accessed June 24, 2019).

Sala, G.; Lin, J. Y. Y.; Graves, V. B.; Ehlers, G. *J. Appl. Crystallogr.* **2018,** *51,* 282–293.

Smeibidl, P.; Tennant, A. D.; Ehmler, H.; Bird, M. *J. Low Temp. Phys.* **2010,** *159,* 402–405.

Strobl, M.; Tremsin, A. S.; Hilger, A.; Wieder, F.; Kardjilov, N.; Manke, I.; Bouwman, W. G.; Plomp, J. *J. Appl. Phys.* **2012,** *112,* 014503.

Takata, S.; Suzuki, J.; Shinohara, T.; Oku, T.; Tominaga, T.; Ohishi, K.; Iwase, H.; Nakatani, T; Inamura, Y.; Ito, T.; Suzuya, K.; Aizawa, K.; Arai, M.; Otomo, T; Sugiyama, M. *JPS Conf. Proc.* **2010,** *8,* 036020.

Tremsin, A. S.; McPhate, J. B.; Vallerga, J. V.; Siegmund, O. H. W.; Veller, W. B.; Lehmann, E.; Dawson, M. *Nucl. Instrum. Methods A* **2011,** *628,* 415–418.

Tremsin, A. S.; Vallerga, J. V.; McPhate, J. B.; Siegmund, O. H. W. *Nucl. Instrum. Methods A* **2015,** *787,* 20–25.

Vickery A.; Deen, P. P. *Rev. Sci. Instrum.* **2014,** *85,* 115103.

(Intentionally left blank)

9. CONTRIBUTORS

ORNL Coordinators of "First Experiments" Chapters

3. *Polymers and Soft Materials*
   Phillip F. Britt, Chemical Sciences Division
   Volker Urban, Neutron Scattering Division
4. *Quantum Matter*
   Ho Nyung Lee, Materials Science and Technology Division
   Mark Lumsden, Neutron Scattering Division
5. *Materials Synthesis and Energy Materials*
   Andrew G. Stack, Chemical Sciences Division
   Matthew G. Tucker, Neutron Scattering Division
6. *Structural Materials*
   Ke An, Neutron Scattering Division
   Easo George, Materials Science and Technology Division and University of Tennessee, Knoxville
7. *Biology and Life Sciences*
   Julie C. Mitchell, Biosciences Division
   Hugh O'Neill, Neutron Scattering Division
   Eric M. Pierce, Environmental Sciences Division
   Jeremy C. Smith, Biosciences Division and University of Tennessee, Knoxville

External Technical Reviewers

Ken Andersen	European Spallation Source
Frank S. Bates	University of Minnesota
Collin Broholm	Johns Hopkins University
Robert Dimeo	NIST Center for Neutron Research
Patricia M. Dehmer	ORNL Science Advisory Board
Janos Kirz	Lawrence Berkeley National Laboratory
Despina Louca	University of Virginia
Robert McGreevy	ISIS Neutron and Muon Source, STFC Rutherford Appleton Laboratory
Sean McSweeney	National Synchrotron Light Source–II, Brookhaven National Laboratory
John B. Parise	Stony Brook University
Roger Pynn	Indiana University, Bloomington
William G. Stirling	Institut Laue-Langevin (retired)
Douglas J. Tobias	University of California, Irvine
Priya Vashishta	University of Southern California
Soichi Wakatsuki	SLAC National Accelerator Laboratory; Stanford University

Additional Contributors

Paul Adams	Lawrence Berkeley National Laboratory
Rigoberto Advincula	Case Western Reserve University
Sean Agnew	University of Virginia

John Ankner	Oak Ridge National Laboratory
Lawrence M. Anovitz	Oak Ridge National Laboratory
Arnab Banerjee	Oak Ridge National Laboratory
Mark Banaszak Holl	Monash University
Christopher M. Bates	University of California, Santa Barbara
Frank S. Bates	University of Minnesota
Cristian D. Batista	University of Tennessee, Knoxville
Edmon Begoli	Oak Ridge National Laboratory
Sergey M. Bezrukov	National Institutes of Health
Hassina Bilheux	Oak Ridge National Laboratory
Jay Billings	Oak Ridge National Laboratory
Kent Blasie	University of Pennsylvania
Reinhard Boehler	Oak Ridge National Laboratory; Carnegie Institution for Science
Jodie Bradby	Australian National University
Collin Broholm	Johns Hopkins University
Frank Brown	University of California, Santa Barbara
Zimei Bu	City College of New York
Paul Butler	National Institute of Standards and Technology
Stuart Calder	Oak Ridge National Laboratory
Bryan C. Chakoumakos	Oak Ridge National Laboratory
Timothy Charlton	Oak Ridge National Laboratory
Sow-Hsin Chen	California Institute of Technology
Wei Chen	Argonne National Laboratory
Wei-Ren Chen	Oak Ridge National Laboratory
Yongqiang Cheng	Oak Ridge National Laboratory
Jaehun Chun	Pacific Northwest National Laboratory
Aurora Clark	Washington State University
Sue Clark	Pacific Northwest National Laboratory
Leighton Coates	Oak Ridge National Laboratory
Piers Coleman	Rutgers University
Matthew Cuneo	Oak Ridge National Laboratory
Luke Daemen	Oak Ridge National Laboratory
Pengcheng Dai	Rice University
Clarina de la Cruz	Oak Ridge National Laboratory
James De Yoreo	Pacific Northwest National Laboratory
Theo Dingemans	University of North Carolina, Chapel Hill
John DiTusa	Louisiana State University
Changwoo Do	Oak Ridge National Laboratory
Antonio dos Santos	Oak Ridge National Laboratory
Nancy Dudney	Oak Ridge National Laboratory
Georg Ehlers	Oak Ridge National Laboratory
Mikhail Eremets	Max Planck Institute for Chemistry
Timothy Ferreira	University of South Carolina
Mike Fitzsimmons	Oak Ridge National Laboratory

Brent Fultz	California Institute of Technology
Franz Gallmeier	Oak Ridge National Laboratory
Yan Gao	GE Global Research
Elena Garlea	Y-12 National Security Complex
Klaus Gawrisch	National Institutes of Health
Al Geist	Oak Ridge National Laboratory
Arne Gericke	Worcester Polytechnic Institute
Van Graves	Oak Ridge National Laboratory
Malcolm Guthrie	European Spallation Source
Yury Gogotsi	Drexel University
Bianca Haberl	Oak Ridge National Laboratory
Lilin He	Oak Ridge National Laboratory
Matt Helgeson	University of California, Santa Barbara
William Heller	Oak Ridge National Laboratory
Russell Hemley	George Washington University
Kenneth Herwig	Oak Ridge National Laboratory
Jason Hodges	Oak Ridge National Laboratory
Axel Hoffmann	Argonne National Laboratory
Christina Hoffmann	Oak Ridge National Laboratory
Kunlun Hong	Oak Ridge National Laboratory
David Hoogerheide	National Institute of Standards and Technology
Ashfia Huq	Oak Ridge National Laboratory
Alex Johs	Oak Ridge National Laboratory
Jacob Jones	North Carolina State University
Udaya Kalluri	Oak Ridge National Laboratory
John Katsaras	Oak Ridge National Laboratory; University of Tennessee, Knoxville
Mark Kester	University of Virginia
Eugenia Kharlampieva	University of Alabama, Birmingham
Patrick Kluth	Australian National University
Alexander Kolesnikov	Oak Ridge National Laboratory
Julie Kornfield	California Institute of Technology
Andrey Kovalevsky	Oak Ridge National Laboratory
Richard Kriwacki	St. Jude Children's Research Hospital
Jessy Labbé	Oak Ridge National Laboratory
Maik Lang	University of Tennessee Knoxville
Ka Yee Lee	University of Chicago
Jue Liu	Oak Ridge National Laboratory
Timothy P. Lodge	University of Minnesota
Mattias Lösche	Carnegie Mellon University
John Loveday	University of Edinburgh
Eugene Mamontov	Oak Ridge National Laboratory
Michael Manley	Oak Ridge National Laboratory
Dougal McCulloch	Royal Melbourne Institute of Technology
Marshall McDonnell	Oak Ridge National Laboratory

Michael A. McGuire	Oak Ridge National Laboratory
David McKenzie	University of Sydney
Sean McSweeney	Brookhaven National Laboratory
Scott Misture	Alfred University
Diana Mitrea	St. Jude Children's Research Hospital
Martin Mourigal	Georgia Institute of Technology
Dean Myles	Oak Ridge National Laboratory
Michihiro Nagao	National Institute of Standards and Technology
Stephen E. Nagler	Oak Ridge National Laboratory
Joerg C. Neuefeind	Oak Ridge National Laboratory
Daniel Olds	Oak Ridge National Laboratory
Brad Olsen	Massachusetts Institute of Technology
Katharine Page	Oak Ridge National Laboratory
E. Andrew Payzant	Oak Ridge National Laboratory
Caroline Pearce	Pacific Northwest National Laboratory
Loukas Petridis	Oak Ridge National Laboratory
Christian Pfleiderer	Technical University of Munich
Philip Pincus	University of California, Santa Barbara
Sai Venkatesh Pingali	Oak Ridge National Laboratory
Shuo Qian	Oak Ridge National Laboratory
Anibal Ramirez-Cuesta	Oak Ridge National Laboratory
James B. Roberto	Oak Ridge National Laboratory (retired)
Ian Robertson	University of Wisconsin–Madison
Lee Robertson	Oak Ridge National Laboratory
Henrik Rønnow	École Polytechnique Fédérale de Lausanne
Peter Rosenblad	Oak Ridge National Laboratory
Stephan Rosenkranz	Argonne National Laboratory
Kevin Rosso	Pacific Northwest National Laboratory
Tatiana Rostovtseva	National Institutes of Health
Michael Rubenstein	Pacific Northwest National Laboratory
Tom Russell	University of Massachusetts
Tomonori Saito	Oak Ridge National Laboratory
Jeff Sakamoto	University of Michigan
Gabriele Sala	Oak Ridge National Laboratory
Gregory Schenter	Pacific Northwest National Laboratory
Mark Schlossman	University of Illinois at Chicago
Gerald Schneider	Louisiana State University
Ivan Schuller	University of California, San Diego
Rachel Segalman	University of California, Santa Barbara
Isaac Silvera	Harvard University
Gregory S. Smith	Oak Ridge National Laboratory (retired)
Olivier Soubias	National Institutes of Health
Philip Sprunger	Louisiana State University
Robert F. Standaert	East Tennessee State University

Christopher Stanley	Oak Ridge National Laboratory
Matt Steiner	University of Cincinnati
Alexandru Stoica	Oak Ridge National Laboratory
Timothy Strobel	Carnegie Institution for Science
D. Alan Tennant	Oak Ridge National Laboratory
Steven Tidrow	Alfred University
Matthew Tirrell	University of Chicago
Douglas Tobias	University of California, Irvine
John Tranquada	Brookhaven National Laboratory
John Tse	University of Saskatchewan
Christopher Tulk	Oak Ridge National Laboratory
Tedi-Marie Usher-Ditzian	Oak Ridge National Laboratory
Sudharshan Vazhkudai	Oak Ridge National Laboratory
Norman Wagner	University of Delaware
Jeffrey M. Warren	Oak Ridge National Laboratory
Lynn Walker	Carnegie Mellon University
Hsiu-Wen Wang	Oak Ridge National Laboratory
Zhe Wang	Oak Ridge National Laboratory
David J. Wesolowski	Oak Ridge National Laboratory
Carol Williams	Medical College of Wisconsin
Travis Williams	Oak Ridge National Laboratory
Stephen Wilson	University of California, Santa Barbara
Thomas A. Witten	University of Chicago
Zuo-Guang Ye	Simon Frasier University
Igor Zaliznyak	Brookhaven National Laboratory
Hans-Conrad zur Loye	University of South Carolina

(Intentionally left blank)

Appendix A.
Community Workshops and Activities in Support of STS, 2013–2018

Science Topical Workshops
[Reports available at https://neutrons.ornl.gov/content/grand-challenge-workshop-reports (accessed July 3, 2019)]

Quantum Condensed Matter Workshop, Lawrence Berkeley National Laboratory, Berkeley, CA, December 9–10, 2013
Organizers: R. J. Birgeneau (University of California–Berkeley), R. Ramesh (Oak Ridge National Laboratory), and S. E. Nagler (Oak Ridge National Laboratory)

Grand Challenges in Biological Neutron Scattering Workshop, University of California–San Diego, San Diego, CA, January 17–18, 2014
Organizers: Susan Taylor (UCSD), Heidi Hamm (Vanderbilt University)

Grand Challenges in Soft Matter Workshop, University of California–Santa Barbara, Santa Barbara, CA, May 17–18, 2014
Organizers: Fyl Pincus (University of California–Santa Barbara), Matt Tirrell (University of Chicago)

Frontiers in Materials Discovery, Characterization and Application, Schaumburg, IL, August 2–3, 2014
Organizers: George Crabtree (University of Chicago and Argonne National Laboratory), John Parise (Stony Brook University and Joint Photon Sciences Institute)

Frontiers in Data, Modeling, and Simulation, Argonne National Laboratory, Argonne, IL, March 30–31, 2015
Organizers: Peter Littlewood (Argonne National Laboratory), Thomas Proffen (Oak Ridge National Laboratory)

Other Workshops

Second Target Station Workshop (general user workshop on STS science and instruments), Oak Ridge National Laboratory, Oak Ridge, TN, October 27–29, 2015
Chairs: M. R. Eskildsen (University of Notre Dame), B. Khaykovich (Massachusetts Institute of Technology)
[Report available at https://neutrons.ornl.gov/sites/default/files/STS%20Workshop%20Report.pdf (accessed July 3, 2019)]

Workshop on Novel Concepts (technical workshop), Oak Ridge National Laboratory, Oak Ridge, TN, April 25–26, 2016
Chair: Roger Pynn (Indiana University)

Very Cold Neutron Source for the Second Target Station Workshop, Oak Ridge National Laboratory, Oak Ridge, TN, April 27–28, 2016
Chair: Mike Fitzsimmons, Oak Ridge National Laboratory
[Report and related documents available at https://conference.sns.gov/event/18/page/414-shared-documents (accessed July 3, 2019)]

Town Hall Discussion at 2016 American Conference on Neutron Scattering (open meeting for users), Long Beach, CA, July 12, 2016

ZEEMANS Instrument Advisory Team Meeting (instrument-specific workshop), Oak Ridge National Laboratory, Oak Ridge, TN, August 19, 2016
Chair: Barry Winn (Oak Ridge National Laboratory)

Early Quantum Materials Science at the STS, Georgia Institute of Technology, Atlanta, GA, January 5–6, 2017
Chairs: Mark Lumsden (Oak Ridge National Laboratory), Travis Williams (Oak Ridge National Laboratory), Martin Mourigal (Georgia Tech)
[Related documents available at https://conference.sns.gov/event/64/overview (accessed July 3, 2019)]

STS Integrated Systems Review (technical status of instruments and target; choice of operating parameters: 15 Hz, 700 kW, short proton pulse), Oak Ridge National Laboratory, Oak Ridge, TN, April 2017
Chair: Robert McGreevy (ISIS)

Instrument Advisory Board (three-source strategy; placement and prioritization of instruments), Oak Ridge National Laboratory, Oak Ridge, TN, January 2018
Chair: Dan Neumann (National Institute of Standards and Technology)

Meetings of the Oak Ridge National Laboratory Neutron Advisory Board, Oak Ridge, TN

April 2013: Development of three-source strategy

March 2014: Three-source strategy; discussion of instrument concepts

May 2015: STS and its instrument suite

June 2016: STS and its technical parameters (short pulse); discussion of Basic Energy Sciences Advisory Committee (BESAC) Facility Upgrade Prioritization Subcommittee report

September 2017: Three-source strategy and instrument optimization

Appendix B.
Acronyms, Abbreviations, and Initialisms

1D	one-dimensional
2D	two-dimensional
3D	three-dimensional
4D	four-dimensional
AAT	aspartate aminotransferase
AI	artificial intelligence
ALS	amyotrophic lateral sclerosis
AM	additive manufacturing
bcc	body-centered cubic
BES	Basic Energy Sciences
CNCS	Cold Neutron Chopper Spectrometer (at SNS FTS)
CNMS	Center for Nanophase Materials Sciences
CORELLI	elastic diffuse scattering spectrometer (at SNS FTS)
CSNS	China Spallation Neutron Source
DAC	diamond anvil cell
DOE	United States Department of Energy
EDA	ethylenediamine
EQ-SANS	Extended Q-Range Small-Angle Neutron Scattering Diffractometer (at SNS FTS)
ESS	European Spallation Source
fcc	face-centered cubic
FRM-II	Forchungsreaktor München II
FTS	First Target Station
hcp	hexagonal close-packed
HEBT	high-energy beam transport
HFIR	High Flux Isotope Reactor
HPC	high-performance computing
HYSPEC	Hybrid Spectrometer (at SNS FTS)
IDP	intrinsically disordered protein
ILL	Institut Laue-Langevin
IMAGINE	Image-Plate, Single-Crystal Diffractometer (at HFIR)
INS	inelastic neutron scattering
ISIS	ISIS Neutron and Muon Source
J-PARC	Japan Proton Accelerator Research Complex
KB	Kirkpatrick-Baez
LEBT	low-energy beam transport
MCP	microchannel plate
MEBT	medium-energy beam transport
ML	machine learning
MM	metamorphic manufacturing
mod-sim	modeling and simulation

NCNR	NIST Center for Neutron Research
NIST	National Institute of Standards and Technology
NR	neutron reflectometry
NSE	neutron spin echo
OEC	oxygen-evolving complex
OLCF	Oak Ridge Leadership Computing Facility
ORNL	Oak Ridge National Laboratory
PLP	pyridoxal-5′-phosphate
PMAA	poly(methacrylic acid)
POWGEN	General-Purpose Powder Diffractometer (at SNS FTS)
PPU	proton power upgrade
PSD	position-sensitive detector
PVP	poly(vinylpyrrolidone)
QCP	quantum critical point
QSL	quantum spin liquid
RF	radiofrequency
RFQ	radiofrequency quadrupole
RTBT	ring-to-beam transport
SANS	small-angle neutron scattering
SEQUOIA	Fine-Resolution Fermi Chopper Spectrometer (at SNS FTS)
SEMSANS	spin-echo-modulated small-angle neutron scattering
SiPM	silicon photomultiplier
SLD	scattering length density
SNS	Spallation Neutron Source
STS	Second Target Station
SWCNT	single-wall carbon nanotube
TBP	tri-*n*-butyl phosphate
TOF	time-of-flight
TOPAZ	Single-Crystal Diffractometer (at SNS FTS)
TS	Target Station
VULCAN	Engineering Materials Diffractometer (at SNS FTS)
WANS	wide-angle neutron scattering